

G8940

# **INFLUENCE OF ALLOYING ADDITIONS ON THE STRUCTURE AND PROPERTIES OF Al-7Si-0.3Mg ALLOY**

Thesis submitted to  
**Cochin University of Science and Technology**  
in partial fulfilment of the requirements  
for the Degree of

**DOCTOR OF PHILOSOPHY**  
in the Faculty of Technology



*By*  
**SREEJA KUMARI. S.S**



**MATERIALS AND MINERALS DIVISION  
REGIONAL RESEARCH LABORATORY (CSIR)  
THIRUVANANTHAPURAM - 695 019  
INDIA**

**April 2006**



COUNCIL OF SCIENTIFIC AND INDUSTRIAL RESEARCH  
**REGIONAL RESEARCH LABORATORY**  
Industrial Estate P.O., Thiruvananthapuram – 695 019, India  
Telegram: Consearch, Fax: 0471-2490186, 2491712  
Email: rrlt@csrrltd.ren.nic.in; Phone: 0471-2490674, 2490811

---

**Dr. R.M. Pillai**

*Senior Deputy Director and Head  
Materials and Minerals Division*

## CERTIFICATE

This is to certify that the thesis entitled '**Influence of Alloying Additions on the Structure and Properties of Al-7Si-0.3Mg Alloy**' embodies the results of bonafide research work carried out by **Mrs. Sreeja Kumari S.S.** for the degree of **Doctor of Philosophy** in the Faculty of Technology of the Cochin University of Technology under my guidance. The content of this thesis or part thereof has not been submitted to any other university or institute for the award of any degree or diploma.

**(R.M. Pillai)**  
**Thesis Supervisor**

## ABSTRACT

Cast Al-Si alloys are widely used in the automotive, aerospace and general engineering industries due to their excellent combination of properties such as good castability, low coefficient of thermal expansion, high strength-to-weight ratio and good corrosion resistance. Recently, sustainability and recycling of resources are of paramount importance with increasing public awareness on environmental issues, energy and depleting natural resources. Therefore, secondary aluminium alloys, requiring only 5% energy compared to primary Al production from ores, are receiving widespread acceptance worldwide. However, the increasing use of recycled aluminium casting alloys warrants strict microstructural control to remove the deleterious effects of impurity elements. Iron is the most common and deleterious impurity in aluminium alloys in general and Al-7Si-0.3Mg alloy, a commercially important one for aerospace, automotive and other critical applications, in particular since it forms different intermetallic compounds with Al, Si and other elements present in the alloy. Among the various Fe-intermetallic phases present, the  $\beta$ -phase is considered to be particularly detrimental to the ductility of the alloy. The platelet and needle-like morphologies of the  $\beta$ -Al<sub>5</sub>FeSi phase make it act as a stress raiser, thereby reducing the mechanical properties of the alloy. Furthermore, the brittle and hard nature of  $\beta$ -Al<sub>5</sub>FeSi makes machining of cast parts difficult and costly because of the increased machining hours required and the associated reduction in tool life. Among the various techniques available to minimize the detrimental effect of iron, the addition of elements called “neutralizers” is most commonly used.

The present investigation is on the “INFLUENCE OF ALLOYING ADDITIONS ON THE STRUCTURE AND PROPERTIES OF Al-7Si-0.3Mg ALLOY”. Calcium, once considered only as a deleterious element in aluminium alloys because of its degrading effect on properties, has some beneficial roles as well. Hence, the primary objective of this present investigation is to study these beneficial effects of calcium on the structure and properties of Al-7Si-0.3Mg-xFe alloys. The second objective of this work is

to study the effects of Mn, Be and Sr addition as Fe neutralizers and also to study the interaction of Mn, Be, Sr and Ca in Al-7Si-0.3Mg-xFe alloys. The structure of the thesis and the details of the studies are given below.

The Chapter 1 deals with the general introduction to Al-Si alloys, Al-Si phase diagram and the applications of these alloys. Further, the importance of recycling has been brought out towards the end of this chapter.

A comprehensive review of the parameters influencing the structure and properties of Al-Si-Mg cast alloys is given in Chapter 2. This chapter also presents an extensive literature survey on the effect of iron in Al-Si foundry alloys and the methods of eliminating the deleterious effects of iron. Further, this review mainly focuses on the literature available on calcium besides the common iron neutralizing elements in Al-Si-Mg cast alloys.

Chapter 3 gives the details of the materials and the experimental methods used in the present investigation. The structural characteristics of the castings are evaluated by optical metallography coupled with Image analyser, Scanning Electron Microscopy and Energy Dispersive X-ray spectroscopy, and X-ray Diffraction analysis. Solidification behaviour was studied by Thermal Analysis and Differential Thermal Analysis. The physical properties such as density and electrical conductivity are measured using Archimedean densitometry and TECHNOFOUR conductivity meter respectively. Mechanical properties (tensile and impact) are evaluated using Instron Universal Testing Machine and Pendulum Type Charpy Impact Testing Machine.

Chapter 4 deals with results of the dual effect of calcium viz., Modification and Fe-neutralization in Al-7Si-0.3Mg alloy. It has been found that calcium modifies the eutectic Si by changing its morphology from acicular to fine fibrous form and the tensile and impact properties obtained are at par with those obtained with the well known modifier viz., Sr. Ca refines the platelet Fe-intermetallic phases causing improved

electrical conductivity, elongation and impact strengths. The proposed mechanism for Fe-neutralization by Ca is the destabilization of the  $\beta$ -phase and fragmentation of the long  $\beta$ -platelets into smaller sizes. One of the interesting observations in the present work is that a low level of calcium reduces the porosity compared to the untreated alloy. However, higher levels of calcium addition lead to higher porosity in the castings. An empirical analysis carried out for comparing the results of the present work with those of the other researchers on the effect of increasing iron content on UTS and % elongation of Al-Si-Mg and Al-Si-Cu alloys has shown a linear and an inverse first order polynomial relationships respectively.

Chapter 5 deals with the effects of Mn, Be and Sr as Fe-neutralizers and their interaction with calcium in Al-7Si-0.3Mg-xFe alloy. Mn and Be additions to Al-7Si-0.3Mg-xFe alloys change the morphology of platelet iron phase to Chinese script form, whereas Sr reduced the size of platelet phases like Ca. This has led to a significant improvement in tensile properties with Mn addition and both tensile and impact properties with Be and Sr additions. Combined additions of Ca + Mn, Be + Mn and Sr + Mn led to improvement in both tensile and impact properties compared to individual additions and a synergistic effect of both the elements is achieved. A trace amount of Be (0.005%) addition to Ca leads to superior tensile properties compared to Ca addition alone.

The summary of the findings of this investigation along with its contributions made to the knowledge and the avenues for further work are presented in Chapter 6.

# CONTENTS

	Page No.
Abstract	i
Acknowledgements	iv
Contents	vi
List of Tables	x
List of Figures	xi
<b>CHAPTER 1: INTRODUCTION</b>	1
1.1 IMPORTANCE OF Al-Si ALLOYS	2
1.2 Al-Si ALLOY SYSTEM	2
1.3 RECYCLING OF ALUMINIUM AND ITS ALLOYS	4
<b>CHAPTER 2: LITERATURE REVIEW</b>	8
2.1 INTRODUCTION	8
2.2 PARAMETERS INFLUENCING THE STRUCTURE AND PROPERTIES OF Al-Si-Mg CAST ALLOYS	8
2.2.1 Alloy Composition	8
2.2.1.1 Major alloying elements	8
2.2.1.2 Trace alloying elements	9
2.2.1.3 Al-7Si-0.3Mg alloy	11
2.2.2 Solidification Characteristics	11
2.2.3 Casting Defects and their Control	14
2.2.3.1 Gas porosity	16
2.2.3.2 Shrinkage porosity	19
2.2.4 Melt Treatments	20
2.2.4.1 Degassing	20
2.2.4.2 Modification	21
2.2.4.3 Grain refinement	29
2.2.5 Effect of Alloying Elements on the Castability of Aluminium Alloys	30
2.2.5.1 Formation of oxides and their effects	30
2.2.5.2 Fluidity	31
2.2.6 Heat Treatment	34
2.2.6.1 Temper selection	34

2.2.6.2	Solution heat treatment	34
2.2.6.3	Quenching	36
2.2.6.4	Aging	37
2.3	IMPURITIES IN CAST Al-Si ALLOYS	37
2.4	IRON IN CAST Al-Si ALLOYS	37
2.4.1	Aluminium – Iron system	38
2.4.2	Iron Intermetallic Phases	38
2.4.3	Effect of Fe on the Properties of Al-Si Alloys	40
2.4.3.1	Physical properties	41
2.4.3.2	Thermal conductivity	41
2.4.3.3	Corrosion resistance	42
2.4.3.4	Mechanical properties	42
2.4.4	Techniques to Neutralize the ill Effects of Fe in Al-Si Alloys	44
2.4.4.1	Rapid solidification	44
2.4.4.2	Melt superheating	45
2.4.4.3	Low temperature working	47
2.4.4.4	Chemical neutralizers	47
2.5	INTERACTION OF TRACE ELEMENTS	55
2.6	APPLICATIONS OF Al-7Si-0.3Mg ALLOY	59
2.7	GENERAL DISCUSSION	59
2.8	SUMMARY	63
2.9	SCOPE OF THE PRESENT INVESTIGATION	64
	<b>CHAPTER 3: MATERIALS AND EXPERIMENTAL DETAILS</b>	<b>66</b>
3.1	MATERIALS	66
3.2	MELTING AND CASTING	66
3.3	HEAT TREATMENT	67
3.4	CHEMICAL ANALYSIS	67
3.5	THERMAL ANALYSIS	67
3.6	DIFFERENTIAL THERMAL ANALYSIS (DTA)	71

3.7	PHYSICAL CHARACTERISTICS	71
3.7.1	Density Measurement and Porosity Calculation	71
3.7.2	Electrical Conductivity	71
3.8	MECHANICAL CHARACTRISTICS	72
3.9	STRUCTURAL STUDIES	72
3.9.1.	Optical Microscopy	72
3.9.2.	Image Analysis	74
3.9.3.	Scanning Electron Microscopy (SEM)/ Energy Dispersive X-ray Spectroscopy (EDS)/ Electron Back Scattered Diffraction (EBSD)	74
	<b>CHAPTER 4: EFFECT OF CALCIUM IN Al-7Si-0.3Mg ALLOY</b>	<b>75</b>
4.1	MODIFICATION	75
4.1.1	Methodology	75
4.1.2	Results and Discussion	76
4.1.2.1	Microstructure	76
4.1.2.2	Physical characteristics	76
4.1.2.3.	Mechanical properties	80
4.1.3	SUMMARY	82
4.2	IRON NEUTRALIZATION	84
4.2.1	Methodology	84
4.2.2	Results	84
4.2.2.1	Microstructure	84
4.2.2.2	Physical characteristics	89
4.2.2.3	Mechanical properties	94
4.2.3	Empirical Analysis of Data	102
4.2.4	Discussion	106
4.2.5	Summary	110
	<b>CHAPTER 5: EFFECT OF Mn, Be AND Sr AND THEIR INTERACTION WITH Ca IN Al-7Si-0.3Mg-xFe ALLOY</b>	<b>111</b>
5.1	INTRODUCTION	111
5.2	METHODOLOGY	111
5.3	RESULTS	112
5.3.1	Microstructure	112

5.3.1	Microstructure	112
5.3.1.1	Effect of Mn, Be and Sr	112
5.3.1.2	Interaction of Mn, Be, Sr and Ca	115
5.3.2	Solidification Behaviour	128
5.3.2.1	Thermal analysis	128
5.3.2.2	Differential thermal analysis	128
5.3.3	Physical Characteristics	138
5.3.3.1	Porosity	138
5.3.3.2	Electrical conductivity	138
5.3.4	Mechanical Properties	139
5.3.4.1	Tensile properties	139
5.3.4.2	Impact strength	142
5.4	DISCUSSION	145
5.5	SUMMARY	150
	<b>CHAPTER 6: CONCLUSIONS</b>	151
6.1	SIGNIFICANT CONTRIBUTIONS OF THE PRESENT INVESTIGATION TO THE KNOWLEDGE	153
6.2	AVENUES FOR FUTURE WORK	153
	<b>REFERENCES</b>	154
	<b>AWARDS AND PUBLICATIONS BASED ON THE THESIS WORK</b>	171

## LIST OF TABLES

<b>Table Number</b>	<b>Caption</b>	<b>Page Number</b>
1.1	Common Al-Si alloys and their mechanical properties	5
2.1	Various Designations of Al-7Si-0.3Mg alloy	12
2.2	Physical properties of LM25 / Al-7Si-0.3Mg alloy	12
2.3	Mechanical properties of LM25/Al-7Si-0.3Mg alloy	13
2.4	Characteristics of elements used as eutectic silicon modifiers in Al-Si alloys	25
2.5	Mechanical Properties of Na and Ca added Silumin (Eutectic Alloy Containing 11.59% Si)	27
2.6	Atomic size, crystal structure and maximum solid solubility of various elements in pure aluminium at eutectic/peritectic temperature	48
2.7	Optimum amount, morphological change, advantages and limitations of various iron neutralizers in Al-Si alloys	49
3.1	Chemical composition (wt.%) of the Al-7Si-0.3Mg (LM25/356) alloy	66
4.1	% Porosity and Electrical Conductivity of Al-7Si-0.3Mg alloy treated without and with Ca	80
4.2	Silicon particle characteristics of T6-heat treated samples	88
4.3	Fitted equation and the correlation coefficient for the plot of % porosity versus % Fe content at various Ca levels	93
4.4	Empirical analysis of data for UTS versus Fe content	104
4.5	Empirical analysis of data for % elongation versus Fe content	105
5.1	Average length of eutectic Si in Al-7Si-0.3Mg-1.0Fe alloy without and with Ca, Be and Ca+Be additions	123
5.2	Alloys, thermal arrests and the phases formed in Al-7Si-0.3Mg-0.8Fe alloy without and with Be, Mn, Ca and Sr additions	134
5.3	% porosity and electrical conductivity of permanent mould cast Al-7Si-0.3Mg-0.6Fe alloy without and with Ca, Mn and Ca + Mn additions	139

## LIST OF FIGURES

<b>Figure Number</b>	<b>Caption</b>	<b>Page Number</b>
1.1	Aluminium's Major Applications	3
1.2	Al-Si alloy phase diagram	3
2.1	Effect of alloying elements on the surface tension of 99.99 aluminium at 973 to 1013 K in argon atmosphere	15
2.2	The solubility of hydrogen at one atmosphere pressure in pure aluminium	17
2.3	Ledge migration mechanism responsible for the growth of Si flakes bounded by atomically flat (111) surfaces	22
2.4	Plot of atomic radii vs atomic number, with range of radii which includes elements capable of producing silicon modification – shaded	23
2.5	Schematic representation of impurity atoms pinning the steps of a silicon crystal growing by the layer growth mechanism at the solid/liquid interface	23
2.6	Microporosity and macroporosity in modified and unmodified A357 alloy	28
2.7	Microstructure of Al-Si-Mg (356) alloy after grain refining with Al-5Ti-1B master alloy	33
2.8	Comparative oxidation losses caused by the addition of various elements to aluminium melt	33
2.9	Equilibrium solubility of Mg and Si in solid aluminium when both $Mg_2Si$ and Si are present	35
2.10	Al-Fe alloy phase diagram	39
2.11	Liquidus surfaces in the Al-rich corner of the Al-Fe-Si equilibrium phase diagram	39
2.12	Micrographs of Al-6Si-3.5Cu-1.0Fe alloy (a) superheated to 1023 K and (b) 1123 K prior to casting (cooling rate = 283 K/s)	46

2.13	Simplified illustration of Fe segregation during solidification of 356 (Al-7Si-0.3Mg) alloy containing 0.48% Fe	51
2.14	$T_{mat}$ and dynamic fracture toughness versus Fe content in AC2B-T6 (Al-6.5Si-4Cu) casting alloy with and without Ca addition	56
2.15	Cooling curves obtained when Ca is used in the presence of Sr	56
2.16	Aura alloy wheel – PCD108 (Hindalco) used in TATA Indica and Ford Ikon cars	60
2.17	Premium quality Al-7Si-0.3Mg (A356) alloy castings for Space application ( <i>PSLV &amp; GSLV Programmes of ISRO</i> )	61
3.1	Dimensions of (a) Rectangular slab mould and (b) Cylindrical mould used	68
3.2	Dimensions of (a) Rectangular slab casting and (b) Cylindrical castings	69
3.3	MeltLab Aluminium Thermal Analyser	70
3.4	DTA equipment	73
3.5	TECHNOFOUR' conductivity meter	73
4.1	Typical as cast microstructures of Al-7Si-0.3Mg alloy treated (a) without and (b) with 0.01% Ca	77
4.2	Typical as cast microstructures of Al-7Si-0.3Mg alloy treated (a) 0.02 % Ca (b) 0.05% Ca and (c) 0.02% Sr	78
4.3	(a) SEM photograph of $Al_2CaSi_2$ phase in Al-7Si-0.3Mg alloy treated with 0.05% calcium (b) EDS spectra showing the distribution of Al, Si and Ca in $Al_2CaSi_2$ phase	79
4.4	Effect of calcium on the (a) UTS (b) % elongation and (c) impact strength of Al-7Si-0.3Mg alloy	81
4.5	SEM micrographs showing the impact fracture surface of Al-7Si-0.3Mg alloy with and without Ca (a) 0% Ca (b) 0.01% Ca (c) 0.02% Ca (d) 0.05% Ca and (e) 0.02% Sr	83
4.6	Typical permanent mould as cast microstructures of Al-7Si-0.3Mg alloy with (a) 0.4 and (b) 0.7% Fe	85

4.7	(a) SEM photograph of $\beta$ -phase in Al-7Si-0.3Mg-0.7Fe alloy and (b) EDS spectra showing the distribution of Al, Si and Fe	86
4.8	Typical microstructures of sand cast Al-7Si-0.3Mg alloy with (a) 0.2% Fe, (b) 0.7% Fe, (c) 0.2% Fe + 0.01% Ca and (d) 0.7% Fe + 0.01% Ca in the as-cast condition	87
4.9	Effect of Ca addition on the average length of the $\beta$ -phase particles in sand cast Al-7Si-0.3Mg-xFe alloy	90
4.10	Typical microstructures of Al-7Si-0.3Mg-0.6Fe alloy treated with 0.05% Ca	90
4.11	SEM micrograph showing very fine Fe intermetallic phases in Al-7Si-0.3Mg-0.6Fe alloy with Ca (0.05%) addition	91
4.12	(a) SEM micrograph showing the formation of $Al_2CaSi_2$ phase in Al-7Si-0.3Mg-0.6Fe alloy with Ca (0.05%) addition (b) EDS spectrum showing Al, Si and Ca distributions.	91
4.13	Typical microstructures of permanent mould cast Al-7Si-0.3Mg-0.7Fe alloy in T6 condition (a) without and (b) with 0.01% Ca	92
4.14	EBSD mapping results of Al-7Si-0.3Mg-0.2Fe+0.01% Ca alloy	92
4.15	Effect of Ca on the % porosity of Al-7Si-0.3Mg-xFe alloy	93
4.16	Micrographs of platelet/needle like Fe intermetallic compound observed within a shrinkage pore in Al-7Si-0.3Mg-0.7Fe alloy (a) Optical and (b) SEM	95
4.17	Effect of Ca on the %IACS of Al-7Si-0.3Mg-xFe alloy	96
4.18	Effect of Ca addition on the (a) UTS and (b) % elongation of Al-7Si-0.3Mg-xFe alloy (T6 condition)	97
4.19	SEM micrographs showing the tensile fractured surface of Al-7Si-0.3Mg alloy (T6 condition) containing (a) 0.2% Fe (b) 0.2% Fe+0.005% Ca (c) 0.4% Fe+0.01% Ca and d) 0.7% Fe+0.005% Ca	99
4.20	Effect of Ca on the quality index of Al-7Si-0.3Mg-xFe alloy in T6 condition	100
4.21	Effect of Ca on the impact strength of Al-7Si-0.3Mg-xFe alloy	101

4.22	Effect of higher amount of Ca (0.05%) on the (a) UTS (b) % elongation and (c) impact strength of Al-7Si-0.3Mg-0.6Fe alloy (T6 condition)	103
4.23	Empirical analysis of the variation of UTS with iron content in Al-Si-Mg and Al-Si-Cu alloys	104
4.24	Empirical analysis of the variation of % elongation with iron content in Al-Si-Mg and Al-Si-Cu alloys	105
4.25	Schematic illustration of decomposition of $\beta$ platelets with Ca addition	107
5.1	Typical microstructures of permanent mould cast Al-7Si-0.3Mg alloy with (a) 0.8% Fe, Circled area showing the branching of $\beta$ -platelet and (b) Higher magnification of the branched platelet, arrow showing nucleation of eutectic Si by $\beta$ -platelets	113
5.2	Typical microstructures of permanent mould cast Al-7Si-0.3Mg-0.6Fe alloy treated with (a) 0.3% Mn and (b) 0.5% Mn [Arrows show the Mn-Fe phases]	114
5.3	SEM micrograph of Al-7Si-0.3Mg-0.8Fe with 0.3% Mn addition	114
5.4	EDS elemental X-ray mapping and elemental distribution of Chinese script Mn-Fe phase in Al-7Si-0.3Mg-0.6Fe alloy treated with 0.3% Mn	116
5.5	Typical as cast microstructures of permanent mould cast Al-7Si-0.3Mg-0.8Fe-0.2Be alloy	117
5.6	Typical microstructure of sand cast Al-7Si-0.3Mg-1.0Fe-0.2Be alloy	117
5.7	X-ray diffraction patterns of (a) Al-7Si-0.3Mg-0.8Fe and (b) Al-7Si-0.3Mg-0.8Fe-0.2Be alloys	118
5.8	Typical microstructures of permanent mould cast Al-7Si-0.3Mg-0.8Fe alloy treated with 0.04% Sr (a) Optical and (b) SEM micrographs	119
5.9	Typical microstructures of permanent mould cast Al-7Si-0.3Mg-0.6Fe-0.3Mn alloy with (a) 0.02 (b) 0.05 and (c) 0.08% Ca	120

5.10	Typical permanent mould cast microstructure of Al-7Si-0.3Mg-0.8Fe alloy with Be (0.005%)+Ca (0.04%) addition	122
5.11	Typical sand mould cast microstructures of Al-7Si-0.3Mg-1.0Fe alloy treated with (a) 0.015% Ca+0.005% Be and (b) 0.008% Ca + 0.007% Be ["1"-Platelet form of iron intermetallic compound]	122
5.12	Average length of $\beta$ phase in Al-7Si-0.3Mg-1.0Fe alloy without and with Ca, Be and Ca + Be additions	123
5.13	SEM micrograph of Al-7Si-0.3Mg-0.8Fe alloy with Be (0.15%) + Mn (0.15%) addition	124
5.14	Typical microstructure of permanent mould cast Al-7Si-0.3Mg-0.8Fe alloy with Mn (0.3%) + Sr (0.04%) addition	124
5.15	EDS elemental X-ray mapping and elemental distribution of Chinese script Mn-Fe phase in Al-7Si-0.3Mg-0.8Fe alloy with Be (0.15%) + Mn (0.15%)	125
5.16	Typical microstructures of Al-7Si-0.3Mg-0.8Fe alloy in T6 condition (a) without and (b) with 0.4% Mn	126
5.17	Typical microstructures of Al-7Si-0.3Mg-0.8Fe alloy in T6 condition with (a) 0.2% Be and (b) 0.04% Sr	127
5.18	(a) Cooling curve and its first derivative and (b) microstructures of Al-7Si-0.3Mg-0.8Fe alloy thermal analysis sample	129
5.19	(a) Cooling curve and its first derivative and (b) microstructures of Al-7Si- 0.3Mg-0.8Fe-0.2Be alloy thermal analysis sample	130
5.20	(a) Cooling curve and its first derivative and (b) microstructures of Al-7Si-0.3Mg-0.8Fe-0.4Mn alloy thermal analysis sample	131
5.21	(a) Cooling curve and its first derivative and (b) microstructure of Al-7Si-0.3Mg-0.8Fe-0.04Ca alloy thermal analysis sample (arrows show $\beta$ -Fe intermetallic phase)	132
5.22	(a) Cooling curve and its first derivative and (b) microstructure of Al-7Si- 0.3Mg-0.8Fe-0.04Sr alloy thermal analysis sample (arrows show $\beta$ -Fe intermetallic phase)	133

5.23	DTA curves of Al-7Si-0.3Mg-0.8Fe alloy (a) Heating and (b) Cooling at 2° K/min.	135
5.24	DTA curves of Al-7Si-0.3Mg-0.8Fe alloy with 0.2% Be addition (a) Heating and (b) Cooling at 2° K/min.	136
5.25	DTA curve of Al-7Si-0.3Mg-0.6Fe alloy with 0.5% Mn addition (a) Heating and (b) Cooling at 2° K/min.	137
5.26	Effect of Ca, Mn and Ca+Mn additions on the (a) UTS and (b) % elongation of Al-7Si-0.3Mg-0.6Fe alloy cast in permanent mould	140
5.27	Effect of Ca, Be and Ca+Be additions on the (a) UTS and (b) % elongation of Al-7Si- 0.3Mg- 1.0Fe alloy cast in permanent mould	141
5.28	Effect of Be, Mn, Sr and Ca individually and in combination on the (a) UTS and (b) % elongation of Al-7Si-0.3Mg-0.8Fe alloy	143
5.29	Effect of Ca, Mn and Ca+Mn additions on the impact strength of Al-7Si-0.3Mg-0.6Fe alloy	144
5.30	Fractographs of impact tested Al-7Si- 0.3Mg- 0.6Fe alloy (a) without and with (b) 0.05% Ca (c) 0.3% Mn and (d) 0.3% Mn+0.05% Ca	146
5.31	Effect of Be, Mn, Sr and Ca individually and in combination on the impact strength of Al-7Si-0.3Mg-0.8Fe alloy	147

---

---

# CHAPTER 1

## INTRODUCTION

---

---

Aluminium is one of the most abundant metals available in the earth's crust as bauxite with wide range of applications in the modern world. There are many reasons for aluminum's continued expansion into newer and wider fields of application. Light weight, excellent specific strength, high thermal and electrical conductivities, high reflectivity, good corrosion resistance, excellent workability, and attractive appearance are some of aluminum's most appealing properties. However, its relatively low strength and poor castability limit its use largely to the production of rotor castings for electrical motors and other applications in which high electrical conductivity is required.<sup>1</sup> Properties of Al are usually enhanced by the addition of major alloying elements such as Cu, Si, Mg, Mn, Zn, Li, Ni and then subjecting the alloys to various thermal, mechanical and thermomechanical treatments. Some of the minor alloying elements added to aluminium are Na, Sr, Sb, Ba and Ca to induce specific changes in the microstructure.<sup>2</sup> Al alloys are available in both cast and wrought forms and about 20% of aluminium produced is used in the cast form mainly in the transport sector.

Figure 1.1 shows the major applications of aluminium. The metal makes a key contribution to fuel-efficient engines in cars and trucks as well as to high speed rail and sea travel. By reducing the vehicles weight, it cuts down on fuel consumption and emissions without compromising the size or the safety of the vehicles. Aluminium facilitates the construction of corrosion-resistant and low maintenance buildings. Around the world, most long distance overhead transmission and distribution lines are made of aluminium. Aluminium in packaging preserves food quality, reduces waste and provides convenience for the users. Aluminium can be rolled into ultra-thin foils, which are light, and strong, have unique barrier and insulation qualities and preserve food, cosmetics and pharmaceutical products by protecting them from ultra-violet light, odours and bacteria.<sup>3</sup>

## 1.1 IMPORTANCE OF Al-Si ALLOYS

Among commercial aluminium casting alloys, those with silicon as the major alloying element are the most important ones mainly because of their excellent casting characteristics. Addition of Si to pure aluminium imparts high fluidity, good feeding characteristics, low shrinkage and good hot cracking resistance. The high strength to weight ratio is one of their most interesting characteristics.<sup>4</sup> While the volume of most metals (including Al) shrinks substantially on solidification, two-phase Al-Si alloys contract relatively less. These are the only Al alloys that are not prone to hot-tearing during solidification. Aluminium has a density of only 2.7 g/cc, approximately one third of steel, copper or brass. As the density of silicon is 2.3 g/cc, it is one of the few elements which may be added to aluminium without loss of weight advantage. For a specific application, the selection of an alloy depends on its castability, the casting process, the required mechanical and physical properties and the end use of the casting. The properties of Al-Si alloys make them very popular in various applications including the automotive, aerospace and defense industries. Over the years, these Al-Si alloys have been specially developed to meet the increasing demands of today's industry, which has resulted in the production of smaller, light-weight components to comply with property, environmental and other specifications. Further, the desirable mechanical properties in these alloys can be obtained by controlling chemical composition and process parameters during melting, casting and heat treatment.<sup>5, 6</sup> By weight, 90% of all shaped Al castings are made from Al-Si-based alloys.

## 1.2 Al-Si ALLOY SYSTEM

Al-Si binary alloy is a eutectic system with the eutectic composition at 12.6 wt.% Si and eutectic temperature at 850 K (Figure 1.2).<sup>7, 8</sup> The two phases in equilibrium will be  $\alpha$ - solid solution (solid solution of Si in Al) and pure Si. The solid solubility of Si in Al at 850 K is 1.65%. Rapid quenching from the liquid raises the solubility up to 16% Si and shifts the eutectic point up to 17% Si.<sup>8</sup> Silicon reduces the thermal expansion coefficient, increases corrosion and wear resistance and improves casting and machining characteristics of the alloy. When the Al-Si alloy solidifies, the primary aluminum forms and grows in dendrites or silicon phase forms and grows in angular primary particles. When the eutectic point is reached, the eutectic Al-Si

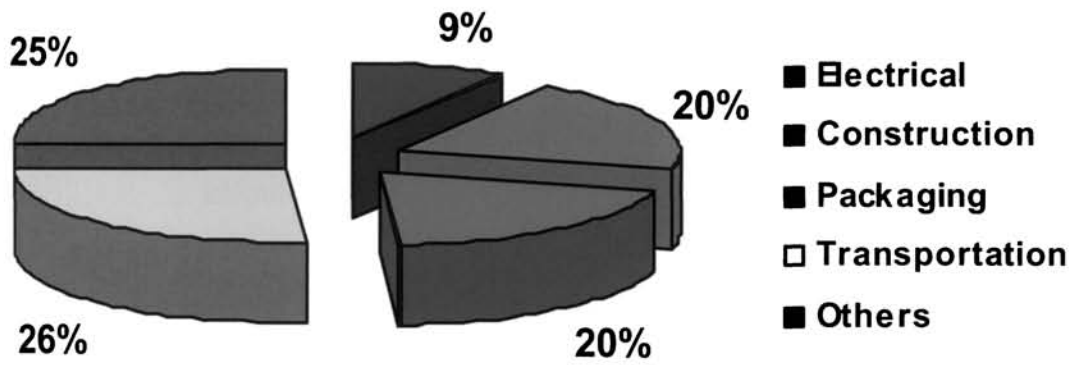


Figure 1.1: Aluminium's Major Applications

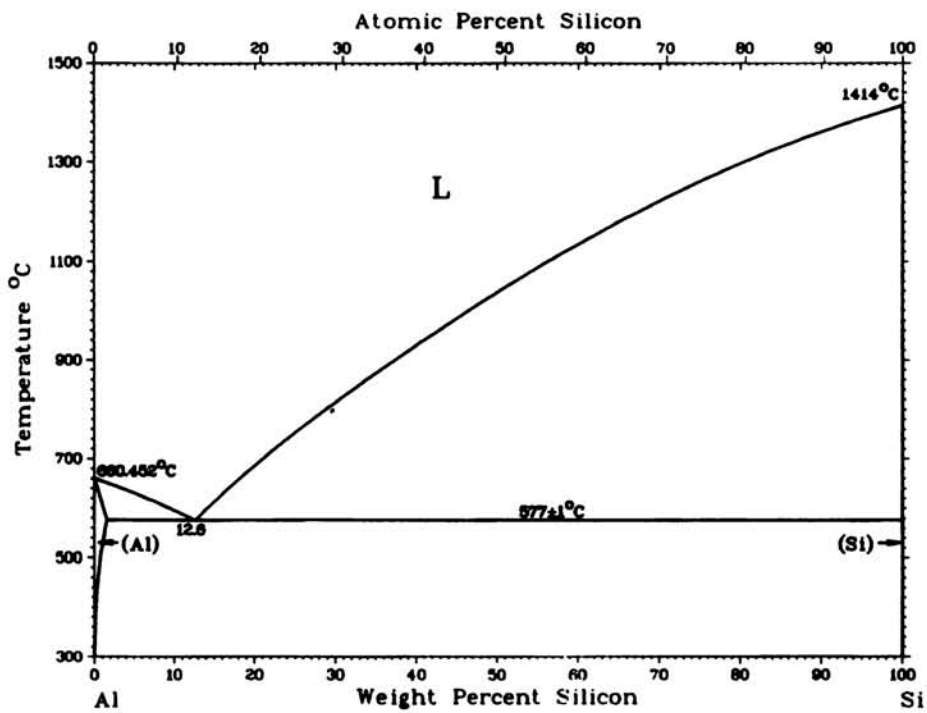


Figure 1.2: Al-Si alloy phase diagram<sup>7</sup>

phases nucleate and grow until the end of solidification. The alloys to the left of the eutectic composition are referred to as hypoeutectic alloys and those to the right as hypereutectic alloys. At room temperature, hypoeutectic alloys consist of a soft and ductile primary aluminium phase and a hard and brittle eutectic silicon phase. Hypereutectic alloy usually contains coarse, primary silicon cuboids as well as angular eutectic silicon phase.

In hypoeutectic alloys, the silicon varies between 5.5 and 10.5%, and primary aluminium is the first phase to solidify. The microstructure consists of primary aluminium dendrites within a eutectic matrix. Eutectic alloys contain 10.5 to 12.5% silicon and have microstructures consisting mainly of aluminium - silicon eutectic. In hypereutectic alloys containing more than 12.6% silicon, the first phase to solidify is silicon, the primary phase. These alloys having a distribution of coarse silicon cuboids provide excellent wear resistance. Although binary Al-Si alloys show excellent casting characteristics, the addition of Mg, Cu and Zn makes the alloys heat-treatable,<sup>9, 10</sup> providing the means to enhance their properties with the use of appropriate heat treatments. Magnesium contents are typically less than about 0.75%, because increased additions impair fluidity and feeding. The most common aluminium casting alloys in the Al-Si-Mg family is Al-7Si-0.3Mg (356) and Al-7Si-0.5Mg (357). The mechanical properties of an Al-Si cast alloy are mainly determined by its cast structure and the microstructural characteristics such as the grain size, dendrite arm spacing (DAS), the size, shape and distribution of the eutectic Si particles, as well as the morphologies and amounts of intermetallic phases present.<sup>11,12</sup> Table 1.1 lists the composition and mechanical properties of some of the common Al-Si casting alloys. Al-7Si-0.3Mg [LM25 (*UK standard*)/356 (*USA standard*)] alloy is perhaps the most widely specified Al-Si-Mg casting alloy for sand and permanent mold castings.

### **1.3 RECYCLING OF ALUMINIUM AND ITS ALLOYS**

Aluminium has been recycled since its first commercial production and today recycled aluminium accounts for one-third of global aluminium consumption.

**Table 1.1: Common Al-Si alloys and their mechanical properties**

<b>Alloy</b>	<b>Composition</b>	<b>Mechanical Properties</b>			
		<b>Ultimate Tensile Strength (MPa)</b>	<b>Modulus (GPa)</b>	<b>Elongation (%)</b>	<b>Hardness (BHN)</b>
<b>356 (T6)</b>	Al-7Si-0.3Mg	300	71	3	105
<b>357 (T6)</b>	Al-7Si-0.57Mg	365	71	5	100
<b>319 (T6)</b>	Al-6.5Si-4.5Cu	276	71	3	95
<b>413</b>	Al-12Si	200	71	13	60
<b>A390 (T6)</b>	Al-17Si-4.5Cu	310	71	1	145

Anything made of aluminium can be recycled repeatedly; not only cans, but also aluminium foil, plates, window frames, garden furniture and automotive components can be melted down and re-used. Aluminium is a sustainable material, whose recyclability and applications justify the high energy requirement of primary aluminium production. The transport sector is forecast to be the most rapidly expanding end-use sector due to the lightweight and energy saving qualities of the material. During an automobile's construction a kilogram of aluminium can replace two kilograms of conventional heavier materials, thus contributing to the reduction of the vehicle's weight and therefore its fuel consumption. This means that, over the vehicle's lifetime, every kilogram of aluminium used saves an equivalent of twenty kilograms of CO<sub>2</sub>.<sup>13</sup> Current estimates<sup>14</sup> show that globally there will be, by the year 2020, a 35% increase of CO<sub>2</sub> emissions from all vehicles. An increased use of aluminium would reduce this increase down to 28% and thus help towards making the transportation sector more sustainable.

Recently, appeal for recycling of resources is becoming more and more intensive with increasing public awareness on environmental issues. Climate change is particularly important to the aluminium industry worldwide because of (i) the relatively high energy consumption and greenhouse gas emissions associated with the production of primary aluminium and (ii) the significant potential to reduce greenhouse gas emissions through increased use of aluminium in transportation applications and recycled aluminium.

Recycling of aluminium brings potential energy savings of up to 95% and produces 99% less emission than primary aluminium production from ores. The metal can also be recycled indefinitely, as reprocessing does not damage its structure.<sup>13</sup> Therefore, secondary aluminium and alloys are getting wide acceptance world-wide. The efficiency of aluminium recycling translates into high recycling rates for the various applications. The lightness of aluminium products contributes to fuel savings and reductions in emissions. Recycling rates for building and transport applications range from 60-90 per cent in various countries.

The aluminium industry is working with the automobile manufacturers to enable easier dismantling of aluminium components from cars in order to improve the sorting and recovery of aluminium. During recycling, most of the parts are mixed together regardless of their chemical composition, as sorting of the parts may not be commercially viable. Efforts are then made to correct the composition of the resulting alloy on line. This practice also has economic limitations. Furthermore, certain elements are either difficult and /or expensive to remove (e.g. iron and magnesium). Iron is always present in commercial aluminium alloys and has consistently emerged as the main impurity element and perhaps the most detrimental to the mechanical properties of these alloys. Hence, the increasing use of recycled aluminum casting alloys raises the necessity for strict process control to remove the ill effects of impurity elements.

---

---

## CHAPTER 2

### LITERATURE REVIEW

---

---

#### 2.1 INTRODUCTION

The popularity of Al-Si casting alloys results in a continuing increase in their demand for components with higher and consistent mechanical properties.<sup>15</sup> Al-7Si-0.3Mg alloy finds widespread applications in automotive, aerospace and general engineering industries due to its excellent combination of properties such as good fluidity, low coefficient of thermal expansion, high strength-to-weight ratio and good corrosion resistance.<sup>5</sup> These foundry alloys possess excellent tensile and fatigue properties and good corrosion resistance.<sup>16</sup>

#### 2.2 PARAMETERS INFLUENCING THE STRUCTURE AND PROPERTIES OF Al-Si-Mg CAST ALLOYS

The physical and mechanical properties attainable in these alloys are strongly influenced by the alloy composition, impurity elements, melt treatments, solidification characteristics, casting defects, and heat treatment.<sup>5</sup>

##### 2.2.1 Alloy Composition

Hypoeutectic alloys in the Al-Si-Mg system containing nominally 7% Si and about 0.25 to 0.7% Mg have widespread applications especially in the aerospace and automotive industries.

##### 2.2.1.1 Major alloying elements

Properties of Al are usually enhanced by the addition of major alloying elements such as Cu, Si, Mg, Mn, Zn, Li, Ni, and then subjecting the alloys to various thermal, mechanical and thermomechanical treatments.

The addition of Si imparts excellent castability and resistance to hot-tearing in these alloys. Further, since Si increases in volume during solidification, the susceptibility of the castings to shrinkage defects is reduced. Consequently, Al-Si alloys are ideally suited for high volume production in the aluminium foundry. Both Yield Strength (YS) and Ultimate Tensile Strength (UTS) increase with Si addition to aluminium up to 7% while ductility decreases. At silicon contents greater than 7%, the rate of increase in strength properties decreases significantly. Tsukuda et al<sup>17</sup> report that elongation and Charpy impact values of Al-Si-0.15Sb alloys decrease rapidly at Si contents greater than about 6%. On the other hand, Harris et al<sup>18</sup> have observed that small variation of Si content within the specification range of Al-7Si-0.3Mg alloy does not have any significant effect on mechanical properties. However, the Si variation can influence the mechanical properties only when the Mg level is below 0.2% in the alloy. Moreover, it is conceivable that Si content towards the upper end of the composition range might yield a relatively more castable alloy.<sup>19</sup> Mechanical properties of cast Al-Si alloy components are determined largely by the shape, size and distribution of Si particles in the matrix, which is influenced by factors such as modification, solidification rate and solution temperature and time.

The presence of Mg in the alloy offers the ability to heat treat Al-Si castings to high strength levels. Mg combines with Si to form the age-hardening compound  $Mg_2Si$ . This compound, when precipitated from solid solution during heat treatment, is responsible for the improvement in mechanical strength. In the as-cast state, Mg is present as fairly large particles of  $Mg_2Si$  and hence has relatively little effect on the as-cast properties of the alloy. Since Si levels are well in excess of the amount required to react with Mg, the degree of strengthening is determined by Mg content.<sup>8, 20</sup>

### ***2.2.1.2 Trace alloying elements***

The role of trace elements in foundry metallurgy, although not fully understood is one of the most important tool available to the foundryman to manipulate the microstructure of the alloys. Trace elements can be beneficial, as well as detrimental to the structure and properties of the alloy. The trace elements may originate from a variety of sources during the processing of the ingot. First, the ingot may indeed inherit the trace elements from the primary ore. Second, additional trace

elements may be added to the aluminium in the reduction cell. A third source of trace elements is pick up from the use of master alloys and fluxes to grain refine, or modify and cleanse the alloy melt. The fourth source of trace elements would be through the use of recycled scrap or secondary ingot. The last source of trace elements would be the intentional addition of an element through fluxes or master alloys.<sup>21, 22</sup> These sources make it extremely difficult to eliminate trace elements in commercial practice.

The principal problem with trace elements is that their effects on the mechanical properties of the alloy are extremely significant even though only a few ppm of the element may be present. Most detrimental trace elements are surface active elements having a very low solubility in the primary aluminium phase. They may contribute to a change in the mechanical properties through several mechanisms. A trace element may (i) react with another trace element to form an intermetallic compound (ii) segregate during solidification to the grain boundaries causing grain boundary embrittlement (iii) get absorbed onto the surface of the primary crystallites causing a change in its growth and shape and (iv) react with a beneficial trace element to form an intermetallic compound removing the beneficial element from its role as a modifier or grain refiner.<sup>23</sup>

Additions of Na, Sr, Ca, Sb, Bi, Be, Mn, Cr, Mo, Co, Ti, B, Rare Earth elements etc have been found to have profound effect on the castability, structure and properties of Al-Si cast alloys.<sup>16</sup> Na, Sr, Sb, Ca and RE modify the coarse acicular morphology of eutectic Si into fine fibrous form thereby improving the mechanical properties of cast Al-Si alloys.<sup>24</sup> Ti, B and Zr lead to grain refinement and result in improved interdendritic feedability, and reduction of porosity and shrinkage defects.<sup>25</sup> Be, Cr, Mn, Co, Sr, Ca and RE change the morphology of platelet iron intermetallic compound to harmless shapes and hence improve the mechanical properties.<sup>26,27</sup> Sb, Bi and P, interacting with eutectic Si modifiers such as Na and Sr, coarsening the eutectic Si and degrading the properties, are to be removed from aluminum cast alloys containing modifiers.<sup>28,29</sup>

Calcium, once considered only as a deleterious element because of its degrading effect on the properties of aluminum alloys, is now being considered to be a

beneficial one in many ways. Calcium, entering the aluminum casting alloys along with the addition of silicon, and appearing as calcium silicides, calcium phosphides, and calcium nitrides, which are considered to be harmful, requires removal to levels below 0.003% (30 ppm) and preferably below 0.001% (10 ppm).<sup>30</sup> However, Ca introduced in the elemental form modifies the eutectic silicon in Al-Si alloys,<sup>31-38</sup> improves the fracture toughness and impact properties of high iron containing recycled aluminum alloys,<sup>27, 39-42</sup> scavenges the effect of Sb from secondary alloys,<sup>43, 44</sup> imparts superplastic properties,<sup>45-49</sup> and enables production of aluminum foams<sup>50-55</sup> and aluminum metal matrix composites.<sup>56-64</sup> Aluminum alloys containing Ca as an intentional alloying element are applied industrially in the form of sacrificial anodes, bearings, electrolytic capacitor cathode foils, packaging and others.<sup>65-86</sup> Based on the extensive literature collection, compilation and analysis, a review paper on “*The Role of Calcium in Aluminum Based Alloys and Composites*”<sup>87</sup> is published in International Materials Reviews, one among a few high impact factor journal in the area of Metallurgy and Materials from UK.

### 2.2.1.3 Al-7Si-0.3Mg alloy

Among the various Al-Si-Mg alloys, the LM25/356 alloy of composition Al-6.5-7.5Si-0.35-0.45Mg is the most widely used one. This alloy is used for investment, sand and permanent mould castings. The designations, physical and mechanical properties of this alloy are given in Tables 2.1, 2.2 and 2.3 respectively.

## 2.2.2 Solidification Characteristics

Generally, aluminium alloys solidify by either skin forming or pasty or mushy manner. The formation of an equiaxed dendritic structure is the normal mode of solidification for commercial Al-Si, Al-Si-Mg and Al-Si-Cu casting alloys. Proper understanding of the solidification behaviour of the alloy helps in overcoming the defects arising during solidification particularly the solidification shrinkage. The secondary dendrite arm spacing (SDAS) is the parameter used to describe the scale of equiaxed dendritic structures. Castings with fine scale SDAS typically display finer intermetallics, finer interdendritic porosity and limited segregation.<sup>88, 89</sup> The SDAS is mainly dependent on solidification rate and temperature gradient. However, it is also dependent on composition, to a lesser degree.<sup>90, 91</sup> It has been observed that addition of

Fe to 319 (Al-6.5Si-4Cu) alloy decreases the SDAS. The mechanism proposed to account for this is that  $\beta$ -Al<sub>5</sub>FeSi needles increase the nucleation rate of eutectic silicon and hence minimise dendrite arm coarsening at eutectic temperature.<sup>91</sup>

**Table 2.1: Various designations of Al-7Si-0.3Mg alloy**

Country	Designation
Great Britain	LM25
USA -Aluminium Association	356
Japan	AC4C
USSR	A19
Spain	L-2651

**Table 2.2: Physical properties of LM25 / Al-7Si-0.3Mg alloy**

Coefficient of Thermal Expansion (per°K at 293-373 K)	22 x 10 <sup>-6</sup>
Thermal conductivity (Wm <sup>-1</sup> K <sup>-1</sup> at 298 K)	151
Electrical conductivity (% copper standard at 293 K)	39
Density (g/cc)	2.68
Freezing range (°K) approx.	888-823

**Table 2.3: Mechanical properties of LM25/Al-7Si-0.3Mg alloy**

Mechanical Properties	LM25-M		LM25-TE		LM25-TB7		LM25-TF	
	Sand	Chill	Sand	Chill	Sand	Chill	Sand	Chill
0.2%Proof Stress (MPa)	80-100	80-100	120-150	130-200	80-110	90-110	200-250	220-260
Tensile Strength (MPa)	130-150	160-200	150-180	190-250	160	230	230-280	280-320
Elongation (%)	2	3	1	2	2.5	5	-	2
Brinell Hardness	55-65	55-65	70-75	75-95	65-75	65-75	90-110	90-110
Modulus of Elasticity (GPa)	71	71	71	71	71	71	71	71
Shear Strength (MPa)	-	-	140	-	-	-	180	250

**M-** As cast condition; **TE-** Precipitation treated condition; **TB7-** solution treated and stabilized condition; **TF-** fully heat treated condition.

### 2.2.3 Casting Defects and their Control

Porosity in cast aluminum and its alloys appears mainly in one of the two forms: (i) the pinhole pores due to the gas evolution and (ii) the shrinkage cavities due to the improper feeding during solidification. Many process and/or design factors, such as local thermal conditions,<sup>92</sup> feeding capability,<sup>93</sup> and applied pressure<sup>94</sup> are known to affect porosity formation. Metal related factors, including dissolved hydrogen,<sup>95</sup> inclusions,<sup>96, 97</sup> modifying elements<sup>98, 99</sup> and other minor elements additions<sup>100</sup> can also influence porosity formation. Cao and Campbell<sup>101</sup> have pointed out the influence of oxide films folded into the melt during pouring as being conducive to porosity formation. Neglecting pore formation due to entrapped air, which is a consequence of bad casting design and practice, the ease of pore formation can be described by the equation<sup>102</sup>,

$$P_g + P_s > P_{atm} + P_h + P_{s-l} \quad \dots\dots\dots (1)$$

Where,  $P_g$  is the equilibrium pressure of dissolved gases in the liquid,

$P_s$  is the pressure drop due to shrinkage,

$P_{atm}$  is the pressure of the atmosphere over the system

$P_h$  is the pressure due to the metallostatic head and

$P_{s-l}$  is the pressure due to surface tension at the pore-liquid interface.

Since the parameters  $P_h$  and  $P_{atm}$  are constant for a given casting, the dissolved gas pressure,  $P_g$ , is a major driving force in microporosity formation. Shrinkage porosity pressure,  $P_s$ , which is directly related to the ease of interdendritic feeding is not easy to control. The remaining parameter in equation (1) is  $P_{s-l}$ , the surface tension effect. Alloying additions to aluminium may decrease or have virtually no influence on surface tension. Figure 2.1 shows the effect of alloying elements on the surface tension of 99.99 Al obtained by the capillary method at 973 to 1013 K in argon atmosphere. It is seen that Bi, Ca, Li, Mg, Pb, Sb and Sn substantially reduce the surface tension of 99.99 Al, whereas Ag, Cu, Fe, Ge, Mn, Si and Zn have little effect.<sup>103</sup> Velasco et al<sup>104</sup> have reported that calcium addition exerts a strong influence on reducing the surface tension in liquid aluminium, and it is expected to have an effect on porosity.

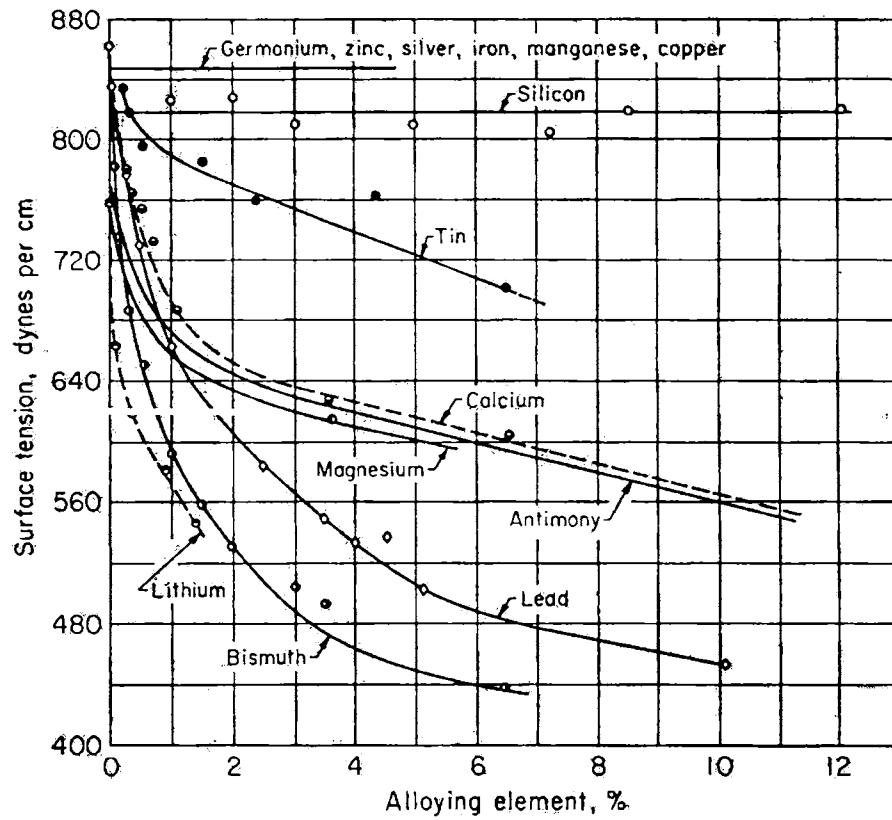
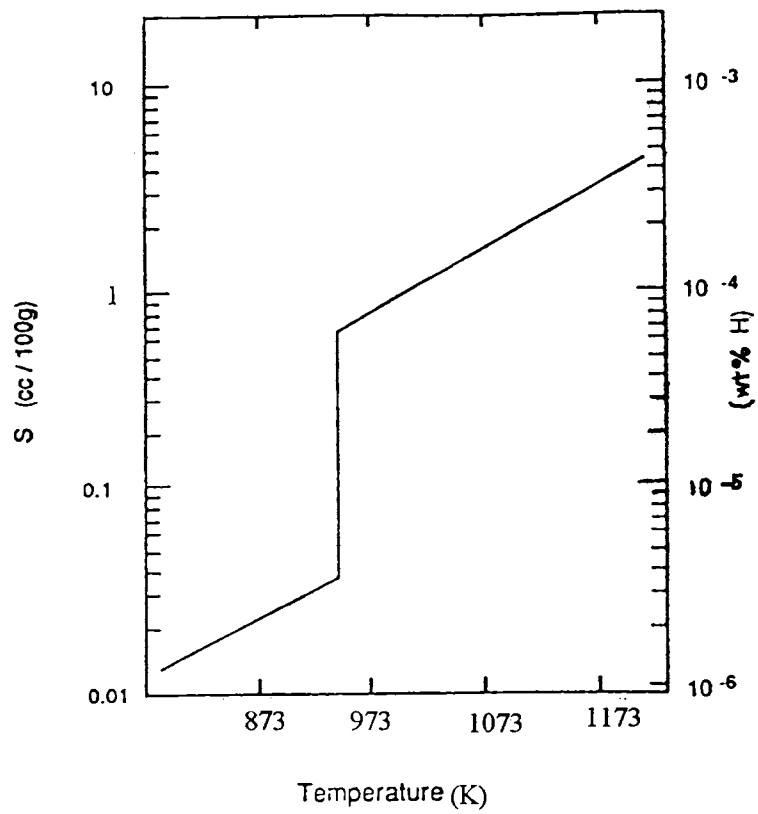


Figure 2.1: Effect of alloying elements on the surface tension of 99.99 aluminium at 973 to 1013 K in argon atmosphere (Courtesy: Van Horn<sup>103</sup>)

Dahle et al<sup>105, 106</sup> have proposed a new theory to understand the porosity formation in Al-Si alloys, which states that the nucleation and growth characteristics of the eutectic must be considered for a thorough understanding of porosity formation because of its 40-100% volume fraction in common casting alloys, and the last solidifying characteristic/nature. The three different eutectic solidification modes theoretically expected in Al-Si alloys are (i) nucleation on/adjacent to the primary phase (ii) independent nucleation in spaces between primary grains and (iii) solidification opposite to the thermal gradient. The operating mode will control the distribution of the remaining liquid at the critical high fraction solid stages of solidification, where feeding is more difficult. The resulting liquid distribution will determine the size, shape, length and connectivity of the feeding channels.

### 2.2.3.1 Gas porosity

Hydrogen is the main gas, which is appreciably soluble in aluminium and its alloys. The presence of dissolved hydrogen in melts of aluminium and aluminium-based alloys is a well known foundry problem.<sup>107, 108</sup> The problem derives from the difference in the solubility of the hydrogen gas between liquid and solid aluminium. This leads to the rejection of almost all of the dissolved hydrogen on the solidification of liquid aluminium and the formation of hydrogen bubbles which ultimately cause porosity in castings and ingots and blisters on sheets and plate.<sup>109-114</sup> Figure 2.2 showing the solubility of hydrogen at one atmospheric pressure in pure aluminium<sup>115</sup> reveals three distinct characteristics viz., a low solubility in solid aluminium, a large change in its solubility at the melting point and a strong temperature dependence in the liquid state. It has been shown that<sup>114</sup> for any given alloy and solidification condition, there is a “threshold hydrogen content” below which no porosity is formed. However, Fang and Granger<sup>108</sup> have indicated that there exists some finite pore volume fraction even at low hydrogen contents. A re-look of the “threshold hydrogen content” has shown that the threshold values increase with cooling rate. Gas porosity has a negative effect, not only on mechanical properties but also on machinability and surface properties of aluminium castings.<sup>99, 108, 116-119</sup>



**Figure 2.2: The solubility of hydrogen at one atmosphere pressure in pure aluminium (Courtesy: Gruzleski and Closset<sup>115</sup>)**

It has been reported that increasing amounts of group IA and IIA elements tend to enhance hydrogen absorption, perhaps because of their tendency for disruption of the protective oxide skin. The use of eutectic silicon modifiers such as Na, Sr, Ca and Li has been observed to cause increase in apparent porosity in a variety of Al-Si based alloy castings.<sup>4</sup> It has been observed that porosity and shrinkage in cast Al-Si alloys are influenced by the formation of the intermetallic compounds.<sup>8, 120</sup> Some foundrymen have claimed that Sr contributes to hydrogen pick up, while others have stated that there is no appreciable gas pick up.<sup>109, 121</sup> Denton and Spittle<sup>121</sup> have studied the effect of Sr (0.04%) addition on the hydrogen absorption by molten LM6 (Al-12Si) alloy. It has been observed that Sr enhances the susceptibility of the alloys to hydrogen pick-up, the hydrogen concentration reaching a plateau during a one hour hold period. Gruzleski et al<sup>109</sup> have measured the hydrogen content of non degassed A356 melt at 983 K before and after the addition of 0.03% Sr to the melt for specific periods of time. No increase in dissolved hydrogen has been found after Sr modification. Baliktay and Honer<sup>38</sup> and Hiroshi and Yoji<sup>122</sup> have observed that calcium increases the hydrogen solubility in aluminium melt as a result of its reaction with moisture in the atmosphere, and hence is often responsible for the casting porosity.

Fakhman et al<sup>123</sup> have noticed increased porosity and gas content with the presence of small amounts of Na, Li and Ca. It has also been observed that addition of calcium has caused significant increase in the casting porosity and an associated reduction in casting density.<sup>124-127</sup> It is a matter of debate whether there is actually an increase in the absolute level of porosity into a more readily observable form. Honer and Zhang<sup>128</sup> have observed that even very low concentrations of Ca give rise to porosity as a result of higher hydrogen pick-up in G-AlSi12 aluminum casting alloy. The oxidation of Ca changes the composition and morphology of the protective oxide skin of the melt, which obviously contributes to a faster pick-up of hydrogen in the melt towards the point of equilibrium.

Velasco et al<sup>104</sup> studying the influence of Ca on microporosity in A319 (Al-6.5Si-4Cu) alloy with Sr modification and titanium refinement have found that the addition of Ca (above 90 ppm) has resulted in an additive effect on Sr modification and reduction in the quantity and size of the pores. In Al-Mg alloys containing 2.5, 5.0 and

10% Mg, it has been reported that calcium addition has reduced the gas content of the alloys.<sup>129</sup>

Investigations on the effect of Ba, Ca, Y and Yb additions on the porosity formation based on their impact on the eutectic solidification mode have shown that these elements increase the porosity level with increasing amount compared to the untreated alloy. However, increasing Ca content reduces and disperses hot tearing as well as causes the eutectic to evolve from the surface of the casting towards the centre of the hot spot resulting in concentrated porosity closer to the hot spot.<sup>130</sup> Tatur test results for Al-11.4Si alloy have shown more dispersed shrinkage porosity with 0.0064% (64 ppm) calcium addition compared to more localized ones in the last solidification area with calcium-free alloy.<sup>131</sup> It is obvious from the foregoing that no consensus exists among the researchers regarding the increase in hydrogen absorption tendency by aluminum melt containing modifiers.

### 2.2.3.2 *Shrinkage porosity*

Shrinkage porosity occurs in regions within the casting, which solidify last, particularly where isolated liquid pools become cut off from feed liquid by either fully solidified metal or partially solidified impermeable dendritic networks. Contraction during solidification leads to microshrinkage particularly in interdendritic areas. Both gas and microshrinkage porosities occur often simultaneously.<sup>4</sup> Calcium concentrations between 0.05-0.1% (500 – 1000 ppm) have increased both gas porosity and shrinkage porosity of the AL2 [Al-12Si-0.6Cu] alloy as well as the tendency of eutectic alloys in forming shrinkage cracks.<sup>132</sup> Holecek<sup>133</sup> has found that the hot tearing tendency is little affected by calcium content in Al-Si alloys, but its effect on shrinkage cavity formation is considerable. However, calcium content above 0.003% (30 ppm) has unfavourably influenced the dissipation of internal shrinkage during solidification of an aluminium alloy containing 12-13% Si.<sup>134</sup> On the other hand, the work of Abdollahi and Gruzleski<sup>135</sup> on Ca addition to A357 alloy reveals no significant increase in melt hydrogen but increased microporosity with a corresponding decrease in macroporosity. This is in agreement with the work of Dahle et al<sup>105, 106</sup> and Knuutinen et al.<sup>130</sup>

Iron is known to cause porosity and shrinkage defects in Al-Si based casting alloys.<sup>136</sup> It has been suggested<sup>137-140</sup> that the intermetallic phase  $\beta$ -Al<sub>5</sub>FeSi is the primary cause of this porosity. The restricted feeding theory suggests that  $\beta$  platelets interfere with liquid feeding, whereas the “pore nucleation theory” suggests that the  $\beta$ -platelets are active sites for pore nucleation. In Al-Si based foundry alloys, Rooy<sup>141</sup>,<sup>142</sup> claims that increase in Fe content leads to reductions in fluidity, poorer feeding characteristics and increased shrinkage cavity formation. Iwahori et al<sup>138</sup> have noted that in a AC2B alloy, increased Fe levels have led to increased shrinkage porosity. Anantha Narayanan et al<sup>143</sup> have confirmed a similar trend between iron level and shrinkage porosity in 319 alloy. Eklund,<sup>139</sup> comparing primary and secondary alloys of various Al-Si compositions, also claims that porosity has been observed to increase as the proportion of Fe containing phases increases in these alloys.

## **2.2.4 Melt Treatments**

Three melt treatment processes commonly employed in the production of aluminium castings to control the porosity level and the microstructure and hence enhance the mechanical properties are degassing modification and grain refinement.

### **2.2.4.1 Degassing**

Virtually gas porosity observed in aluminium castings is attributable to hydrogen. The solubility limit of hydrogen in molten aluminium is 0.68ml/100g about 20 times greater than that in solid aluminium (0.037ml/100g) at the melting point. As solidification progresses, hydrogen is rejected at the solid-liquid interface forming hydrogen gas bubbles. If these bubbles cannot escape, porosity will be present in the solidified casting. Since the precipitation of hydrogen during the solidification process is inevitable, the only effective means to limit gas porosity is to reduce the hydrogen content of the molten metal.<sup>111, 144</sup> Reduction of hydrogen level is extremely important for critical component castings. In order to obtain sound castings with a minimum of porosity, it is necessary to decrease the hydrogen levels in the order of 0.10ml/100 g of aluminium before casting. The use and the mode of degassing will depend on the level of hydrogen desired. Among the many methods in use to reduce hydrogen levels, the most common methods are natural degassing, gas purging, vacuum degassing and treatment with a flux/tablet. Inert gases or mixtures of inert gases and reactive gases are

injected via a lance usually made of graphite or silicon carbide. Various lance designs including open-end, perforated end and porous plug head are available to achieve degassing. Recently, lances with rotary impellers or spinning heads have increased the degassing efficiency by a factor of 5 to 10.

#### **2.2.4.2 Modification**

In the Al-Si system, silicon is a non-metal with directed covalent bonds; therefore, it tends to grow anisotropically into faceted crystals and hence requires more undercooling for its growth than the isotropic aluminium phase. Consequently, the coupled region in the Al-Si system is asymmetric.<sup>145</sup> The morphology of eutectic silicon is the predominant factor determining the mechanical properties. The silicon particles in the aluminium rich matrix generally grow in the form of coarse platelets and act as crack initiation sites because of their stress concentration effect<sup>146, 147</sup> resulting in poor mechanical properties. When Si freezes out from an Al-Si melt, it grows as flakes with atomically flat, (111)Si-oriented surfaces. These flakes grow by nucleation of mono-atomic ledges on the (111) surfaces, which subsequently migrate rapidly over the surface by incorporating further atoms at the ledge. This common growth process via ledge migration is schematically shown in Figure 2.3.

In silicon, twins form readily across the (111) planes and this has the effect of producing a self-perpetuating groove of 141 degrees at the solid liquid interface. In the growth of Si flakes from an Al-Si melt, however, the growth takes place near the thermodynamic equilibrium. Therefore, the density of these planar defects is usually rather low. Consequently, the flakes cannot “branch,” which results in a microstructure in which the Si particles are large plates.

The process of changing morphology of platelet/acicular Si to a fine fibrous form is known as modification, which results in considerable improvement in the mechanical properties. The modification of the eutectic Si can be achieved through rapid rates of solidification and by the addition of modifying agents (modifiers) to the melt. Full modification is difficult to achieve by only increasing the solidification cooling rate of the casting, which has varying section thickness and hence different cooling rates. It is therefore essential to modify the eutectic structure by introducing

modifying agents. One possible explanation for the modification is that when a modifying element of correct atomic size (Figure 2.4) with respect to Si ( $r_{\text{modifier}} : r_{\text{silicon}} = 1.646$ ) is incorporated into the melt, the accumulation of such atoms in sufficient density by adsorption at the liquid-solid growth front poisons the growth of silicon in a particular direction (Figure 2.5). This phenomenon has been named impurity-induced twinning and is supported by the observation that the modifier becomes concentrated in the Si and not in the aluminium phase. It has been observed that modified fibres contain orders of magnitude more twins than do unmodified Si plates and that the surface of the fibres is microfacted and rough as a consequence of the intersection of myriads of twin planes with it. Si fibres are crystallographically imperfect and each surface imperfection is a potential site for branching to occur. As a result, fibres in the chemically modified eutectic are able to bend, curve and split to create a fine microstructure; the platelets of the unmodified structure are inhibited by their relative crystallographic perfection and can do little except forming in a coarse acicular fashion.<sup>24, 115</sup>

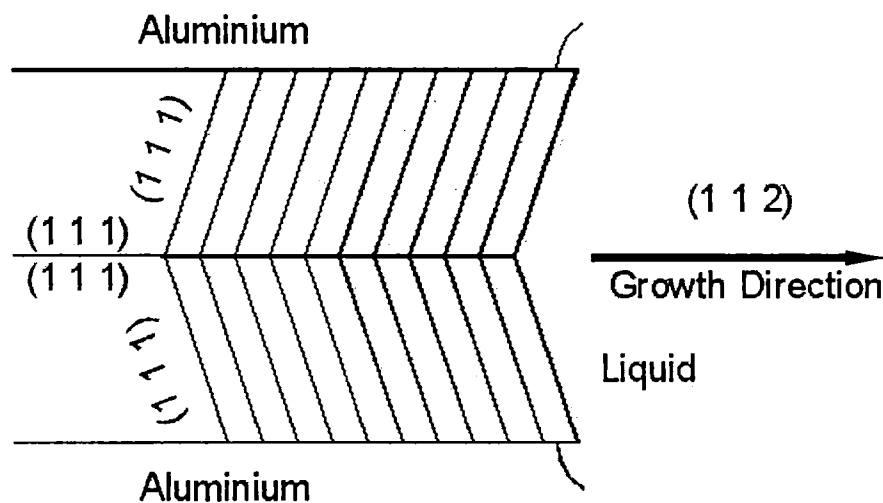


**Figure 2.3: Ledge migration mechanism responsible for the growth of Si flakes bounded by atomically flat (111) surfaces**

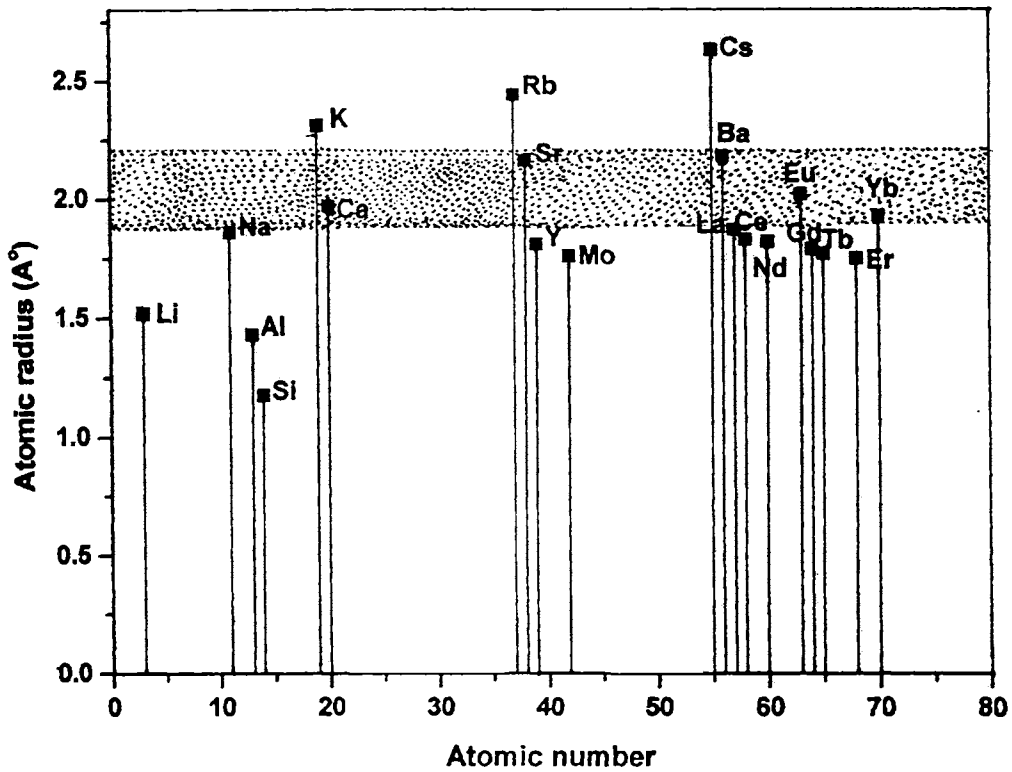


Figure 2.4: Plot of atomic radii vs atomic number, with range of radii which includes elements capable of producing silicon modification – shaded

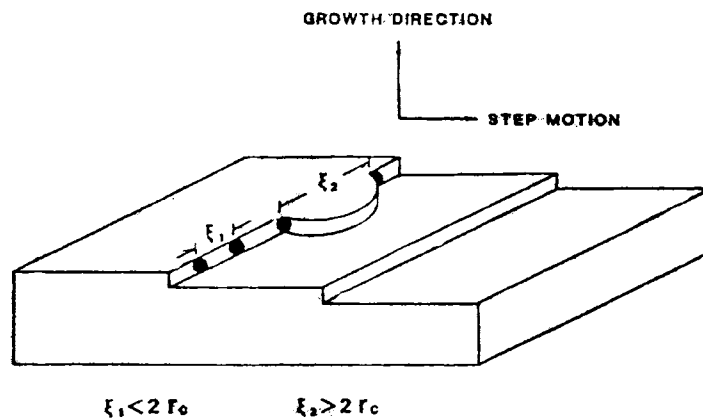


Figure 2.5: Schematic representation of impurity atoms pinning the steps of a silicon crystal growing by the layer growth mechanism at the solid/liquid interface<sup>24</sup>

Although the group IA and IIA elements of the periodic table, rare earths (La, Ce or mischmetal), As, Sb, Se, and Cd have been reported to modify the Al-Si eutectic, only Na and Sr find extensive commercial application.<sup>148-155</sup> The works of Hogan and Shamsuzzoha<sup>156, 157</sup> and Lu and Hellawell<sup>24</sup> have shown the importance of twinning in the growth of silicon and that modified silicon contains more twins and has a rough microfaceted surface. They have shown that impurity atoms of the appropriate size can force the nucleation of twins and stacking faults at the solid-liquid (Si-metal) interface. These twins create sites for atom attachment at the interface, encouraging growth in a manner similar to that of an atomically rough interface. As a consequence, the morphology of the Si particles changes from flakes to fibers. The primary Al dendrites do not exhibit shape modification.

It has been concluded that the nucleation of the silicon controls the solidification of the eutectic, whose subsequent growth is led by silicon having the smallest constitutional undercooling. However, today, the change in growth mechanism has been accepted as the reason for Si morphology change with the addition of modifiers. Several studies<sup>105, 158-160</sup> have recently shown that widely different eutectic solidification modes can occur in hypoeutectic Al-Si alloys as a result of the addition of modifying elements. The three different eutectic solidification modes theoretically expected in Al-Si alloys are (i) nucleation on/adjacent to the primary phase (ii) independent nucleation in spaces between primary grains and (iii) solidification opposite to the thermal gradient. The operating mode will control the distribution of the remaining liquid at the critical high fraction solid stage of solidification, where feeding is more difficult. The resulting liquid distribution will determine the size, shape, length and connectivity of the feeding channels. Moreover, it has been found that it is possible for all these mechanisms to occur in Al-Si alloys, either independently or combined, based on the alloy and presence of certain elements, namely Na, Sr, Ca and their levels. A comparison of some characteristics of different modifiers<sup>25, 115, 161, 162</sup> is given in the Table 2.4.

Table 2.4: Characteristics of elements used as eutectic silicon modifiers in Al-Si alloys<sup>41, 61, 68, 69</sup>

Modifier	-ΔG oxide at 1000K, (KJ/mol)	Optimum amount, %	Incubation period, hrs	Twin Spacing	Recovery	Fading	Remarks
Na AR(A°)=1.58 M.P(K)=374 V.P(Pa)=20,265.0	367	0.01	Exists	564	Poor, 20 to 30 %	Rapid fading	i) Difficulty to store and handle ii) Difficulty in controlling additions can lead to over modification iii) Increases porosity
Sr AR(A°)=1.84 M.P(K)=1042 V.P(Pa)=101.325	480	0.01 to 0.02	1-2	30	High, about 90%	More slowly than Na	i) Much easier to store and handle as master alloy ii) Semi permanent effect iii) Overmodification not as serious as with Na (iv) Increases porosity more than Na
Sb AR(A°)=1.45 M.P(K)=904 V.P(Pa)=7,447.39	-	0.10 to 0.15	Not known	NA	55 %	No fading	i) Forms poisonous SbH <sub>2</sub> with hydrogen ii) Unaffected by holding time iii) Fully modified structure can never be achieved
Ca AR(A°)=1.68 M.P(K)=1112 V.P(Pa)=26.3445	509	0.004	NA	100	High, about 70%	Very slow	i) Much easier to store and handle as master alloy (ii) Over modification not as serious as with Na (iii) Fully modified structure can be achieved (iv) Adds hydrogen to the melt v) Increases porosity
Ce, AR(A°)=1.56 M.P(K)=1071	497	1.0	-	NA	50 %	Very slowly than Na	Not a strong modifier
La, AR(A°)=1.59 M.P(K)=1193	487	0.05-0.2	-	NA	-	Very slow	Not a strong modifier

AR- Atomic Radius Ratio; M.P.- Melting Point (K); V.P - Vapour Pressure at 1000 K (Pa); NA-Not Available

Although modification of the eutectic silicon in Al-Si alloys is commercially performed by Na and Sr addition, calcium also influences modification and is well recognized as a modifier. Several authors reporting the modification of Al-Si alloys by calcium have found that its effect persists through remelting.<sup>5, 31-38</sup> It has been reported that the calcium modified eutectic structure of an SAE332 alloy (Al-9.5Si-3.0Cu-1.0Mg) is maintained for about 13 hours at 938.6 K while the sodium modified eutectic structure is sustained only for about 3-4 hours.<sup>163</sup> Since the radius ratio for Ca is 1.68, which is close to the needed ratio of 1.646 for modification, Ca also modifies the eutectic silicon. Gokhshtein and Vasil'eva,<sup>164</sup> studying the mechanism of modification of silumins (Al-Si alloys) by Ca, Na and other elements, have found that the principal influence of Ca is to deactivate the impurity particles, which in unmodified silumin act as crystallization centres for eutectic Si. This is in line with the work of Belov et al.<sup>165</sup>

The eutectic solidification mode in A356.0 (Al-7Si-0.37Mg) alloy modified with Ba, Ca, Y and Yb additions has been determined by comparing the crystallographic orientation of the aluminium in the eutectic to the surrounding primary aluminium dendrites. It has been shown that each of the elements added promotes heterogeneous nucleation of eutectic grains in the interdendritic liquid, while the aluminium in the unmodified alloy grows epitaxially from the dendrites. Furthermore, Ca and Y have resulted in a strong dependency of eutectic solidification on the thermal gradient, i.e, the eutectic evolves from the walls towards the centre of the sample on a macro-scale.<sup>166</sup>

Tsumura<sup>167</sup> has found that addition of 0.05% (500 ppm) Ca modifies a eutectic Al-Si alloy (Al-11.59Si-0.21Fe-0.01Cu-0.006Na-0.009Ti) and results in maximum tensile strength and elongation [Table 2.5]. While the tensile strength is almost the same as the eutectic alloy modified with 0.02% Na, elongation is significantly (50%) lower. Further increase in calcium addition has resulted in decreased properties owing to the formation of CaSi<sub>2</sub>.

Baliktay and Honer<sup>38</sup> studying the effect of calcium on eutectic modification and porosity formation in G-ALSi10Mg alloy have observed (i) reduction of ~ 4° K in eutectic temperature with 150 ppm Ca containing alloy cast in graphite mould

(ii) initiation of eutectic modification with 35 ppm Ca containing alloy cast in Cu mould (iii) burning of Ca with holding time as per the first order rate equation and (iv) increase in porosity with increasing Ca content for a given holding time. Further, an increase in the microdefects has also been observed with Ca contents exceeding 30 ppm in Al-Si alloys cast in both sand and permanent moulds.

**Table 2.5: Mechanical Properties of Na and Ca added Silumin, (Eutectic Alloy Containing 11.59% Si) <sup>167</sup>**

Ca	Na	Tensile Strength (MPa)	Elongation (%)
-	0.01	155.8	6.3
-	0.02	199.9	13.4
0.01	-	166.6	5.7
0.02	-	176.4	6.8
0.03	-	184.2	7.0
0.05	-	197.0	8.9
0.10	-	179.3	7.6
0.20	-	151.9	3.5

Velasco et al<sup>104</sup> have studied the effect of Ca on the microstructure of a cast A319 (Al-6.5Si-4Cu) alloy and its interaction with that of conventional modifier, Sr. Image analysis and thermal analysis studies have indicated that Ca contributed to the reduction in the number of pores and enhancement in the modification effect of Sr.

Abdollahi and Gruzleski<sup>135</sup> have investigated the effect of Ca on modification rating, porosity and mechanical properties of A357 (Al-7Si-0.5Mg) alloy and compared with that of conventional modifiers. Metallographic observation and thermal analysis studies have revealed that the effect of Ca as a modifier is not as strong as that

of Na or Sr at low cooling rates but a fully modified structure is obtained at high cooling rates. Contrary to the results of Baliktay and Honer,<sup>38</sup> the above authors have observed that the recovery of Ca in the melt is high and does not fade with long holding times. Figure 2.6 presents the average microporosity and pipe volume (measure of macroporosity) in modified and unmodified Tatur samples. It is seen that modification treatment with either Sr or Ca increases microporosity, but the increase is greater in the case of calcium. However, modification decreases the pipe volume, with a greater decrease in the case of Ca than Sr. Further, Ca modification improves the mechanical properties especially elongation.

Sasaki and Yamada<sup>168</sup> have invented an Al-Si alloy having fine silicon crystals evenly distributed throughout the whole thickness of the casting with excellent mechanical characteristics and significantly reduced surface porosity. This alloy has been pressure cast after modifying with a flux containing at least one element selected from the group of Na, Sb, Sr, and /or Ca.

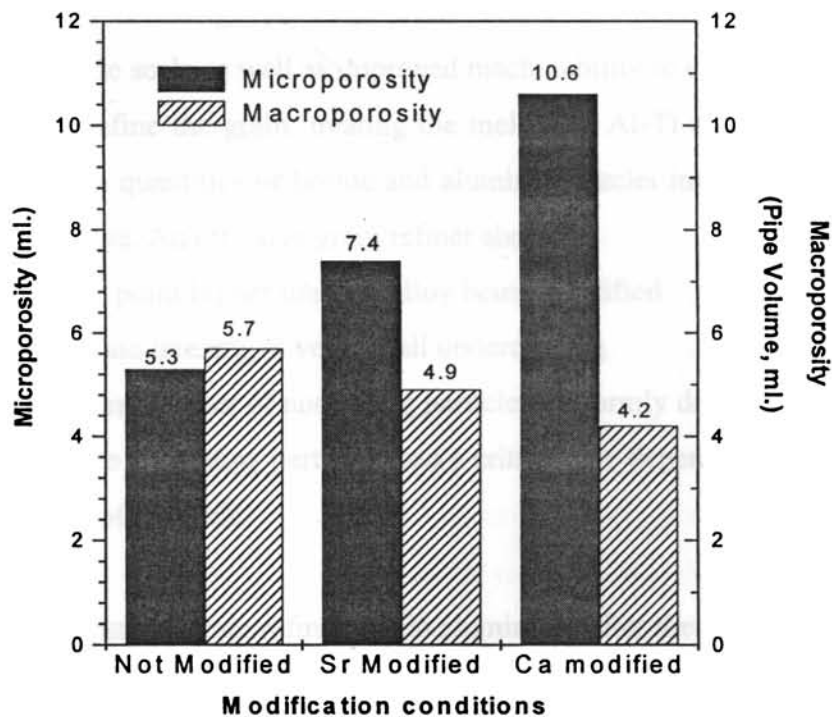


**Figure 2.6: Microporosity and macroporosity in modified and unmodified A357 alloy**

Knuutinen et al<sup>169</sup> investigating the modifying action of Ba, Ca, Y and Yb in Al-7Si-0.3Mg alloy have found that Ca modifies the eutectic silicon to fine, fibrous Si structure and the modification level increases with increasing level of Ca. Thermal analysis study has shown that with Ca addition (36 ppm), the eutectic arrest changes dramatically and further increase in Ca concentration has only a minor impact on the eutectic arrest in terms of nucleation temperature, growth temperature and recalescence.

#### **2.2.4.3 Grain refinement**

Grain refinement refers to the development of an increased number of sites for the nucleation of the primary alpha aluminium phase during casting solidification. Two recent reviews on grain refinement of Al and its alloys published in 2002 and 2003 by Murty et al<sup>25</sup> and Greer et al<sup>170</sup> respectively are available for reference. McCartney<sup>171</sup> has defined grain refinement as the deliberate suppression of columnar grain growth in ingots and castings and formation of fine equiaxed solidification structure throughout the material. Grain size in metals and alloys influences the properties. An equiaxed grain structure ensures uniform mechanical properties, reduced hot tearing, improved feeding to eliminate shrinkage porosity, even distribution of second phases and microporosity on a fine scale as well as improved machinability in castings. Among the various methods to refine the grain, treating the melt with Al-Ti and Al-Ti-B master alloys providing large quantities of boride and aluminide nuclei into the molten metal is known to be effective. An effective grain refiner should:<sup>25</sup>

- (i) have a melting point higher than the alloy being solidified
- (ii) be able to initiate freezing at very small undercooling
- (iii) have a sufficient number of nucleating particles uniformly distributed
- (iv) have larger size nucleating particles than a critical size depending on the undercooling of the melt.

The mechanism of grain refinement in aluminium after the addition of Al-Ti-B master alloys is still a subject of controversy. Several mechanisms have been postulated and are reviewed elsewhere.<sup>25</sup> According to Jones and Pearson,<sup>172</sup> a grain refiner is effective if the grain size of aluminium falls below an acceptance level (220  $\mu\text{m}$ ). It has been found that grain refinement of 356 (Al-7Si-0.3 Mg) alloy with

Al-5Ti-1B master alloy leads to fine dendrite arm spacing of the solidified structure (Figure 2.7).<sup>173</sup> The alloying elements as well as the impurities present in the aluminium alloys play significant roles in deciding their grain refining behaviour. While a large number of alloying elements and some impurities (Ca, Be, Mg, Sr, Bi, In, Pb, Sb, Sn and Co) in the aluminium alloys enhance their grain refining capabilities, elements such as Cr, Si, Zr, Li lead to poisoning when aluminium is grain refined by the conventional addition of 0.01%Ti of the Al-5Ti-1B master alloy. However, master alloys such as Al-B and boron rich Al-Ti-B appear to have better grain refining capability in the case of aluminium alloys containing poisoning elements.<sup>25</sup>

It has been reported that calcium enhances the grain refining action of titanium.<sup>174</sup> Abdel-Rahim et al<sup>175</sup> have observed that the grain refinement of aluminium by titanium is enhanced by additional alloying with < 0.1% Be, Sr, Ca or Mg in the form of respective master alloys. The increase in the seed crystal formation rate in the presence of alkaline earth metals is due to the isomorphic growth of ternary or quaternary phases on Al<sub>3</sub>Ti.

## **2.2.5 Effect of Alloying Elements on the Castability of Aluminium Alloys**

Castability is the ability of an alloy to effectively fill a mould and form a dimensionally accurate casting of acceptable soundness and integrity. It refers principally to two measurable foundry parameters: molten alloy fluidity and the casting soundness as measured by the type and distribution of solidification shrinkage. Calcium is expected to affect the casting characteristics of aluminium casting alloys because of its significant influence on the viscosity and surface tension of the melt.<sup>176</sup>

### **2.2.5.1 Formation of oxides and their effects**

Aluminium readily oxidizes in the presence of air or moisture rapidly forming a strong, thin impermeable film of protective oxide on any exposed metal surface. Most of the group IA and IIA elements also readily form very stable oxides. These oxides have lower densities than the corresponding parent metal and so tend to be broken and porous to both air and moisture (BeO is an exception). Fox and Nilmani<sup>177</sup> have used the Pilling – Bedworth (PB) ratio (oxide density to metal density) to explain this tendency. Elements with PB ratios < 1 form discontinuous and non-protective oxides,

while those with PB ratios  $> 1$  form continuous and protective oxides. PB ratios of BeO, MgO, CaO,  $\alpha$ -Al<sub>2</sub>O<sub>3</sub> and  $\gamma$ -Al<sub>2</sub>O<sub>3</sub> are 1.68, 0.78, 0.65, 1.28 and 1.45 respectively. Thus, the melt containing Ca and Mg cannot maintain its continuous protective Al<sub>2</sub>O<sub>3</sub> skin even when the melt is quiescent. Instead, it will be subjected to a rapid and continuous oxidation leading to formation of more oxides. These oxides appear to play a major role in providing nucleation sites for porosity. Further, entrained oxides lead to increased melt viscosity and hence reduced fluidity and poor feeding of castings. Figure 2.8 shows the comparative oxidation losses caused by the addition of various elements to aluminium melt and it should be noted that the group IA and IIA elements (Na, Ca and Mg) have a considerable oxidation loss than the very little of silicon.

A strong oxide will protect the metal from further reactions with the environment (good aspect) and may prevent the liquid from flowing into intricate parts of the mould (bad aspect) but staying on the surface of the advancing metal front, so that its final location can be controlled (good aspect). On the other hand, a weak oxide in a turbulent flow will break up and get incorporated in the bulk of the casting in the form of inclusions (bad aspect).<sup>178</sup>

### 2.2.5.2 Fluidity

Fluidity describes the ability of a metal to fill a mould completely. Campbell<sup>94</sup> defines fluidity as “the maximum distance to which the metal will flow in a standard mould”. It is a complex characteristic influenced by surface tension, viscosity, alloy freezing range, melt cleanliness, superheat and solidification conditions. For good castability, fluidity needs to be sufficient but not so excessive as to cause mould penetration or flashing along parting lines. There are two groups of variables that affect the fluidity: 1) alloy parameters and 2) mould parameters. The effect of chemical modifiers on casting fluidity has been investigated by a number of researchers. Venkateswaran et al,<sup>179</sup> in an extensive study using the vacuum suction technique on eutectic Al-Si alloy, have concluded that both Na and Sr additions, individually or in combination, with or without accompanying Ti-based grain refiner, have resulted in reduction in casting fluidity. However, additions of either Sb, or Sb plus Ti have

resulted in increased fluidity. However, Argo and Gruzleski<sup>180</sup> studying the effect of Na and Sr additions to 319, 356 and 413 alloys have found no significant effect on fluidity. On the other hand, Alsem et al<sup>181</sup> have found that additions of Al-10Sr master alloy in combination with TiB grain refiner to an Al-7Si alloy have improved fluidity. Ca addition to Al-Si alloys is expected to increase their fluidity because Sr, its neighbouring element in the Periodic Table, increases fluidity of Al-Si alloys significantly. The possible reason is the straightening of the solidification front due to the transition from dendritic (in which the extensions of the dendrites into the flow causes drag) to cellular growth mode.<sup>182</sup> On the other hand, Tsumura et al<sup>183</sup> have found that a small addition of calcium reduces fluidity as indicated by a reduction in the flow length in the spiral fluidity mold for the AC2A (Al-4.45Si-4.01Cu), AC3A (Al-12.9Si) and ADC12 (Al-10.9Si-3.07Cu) alloys. It has been found that grain refiners increase the fluidity and feedability.<sup>173</sup> The feedability (the subsequent interdendritic feeding stage, wherein the metal flow and transfer occurring after the mould has been completely filled.<sup>182</sup>) of these three alloys is also notably reduced by calcium additions up to about 0.01% (100 ppm). Further, it has been observed that additions of Ca and Li reduce the casting fluidity of AL2 [Al-12Si-0.6Cu] and AMg6 [Al-(5.8-6.8)Mg-(0.5-0.8)Mn-0.4Si-0.4Fe-0.2Zn-0.1Cu-(0.02-0.10)Ti-(0.0002-0.005)Be-0.1other impurities] Al alloys.<sup>132</sup>

The reduced fluidity with Ca addition may be attributed to the increased effective viscosity of the melt as a result of entrained surface oxides. These can be introduced by accidental enfolding of the surface during pouring, especially if the design of the filling system of the casting is bad. Thus, in practice, depending on the freedom of the liquid metal from oxides entrained previously (i.e. already present in the original ingot material as bought) or by the alloying action and casting the fluidity test piece, the apparent effect of Ca can either increase or decrease the fluidity.<sup>182</sup> Chai<sup>184</sup> has demonstrated that the delayed coherency points obtained with the addition of grain refiner in Al-17Si-Mg and Al-11Si alloys have resulted in increased casting fluidity and feedability. Fang and Granger<sup>108</sup> have shown that grain refining additions promote a more uniform porosity distribution in Al-7Si-0.3Mg alloy, presumably because of an improvement in feedability. However, Venkateswaran et al<sup>179</sup> and Morimoto et al<sup>185</sup> claim that casting fluidity decreases with the addition of Ti-based grain refiners.

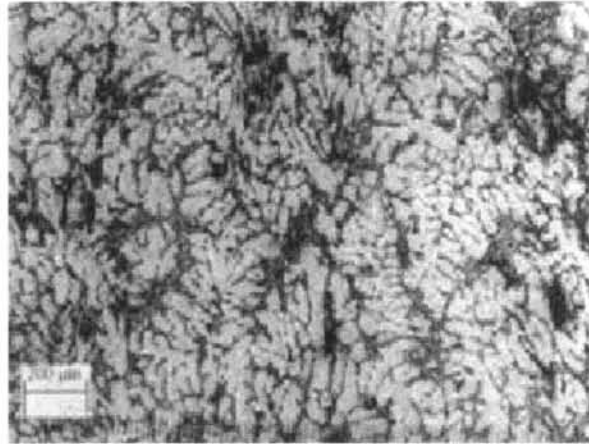


Figure 2.7: Microstructure of Al-Si-Mg (356) alloy after grain refining with Al-5Ti-1B master alloy (Courtesy: Kashyap and Chandrashekar<sup>173</sup>)

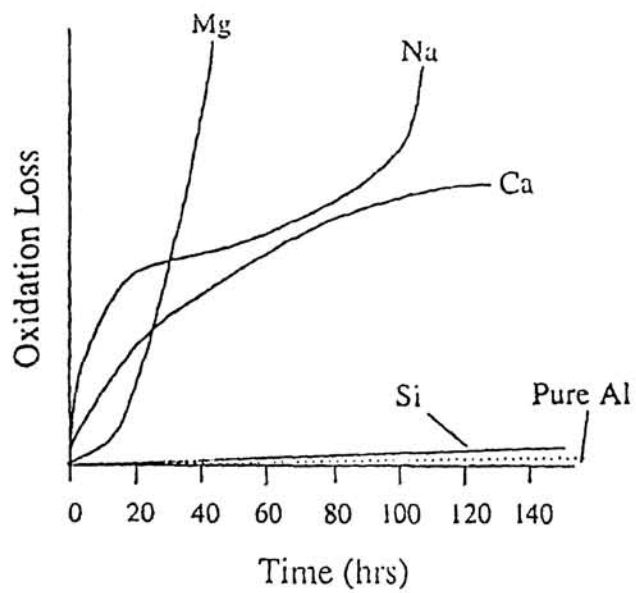


Figure 2.8: Comparative oxidation losses caused by the addition of various elements to aluminium melt (Courtesy: Fox and Nilmani<sup>177</sup>)

## 2.2.6 Heat Treatment

Cast Al-Si-Mg alloys can be heat treated to obtain an optimum combination of strength and ductility. The heat treatment consists of solutionizing at temperatures close to eutectic temperature, quenching and a combination of natural and artificial aging. The enhancement in tensile properties after the thermal treatment has largely been attributed to the formation of non-equilibrium precipitates of  $Mg_2Si$  within the primary dendrites during aging and the changes occurring in Si particle characteristics from the solution treatment. The properties attainable in the casting are determined by the temperature and the duration of both solutionizing and aging processes.<sup>186</sup>

### 2.2.6.1 Temper selection

Several heat treatment tempers such as T4, T5, T6 and T7 have been developed for Al-Si-Mg alloys. Fully heat treated structures such as T6 produce higher strengths because of the formation of greater amounts of fine  $Mg_2Si$  precipitates during aging. At low Mg contents and low aging times, ductility obtained with a T6 treatment is greater than in a T7 temper. The T7 temper exhibits high ductility with minimum internal stresses in the casting. Compared to T1 (as-cast) condition, the yield strength for a T7 temper is greatly enhanced without any loss in ductility. The response of the casting to a T5 treatment is determined primarily by the cooling rates, (as in small permanent mould castings) with some Mg retained in solid solution precipitating as  $Mg_2Si$  during aging. This temper may be an economic proposition in modified alloys when moderate strengths are required. The T6 (in some cases T7) treatment gives the optimum balance of strength and ductility and is most commonly employed with aluminium alloy castings.<sup>161, 186</sup>

### 2.2.6.2 Solution heat treatment

The solution treatment of the casting produces the following effects:

- Dissolves  $Mg_2Si$  particles
- Homogenizes the casting
- Changes the morphology of eutectic Si

Heat treatable aluminium alloys display appreciable solid solubility of the precipitating  $Mg_2Si$  phase at the solidus temperature. Under equilibrium conditions,

solubility decreases with temperature and the second phase precipitates out as coarse particles. This decrease in solubility is a prerequisite to a significant response to heat treatment. In order to obtain a maximum concentration of Mg and Si particles in solid solution, the solution temperature should be as close as possible to the eutectic temperature. In most cases, the Al-7Si-0.3Mg (356) and Al-7Si-0.5Mg (357) type alloys are solutionized at  $813 \pm 5$  K. At this temperature, about 0.6% Mg can be placed in solution (Figure 2.9).

The solution treatment homogenizes the cast structure and minimizes segregation of alloying elements in the casting. The segregation of solute elements resulting from dendritic solidification may have an adverse effect on mechanical properties. The time required for homogenization is determined by the solution temperature and dendrite arm spacing. In the case of Al-Si-Mg casting alloys, there is no strong segregation of Mg and Si.<sup>186</sup> Closset et al<sup>187</sup> have found that homogenization was essentially complete within 30 min at 823K. No difference in the rate of homogenization between modified and unmodified samples has been observed.

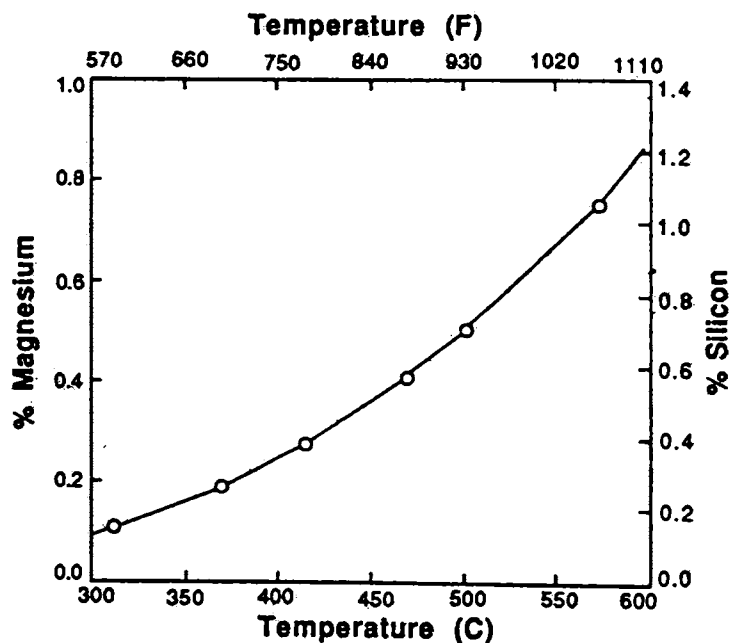


Figure 2.9: Equilibrium solubility of Mg and Si in solid aluminium when both Mg<sub>2</sub>Si and Si are present<sup>186</sup>

The eutectic Si morphology plays a vital role in determining the mechanical properties. Particle size, shape, and spacing are all factors that characterize silicon morphology. During heat treatment, Si particles are initially broken down into smaller fragments and gradually spheroidized. Prolonged solution treatment leads to coarsening of the particles. Both spherodization and coarsening are surface energy driven, i.e the system tries to reduce excess surface area to the minimum possible. In modified alloys, a high degree of spherodization is observed only after 12 hr of solution treatment, while in unmodified alloys, even after 12 hr, coarse needles of Si are visible.<sup>186</sup> It has been reported<sup>188</sup> that rapid spherodization of well modified fibrous eutectics occurs during solutionizing at 813 K in a Sr modified Al-7Si-0.45Mg alloy. Similar results have been reported by Rhines and Aballe.<sup>189</sup> The rates of spheroidization and coarsening increase with the solution temperature.<sup>190, 191</sup> Zhu et al<sup>192</sup> have proposed that changes in Si morphology occur in two stages: dissolution separation and spheroidization. In the first stage, Si is separated into segments at corners or thin growth steps, but they retain their flake morphology. In the second stage, the broken segments spheroidize and the aspect ratio decreases. Theoretical analysis suggests that interfacial instabilities cannot readily occur in plate-like (unmodified) eutectics and consequently the structure is resistant to spheroidization.<sup>193</sup> Fibrous eutectics, however, are susceptible to shape perturbations and the particles are easily fragmented. Consequently, higher rates of spheroidization are observed in modified than in unmodified specimens. The solution temperature has a greater effect on tensile properties than solution time.

### **2.2.6.3 Quenching**

Following solutionizing, the castings are usually quenched in water. The purpose of quenching is to suppress the formation of equilibrium Mg<sub>2</sub>Si phase during cooling and retain maximum amount in solution to form a supersaturated solid solution at low temperature. The quench media and quench interval are the parameters that control the effectiveness of this treatment. In most cases, the samples are quenched in water whose temperature is between 298 to 373 K. The ASTM standard recommends that for A356 and A357 alloys, which are quench sensitive, a quench delay of not more than 10s may be necessary to attain tensile requirements in the product specification.<sup>186</sup>

#### 2.2.6.4 Aging

Maintaining quenched samples at a temperature below the final artificial aging temperature for extended periods is termed preaging. This temperature may be equal to, above or below the room temperature. The precipitation of very fine  $\beta'$ (Mg<sub>2</sub>Si) during aging leads to pronounced improvements in strength properties. Both aging time and temperature determine the final properties. Among the alloying elements that may be present in cast Al-Si-Mg alloys, only Ti seems to have a major influence on the aging process. The presence of TiAl<sub>3</sub> particles in the matrix may delay the precipitation of Mg<sub>2</sub>Si. It has been reported that this delay gives rise to a secondary peak in the elongation at times greater than about 10hr.<sup>186</sup>

### 2.3 IMPURITIES IN CAST Al-Si ALLOYS

The influence of impurities in aluminium casting alloys has become increasingly important. Small quantities of many elements can occur in Al-Si alloys and have a marked influence on the structure and properties of the castings. Some are present as deliberate additions while others arise from trace impurities in the raw materials. Several of these elements have beneficial effects, while others are very damaging and must be avoided as far as possible. The increasing use of recycled aluminium casting alloys raises the necessity for strict process control to remove the ill effects of impurity elements.<sup>194</sup> The main impurities that exist in recycled Al-Si foundry alloys are iron (Fe), manganese (Mn), copper (Cu), and zinc (Zn).<sup>195</sup>

### 2.4 IRON IN CAST Al-Si ALLOYS

Iron is always present in commercial aluminium alloys and has consistently emerged as the main impurity element and perhaps the most detrimental to the mechanical properties of these alloys. It gets readily picked up by aluminium from numerous sources, namely, crucible, tools, etc., and its permissible limit gets easily exceeded if proper care is not exercised.<sup>4</sup> Aluminium foundry alloys always contain a certain quantity of iron. In addition, it is sometimes unintentionally added to the molten metal by various means, particularly the iron tools that are often used during melting and casting. The raw materials such as aluminium and silicon used for the preparation of alloys as well as the secondary Al alloys from recycling also contain a certain unavoidable amount of iron.<sup>196</sup> Consequently, the cost of aluminium alloys is inversely

related to its Fe content. Indian commercial grade Al is well known for its higher iron content and an understanding on the effects of Fe in Al alloys is a prerequisite for getting the best mechanical properties.<sup>197</sup>

#### 2.4.1 Aluminium – Iron System

The Al-Fe alloy phase diagram<sup>7</sup> is shown in Figure 2.10. There is a eutectic, Al-FeAl<sub>3</sub>, at the aluminium end, at 928 K, with a probable composition within the range 1.7-2.2% Fe. The solubility of iron in molten aluminium is quite high leading to the ready dissolution of ferrous material coming in contact with it. In contrast, the equilibrium solid solubility is of the order of 0.03-0.05% at eutectic temperature. Its solubility is even less at room temperature or in the presence of alloying elements that form compounds with Fe. Hence, iron in aluminium alloys forms second phase particles. By quenching from the liquid, supersaturated solutions can be produced, containing up to 8.4% Fe, in which the iron atoms are clustered.

#### 2.4.2 Iron Intermetallic Phases

A number of Fe-rich phases have been identified in Al-Si alloys. The chemical composition and local cooling rate are the controlling factors determining the phases to be formed and their particle size.<sup>198</sup> The ternary Al-Si-Fe equilibrium diagram (Figure 2.11) indicates the different phases formed at various temperatures and compositional ranges.<sup>199</sup>

In Al-7Si-0.3Mg alloy, Fe combines with Al, Si and Mg to form intermetallic compounds such as  $\beta$ (Al<sub>5</sub>FeSi),  $\alpha$ (Al<sub>8</sub>Fe<sub>2</sub>Si) and  $\pi$ (Al<sub>8</sub>FeMg<sub>3</sub>Si<sub>6</sub>). These iron rich phases affect the mechanical behaviour, corrosion resistance and machinability of the castings, depending on their chemical composition, morphology and distribution. Of these,  $\beta$ -phase (Al<sub>5</sub>FeSi) in particular is considered to be detrimental for the ductility of the material. The platelet morphology of this phase appearing as needles in the interdendritic regions acts as a stress raiser decreasing the mechanical properties of the cast part. Further, its brittle and hard nature makes machining of cast parts containing Al<sub>5</sub>FeSi difficult and costly because of increased machining hours requirement and associated reduction in tool life. Moreover, the large platelets of

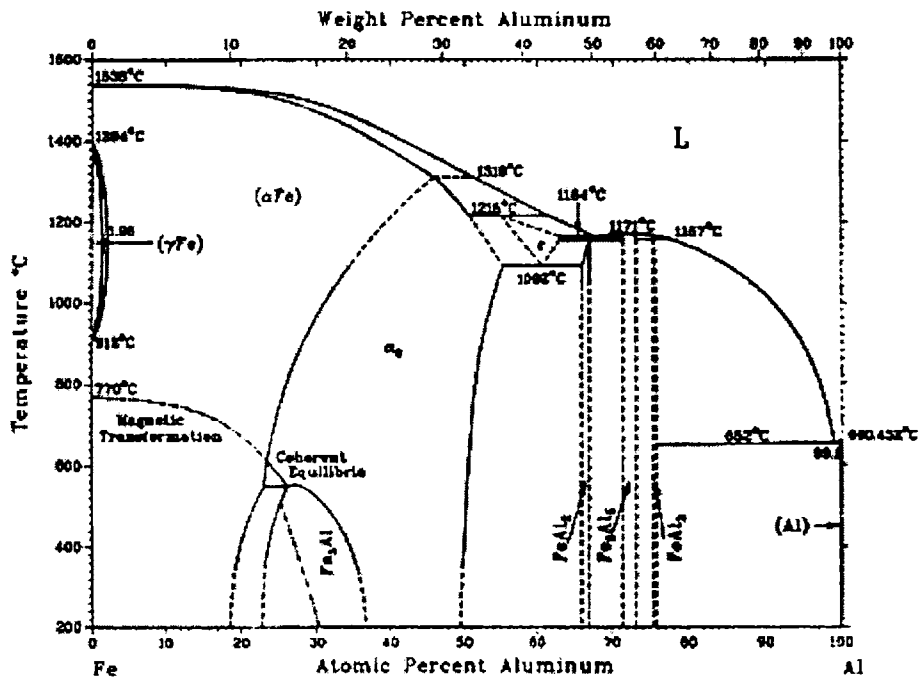


Figure 2.10: Al-Fe alloy phase diagram<sup>7</sup>

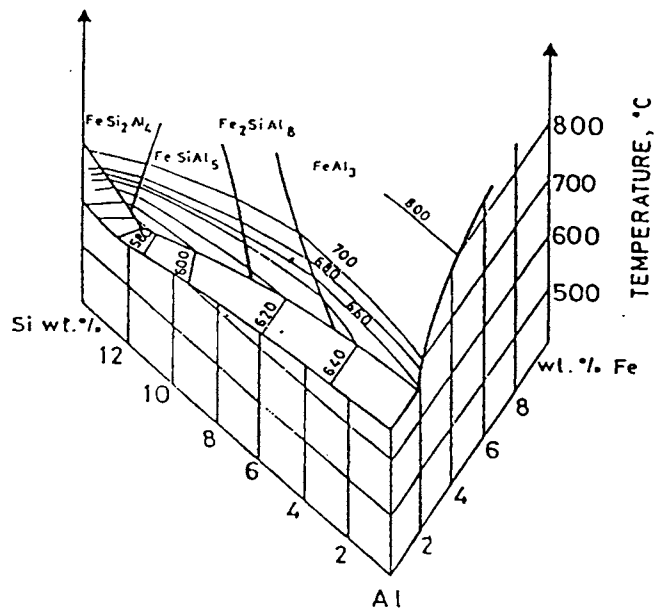


Figure 2.11: Liquidus surfaces in the Al-rich corner of the Al-Fe-Si equilibrium phase diagram<sup>199</sup>

Al<sub>3</sub>FeSi forming early during solidification tend to prevent the flow of liquid metal through the feeding channels causing unsoundness. Although other Fe-rich phases are also as hard and brittle as the  $\beta$ -phase, they have less detrimental shapes.

The conditions favouring the formation of  $\alpha$  or  $\beta$  intermetallic phase depend not only on the alloy composition but also on the solidification conditions. The interesting aspect of  $\beta$ -phase reaction is that unlike the silicon eutectic temperature, which is only slightly affected by variations in cooling rate, the  $\beta$ -phase start temperature decreases with decreasing iron content, increasing cooling rate and increasing melt superheat temperature until it eventually starts with the silicon eutectic temperature.<sup>143, 200, 201</sup> The formation and presence of Fe containing intermetallic phases (in particular  $\beta$ -phase) are also believed to produce significant reductions in the castability of aluminium alloys. When Fe is added to aluminium to produce a binary alloy, increased Fe levels result in increases in both the shrinkage porosity and the melt viscosity without any change to surface tension.<sup>4</sup>

On the other hand, the presence of Fe (in excess of 1%) is also necessary particularly in the case of die casting to prevent the molten alloy from sticking to the casting die, often referred to in the trade as “soldering to the die”. However, such high amount of Fe poses problems due to  $\beta$ -phase formation.<sup>30</sup> In order to obtain very good mechanical properties, either the Fe content in the alloy has to be maintained as low as possible or the morphology of the  $\beta$  plates has to be altered to harmless shapes.<sup>110</sup> Since Fe cannot be economically removed from the melt, it is technically important to understand the effects of iron and the means to reduce its ill effects.

#### **2.4.3 Effect of Fe on the Properties of Al-Si Alloys**

Three reviews on the effect of Fe in Al casting alloys published in 1981, 1997 and 2003 by Couture<sup>202</sup>, Crepeau<sup>110</sup> and Mbuya et al<sup>203</sup> respectively are available for ready reference. However, because of the topic’s continued significant importance in Al industry, further contributions have been confirmed to be made by researchers.

### **2.4.3.1 Physical properties**

The electrical resistivity of aluminium increases from about  $2.6548 \times 10^{-8} \Omega \text{ m}$  at  $20^\circ \text{C}$  to about  $2.75 \times 10^{-8} \Omega \text{ m}$  and  $2.9 \times 10^{-8} \Omega \text{ m}$  with the addition of 0.05% Fe and 1% Fe respectively. The lattice parameter of aluminium is practically unchanged up to the equilibrium solid solubility limit (0.05% Fe), but shrinks from  $4.049596 \times 10^{-10} \text{ m}$  at  $25^\circ \text{C}$  to  $4.012 \times 10^{-10} \text{ m}$  when 8.4% Fe is retained in solid solution by quenching from the liquid. The density varies linearly from  $2690 \text{ kgm}^{-3}$  at 0%Fe to  $3770 \text{ kgm}^{-3}$  at 36%Fe. Iron decreases the thermal expansion coefficient of aluminium linearly. The solidification shrinkage of aluminium also decreases linearly from 6.5% to 3% for a 5% Fe alloy. The viscosity of molten alloy increases with addition of Fe, but there is no appreciable change in surface tension. When Fe is deposited on aluminium, a layer of  $\text{Al}_3\text{Fe}$  forms and this slows down diffusion. Solution of Fe in molten aluminium is diffusion dependent and its activation energy is 1.04eV. Iron does not appreciably affect other metals in solid aluminium, but the activation energy for diffusion of Fe dissolved in aluminium is lowered by silicon from a value of 1.65eV for pure Al-Fe alloy to 1.35eV for the alloy containing 0.12%Si.<sup>8</sup>

### **2.4.3.2 Thermal conductivity**

In the Al-Fe system, increasing the Fe content reduces the thermal conductivity of aluminium. Makhlouf et al<sup>204</sup> have studied the effect of Fe on the thermal conductivity of Al-Si die casting alloys (based on 7 and 13% Si) and found that Fe decreases the thermal conductivity. In the alloys studied by Makhlouf et al,<sup>204</sup> the Fe-rich phases containing mainly Fe, Al, Mn, Cr and Ni have existed in the form of needles, Chinese script and/or polyhedral (star-like) crystals. The needle phase has the largest surface/volume ratio and hence has the largest interfacial area with the alloy matrix. Consequently, this phase affects the thermal conductivity more than the other phase morphologies. Manganese additions can transform the needle Fe-bearing phases to Chinese script or polyhedral crystals, thus reducing the negative influence of Fe on thermal conductivity. Other elements that change the needle morphology of the Fe-bearing phases to morphologies with less surface/volume ratios are also expected to reduce the negative effect of Fe on thermal conductivity.

### 2.4.3.3 Corrosion resistance

Although the difference in the electrolytic potential between that of  $\text{Al}_3\text{Fe}$  particles (ranges between  $-0.39$  and  $-0.58$  V) that are usually present in the Al-Fe system and that of the aluminium matrix ( $\sim -0.80$  V) is small ( $\sim 0.40$  V), it leads to a reduction in corrosion resistance of Fe added aluminium. The purer the aluminium, the more pronounced the effect; the first few hundredths per cent of Fe are in solid solution, and are segregated at the sub-grain boundaries and grain boundaries of the aluminium and therefore lead to intergranular corrosion. Successive additions of Fe form  $\text{Al}_3\text{Fe}$  particles dispersed throughout and shift the corrosion from intergranular to the pitting type.<sup>8</sup> Hatch<sup>205</sup> reported that Fe forms constituents ( $\text{Al}_3\text{Fe}$ ) that are cathodic to the aluminium matrix. When these are present on the surface, the oxide film over them is thin or non-existent. The local cells produced by these impurities promote pitting attack of the surface in a conductive liquid. In Al-Si foundry alloys, Fe reduces significantly the corrosion resistance unless corrected with Mn or Cr. However, Fe together with Ni in Al-Si alloys produces particularly good resistance to the effects of high temperature water or steam.<sup>206</sup>

### 2.4.3.4 Mechanical properties

The mechanical properties of cast aluminium alloys are adversely affected by Fe because it is generally present as large primary or pseudo-primary crystals or as Fe-bearing intermetallic compounds increasing the hardness but decreasing most other mechanical properties such as ductility. The morphology of Fe-bearing intermetallic compounds plays a deciding role in determining the mechanical properties of the alloy. Although many Fe-rich phases are likely to form, the most detrimental phase to mechanical properties is the needle/platelet  $\beta$ -phase. Wang et al.<sup>207</sup> have reported that this is mainly because of the more severe stress concentration effect introduced by the sharp edges of the needles into the alloy. Despite the availability of number of publications on the effect of Fe in aluminium alloys, there is no unanimity on the degree of its influence on mechanical properties. This is especially so when its effect on the tensile and yield strengths of Al-Si based foundry alloys is considered. Some researchers<sup>4, 8, 88, 205</sup> have reported that Fe slightly increases the tensile and yield strengths of aluminium alloys although others<sup>208-213</sup> have observed a decrease in both tensile and yield strength with increasing levels of Fe in

these alloys. However, there seems to be consensus on the fact that Fe increases hardness and it greatly reduces the fracture toughness,<sup>4, 8, 88, 205, 210, 211, 213-217</sup> ductility,<sup>4, 8, 88, 205, 208-210, 212-217</sup> fatigue resistance<sup>42, 213, 218</sup> and impact energy.<sup>88, 210, 216</sup>

According to Couture,<sup>202</sup> although there is no unanimity amongst various sources in the literature as to the level of enhancement in mechanical properties obtained with the addition of iron, there is consensus, however, on its detrimental influence in the form of the  $\beta$ -phase. It has been found that at higher Fe content ( $>0.6$  wt.%) in Al-Si alloys, the Fe-rich intermetallic phases are potential fracture initiating sites than the eutectic Si.<sup>219</sup> Appearing as needles in the microstructure, the amount and size of the  $\beta$ -phase platelets formed are strongly dependent on the Fe content and solidification rate.<sup>199, 208</sup> According to Mascres,<sup>220</sup> the  $\beta$ -phase has a detrimental influence on the properties only when it is in the primary state; when it is part of a eutectic, its effect may be negligible or even beneficial. Grand<sup>221</sup> has found that increasing iron from 0.17 to 0.60% in Al-7Si-0.3Mg alloy cast in shell moulds has no effect on the tensile strength but has markedly reduced elongation. Lemon and Hunsicker<sup>222</sup> have observed that Fe up to 0.5% decreases the elongation markedly but has little effect on the tensile and yield strengths of Al-5Si-1.3Cu-0.5Mg and Al-7Si-0.3Mg alloys cast in permanent moulds. Murali et al<sup>223</sup> have found that an increase in Fe from 0.2 to 0.8% in Al-7Si-0.3Mg alloy decreases the strength (15%) and ductility (50%) but increases the hardness (12%). Further, it has been observed that  $\beta$ -phase ( $\text{Al}_3\text{FeSi}$ ) formation in Al-7Si-0.3Mg alloy reduces the dynamic fracture toughness sharply.<sup>224</sup> With increase in volume percent of  $\pi$  phase, a portion of Mg available in the alloy will be consumed whereby the amount of Mg available for  $\text{Mg}_2\text{Si}$  precipitate formation is reduced. This will lead to decreased strength properties in the heat treated Al-7Si-0.3Mg alloy containing large amount of Fe. Closset and Gruzleski<sup>225</sup> have studied the effects of Fe and Mg on the properties of Sr-modified alloys. It has been observed that Fe decreases the quality index dramatically. This decrease is primarily due to its effect on elongation, which decreases from 12.7% at 0.1% Fe to about 3.8% when Fe reaches 0.36% (Mg has also caused a slight decrease in elongation). Variations in Fe and Mg have given rise to several changes in the intermetallic compounds observed in the eutectic. Vorren et al<sup>88</sup> have observed that a reduction in the Fe content from 0.30 to 0.15% in Al-7Si-0.3Mg alloy has resulted in a 20-25%

increase in fracture toughness. They have also reported about 47% and 20-25% reduction in tensile elongation and impact energy respectively with increasing iron content from 0.15 to 0.30%. Murali et al<sup>26</sup> have reported that the maximum allowable amount of Fe in Al-7Si-0.3Mg alloy should be between 0.3 to 0.4% to obtain the desired mechanical properties and fracture toughness. The upper permissible limit of Fe content in Al-7Si-0.3Mg cast components for general use is approximately 0.25%, while it is 0.10% or lower for castings used in critical load-bearing applications.

#### **2.4.4 Techniques to Neutralize the Ill Effects of Fe in Al-Si Alloys**

The detrimental effect of iron can be minimized by one of the following techniques and/or their combinations: (i) Rapid solidification (ii) Superheating of melt (iii) Addition of trace elements and (iv) Low temperature working. All of these methods convert the crystallization of the platelet/needle like  $\beta$ -Al<sub>5</sub>FeSi phase to either the less harmful Chinese script form or reduce the platelet size to finer sizes. Each one of these methods has its own advantages and limitations.

##### **2.4.4.1 Rapid solidification**

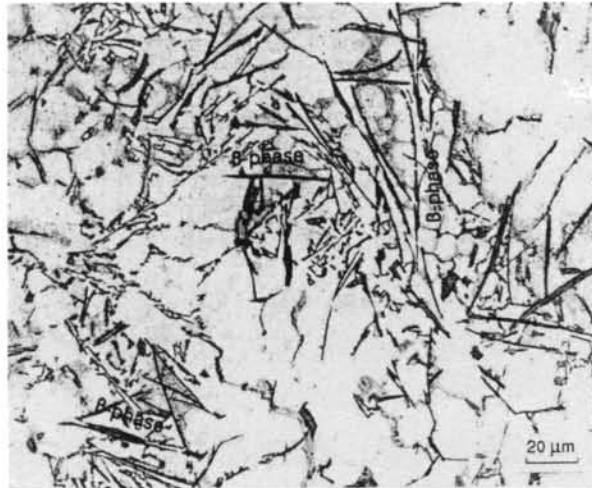
Rapid solidification is one of the methods of improving the mechanical properties of Al-Si-Fe alloys by controlling the size of intermetallic compounds.<sup>226, 227</sup> It involves solidifying the melt at a very high cooling rate and is applicable only at low levels of iron and silicon.<sup>227</sup> It has been found that higher cooling rate increases the maximum solubility of Fe in the aluminium matrix and limits the time for growth, resulting in fine  $\beta$ -phase in the case of metallic mould castings and the disappearance of all intermetallics when the cooling rate is as high as  $\sim 150^\circ$  K/s experienced in water quenched samples.<sup>228</sup> At low cooling rates  $\sim 0.5^\circ$  K/s, the  $\beta$ -Al<sub>5</sub>FeSi needles are thick and precipitate mainly at grain boundaries leading to serious alloy embrittlement. Increasing the cooling rate ( $\geq 10^\circ$  K/s) results in the precipitation of fine  $\beta$ -phase needles well distributed in the microstructure. It also increases the maximum solubility of Fe in the Al matrix. Consequently, a higher iron concentration could be tolerated in Al-Si foundry alloys, especially for die casting applications, where the presence of iron is essential to prevent problems of welding or soldering of the castings to the die.<sup>229</sup> However, this method is not amenable for mass production due to its high cost and low productivity. Further, it is impossible to produce the same

high solidification rates throughout the castings having varying section thicknesses made by conventional casting processes.

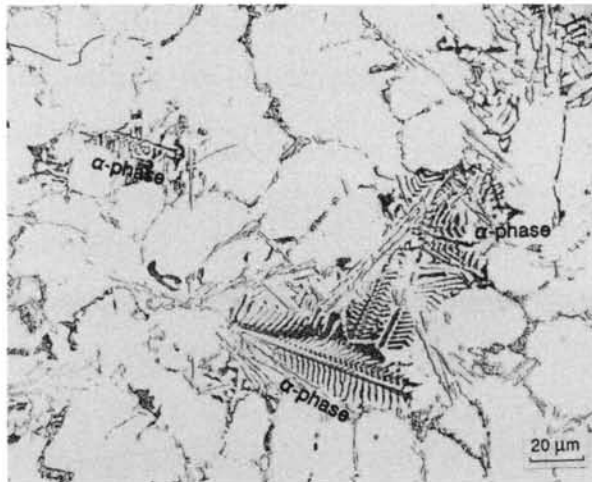
#### **2.4.4.2 Melt superheating**

Mondolfo and Barlock<sup>230</sup> have studied the effect of superheating of several aluminium alloys cast at different cooling rates ( $< 0.1$  to  $< 20^\circ$  K/s) and found that the higher superheat has resulted in faster solidification rate and finer the microstructural constituents. Awano and Shimizu<sup>231</sup> have demonstrated a novel method of neutralizing the effect of Fe (0.1, 0.5 and 0.9%) in Al-7Si-0.3Mg alloy by superheating the melt to high temperatures (973–1223 K) before pouring. It has been found that superheating of the melt transforms the Al<sub>5</sub>FeSi needle shaped compounds to Chinese scripts and thus increases the toughness of T6-treated squeeze cast alloy experiencing high solidification rate. Iglessis et al<sup>227</sup> have explained the growth process of  $\alpha$  and  $\beta$  phases in the ternary Al-Si-Fe system when the melt is superheated to a high temperature. Anantha Narayanan et al<sup>143</sup> studying the effect of superheating (200 to 300 degrees above the liquidus temperature) on the crystallization behaviour of iron containing intermetallic compounds in Al-6Si-3.5Cu-1.0Fe aluminium alloy have observed the crystallization of Fe compounds in  $\alpha$  - phase (Figure 2.12). This is due to the fact that when the melt is superheated to a high temperature, the  $\gamma$  alumina transforms to  $\alpha$  alumina, which is a poor nucleus for the  $\beta$  phase crystallization leading to the formation of  $\alpha$  phase. Superheating of Al-7Si-0.55Mg melt has been found to change the morphology of the Fe-rich phase from a needle like to a skeleton-like structure.<sup>232</sup> Ahmad and Marshall<sup>196</sup> have found that superheating (983 to 1273 K) of Al-Si alloys (Al-7.85Si-0.42Mn-1.12Fe-3.5Cu-2.2Zn and Al-11.86Si-0.44Mn-1.94Fe) refines the massive plates to compact globular forms and hence results in improved strength values of the alloys.

Bian et al<sup>233</sup> and Liu et al<sup>234</sup> have investigated another aspect of the conversion of the  $\beta$ -platelets through melt superheating. According to them, in any Al-Si alloy where the iron content is between 0.8 and 1.8%, the morphology of the iron compounds changes from a long needle-like form to rosettes and thereafter to a spheroidal shape as the melt temperature changes from low to high (from  $< 1113$  to



(a)



(b)

**Figure 2.12: Micrographs of Al-6Si-3.5Cu-1.0Fe alloy (a) superheated to 1023 K and (b) 1123 K prior to casting (cooling rate=283 K/s) [Courtesy: Anantha Narayanan et al<sup>143</sup>]**

1253 K). This spheroidization treatment has increased the tensile strength and ductility of the alloy considerably and the spheroidal form is retained even after remelting. Samuel et al<sup>228</sup> investigating the effect of melt superheat (923, 1023 and 1296 K) on  $\beta$ -Al<sub>5</sub>FeSi phase formation in A380.1 (Al-9.14Si-3.22Cu-1.01Fe), 319.2 (Al-6.23Si-3.77Cu-0.46Fe) and eutectic Al-13Si-1.5Fe-(0-0.6)Mg alloys, have found that higher superheat temperature leads to refinement of the eutectic Si and  $\beta$ -Al<sub>5</sub>FeSi intermetallics. However, it should be borne in mind that superheating the molten metal to high temperatures will lead to increased hydrogen and oxide inclusion contents apart from spending more for energy.

#### **2.4.4.3 Low temperature working**

Kim et al<sup>235, 236</sup> and Umezawa and Nagai<sup>237, 238</sup> have applied a new low temperature working process to Al-7Si-1Fe alloy to control the size and shape of intermetallic compounds and eutectic Si particles. The process consists of repeated cold working at 77 K and recovery treatment at 793 K. It has been found that the eutectic Si and acicular  $\beta$ -Al<sub>5</sub>FeSi phases are broken down to spherical shape of 2-3  $\mu$ m size. The refined particles are also uniformly distributed increasing the strength and the elongation of the alloy.

#### **2.4.4.4 Chemical neutralizers**

The most common method of mitigating the ill effects of Fe in Al-Si alloys is by adding trace elements. Various elements like Mn, Cr, Be, Co, Mo, Cd, Ni, S, V, Cu, Ca, and RE (La, Ce, Y, Nd) have been found to neutralize the ill effects of Fe in the cast alloys to different levels either individually or in combination with other elements. Each element has its own advantages and limitations. In all the cases, neutralization results in modifying the morphology of Fe – rich compound from a brittle to a less brittle form – i.e. from platelets/needles to globules or even Chinese script. Table 2.6 gives the atomic size, crystal structure and maximum solid solubility of various elements in pure aluminium at eutectic temperature. There is a critical ratio between the trace element and Fe content for effective neutralization. Higher ratios can form other undesirable intermetallic compounds. Table 2.7 lists the optimum amount, the resulting morphological change, the advantages and the limitations of various Fe neutralizers investigated for Al-Si alloys.

**Table 2.6: Atomic size, crystal structure and maximum solid solubility of various elements in pure aluminium at eutectic/peritectic temperature**

Element	Atomic Size (Å <sup>o</sup> )	Crystal structure	Eutectic (Peritectic*) temperature (°K)	Maximum solid solubility (wt.%)
Be	1.133	Hexagonal close packed	918	0.063
Mn	1.24	Cubic	931	1.82
Cr	1.249	Body-centred cubic	933*	0.77
Co	1.243	Hexagonal close packed	933	< 0.02
Sr	2.151	Cubic close-packed	-	-
Ca	1.973	Cubic close-packed	893	< 0.01

**Table 2.7: Optimum amount, morphological change, advantages and limitations of various iron neutralizers in Al-Si alloys**

Element	Optimum amount	Morphological change	Advantages	Limitations	Ref.
Mn	Mn:Fe = 1:2	platelet $\beta$ -phase to $\alpha$ - Chinese script $Al_{15}(FeMn)_3Si_2$ phase	i) Improves strength and ductility ii) Least expensive element.	i) "sludge" formation when (Mn+Fe) >0.8 ii) hot tearing iii) damaging of furnace walls iv) Do not improve fracture toughness	26, 88, 195, 202
Be	0.26% per 1%Fe	platelet $\beta$ -phase to $\alpha$ - Chinese script $BeSiFe_2Al_8$ phase	i) Improves strength ductility and fracture toughness	Toxic	26, 88, 195, 202, 239
Cr	(Cr+Fe)/Si=2.2	platelet $\beta$ -phase to $\alpha$ - Chinese script $\alpha-Al_{13}(CrFe)_4Si_4$ phase	Better than Mn addition as evidenced by higher ductility	i) Sludge formation ii) Do not improve fracture toughness	26, 88, 195, 199, 202
Co	Fe/Co=1 to 2	platelet $\beta$ -phase to $\alpha$ - Chinese script $Al_9(CoFe)_2$ phase	i) Improves tensile properties ii) less tendency to segregate during solidification	i) poor ductility ii) large amount of Co is required	26, 202
Ca	0.0035-0.02 % in hypoeutectic	Reduces the size of platelet $\beta$ -phase to finer size	i) Improves Impact fracture toughness, dynamic fracture toughness, tensile properties	i) Higher amounts lead to porosity ii) Excessive addition leads to the precipitation of Ca-containing intermetallics	30, 27, 39, 42
Sr	0.02-0.04% in hypoeutectic > 0.1 in eutectic	Reduces the size of platelet $\beta$ -phase to finer size	Improves tensile properties	i) Higher amounts lead to porosity ii) Excessive addition leads to the precipitation of Sr-containing intermetallics	228, 195, 240, 241
Rare earths	1%	platelet $\beta$ -phase to Spheroidal	Improves mechanical properties	High amount (>1%) reduces ductility and strength	155

#### 2.4.4.4.1 Manganese

Mn is the most commonly used and the least expensive element for Fe neutralization in Al-Si alloys. Since Mn is an impurity in secondary metal, it is not always necessary to add it deliberately. It encourages the formation of  $\alpha$ -phase, which forms in the interdendritic regions as well in the  $\alpha$ -Al matrix.<sup>26, 242</sup> In this respect, Mn is considered to be more effective compared to Cr, Ni, Co and Mo.<sup>243</sup> The addition of Mn to Al-Si alloys leads to the formation of quaternary (Al-Fe-Mn-Si) intermetallics.

According to the solidification conditions, the Fe-phase can precipitate as three distinct morphologies: (a) polyhedral or star-like particles of sludge, favoured by a high Mn/Fe ratio ( $\geq 0.5$ ),<sup>195</sup> where this sequence of precipitation is based on the phase formation temperature), b)  $\alpha$ -Chinese script ( $\text{Al}_{15}(\text{FeMn})_3\text{Si}_2$ ) form that is less harmful to mechanical properties, and c)  $\beta$ - $\text{Al}_5\text{FeSi}$  phase needles/platelets. Figure 2.13 illustrates Fe segregation during solidification of Al-7Si-0.3Mg alloy containing 0.48% Fe forming  $\text{Al}_{15}(\text{FeMn})_3\text{Si}_2$  and  $\text{Al}_5\text{FeSi}$  phases. As solidification progresses, the composition of the remaining liquid follows lines 1, 2a and 2b.  $\text{Al}_{15}(\text{FeMn})_3\text{Si}_2$  phase precipitates along line 2a. Both the phases precipitate along 2b and at point 3, where the Al-Si eutectic also solidifies.<sup>244</sup> However, the addition of Mn results in other problems such as hot tearing or damaging of crucibles due to the crystallization of a coarse  $\text{Al}_{15}(\text{FeMn})_3\text{Si}_2$  compound, usually termed “sludge” or “fallout”. This problem usually arises in the die casting industry, where the melt holding temperatures are generally kept low.<sup>228</sup> The formation of sludge depends on the cooling rate and the concentrations of Fe, Mn, Cr. Several empirical formulae have been introduced in order to correlate the ratio between these elements and precipitation of sludge. From the following formula<sup>195</sup> for the segregation or sludge factor,

$$\text{Sludge factor (S.F)} = \% \text{Fe} + 2(\% \text{Mn}) + 3(\% \text{Cr}) \quad \dots\dots\dots(2)$$

a value of 1.8 has been established for the formation of sludge. Under die-casting conditions, the sludge factor could be as low as 1.4. The ASTM specification indicates that in order to suppress the harmful influence of Fe in sand castings, Mn content should be greater than one half of Fe content. The work of Gustafsson et al<sup>199</sup> confirms that when the Fe content exceeds 0.45%, it is preferable to increase the Mn concentration to almost half that of the iron.

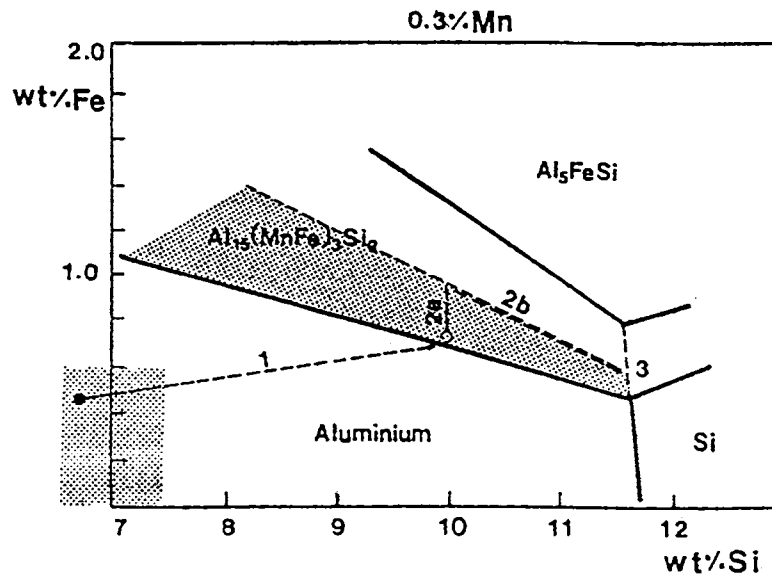


Figure 2.13: Simplified illustration of Fe segregation during solidification of 356 (Al-7Si-0.3Mg) alloy containing 0.48%Fe.<sup>244</sup>

#### 2.4.4.4.2 Chromium

Cr addition also exhibits a similar behaviour like Mn. Gustafsson et al,<sup>199</sup> studying the influence of Fe and Cr on the microstructure of cast Al-7Si-0.3Mg alloy have found that the coarse  $\beta$ -phase ( $Al_5FeSi$ ) platelets, which form during solidification of alloys containing Fe, are replaced by Chinese script  $\alpha$ (bcc)- $[Al_{13}Si_4(Cr,Fe)_4]$  dendritic particles when Cr is added. Coarse  $\beta$ -phase platelets are found to be replaced by  $\alpha$ -script when Cr is added to 356 alloy containing  $\sim 0.5\%$  Fe.<sup>2</sup> However, its tendency to contribute to sludge formation limits its usefulness. The precipitation of the  $\alpha$ -phase in the form of large dense particles (sludge) in 339 alloys containing relatively high-Cr has been reported by Granger.<sup>245</sup> Mn and Cr additions, however, do not significantly reduce the deleterious effect of Fe on fracture toughness.<sup>88</sup>

#### 2.4.4.4.3 Beryllium

Among the various iron neutralizers available, Be has been found to be the most effective in improving the mechanical properties (optimum level is 0.26% Be

per 1% Fe) by exhibiting a constant hardness, strength and ductility irrespective of the Fe level.<sup>26, 246</sup> Belov and Kurdyumova<sup>247</sup> have studied the Al-Si-Fe-Be alloy system and found that Be is the most effective ferrous phase neutralizer in silumins. Tan et al<sup>212, 214</sup> have found that the addition of Be to A357 alloys is effective in decreasing the deterioration of mechanical properties due to the presence of Fe. Be-Al-Fe phases ( $\text{Al}_4\text{Be}_5\text{Fe}_2$  and  $\text{AlFeBe}_4$ ) have also been observed in spheroidal compact forms with 0.2-0.5% Be addition.<sup>248</sup> Warnig et al<sup>249</sup> have investigated the effect of Be addition on microstructures and mechanical properties of B319 alloy. It has been found that the addition of Be (i) reduces the amount and modify the morphology of iron intermetallics from platelet like  $\beta\text{-Al}_5\text{FeSi}$  phases to comparatively harmless Chinese script  $\alpha\text{-Al}_8\text{Fe}_2\text{Si}$  phases, (ii) enhances the precipitation kinetics and increases the amount of strengthening precipitates, (iii) spheroidizes and decreases the size of silicon particles, (iv) increases the melting point of Al-Al<sub>2</sub>Cu eutectic by about 280°K, and (v) improves the tensile properties. Murali et al<sup>210</sup> have studied the changes in morphology of the  $\beta$ -phase in the presence of Be in Al-7Si-0.3Mg alloy containing 0.6% Fe. Further, Be-Fe phases are seen only inside the  $\alpha$ -Al dendrites resulting in cellular fracture whereby improving the fracture toughness unlike the mixed mode of intergranular and brittle cleavage fracture in high Fe containing alloys without Be addition. It has been found that Be addition is the most effective means in improving the ductility and the tensile strength of Al-Si-Mg alloys.<sup>26, 224</sup> Moreover, Be addition has few other benefits apart from altering the morphology of the  $\beta$  phase. It acts as a grain refiner and preferentially oxidizes forming BeO on the surface of the melt, reducing Mg loss and making Mg available for forming the required volume of  $\text{Mg}_2\text{Si}$  for strengthening. In addition, Be improves the alloy fluidity/castability, especially in the case of automotive alloys.<sup>240, 250</sup> However, since Be is toxic, foundrymen are reluctant to use even small quantities of Be. Hence, efforts have been made to minimise its amount by combining with other elements. Murali et al<sup>26</sup> have found that Be added together with Mn and/or Cr seems to be the most effective way in providing better tensile properties than individual Be addition. Samuel et al<sup>195</sup> have studied the effect of Be, Sr, Mn and Cr individually and in combination on  $\beta\text{-Al}_5\text{FeSi}$  characteristics and found that the classic neutralization treatment of using a Mn

addition with or without Cr could be replaced by the combined Be (0.08%) + Sr (0.02%) addition.

#### 2.4.4.4.4 Strontium

There are considerable evidences<sup>251-254</sup> that Ca and Sr refine the detrimental intermetallic compounds in wrought Al alloys. Morris and Miners<sup>253</sup> have found that addition of Sr or Ca in the range of 0.02-0.05% changes the  $\beta$  phase to  $\alpha$  phase thereby improving the surface characteristics of the extrusions and Ca and/or Sr content above 0.02-0.05% has decreased the strength of the alloy. Sigworth<sup>255</sup> has reported that the formation of large brittle iron intermetallic phases can be suppressed in an exceedingly well modified alloy. Haque and Kondic<sup>256</sup> have indicated that Sr has some positive effect on the reduction of the amount of intermetallics during solidification of an Al-12.2%Si alloy. The amount of iron-bearing phase as well as the primary Si phase are reduced or become negligible and the tensile properties are improved by Sr treatment. The effect of Sr on changing the needle ( $\beta$ -phase) to Chinese script ( $\alpha$ -phase) morphology and also on the fragmentation of needles may be compared with the effect of Sr on the modification of Si in Al-Si alloys. It appears that there are many similarities in nucleation and growth between intermetallics and silicon.

Samuel et al<sup>241</sup> have studied the effect of strontium (Sr) on the size and distribution of  $\beta$ -phase needles formed in 319 type alloys. The addition of 300 ppm Sr seems to accelerate the dissolution of the  $\beta$ -phase through fragmentation of the long, intercepting needles that occur in the as-cast condition into small pieces. At such Sr concentrations, the average  $\beta$ -needle length is found to decrease from 130 to 70  $\mu\text{m}$ . These observations have been supported by the microstructural analysis carried out by Pennors et al,<sup>257</sup> where the authors have attributed the decomposition of the  $\beta$ -Al<sub>5</sub>FeSi intermetallic phase to the possibility of Si rejection.

The influence of the addition of Sr as well as (Sr and Mn) on the Fe-containing intermetallic compounds in Al-6.5Si-3.5Cu-1.0Fe and Al-6.5Si-3.5Cu-1.0Fe-0.3Mn (in mass %) cast alloys has been investigated. It has been found that Sr successfully modifies the large highly branched  $\beta$ -needle like phase ( $\beta$ -Al<sub>5</sub>FeSi) into

the individual less branched and finer ones. The combined addition of (Mn and Sr) results in modification of the needle like  $\beta$ -phase as well as promotion of Chinese script and sludge morphology formation. The mechanism of the above morphological changes has been discussed in accordance with the mechanism of nucleation and growth of the  $\beta$ -needle phase during solidification.<sup>258</sup>

#### 2.4.4.4.5 Calcium

It has been reported that a small amount of Ca (40 ppm) is effective in improving the fracture toughness even in alloys having relatively high iron content.<sup>39</sup> An Al alloy containing 0.45-0.9% Mg and 0.2-0.6% Si has been widely used for the production of aluminum extrusions. However, a principal cause of defects in the quality of the extrusions is the breaking away of solid components from the surface of the metal as it is forced through the die orifice, which is due to the presence of the iron intermetallic,  $\beta$  Al-Fe-Si phase in the ingot during the extrusion process. Morris and Miners<sup>253</sup> have found that addition of Sr or Ca in the range of 0.02-0.05% has changed the  $\beta$  phase to  $\alpha$  phase thereby improving the surface characteristics of the extrusions and Ca and/or Sr content above 0.02-0.05% has decreased the strength of the alloy. It has been reported<sup>251</sup> that the addition of 0.001-0.008% Ca has avoided the formation of fir tree surface structures on the unidirectionally solidified billets [177-305 mm diameter] and the sheet ingots of AA1100 [Al-0.95(Si + Fe)-(0.05-0.20)Cu-0.05Mn-0.10Zn], AA1050 [Al-0.25Si-0.40Fe-0.05Cu-0.05Mn-0.05Mg-0.05Zn-0.03Ti-0.05V] and AA5005 [Al-(0.5-1.1)Mg-0.20Mn-0.30Si-0.70Fe-0.20Cu-0.10Cr] Al alloys regardless of the size of the billet/ingot. Further, a combined addition of calcium 0.0005-0.05% (5-500 ppm), Ti 0.0005-0.1% (5-1000 ppm) and B 0.0001-0.02% (1-200 ppm) to iron containing (more than 0.2%) direct chill cast (D.C) Al alloy (AA1000 to AA5000 series) for rolling operation has eliminated the occurrence of unwanted fir-tree structure on the surface, thus improving productivity.<sup>252</sup>

Kobayashi et al<sup>27, 39-42</sup> have determined the effect of Fe and Ca on the mechanical properties and microstructural changes of JIS AC4C-T6 (Al-7Si-0.3Mg), JIS AC2B-T6 (Al-6.5Si-4Cu), and JIS AC4D-T6 (Al-5Si-1.5Cu-0.5Mg) alloys. The properties are in general reduced when Fe is increased from 0.2 to 0.6% in the absence of Ca. But, a distinct improvement in properties is noticed when Ca is added.

The addition of Ca (~ 40 ppm) has refined the harmful plate-like Al-Fe based intermetallic compound especially in high Fe content specimens as well as eutectic silicon to a certain degree leading to the improved mechanical properties in all the above alloys. The decreasing impact fatigue fracture toughness  $K_{fc}$  with increasing iron content is found to improve with Ca addition. Similar beneficial effect of Ca is observed with both the dynamic fracture toughness,  $J_d$  and the tearing modulus,  $T_{mat}$ , of AC2B -T6 aluminium casting alloy (Figure 2.14). Except the observation by Kobayashi et al,<sup>27, 39-42</sup> there is no comprehensive investigation of the effect of Ca on Fe-intermetallics and its interaction with other elements in Al-Si casting alloys.

## 2.5 INTERACTION OF TRACE ELEMENTS

The interaction between trace elements present in aluminium alloys can be either beneficial or detrimental to the properties of the alloys.

Among the various trace elements reported to react with Sr to neutralize its modifying effect, both Sb and P are quite effective. Suzuki and Oshiro<sup>259</sup> have invented an improved method of eliminating P and/or Sb from molten aluminium by Ca addition at a temperature of 923 to 1123 K and blowing chlorine gas or a chloride to remove calcium phosphide or Ca-Sb compound forming dross. Bonsignore and Daniels<sup>43, 44</sup> have found that additions of either Sr or Ca could scavenge Sb from secondary molten aluminium. Sb content could be reduced to 50 from 2800 ppm by treating the melt with 1500 ppm Ca. Ca and Sb form an insoluble intermetallic compound, which separates out and probably combines with the aluminium oxide surface dross. It is also observed that a minimum ratio of ~ 4:1, by weight of Ca to Sb appears to be necessary in ensuring an effective scavenging of Sb in A356 Al alloy.

Abdollahi and Gruzleski<sup>135</sup> have investigated the interactions between Sr and Ca in sand cast A357 alloy through microstructural and thermal analysis studies. It has been observed that deleterious calcium–strontium interactions take place when both the elements are present simultaneously in the melt. This can be overcome by the addition of higher amounts of calcium. Figure 2.15 shows the thermal analysis curves obtained when Sr is present alone and in combination with varying amounts of Ca.

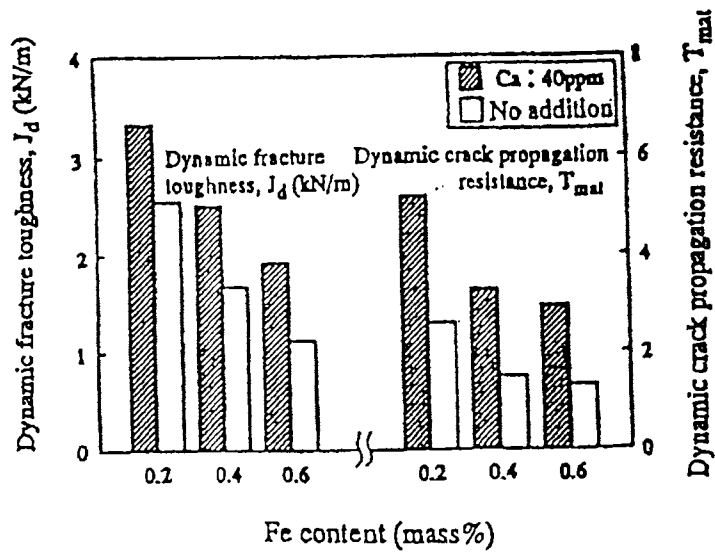


Figure 2.14:  $T_{mat}$  and dynamic fracture toughness versus Fe content in AC2B-T6 (Al-6.5Si-4Cu) casting alloy with and without Ca addition (Courtesy: Kobayashi et al<sup>27</sup>)

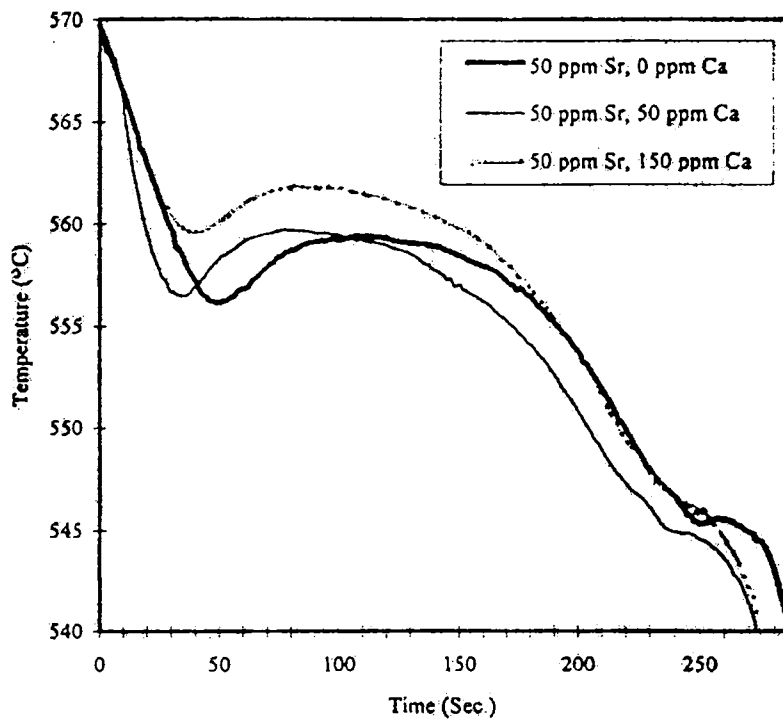


Figure 2.15: Cooling curves obtained when Ca is used in the presence of Sr (Courtesy: Abdollahi and Gruzleski<sup>135</sup>)

It is seen that the eutectic plateau is depressed to a greater extent when Ca is not added and is raised when both Sr and Ca are present together. The greater depression of eutectic plateau observed without Ca indicates a high degree of modification and the raising of plateau with both Ca and Sr indicates a reduction in modification. In addition, it has been reported that 0.005% (50 ppm) Ca addition in AC4CH alloy (Al-7Si-0.3Mg) influences the modification effect of Sr and shows a coarse eutectic Si structure, indicating a reduced modification effect.<sup>260</sup>

Nakae et al<sup>261</sup> probing the influence of impurity elements like Ca on modification of eutectic Si in Al-Si alloys treated with Sr have observed (i) reduced modification in commercial grade Al-Si alloy solidified with a cooling rate < 1 K/min due to the reaction between Sr and Ca released either from Al-Si-Sr master alloy or furnace refractory (ii) perfect modification in high purity Al-Si alloy melted in a high purity alumina tube and treated with Sr and cast even at slow cooling rate of 0.025 K/min. (iii) significant obstruction to or total stoppage of modifying action of Sr with the presence of 0.02 and 0.06 mass % Ca respectively and (iv) 0.01 to 0.02 mass % Ca as the allowable limit in Al-Si alloy for modification by Sr. The mechanism proposed is that Ca in the Al-Si-Sr alloy forms  $\text{CaSi}_2$ , which reacts with Sr forming strontium – calcium – silicide.

El-Hadad et al<sup>262</sup> have investigated the effect of Ca addition on the characteristics of eutectic Si particles in Sr modified 319 (Al-6.5Si-4Cu) alloys. It has been found that Ca additions of 50 ppm and higher coarsened the Si particles due to the formation of Al-Si-Ca-Sr compounds. Further, the form (rod or plate) and chemical composition  $[\text{Al}_7(\text{Ca,Sr})\text{Si}_7$  or  $\text{Al}_2(\text{Ca,Sr})\text{Si}_2]$  of these intermetallic compounds have been found to be strongly dependent on the Mg concentration in the alloy.

Kurdyumov et al<sup>132</sup> studying the effect of Li and Ca on the structure, shrinkage, crack resistance and flowability of AL2 [Al-12Si-0.6Cu] and AMg6 [Al-(5.8-6.8)Mg-(0.5-0.8)Mn-0.4Si-0.4Fe-0.2Zn-0.1Cu-(0.02-0.10)Ti-(0.0002-0.005)Be-0.1other impurities] Al alloys have established that Li and Ca affect the alloy characteristics degrading their properties.

Vakhovbov et al<sup>263</sup> have studied the combined solubility of Ca, Sr, Ba and Ti in aluminium and detected the phase - equilibrium boundaries in the Al corner for Ca-Ti-Al and Ba-Ti-Al systems at 773 K. The positive role of Ti, Ca, Sr and Ba in strengthening Al alloys has been reported. This has been attributed to the formation and dispersion of TiAl<sub>3</sub>, CaAl<sub>4</sub>, BaAl<sub>4</sub> and SrAl<sub>4</sub> intermetallic phases, whose amounts have increased with increasing content of Ti, Ca, Ba and Sr.

Kobayashi et al<sup>264</sup> investigating the influence of impurity elements on the morphology of primary silicon precipitates in hyper eutectic JIS AC3A Al-Si alloy (Al-12.9Si) have observed the morphology of primary silicon as long and thin as well as blocky shapes in super high (99.99%) and commercial purity (95%) hypereutectic Al-Si alloys respectively. Further, the primary Si grows longer with lower solidification rate in the former alloy, which could be suppressed by the addition of small amount of Ca (150 ppm) and Fe (400 ppm). However, the growth rate of primary Si morphology has not been affected by solidification rate in Ca and Fe containing Al-Si alloy.

Afanas'ev and Prudnikov<sup>265</sup> have investigated the method of improving the mechanical properties and formability of Al-Si piston alloys by optimising their chemical composition. Such an Al alloy containing 18-20Si, 0.9-1.1Cu, 0.5-0.6Mg, 0.8-0.9Mn, 0.07-0.09Ca, 0.2-0.4N, 0.1-0.2Ti, 0.01-0.03P and 0.00008-0.00025% H has shown better mechanical properties than the known piston alloys of the Al-Si system, as well as lower linear thermal expansion coefficient compared to the Al-Cu alloys.

Studying the effects of increasing Ca content on the modification of Al-7Si-0.3Mg alloy with Sr, Kwon et al<sup>266</sup> have observed (i) deterioration of eutectic modification rate and increase in both primary  $\alpha$  and eutectic temperatures in 50 ppm Sr treated alloy and (ii) decreased UTS and elongation as well as increased intergranular fracture. Meanwhile, coexistence of Ca and P has been found to increase eutectic modification rate and depress the eutectic temperature.

## 2.6 APPLICATIONS OF Al-7Si-0.3Mg alloy

Al-7Si-0.3Mg alloy finds widespread applications in automotive, aerospace and general engineering industries. Sand cast Al-7Si-0.3Mg alloy finds applications in flywheel castings, automotive transmission cases, oil pans and pump bodies. Permanent mould cast alloy is used in machine tool parts, aircraft wheels, airframe casings and bridge railings. It is a general purpose high strength casting alloy, whose range of applications is increased by its availability in the as-cast and heat-treated condition as well. Figure 2.16 shows an Al-7Si-0.3Mg alloy wheel used in TATA Indica and Ford Ikon cars. A typical strategic application of this alloy in Polar Satellite Launch Vehicle (PSLV) and Geosynchronous Satellite Launch Vehicle (GSLV) programmes of Indian Space Research Organization (ISRO) is for making U-bracket, Interface and Engine mounting frame castings (Figure 2.17), which have been developed at the Regional Research Laboratory.

## 2.7 GENERAL DISCUSSION

Various alloying elements have been found to have tremendous effect on cast Al-Si alloys. However, each element has its own advantages and limitations. A detailed literature survey carried out on the role of Ca in Al alloys<sup>87</sup> reveals its potential in enhancing certain important properties. However, a number of aspects remain unclear and unanswered requiring detailed investigation for thorough understanding. Na and Sr are the commonly used modifiers in Al-Si alloys changing the eutectic silicon structure from acicular or plate-like to fine fibrous shape. Variation in the efficiency of individual elements to promote modification is discussed in terms of factors such as melting point, vapour pressure, free energy of oxide formation, etc (Table 2.4). Na rapidly dissolves but does not oxidize; it has a high vapour pressure and therefore evaporates easily. Hence, rapid fading and the difficulties in storing and handling are the major drawbacks of Na. Sr tends to oxidize fairly readily but much less than Ca. Unlike elemental Ca, Al-Ca master alloys are easy to handle and store like Al-Sr master alloys. However, Ca readily gets oxidized to CaO affecting the castability especially fluidity. This can be overcome by adding trace amount of Be. The melting points of both Ca and Sr are comparable with the melt temperature. On the other hand, the vapour pressure of Sr is nearly four times that of Ca, although, both are relatively low compared to Na. However, contradicting

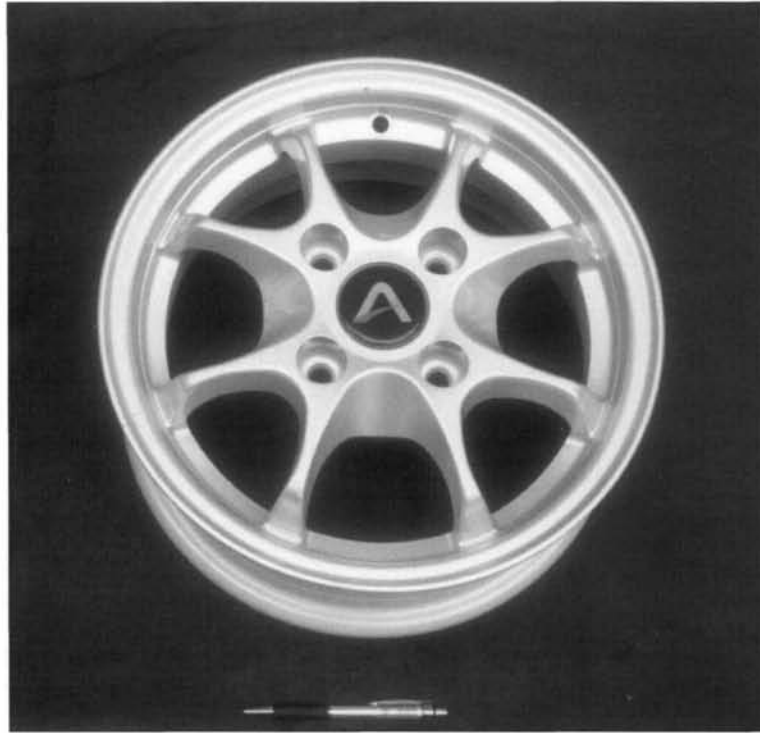
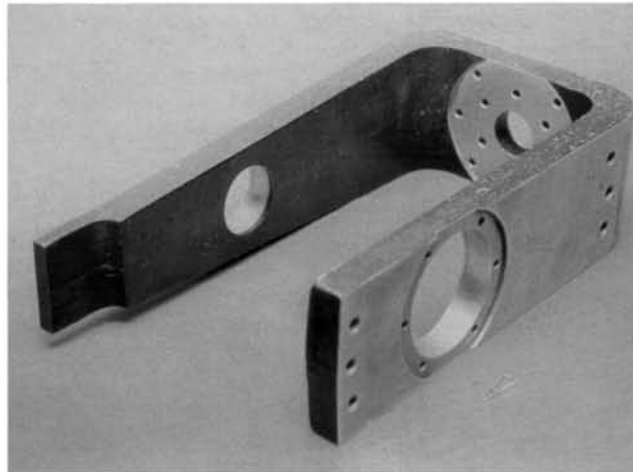
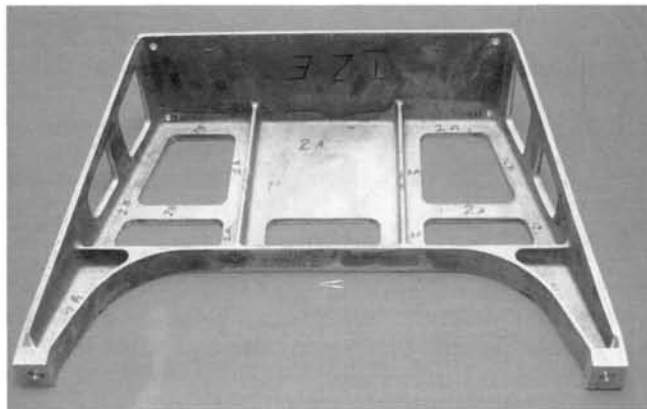


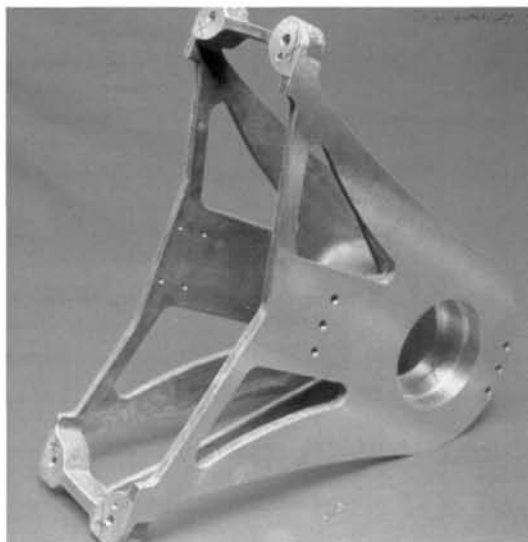
**Figure 2.16: Aura alloy wheel – PCD108 (Hindalco) used in TATA Indica and Ford Ikon cars**



**U-bracket**



**Interface frame**



**Engine mounting frame**

**Figure 2.17: Premium quality Al-7Si-0.3Mg (A356) alloy castings for Space application (PSLV & GSLV Programmes of ISRO)**

results are reported regarding modification effect, the fading behaviour and the optimum amount of calcium for modification. The formation of Ca compound,  $\text{CaSi}_2$  in Al-Si alloys with a Ca concentration greater than 500 ppm, detrimentally influences the mechanical properties of these alloys. Hence, there is a critical concentration of calcium up to which it is beneficial as a modifier in Al-Si alloys and beyond that it is harmful. In addition, modification of eutectic silicon by Ca does not occur below a critical cooling rate, regardless of the Ca concentration. Further, the mechanism of modification by Ca is considered to be similar to that of Na<sup>165, 267</sup> and needs further investigation.

Similarly, contradictory results have been observed in the case of hydrogen pick-up in Ca modified Al-Si melt. Some authors have found that Ca does not add hydrogen to the melt but increases the amount of microporosity and reduces the quantity and size of the macroporosity whereas others have observed hydrogen pick-up. In the case of Sr modified Al-Si melts, it has been reported that Sr does not alter the regassing rate of melts and it ties up with the additional hydrogen in the melt as hydrides.<sup>268</sup> Since the values of free energy of formation of  $\text{SrH}_2$  and  $\text{CaH}_2$  are of the same order viz., -14.63 and -14.76 kcal/mole respectively, like Sr, Ca at very low levels may tie up with the hydrogen present in the melt as hydrides leading to low porosity. Beyond this critical level of Ca, Ca containing oxide film formed ruptures the protective  $\text{Al}_2\text{O}_3$  film leading to faster pickup of hydrogen. It may also be noticed that the technique used by individual researcher, namely inert gas-melting (sintering)<sup>128</sup> and Alscan<sup>135</sup> methods for hydrogen measurement is different. Hence, the effect of Ca on the hydrogen pickup by aluminium melts is still in dispute and needs further investigation.

Calcium interacts with other elements present in aluminium alloys. It scavenges Sb from secondary Al alloys. However, admixtures of Li and Ca in Al alloys affect the alloy characteristics degrading their properties. The simultaneous presence of both Sr and Ca in the melt results in deleterious calcium-strontium interactions. On the other hand, calcium addition results in an additive effect on Sr modification and reduction in quantity and size of pores.<sup>135</sup> These observations are to

be taken into account for better understanding of the roles of Ca in Al-Si-Mg alloys.

It is evident<sup>39</sup> that only a very small amount of Ca (0.004% = 40 ppm) is sufficient to improve the tensile properties, fracture toughness, fatigue strength and impact properties of even high iron containing Al alloys. Apart from changing the morphology of the platelet Fe phase, since Ca also modifies the eutectic silicon, a combined effect of iron neutralization and eutectic modification can be achieved by Ca addition (40 ppm) to Al alloys having high Fe content. Except for the observation by Kobayashi et al,<sup>39-42</sup> there appears to be no comprehensive investigation on the effect of Ca on Fe-intermetallics in Al-Si casting alloys. Be and Mn are the most effective iron neutralizers in Al-Si cast alloys. Since Be is toxic, foundrymen are reluctant to use even small quantities of Be. Hence, efforts have been made to minimise its amount by combining with other elements. Higher amounts of Mn lead to sludge formation which is deleterious to the properties of the alloys. Ca in combination with Be and Mn can give better properties than both of these elements added individually. Till date, no work has been done on the combined addition of trace amount of Be, Mn and Ca. Further investigation needs to be carried out to study the effect of Ca as an iron neutralizer and its combined effect with Be and other alloying elements in high Fe containing Al alloys. The mechanism of Fe-neutralization by Ca addition also needs to be understood.

## 2.8 SUMMARY

Properties of Al are usually enhanced by the addition of the major alloying elements such as Cu, Si, Mg, Mn, Zn, Li, Ni, and then subjecting the alloys to various thermal, mechanical and thermomechanical treatments. Some of the minor alloying elements added to aluminium are Na, Sr, Sb, Ba, Ca, Be, Mn, Cr etc., to induce specific changes in the microstructure. Iron is the most deleterious impurity element found in cast aluminium alloys since it forms different intermetallic compounds with Al, Si and other elements. Of these,  $\beta$  phase ( $Al_5FeSi$ ) is the most detrimental one in degrading the mechanical properties especially ductility. The ill effects of iron can be neutralized by either increasing the cooling rate or superheating the melt or adding trace elements or low temperature working process. Among these, neutralization by trace element addition is commonly practiced. Be, Cr, Mn, Co, and Rare Earths changes the morphology of platelet iron intermetallic compound to harmless shapes

and improves the mechanical properties. Ca and Sr modify the eutectic Si and refine the platelet iron intermetallic compounds thereby improving the mechanical properties. A study on the role of Ca in Al alloys and their composites reveals its potential in enhancing certain important properties. However, a number of aspects remain unclear and unanswered requiring detailed investigation for understanding. Some of them are: The fading characteristics of Ca in Al-Si melts and the exact mechanism for modification of eutectic silicon by Ca and contradicting views on the influence of Ca on hydrogen pickup by aluminum melts. Since Be is toxic, attempts have been made to reduce the amount of Be by combining with other elements. Till date, no work has been done on the combined addition of Be and Mn with Ca. Further investigation needs to be carried out to study the effect of Ca as an iron neutralizer and its combined effect with Be and other alloying elements in high Fe containing Al alloys.

## **2.9 SCOPE OF THE PRESENT INVESTIGATION**

Cast Al-Si alloys have widespread applications for structural components in the automotive, aerospace, and general engineering industries because of their excellent castability, corrosion resistance and high strength-to-weight ratio in the heat treated condition in particular. However, the use of these cast alloys is still limited in comparison with wrought alloys, even though casting would be a more economical production method. Aluminium alloys make up about 78% of the structural weight of commercial aircraft, of which castings comprise only about 6%. Better quantitative understanding of the microstructure-property relationships in cast Al alloys coupled with improved foundry practice will allow wider application of reliable castings in low mass structures. Further, in commercial purity aluminium there are many naturally occurring impurities that can only be removed at great cost. Iron is probably the most important one of these elements and detrimental impurity in cast aluminium and its alloys and degrades the mechanical properties and fracture toughness. The cost of aluminium alloys is inversely related to its Fe content. Indian commercial grade Al is well known for its higher iron content and an understanding on the effects of Fe on its alloys is a prerequisite for getting the best mechanical properties. Among the various methods available to neutralize the ill-effects of iron, neutralization by adding trace elements such as Mn, Cr and Be is commonly practiced. Mn is the most

commonly used and least expensive element. However, Be is carcinogenic and the higher amounts of Mn and Cr required for neutralization lead to sludge formation affecting machinability. Recent investigations<sup>27, 39-42, 241, 251-254, 258</sup> have revealed the importance of eutectic Si modifiers for iron neutralization. However, very little work has been carried out using modifiers viz., Ca and Sr in Al-7Si-0.3Mg alloy, a commercially important alloy. In view of the fact that, modification is normally carried out as a rule, and Fe content is unavoidable in Al-Si alloys, looking at Ca and Sr and their combination with other elements used as Fe neutralizers would certainly be worthwhile.

The objectives of the present investigation are:

- (i) To study the dual roles (modification and Fe-neutralization) of Ca in Al-7Si-0.3Mg alloy
- (ii) Effect of Be, Mn and Sr as Fe neutralizers in Al-7Si-0.3Mg-xFe alloy
- (iii) Comparison and interaction of the effect of Be, Mn, Ca and Sr added Al-7Si-0.3Mg alloy at a constant Fe content on the morphological change of  $\beta$ -phase and the tensile and impact properties.

---

---

## CHAPTER 3

### MATERIALS AND EXPERIMENTAL DETAILS

---

---

#### 3.1 MATERIALS

Commercial grade Al-7Si-0.3Mg (LM25/356) alloy was used as the base alloy. The chemical composition of the alloy is given in Table 3.1. Required amounts of Ca, Be, Mn, Sr and Fe were added in the form of Al-10% Ca, Al-5% Be, Al-10% Mn and Al-10% Sr master alloys and ALTAB Fe compact (75% Fe and 25% Al) respectively.

Table 3.1: Chemical composition (wt.%) of the Al-7Si-0.3Mg (LM25/356) alloy

Si	Fe	Cu	Mn	Mg	Ni	Zn	Sn	Pb	Ti	Balance
7.0	0.2	0.1	0.3	0.35	0.1	0.1	0.05	0.1	0.25	Al

#### 3.2 MELTING AND CASTING

The alloy was melted in clay graphite crucibles of varying sizes in an electric resistance furnace. Standard fluxing and degassing procedures using proprietary salt fluxes and hexachloroethane tablets respectively were employed. For Fe-neutralization experiments, pre-alloyed ingots of Al-7Si-0.3Mg-xFe were prepared in 20 kg capacity crucible using ALTAB Fe compact (75% Fe and 25% Al). For all the experiments, the processing temperature of the melt ranged between 993-1013 K. Further details about processing are given in the individual chapters.

The alloying additions in the form of master alloys were immersed in the melt at  $1003 \pm 5$  K using coated and preheated mild steel plunger and stirred for 2-3 minutes to enable complete dissolution and homogenization and the melt was held at this temperature for about 20 minutes (holding time). The melt was thoroughly

stirred, skimmed and poured (pouring temperature ranged between 993-1003 K) into a preheated rectangular permanent mould (preheat temperature 573 K) and cylindrical permanent and sand moulds (preheat temperatures 473 and 573 K respectively). Figures 3.1 and 3.2 show the dimensions of the moulds used and castings made respectively.

### 3.3 HEAT TREATMENT

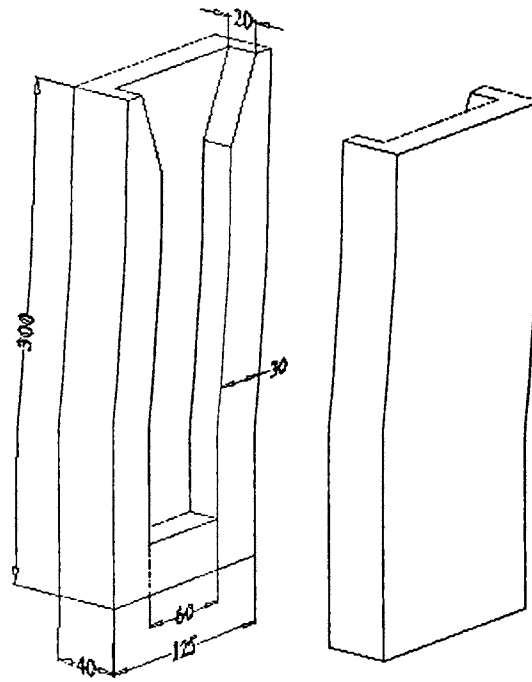
Al-7Si-0.3Mg is a precipitation hardening alloy. The common heat treatment procedure applied is solution treatment followed by quenching in warm water and then precipitation or age hardening (T6 condition). The prescribed<sup>269</sup> solution treatment schedule is at 798-818 K for 12 hrs and age hardening at 428-448 K for 8-12 hrs. In the present work all the tensile and impact specimens were solutionised at 808 K for 12 h, quenched in warm water (353 K) and aged at  $438 \pm 5$  K for 8 h prior to tensile and impact testing.

### 3.4 CHEMICAL ANALYSIS

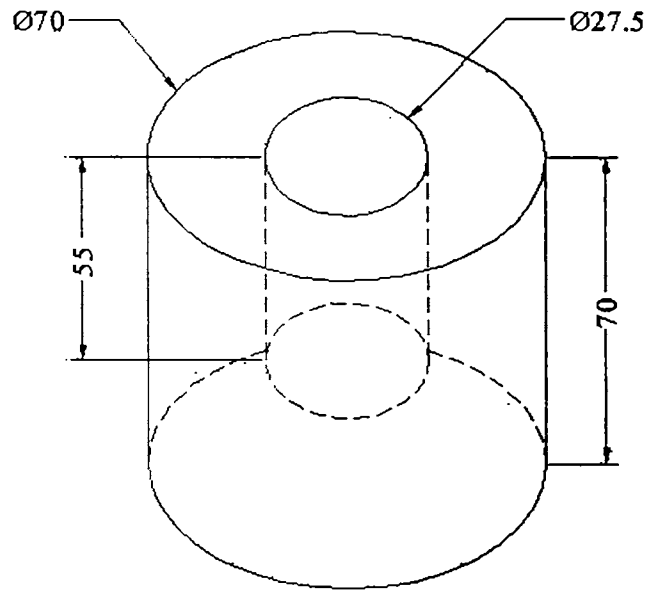
The chemical analysis of the alloys studied (representative sample chips taken by drilling) were measured by ASTM E 34 and Instrumental- Inductive Coupled Plasma (ICP) analyzer elsewhere. Recovery of about 90 and 75-80% was obtained with Fe and Ca and Sr additions respectively.

### 3.5 THERMAL ANALYSIS

In thermal analysis, the cooling curve of a solidifying sample is recorded as it cools from liquid state through the solidification range to solid. Thermal analysis was carried out using MeltLab Aluminium Thermal Analyser (Figure 3.3). The molten metal (about 100g) was poured into a preheated standard steel cup at  $993 \pm 5$  K. The solidification rate from the initial melt temperature was  $1.5^\circ$  K/min. Thermocouple was placed at the centre of the cup and connected to a computer through an analog/digital converter. The computer software program reads the temperature in real time and plots a cooling curve on the monitor. For each melt, two cooling curves were recorded to ensure the quality of the results. The liquidus temperatures, eutectic temperature as well as the temperatures of formation of other precipitating phases were determined from the cooling curves. Additionally, metallographic examinations

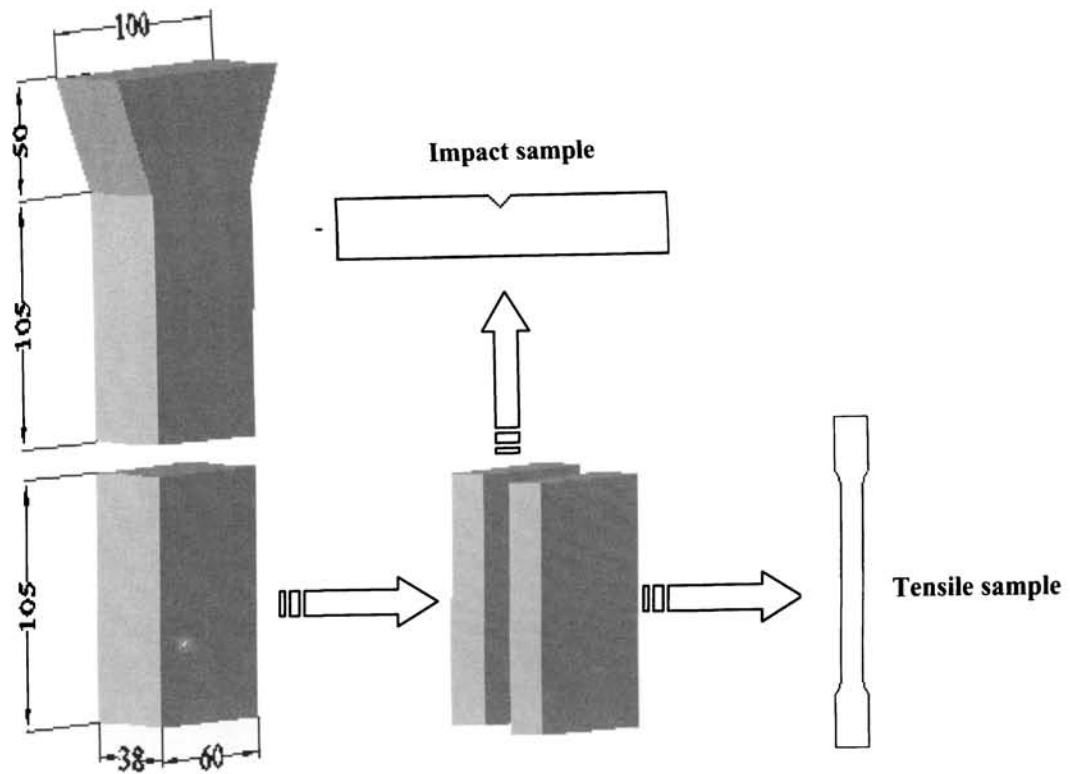


(a)

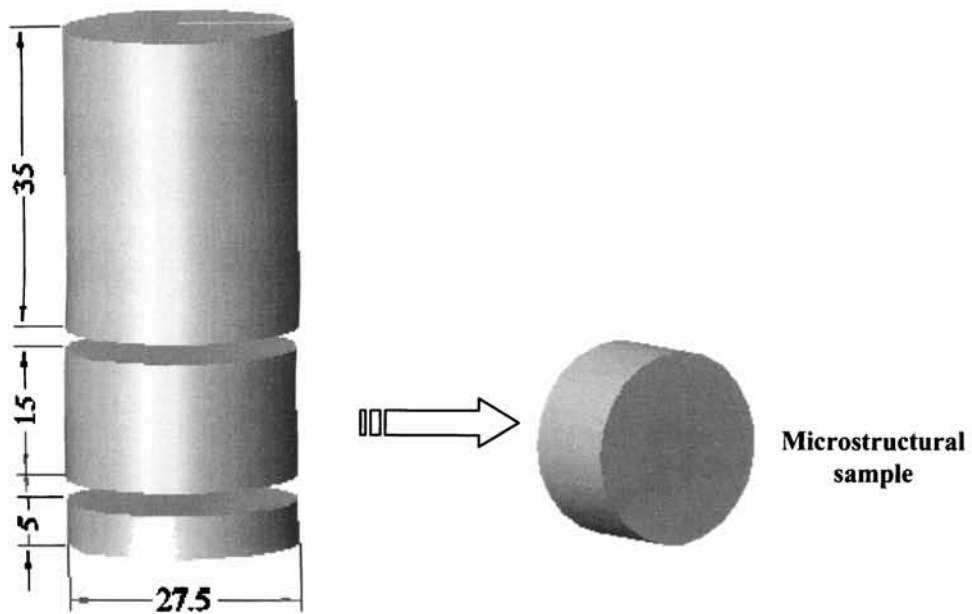


(b)

**Figure 3.1: Dimensions of (a) Rectangular slab mould and (b) Cylindrical mould used (All dimensions in mm)**



(a)



(b)

Figure 3.2: Dimensions of (a) Rectangular slab casting and (b) Cylindrical casting (All dimensions in mm)



**Figure 3.3: MeltLab Aluminium Thermal Analyser**

were carried out to correlate the results of thermal analysis with the corresponding microstructures. The specimens were polished near the thermocouple region and etched for microstructural observation.

### 3.6 DIFFERENTIAL THERMAL ANALYSIS (DTA)

The samples were subjected to differential thermal analysis using a SETSYS apparatus from SETARAM (Figure 3.4). The DTA signal was recorded both on heating and cooling at the scanning rate of 2° K/min over the temperature range from 313 to 1073 K. After a sample has been introduced in the sample crucible, this latter was evacuated and filled with argon twice. A low argon flux was then fixed and heating started. Each sample was analyzed twice to check the repeatability.

### 3.7 PHYSICAL CHARACTERISTICS

#### 3.7.1 Density Measurement and Porosity Calculation

The density of the samples was measured using Archimedes' principle and computed using the expression given below:

$$\rho = \frac{W_a \rho_l - W_l \rho_a}{W_a - W_l} \dots\dots\dots (3)$$

where 'W' is the weight and the subscripts 'a' and 'l' refer to air and liquid (water in the present work). From the density values, the % porosity can be calculated using the following expression:

$$\% Porosity = \frac{(Theoretical\ density - Measured\ density)}{Theoretical\ density} \times 100 \dots\dots\dots (4)$$

#### 3.7.2 Electrical Conductivity

The electrical conductivity of the alloys was carried out using 'TECHNOFOUR' conductivity meter type 901 (Figure 3.5). The instrument works on the principle of eddy currents. The probe induces eddy currents of a fixed frequency

in the test part. The magnitude of these eddy currents is directly proportional to the electrical conductivity of the metal. These eddy currents generate their own electromagnetic field which affects the electrical-impedance of the probe. Thus, conductivity can be measured by measuring the corresponding changes in the probe impedance. It reads the conductivity in percentage of International Annealed Copper Standards, in the range of 10-110% IACS. The instrument was standardised often by setting the instrument for the reference copper plates of 99% IACS and 17% IACS for accuracy.

### **3.8 MECHANICAL CHARACTERISTICS**

The rectangular (210 x 60 x 38 mm) casting was used for making tensile and V-notch impact specimens. Figure 3.1 shows the dimensions of tensile and impact specimens. Tensile and impact testing were carried out in an Instron Universal Testing Machine at a cross head speed of 2 mm/min and Pendulum type Charpy Impact Testing Machine (PSW-423) respectively. For each composition, four tensile and impact specimens were tested and the average value was computed.

### **3.9 STRUCTURAL STUDIES**

The structural features of the samples have been characterized using optical microscopy, Image Analyzer, Scanning Electron Microscopy, Energy dispersive X-ray spectroscopy and Electron Back Scattered Diffraction analyzer.

#### **3.9.1 Optical Microscopy**

The specimens for microscopic examination were machined out from the cylindrical castings [Figure 3.2(c)]. Additionally, metallographic examinations were carried out in the thermal analysis samples (near the thermocouple region). The samples were ground with emery papers of progressively fine grade 80, 220, 400 and 600 grits. The samples were turned through 90° between papers and washed thoroughly with water before proceeding from one paper to the next. Final polishing was performed in rotating discs of proprietary cloth (Selvyte cloth) charged with diamond paste of 6, 3 and 0.25 μm particle size in sequence. Then the samples were washed thoroughly with water and dried. The samples were etched in 0.5% HF solution (0.5mlHF in 99.5ml water). Leitz metalloplan optical microscope was used for metallographic analysis.



**Figure 3.4: DTA equipment**



**Figure 3.5: TECHNOFOUR' conductivity meter**

### **3.9.2 Image Analysis**

Quantitative analysis of the microstructure was done using a Leica 2001 image analyzer in conjunction with the optical microscope. The silicon particle characteristics (length, breadth, area, aspect ratio, equivalent diameter and density) were measured. The fields of observations were selected randomly at different locations of the sample. The size of  $\beta$ -Fe intermetallic phase was measured manually. In each case, at least ten fields were analyzed from a single specimen and the average was computed.

### **3.9.3 Scanning Electron Microscopy (SEM)/ Energy Dispersive X-ray Spectroscopy (EDS)/Electron Back Scattered Diffraction (EBSD)**

The microstructures of the polished and fractured sample surfaces were examined using 'JEOL' Scanning Electron Microscope. The various phases observed were identified using Energy Dispersive X-ray Spectroscopy coupled with the SEM. A JEOL-6460LA Scanning Electron Microscope equipped with an HKL EBSD analyzer was used for studies by EBSD characterization. The system was operated at 20 keV with the sample tilted to 70°. The sample preparation includes mechanical thinning of small specimens, polishing to a 1  $\mu\text{m}$  finish and then ion beam milling. Ion beam milling was conducted with 4kV  $\text{Ar}^+$ , 10° beam tilt for 2 hours, and cooling with liquid  $\text{N}_2$ .

---

---

## CHAPTER 4

### EFFECT OF CALCIUM IN Al-7Si-0.3Mg ALLOY

---

---

Initially, Ca has been considered as one of the deleterious elements in aluminum and its alloys and hence techniques have been developed for its removal.<sup>32</sup> Calcium, entering the aluminum casting alloys along with the addition of silicon and appearing as calcium silicides, calcium phosphides and calcium nitrides, which are considered to be harmful, requires removal to levels below 0.003% (30 ppm) and preferably below 0.001% (10 ppm).<sup>30</sup> However, Ca introduced in the elemental form modifies the eutectic silicon in Al-Si alloys,<sup>30-37</sup> improves the fracture toughness and impact properties of high iron containing recycled aluminum alloys,<sup>27, 39-42</sup> scavenges the effect of Sb from secondary alloys,<sup>43, 44</sup> imparts superplastic properties,<sup>45-49</sup> and enables production of aluminum foams<sup>50-55</sup> and aluminum metal matrix composites.<sup>56-64</sup> Aluminum alloys containing Ca as an intentional alloying element are applied industrially in the form of sacrificial anodes, bearings, electrolytic capacitor cathode foils, packaging and others.<sup>65-86</sup> The present study aims to investigate the first two beneficial effects of calcium viz., modification and Fe-neutralization on the structure and properties of Al-7Si-0.3Mg and Al-7Si-0.3Mg-xFe alloys respectively.

#### 4.1 MODIFICATION

##### 4.1.1 Methodology

Al-7Si-0.3Mg alloy was used as the base alloy. For each experiment, about 3-4 kg of the alloy was melted in a clay-graphite crucible of 10 kg capacity using an electric resistance furnace. The required amounts of calcium in the form of Al-10% Ca master alloy to make calcium levels in the range 0-0.05% were immersed in the melt at 1003 K using coated and preheated mild steel plunger and stirred for 2-3 minutes to enable complete dissolution and homogenization and the melt was held at this temperature for about 20 minutes (holding time). The modification effect of Ca

has been compared with the well known modifier viz., Sr (0.02%), which was added in the form of Al-10% Sr master alloy. Figure 3.1 shows the dimensions (in mm) of the moulds used and castings made. The casting and heat treatment procedures are given in chapter 3.

## **4.1.2 Results and Discussion**

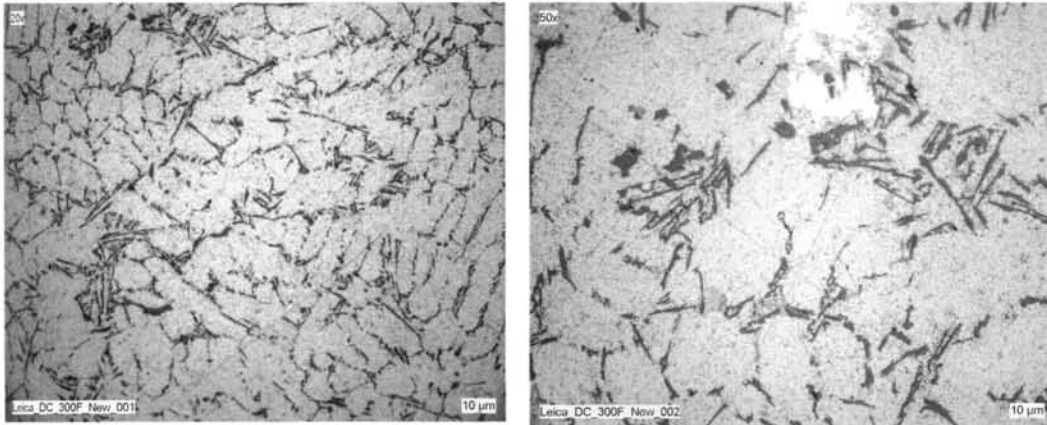
### **4.1.2.1 Microstructure**

Figure 4.1 shows the typical as cast microstructures of Al-7Si-0.3Mg alloy without and with 0.01% Ca, while Figure 4.2 shows those of the alloy treated with 0.02% Ca, 0.05% Ca and 0.02% Sr. It is seen that in Figure 4.1(a), eutectic Si particles are in coarse acicular and platelet form. Only partial modification has been observed in the alloy treated with 0.01% Ca [Figure 4.1(b)]. However, 0.02% Ca shows a modified eutectic Si structure [Figure 4.2(a)]. On the other hand, 0.05% of Ca addition has yielded a very fine fibrous eutectic Si [Figure 4.2 (b)] as well as leads to the formation of an Al-Ca-Si compound which is identified as  $\text{Al}_2\text{CaSi}_2$  by SEM/EDX analysis (Figure 4.3). When comparing the effects of Ca and Sr additions, it has been observed that Sr addition leads to very fine globular eutectic Si. On the other hand, Ca addition leads to the formation of both network and individual globular eutectic Si. Quantification of the silicon particle characteristics using image analysis in the as cast Ca added Al-7Si-0.3Mg alloys could not be done because of the formation of eutectic Si in networks of fibrous form, wherein the identification of individual Si is difficult.

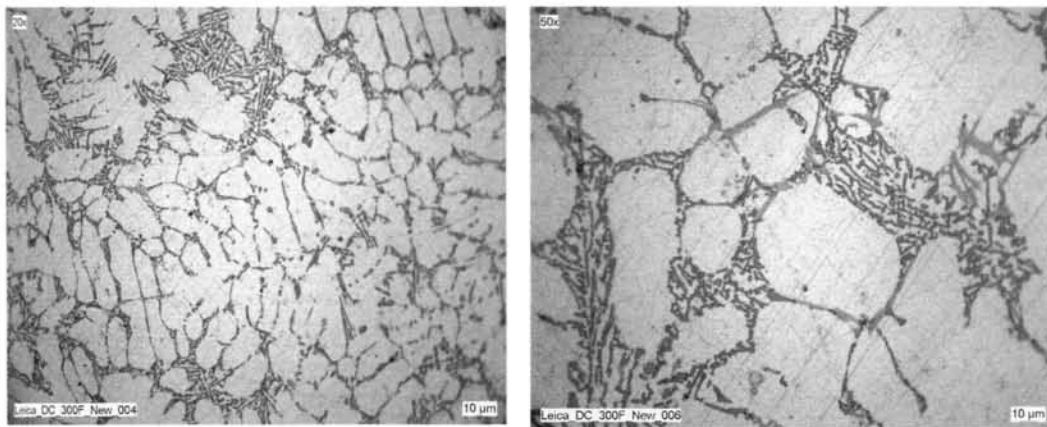
### **4.1.2.2 Physical Characteristics**

#### *Porosity and electrical conductivity*

Table 4.1 shows the effects of various amounts of calcium on the porosity and electrical conductivity of Al-7Si-0.3Mg alloy. It is seen that the % porosity increases as the calcium content increases. The increased porosity at higher Ca levels may be due to the increased melt affinity for gas absorption. When comparing the porosities of 0.02% Ca and Sr added Al-7Si-0.3Mg alloys, it is seen that the porosity with Sr addition is higher than that with Ca addition.

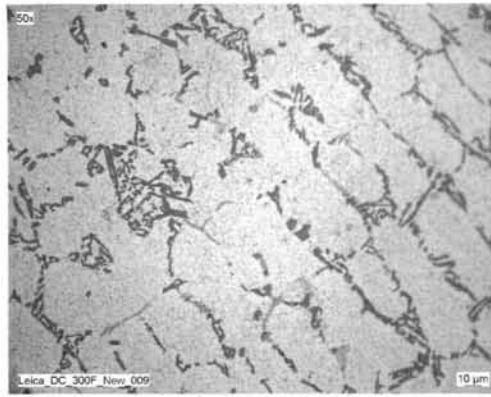


(a)

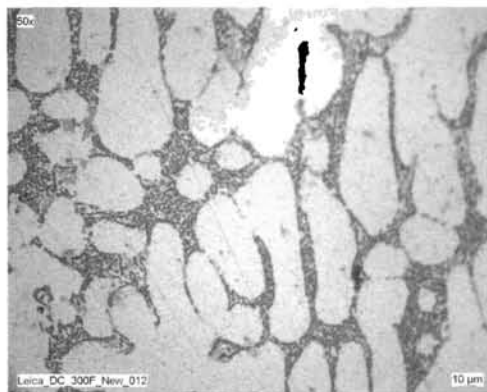


(b)

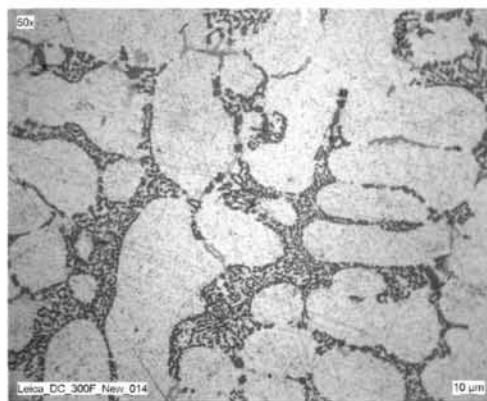
**Figure 4.1: Typical as cast microstructures of Al-7Si-0.3Mg alloy treated (a) without and (b) with 0.01% Ca**



(a)

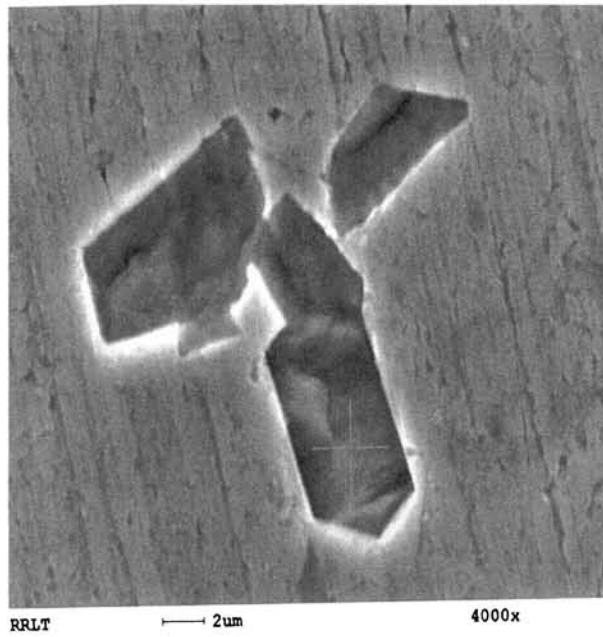


(b)

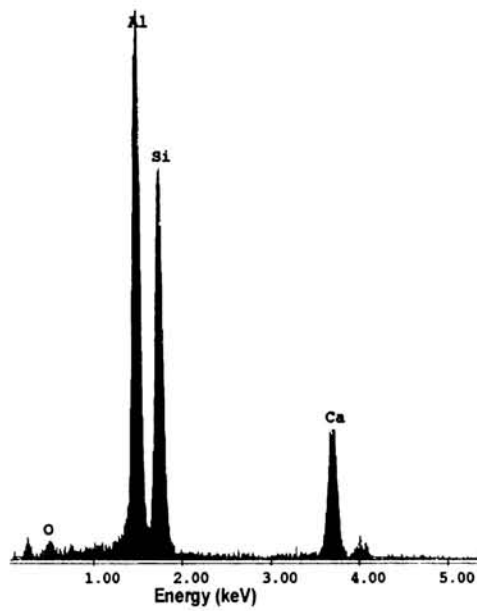


(c)

**Figure 4.2: Typical as cast microstructures of Al-7Si-0.3Mg alloy treated (a) 0.02% Ca (b) 0.05% Ca and (c) 0.02% Sr**



(a)



(b)

**Figure 4.3: (a) SEM photograph of  $\text{Al}_2\text{CaSi}_2$  phase in Al-7Si-0.3Mg alloy treated with 0.05% calcium (b) EDS spectra showing the distribution of Al, Si and Ca in  $\text{Al}_2\text{CaSi}_2$  phase**

**Table 4.1: % Porosity and Electrical Conductivity of Al-7Si-0.3Mg alloy treated without and with Ca**

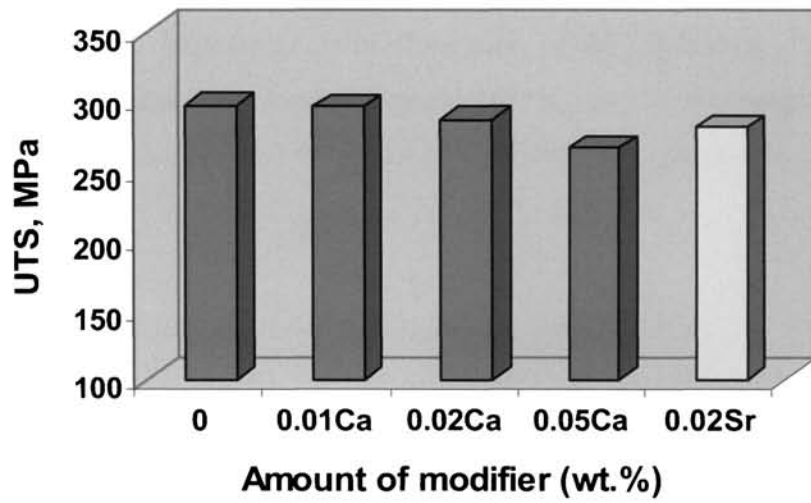
Alloy	% Porosity	Electrical Conductivity
Al-7Si-0.3Mg	1.47	31.2
Al-7Si-0.3Mg + 0.01% Ca	1.40	34.8
Al-7Si-0.3Mg + 0.02% Ca	1.68	35.5
Al-7Si-0.3Mg + 0.05% Ca	2.84	33.9
Al-7Si-0.3Mg + 0.02% Sr	2.08	35.0

It is seen that Ca and Sr additions have increased the electrical conductivity (in %IACS) compared to the untreated alloy. This is due to the modification of eutectic Si by Ca addition, which allows easier flow of electrons compared to the untreated alloy, where the platelet morphology of eutectic Si poses serious impediment to the flow of electrons. On the other hand, the decrease in conductivity with increasing calcium contents may be due to the higher amount of porosity present in the samples. Nevertheless, the conductivity values of Ca treated alloys are still higher than that of an untreated or unmodified alloy. When considering the effect of porosity on %IACS, it is evident from the Table 4.1 that porosity has a significant effect on %IACS. Though a very fine fibrous eutectic Si structure is obtained with 0.05% Ca addition, the presence of higher porosity has reduced the %IACS.

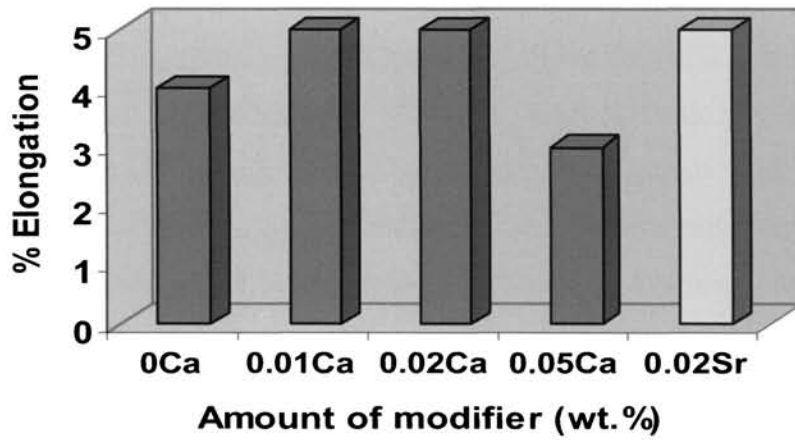
#### **4.1.2.3 Mechanical Properties**

##### *Tensile properties*

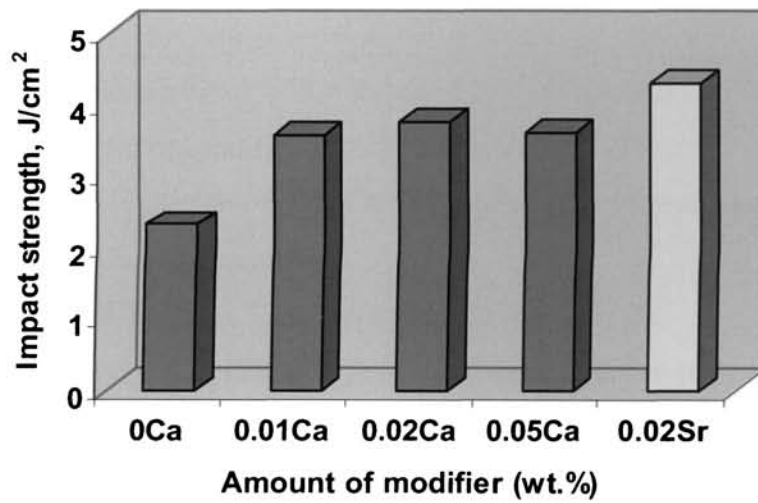
The effect of calcium on the tensile properties of T6-heat treated Al-7Si-0.3Mg alloy is shown in Figures 4.4 (a) and (b). Comparing the tensile strengths of Al-7Si-0.3Mg alloy treated with and without Ca and Sr, it has been observed that the tensile strength is decreased marginally with both Ca and Sr. This is due to the higher porosity formation with the above additions. Similarly, comparing Ca and Sr additions, UTS is lower in the case of Sr addition, which is due to the higher porosity



(a)



(b)



(c)

Figure 4.4: Effect of calcium on the (a) UTS (b) % elongation and (c) impact strength of Al-7Si-0.3Mg alloy

associated with Sr added sample. Both Ca and Sr additions lead to a significant improvement (25% improvement) in elongation of Al-7Si-0.3Mg alloy. However, when the Ca content is increased beyond 0.02%, the % elongation is decreased dramatically. This is attributed to the over modification of eutectic Si, presence of Al-Ca-Si intermetallics and also higher porosity in the samples.

#### *Impact strength*

Figure 4.4 (c) shows the impact strength of Al-7Si-0.3Mg alloy with and without Ca and Sr additions. It has been found that Ca and Sr additions improve the impact strength significantly compared to the untreated alloy. Impact strength of Al-7Si-0.3Mg alloy has been improved by 53, 62, 55 and 85% by treating the alloy with 0.01, 0.02, 0.05% Ca and 0.02% Sr respectively. This is due to the modification of platelet eutectic Si to fibrous form. Figure 4.5 shows the SEM micrographs of the fractured surface of impact tested Al-7Si-0.3Mg alloy without and with Ca and Sr. Figure 4.5 (a) shows cleavage pattern typical of brittle fracture while Figure 4.5 (b) shows few dimples along with the cleavage pattern. On the other hand, Figures 4.5 (c)-(e) show more dimples, a characteristic of ductile fracture. Though very fine eutectic Si and more dimples are observed with 0.05% Ca, impact strength is almost the same as that of 0.01% Ca added sample. This is attributed to the detrimental effect of Al-Ca-Si intermetallics at higher calcium content.

#### **4.1.3 Summary**

1. The optimum level of Ca required for modification so as to get the best mechanical properties lies in the range 0.01-0.02%.
2. Like Sr, higher amount of Ca also leads to the formation of higher porosity and Al-Ca-Si intermetallics.
3. At 0.02% addition, Sr shows more porosity than Ca.
4. The properties obtained with Ca modification are at par with those obtained with the well known modifier viz., Sr.

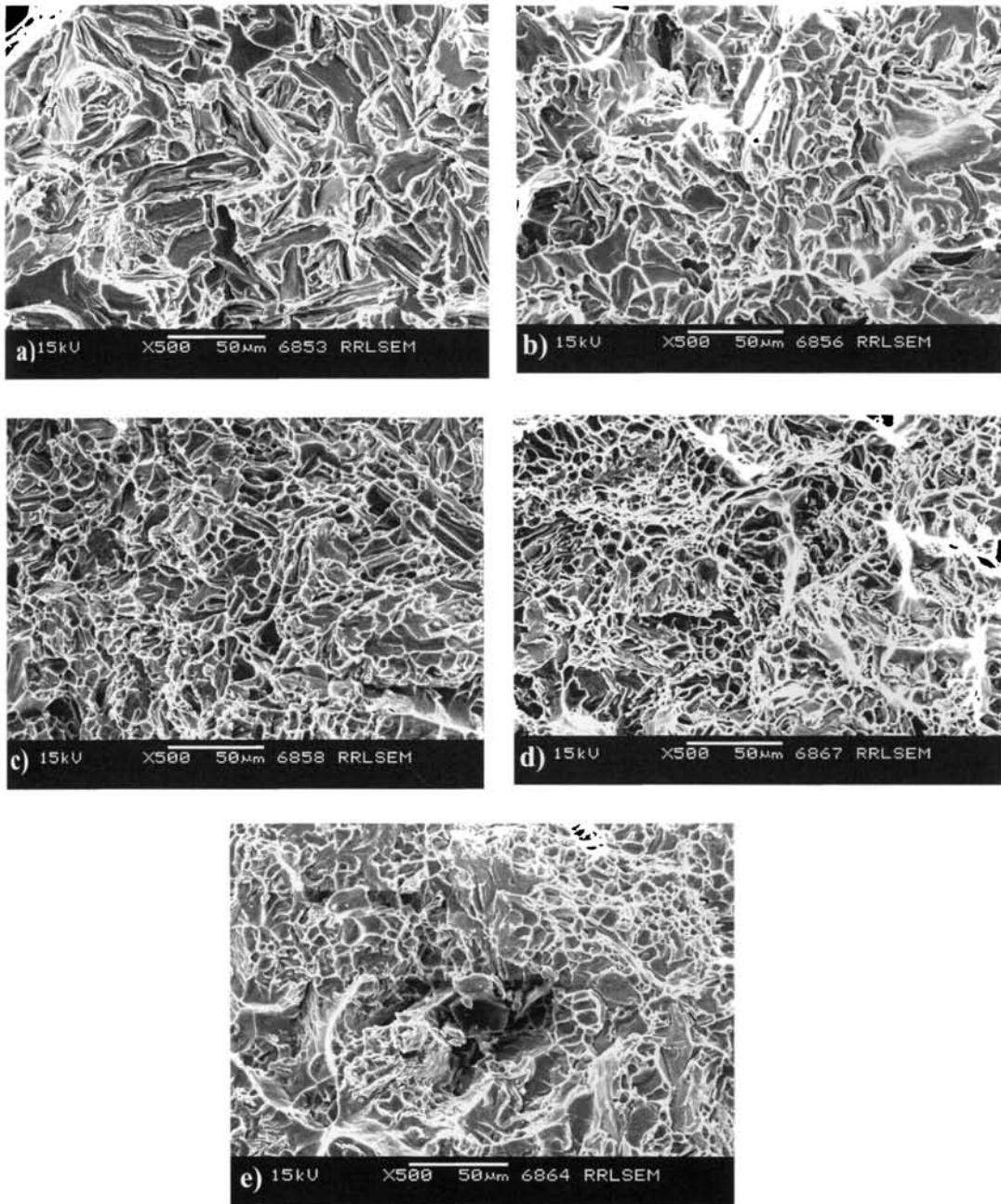


**Figure 4.5: SEM micrographs showing the impact fracture surface of Al-7Si-0.3Mg alloy with and without Ca (a) 0% Ca (b) 0.01% Ca (c) 0.02% Ca (d) 0.05% Ca and (e) 0.02% Sr**

## 4.2 IRON NEUTRALIZATION

### 4.2.1 Methodology

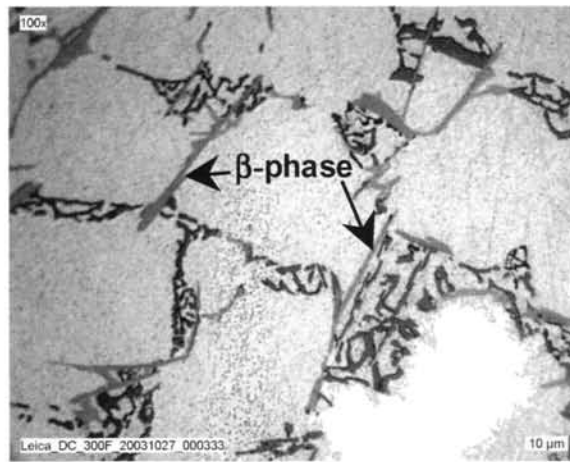
Al-7Si-0.3Mg-xFe ( $x = 0.2 - 0.7\%$ ) alloys were prepared in a 20 kg capacity crucible using ALTAB Fe compact (75% Fe and 25% Al). For each experiment, about 3 kg of the alloy of known iron content was melted in a clay-graphite crucible of 5 kg capacity using an electric resistance furnace. The melt was subjected to fluxing and degassing using commercially available fluxes and degassing tablets respectively. The required amount of calcium in the form of Al-10% Ca master alloy was immersed in the melt at 1003 K using coated and preheated plunger and stirred for 2-3 minutes to enable complete dissolution and homogenization and the melt was held at this temperature for about 20 minutes (holding time). The casting, heat treatment and testing procedures are given in chapter 3. The melt was cast into both cylindrical and rectangular shapes, whose dimensions are given in Figure 3.2.

### 4.2.2 Results

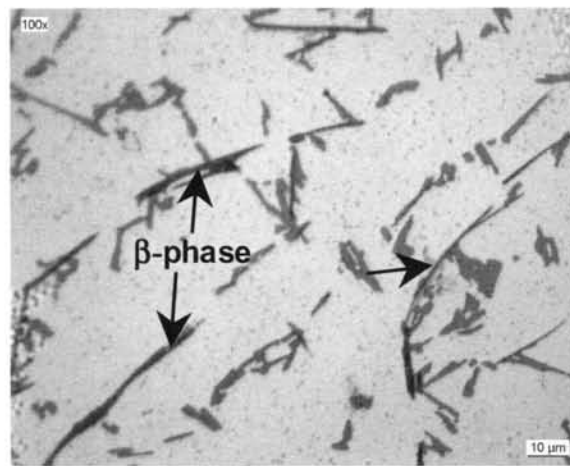
#### 4.2.2.1 Microstructure

Figures 4.6 (a) and (b) show the typical permanent mould as cast microstructures of Al-7Si-0.3Mg alloy with 0.4 and 0.7wt.% Fe contents respectively. It is seen that the microstructure consists of a large number of platelet Fe intermetallics, platelet eutectic Si and primary aluminium. Further, it has been observed that the size and volume fraction of the  $\beta$  phase increases with increasing iron content. The platelet  $\beta$ -phase has been confirmed as  $Al_5FeSi$  by SEM/EDX analysis (Figure 4.7), which agrees well with the reported results.<sup>4, 8</sup>

Figures 4.8 (a-d) show the typical sand cast microstructures of Al-7Si-0.3Mg-xFe ( $x = 0.2$  and  $0.7\%$ ) alloys without and with calcium addition. As observed in the permanent mould cast samples, the size and volume fraction of the  $\beta$ -phase increases when the iron content is increased from 0.2 to 0.7wt.%. This observation has also been confirmed by the significant increase in the average length of the  $\beta$ -needles measured by image analysis with increasing iron content (Figure 4.9). It can also be seen that Ca addition reduces the size of the platelets, which is again confirmed by



(a)



(b)

Figure 4.6: Typical permanent mould as cast microstructures of Al-7Si-0.3Mg alloy with (a) 0.4 and (b) 0.7% Fe

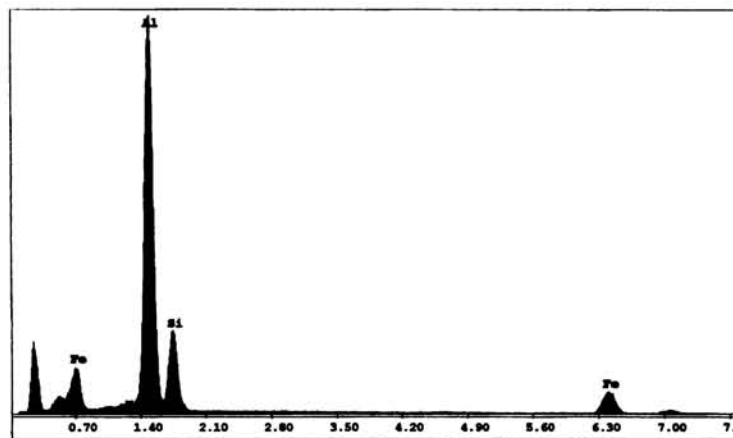
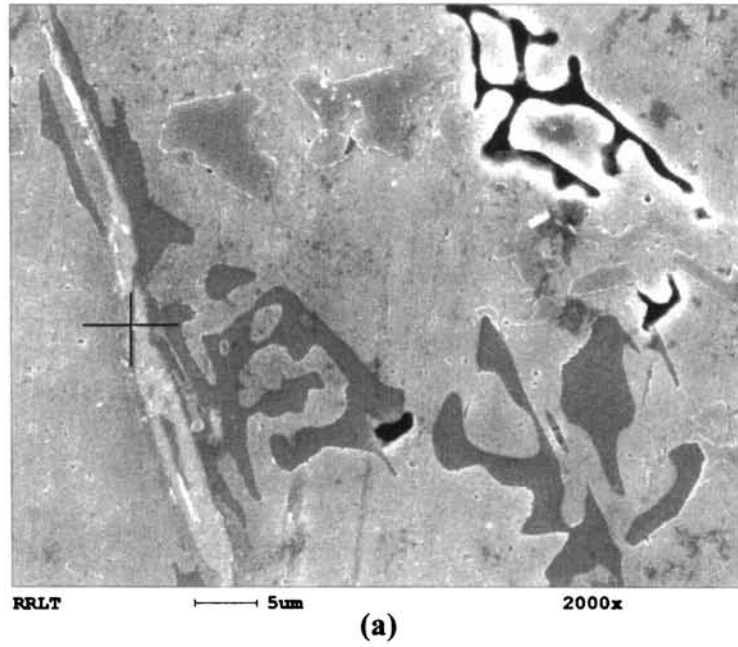
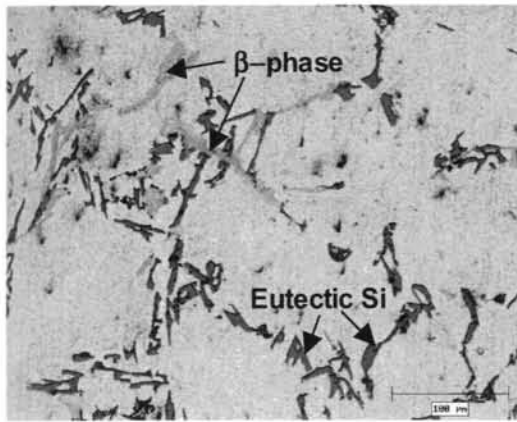
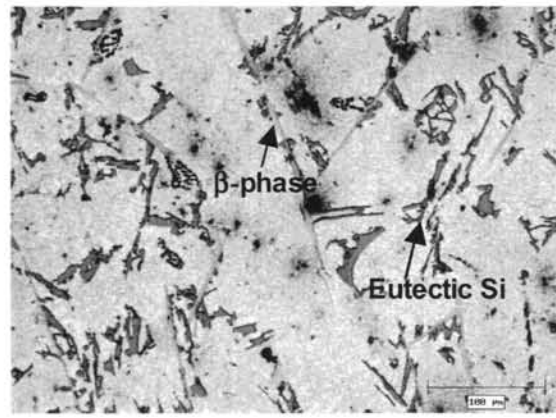


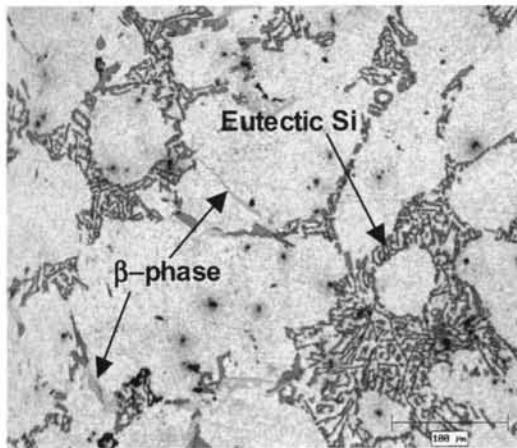
Figure 4.7: (a) SEM photograph of  $\beta$ -phase in Al-7Si-0.3Mg-0.7Fe alloy and (b) EDS spectra showing the distribution of Al, Si and Fe



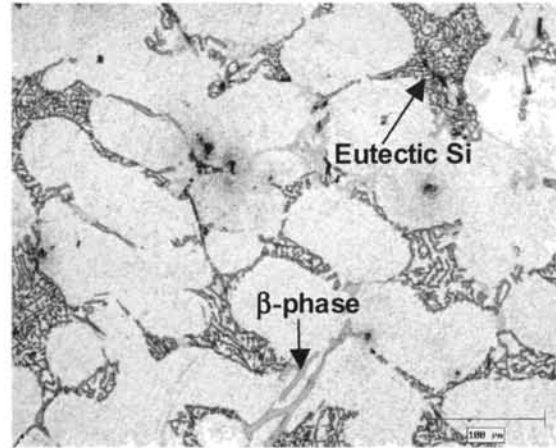
(a)



(b)



(c)



(d)

**Figure 4.8: Typical microstructures of sand cast Al-7Si-0.3Mg alloy with (a) 0.2% Fe, (b) 0.7% Fe, (c) 0.2% Fe + 0.01% Ca and (d) 0.7% Fe + 0.01% Ca in the as-cast condition**

image analysis (Figure 4.9). Further, it has been observed that a higher amount of Ca (0.05%) addition to Al-7Si-0.3Mg-0.6Fe alloy reduces the size of the platelet Fe-intermetallics to very fine form (Figure 4.10). It has also been seen that fine  $\beta$ -platelets are precipitated along with the eutectic Si as clearly shown in the SEM micrograph (Figure 4.11). Moreover, precipitation of Al-Si-Ca intermetallic has also been observed (Figure 4.10) which has been identified by SEM/EDX as  $Al_2CaSi_2$  (Figure 4.12). This result is in agreement with the observations of Ware et al<sup>270</sup> that Ca-containing intermetallics form at high levels of Ca addition.

The eutectic Si in untreated alloys [Figures 4.6 and 4.8 (a) and (b)] is in coarse acicular and platelet form, while it is in fine fibrous form in the alloys treated with calcium [Figures 4.8 (c) and (d) and 4.10]. This shows the modification effect of calcium. Quantification of the silicon particle characteristics in the as cast Ca added alloys using image analysis could not be done because of the formation of eutectic Si in networks of fibrous form, wherein the identification of individual Si is difficult. The microstructures of Al-7Si-0.3Mg-xFe alloys with and without Ca in T6 condition are shown in Figures 4.13 (a) and (b). The eutectic Si particles are more spheroidized by Ca addition [Figure 4.13 (b)], although they are spheroidized to some extent by T6 treatment. This observation has been confirmed by quantitative image analysis and the various parameters measured are given in Table 4.2.

**Table 4.2: Silicon particle characteristics of T6-heat treated samples**

<b>Silicon particle characteristics</b>	<b>Al-7Si-0.3Mg-0.7Fe Alloy</b>	<b>Al-7Si-0.3Mg-0.7Fe + 0.01% Ca alloy</b>
Length ( $\mu\text{m}$ )	$5.83 \pm 3.41$	$5.42 \pm 3.54$
Breadth ( $\mu\text{m}$ )	$3.56 \pm 1.47$	$3.40 \pm 1.67$
Aspect Ratio	$1.61 \pm 0.44$	$1.55 \pm 0.41$
Equivalent diameter ( $\mu\text{m}$ )	$4.12 \pm 1.68$	$3.89 \pm 1.89$

*The  $\pm$  value in each case represents the standard deviation*

Figure 4.14 shows the EBSD mapping result with back-scattered electron image of Al-7Si-0.3Mg-0.2Fe+0.01% Ca sample. If the crystallographic orientation of neighbouring grains of aluminium in eutectic and primary dendrite is less than  $5^\circ$ , the colour of mapping images is identical. The presence of many grains with different orientations in eutectic area of Ca modified specimen (Figure 4.14) indicates the existence of more than  $5^\circ$  orientation difference between neighbouring grains. It is expected that neighbouring aluminium and silicon in the eutectic display the same orientation. The EBSD patterns from aluminium and silicon are very similar since aluminium has a fcc structure and silicon has a diamond structure. In the case of the present measurement, the EBSD program was set for indexing of aluminium EBSD patterns. This mapping result is in good agreement with the results of Nogita et al<sup>166</sup> and Ware et al<sup>270</sup>. This shows the direct evidence of nucleation of the eutectic heterogeneously in the interdendritic liquid and not from the primary dendrites. Further, this suggests that the eutectic nucleated separately in the interdendritic melt, but silicon and aluminium in the eutectic would still be expected to have a common solidification interface.

#### ***4.2.2.2 Physical Characteristics***

##### *Porosity*

The porosity of the sand cast cylindrical samples of Al-7Si-0.3Mg-xFe alloys were calculated as per the details given in chapter 3. Figure 4.15 shows the effect of various amounts of calcium on the porosity of Al-7Si-0.3Mg-xFe alloys and Table 4.3 gives the linear fit equations and the corresponding correlation coefficients. It can be observed that the porosity level of the alloy increases as the iron content increases from 0.2 to 0.7% for all calcium levels linearly with a correlation coefficient near to 1.0 for unmodified and 0.005% Ca added alloys. For the samples treated with 0.01% Ca, it appears that the porosity increases for 0.2-0.4% Fe and then remains constant for 0.4-0.7% Fe. Hence, the fitted equation shows a lower coefficient of correlation of 0.8. Except for the 0.4% Fe + 0.01% Ca sample, the other calcium containing samples showed lower porosity levels than the unmodified samples for each iron level. The porosity for 0.2, 0.4 and 0.7% Fe containing alloys is consistently reduced by the addition of 0.005% Ca, which may be attributed to the degassing effect produced by low levels of calcium. Beyond this critical level of Ca, Ca containing oxide film

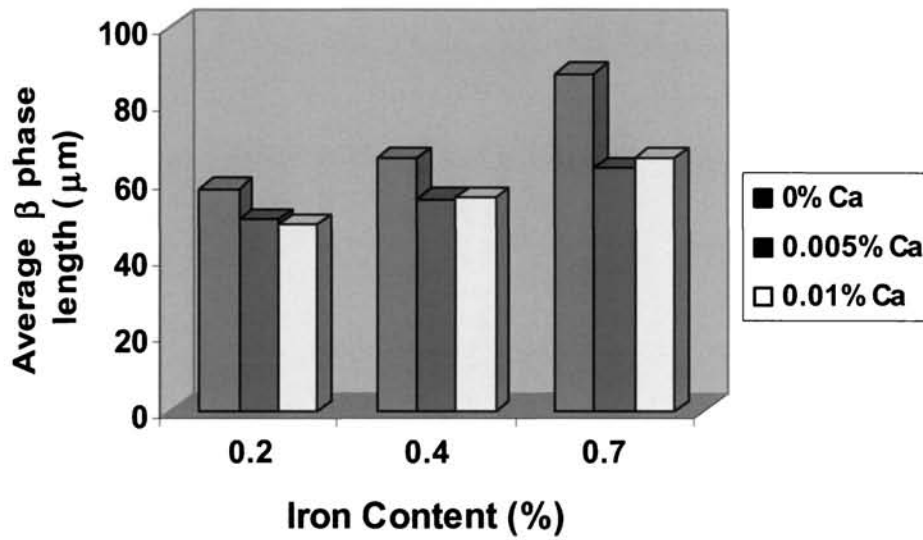


Figure 4.9: Effect of Ca addition on the average length of the  $\beta$ -phase particles in sand cast Al-7Si-0.3Mg-xFe alloy

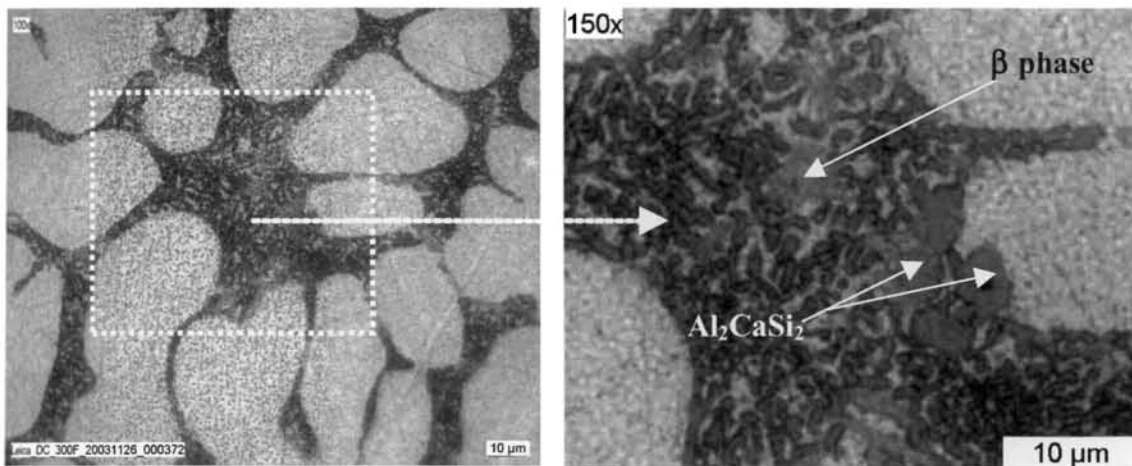
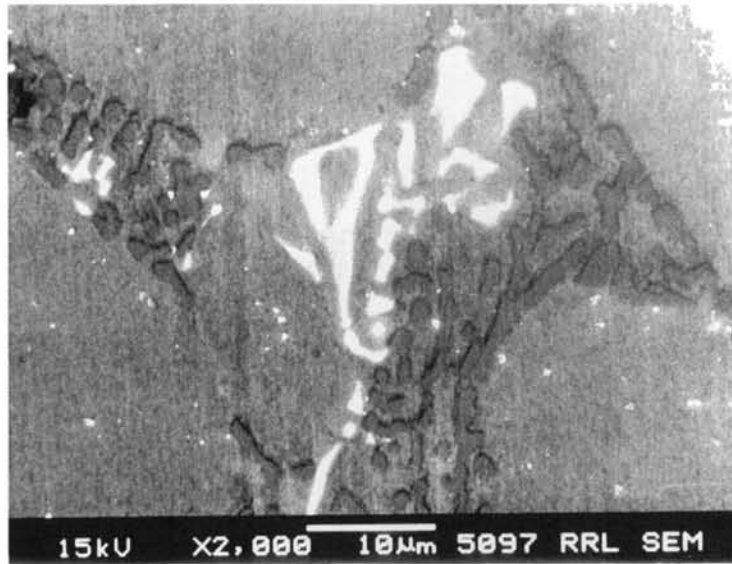
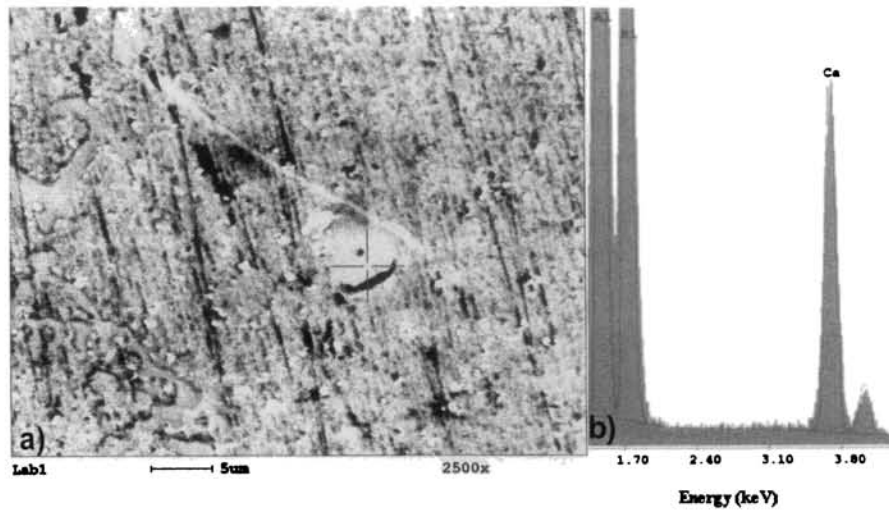


Figure 4.10: Typical microstructures of Al-7Si-0.3Mg-0.6Fe alloy treated with 0.05% Ca



**Figure 4.11: SEM micrograph showing very fine Fe intermetallic phases in Al-7Si-0.3Mg-0.6Fe alloy with Ca (0.05%) addition**



**Figure 4.12: (a) SEM micrograph showing the formation of  $\text{Al}_2\text{CaSi}_2$  phase in Al-7Si-0.3Mg-0.6Fe alloy with Ca (0.05%) addition (b) EDS spectrum showing Al, Si and Ca distributions.**

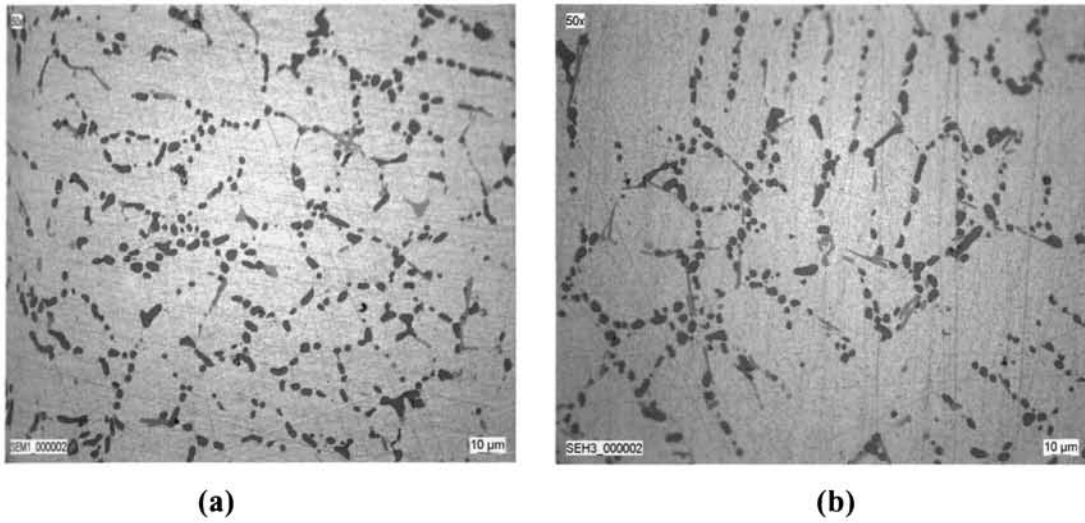


Figure 4.13: Typical microstructures of permanent mould cast Al-7Si-0.3Mg-0.7Fe alloy in T6 condition (a) without and (b) with 0.01% Ca

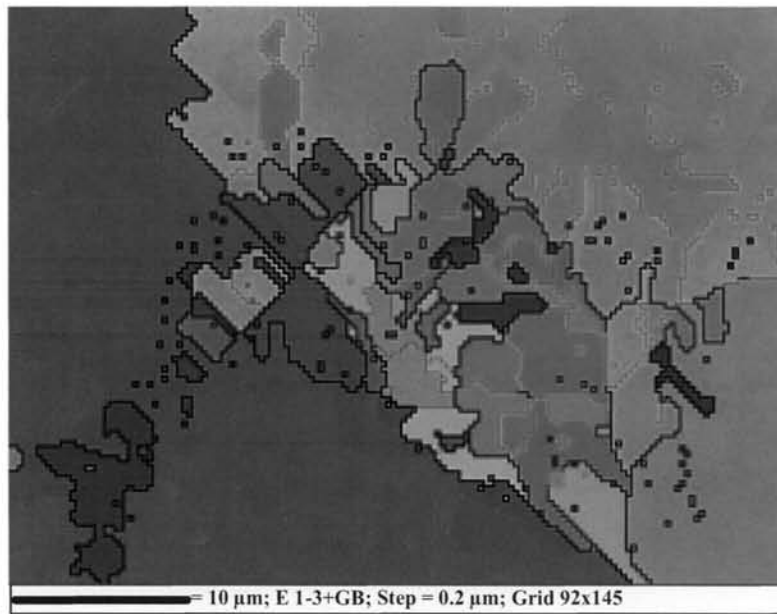


Figure 4.14: EBSD mapping results of Al-7Si-0.3Mg-0.2Fe+0.01% Ca alloy

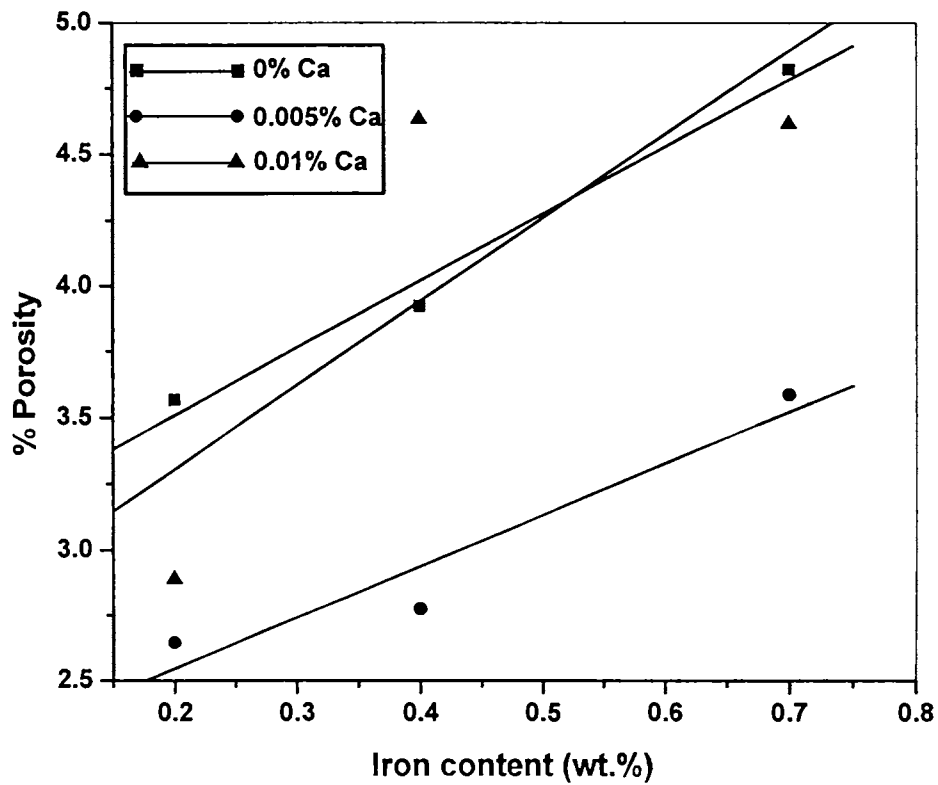


Figure 4.15: Effect of Ca on the % porosity of Al-7Si-0.3Mg-xFe alloy

Table 4.3: Fitted equation and the correlation coefficient for the plot of % porosity versus % Fe content at various Ca levels

Amount of calcium (wt.%)	Fitted equation	Correlation coefficient, $R^2$
0	% Porosity = 2.9998 + 2.5490 (% Fe)	0.9914
0.005	% Porosity = 2.1539 + 1.9571 (% Fe)	0.9609
0.01	% Porosity = 2.6698 + 3.1766 (% Fe)	0.7976

might have caused ruptures in the usually protective  $\text{Al}_2\text{O}_3$  oxide film, leading to faster pickup of hydrogen. Figures 4.16 (a) and (b) are the optical and SEM micrographs of platelet/needle like Fe intermetallic compound observed inside a shrinkage pore in Al-7Si-0.3Mg-0.7Fe alloy.

#### *Electrical conductivity*

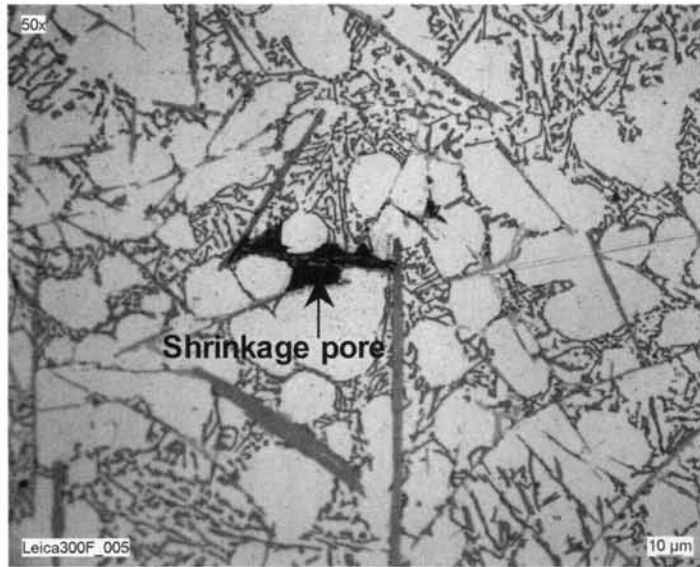
Figure 4.17 shows the effect of calcium on the electrical conductivity (in %IACS) of Al-7Si-0.3Mg-xFe alloys. In the case of low Fe (0.2%) containing alloy, conductivity increases with increasing calcium addition. This is due to the modification of eutectic Si by Ca addition, which allows easier flow of electrons compared to the untreated alloy, where the platelet morphology of eutectic Si poses serious impediment to the flow of electrons. However, in the case of 0.4% iron containing alloy, conductivity initially increases and then decreases with increased Ca level. On the other hand, the conductivity of 0.7% iron containing alloy reduces with increasing calcium content. The reasons for these observations are not fully understood and may be attributed to the higher amount of porosity (Figure 4.16) present in these samples.

### **4.2.2.3 Mechanical Properties**

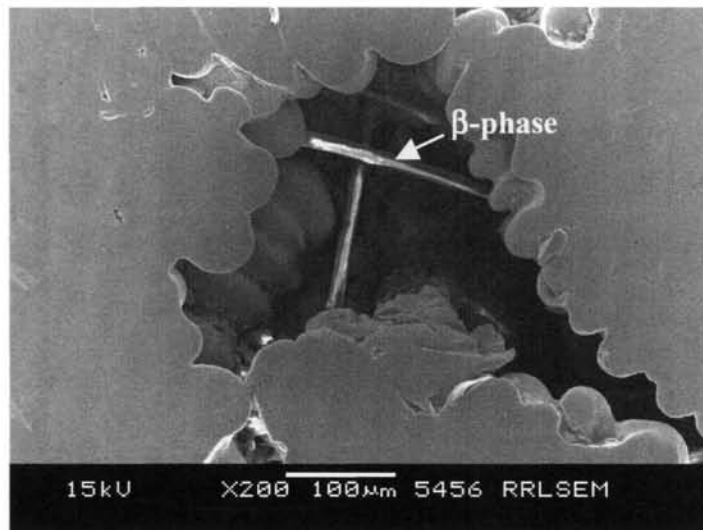
#### *Tensile properties*

Tensile testing was carried out on samples machined from the permanent mould castings. Figure 4.18 shows the tensile properties of the alloys in the T6 heat treated condition. It can be observed that the ultimate tensile strength (UTS) increases marginally (2.2% improvement) as the Fe content increases from 0.2 to 0.4% for the alloys without Ca addition. However, the UTS for the higher Fe content (0.7%) sample remains the same as that of the 0.2% Fe alloy. Comparing the tensile strengths of 0.2, 0.4 and 0.7wt% Fe containing alloys treated with and without Ca addition, the tensile strength is decreased slightly with Ca addition.

Figure 4.18 (b) shows a drastic decrease (74.3%) in % elongation of the alloys without Ca addition as the Fe content is increased from 0.4 to 0.7%. This effect is due to the increased amounts of  $\beta$ -Fe intermetallic platelets dispersed throughout the microstructure at higher Fe contents, leading to crack initiation and rapid crack



(a)



(b)

**Figure 4.16: Micrographs of platelet/needle like Fe intermetallic compound observed within a shrinkage pore in Al-7Si-0.3Mg-0.7Fe alloy (a) Optical and (b) SEM**

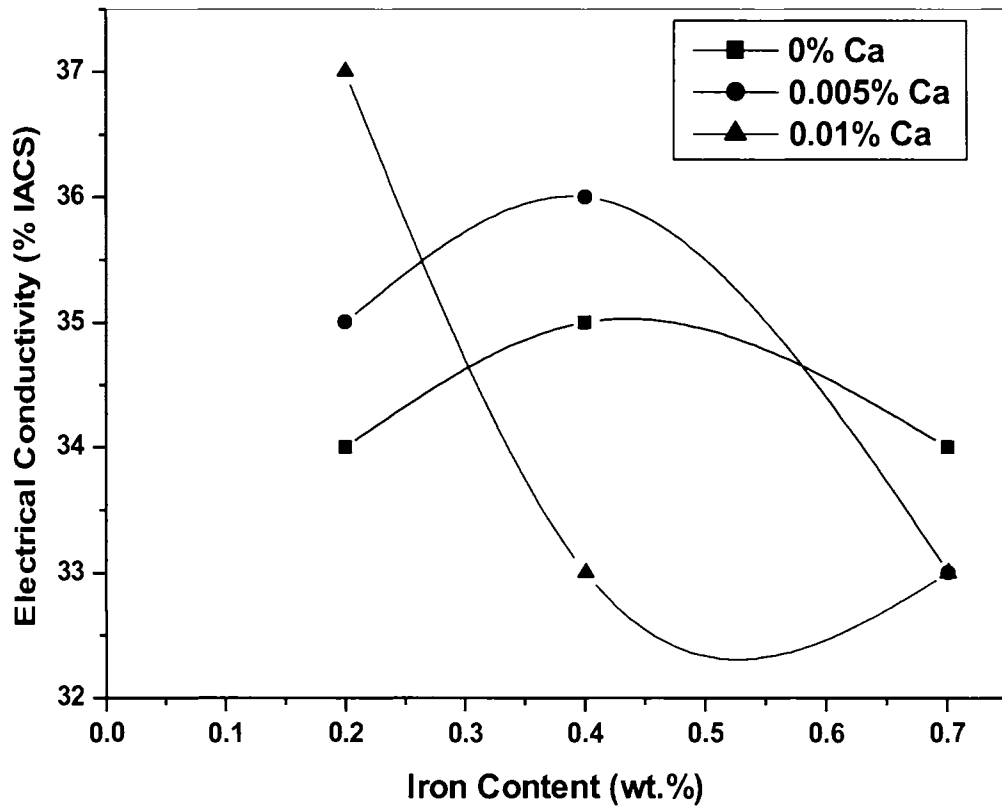
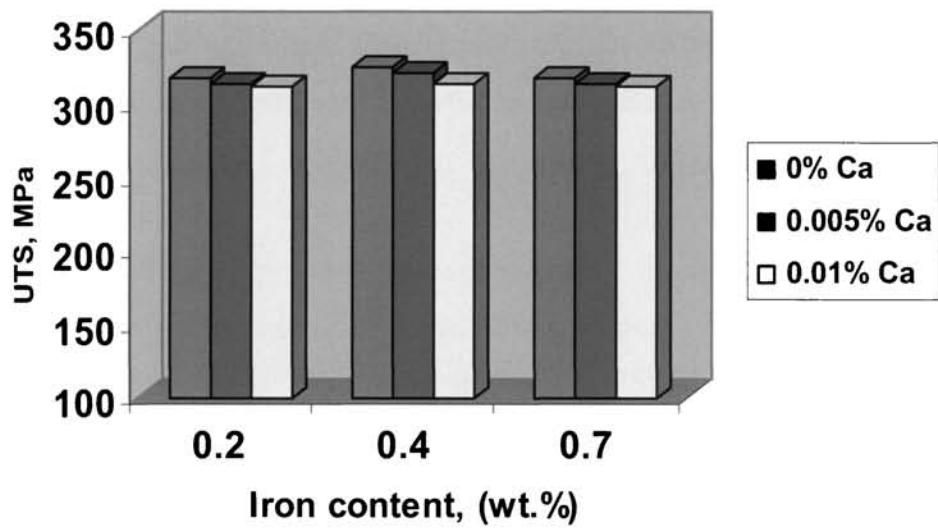
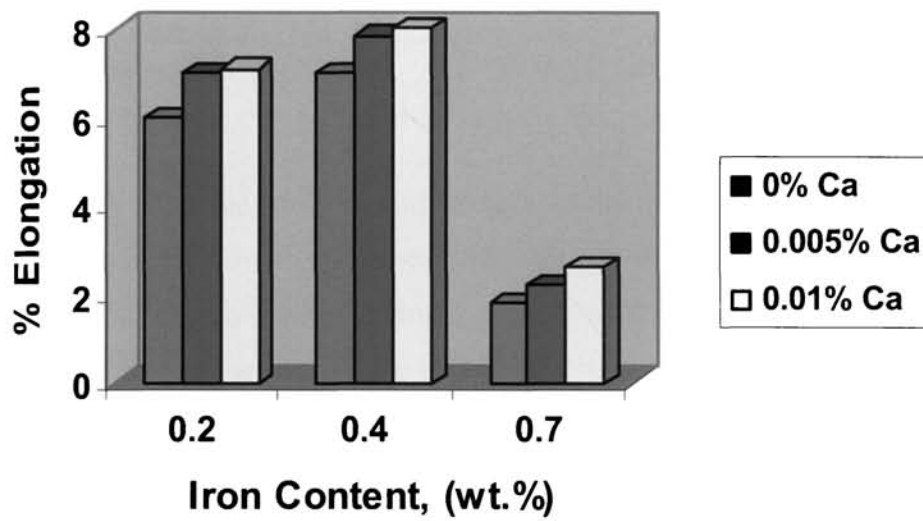


Figure 4.17: Effect of Ca on the %IACS of Al-7Si-0.3Mg-xFe alloy



(a)



(b)

Figure 4.18: Effect of Ca addition on the (a) UTS and (b) % elongation of Al-7Si-0.3Mg-xFe alloy (T6 condition)

propagation in the alloy. The addition of Ca has improved the elongation of 0.2, 0.4 and 0.7% Fe containing alloys. The addition of 0.005% Ca to the 0.2, 0.4 and 0.7% Fe alloys leads to a 17, 12 and 22% improvement in % elongation respectively. Addition of 0.01% Ca improved the % elongation by 18, 14 and 44% respectively compared to the unmodified alloy. These observations are supported by the microstructural observations on modification of eutectic Si and refinement of  $\beta$ -platelets with Ca addition.

Figure 4.19 shows the SEM micrographs of the fractured surface of tensile samples. At low Fe contents (0.2 and 0.4%) [Figures 4.19 (a)-(c)], there is no significant difference in the fractographs of Al-7Si-0.3Mg-xFe alloys with and without Ca. These fractographs exhibit dimpled structure typical of ductile fracture. However, the embrittling nature of the  $\beta$ -platelets is evident in high Fe content (0.7%) alloy [Figure 4.19 (d)].

The quality index ( $Q$ )<sup>271</sup> values for the alloys have also been calculated using the following equation and plotted in Figure 4.20.

$$\text{Quality index (Q)} = \text{UTS} + 150 \log (\% \text{ elongation}) \dots\dots\dots (5)$$

Higher the Q-value, the material will be both strong and ductile. It is seen from the Figure that the quality index increases with increasing iron from 0.2 to 0.4% and then decreases rapidly with further increase in iron to 0.7%. This is due to the rapid decrease in the % elongation as the iron content increases from 0.4 to 0.7% [Figure 4.18 (b)] indicating that the quality index represents the relative ductility of the material. Further, the higher Q-value with Ca addition compared to untreated alloys is due to the improved % elongation with Ca addition.

*Impact strength*

Figure 4.21 shows the impact strength of Al-7Si-0.3Mg-xFe alloys with and without Ca addition. It is seen that Ca addition significantly improves the impact strength of the alloys compared to the untreated alloys. Improvement in impact strength obtained in the 0.2, 0.4 and 0.7% Fe containing alloys with Ca addition are 44, 48 and 16% respectively.

G8940

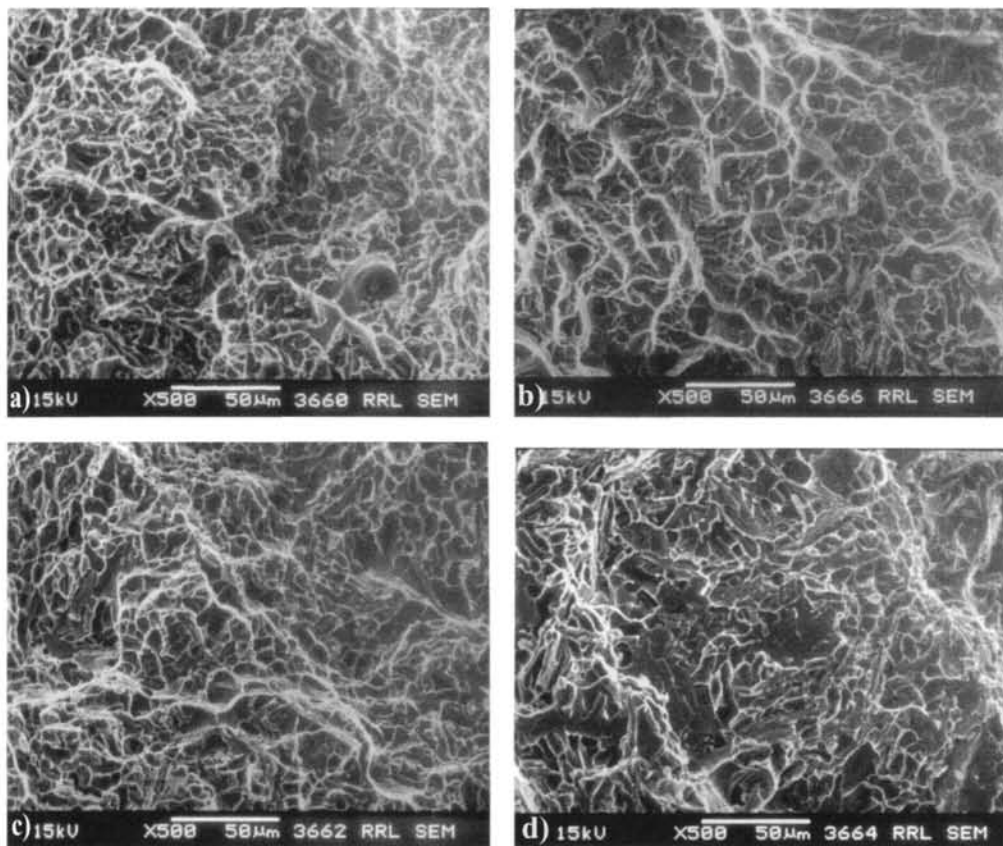


Figure 4.19: SEM micrographs showing the tensile fractured surface of Al-7Si-0.3Mg alloy (T6 condition) containing (a) 0.2% Fe (b) 0.2%Fe + 0.005% Ca (c) 0.4% Fe + 0.01% Ca and (d) 0.7% Fe + 0.005% Ca



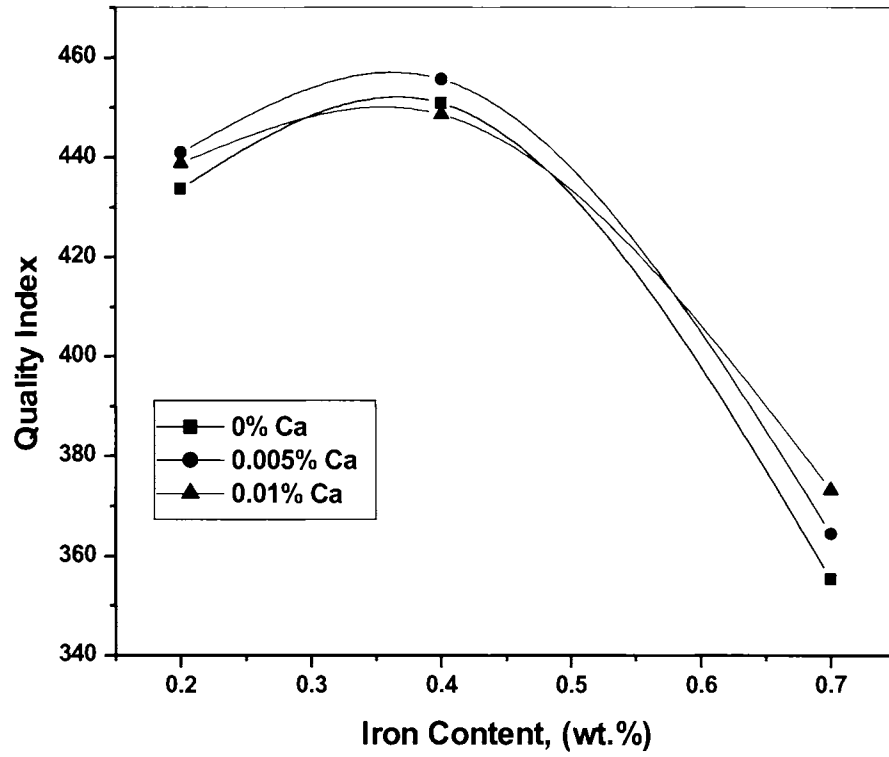


Figure 4.20: Effect of Ca on the quality index of Al-7Si-0.3Mg-xFe alloy in T6 condition

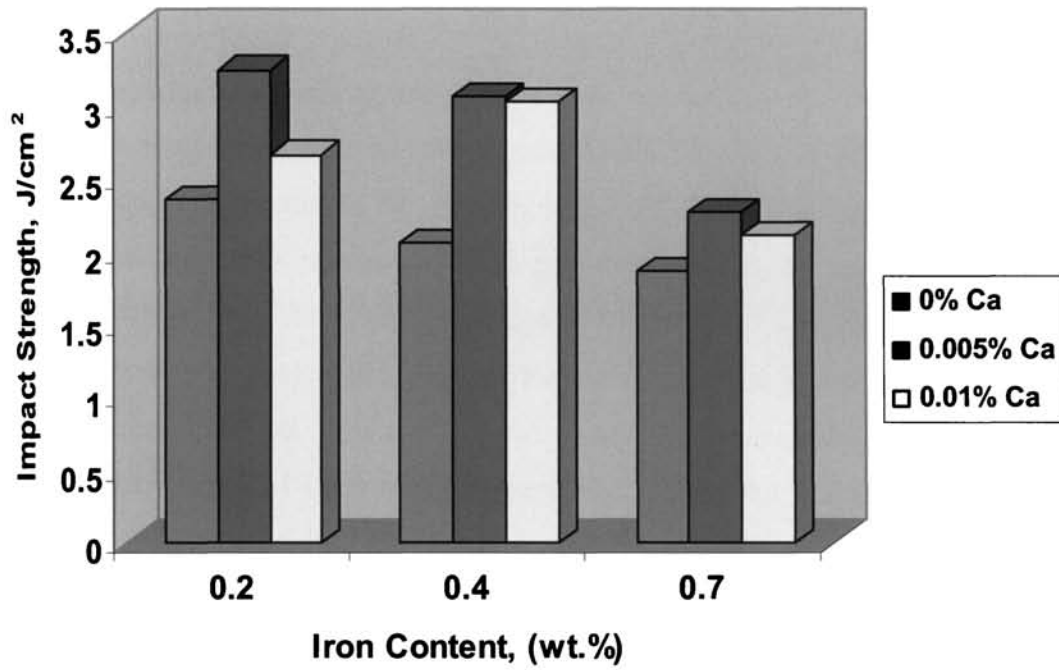
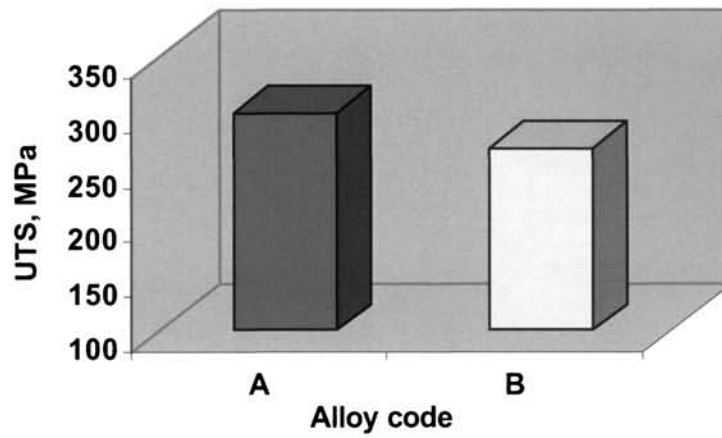


Figure 4.21: Effect of Ca on the impact strength of Al-7Si-0.3Mg-xFe alloy

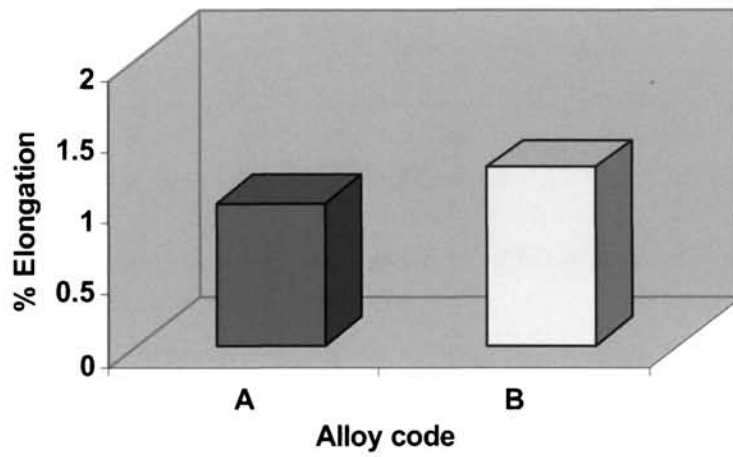
Attempts were made to study the influence of high calcium addition to Al-7Si-0.3Mg-0.6Fe alloy on UTS, % elongation and impact strength and the results are given in Figures 4.22 (a)-(c). It has been seen that a higher amount of Ca (0.05%) addition to Al-7Si-0.3Mg-0.6Fe alloy leads to 10.8% reduction of UTS [Figure 4.22 (a)] and 25% improvement of elongation [Figure 4.22 (b)] compared to the alloy without Ca addition. Further, a maximum improvement of 79.6% in impact strength has been achieved by 0.05% Ca addition to Al-7Si-0.3Mg-0.6Fe alloy [Figure 4.22 (c)]. This improvement in impact strength is due to the modification of the eutectic Si and refinement of the  $\beta$ -Fe intermetallic platelets caused by the Ca addition.

#### 4.2.3 Empirical Analysis of Data

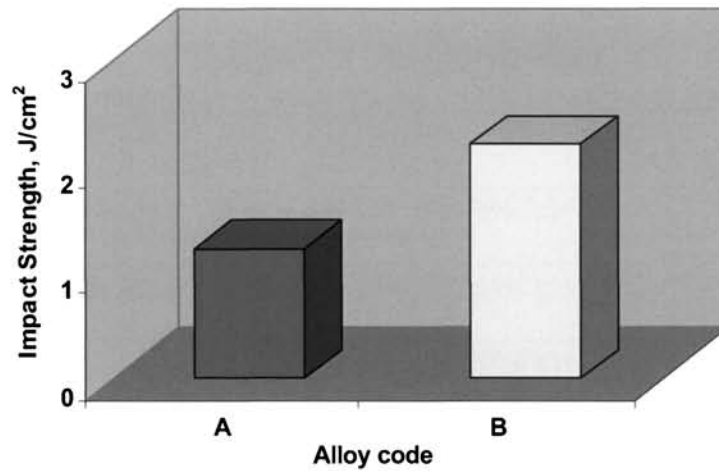
Extensive literature has been published on the effect of Fe in aluminium alloys, but there seems to be no consensus on the degree of its influence on mechanical properties especially tensile properties. Hence, an empirical analysis on the published data of the tensile properties of Al-Si-Mg<sup>26, 88, 211</sup> and Al-Si-Cu<sup>42</sup> alloys with increasing Fe content has been carried out and compared with the present work. The data for UTS and % elongation for various Fe contents have been plotted in Figures 4.23 and 4.24 (a) and (b) respectively. Tables 4.4 and 4.5 summarize the casting conditions, the best fit equations and the correlation coefficients for UTS versus Fe content and % elongation versus Fe content respectively for Al-Si-Cu and Al-Si-Mg alloys. It is to be noted that except the work by Murali et al<sup>26</sup> and Wang and Xiong<sup>211</sup> (sand casting), others are on permanent mould casting. By carrying out regression analysis of the data for UTS for various Fe content, it has been found that a linear relationship with correlation coefficient near to one exists in all cases. UTS decreases with increasing Fe content in all cases except in the work of Kim et al<sup>42</sup> and the present work, where the variation is not much. Similarly, the regression analysis of the data for % elongation for various Fe content has shown that the best fit equations are inverse first order polynomials. The fitted equations for % elongation versus Fe content predict that as the Fe content increases, % elongation decreases rapidly with increasing iron content upto a certain Fe content and thereafter show a tendency to remain constant.



(a)



(b)



(c)

Figure 4.22: Effect of higher amount of Ca (0.05%) on the (a) UTS (b) % elongation and (c) impact strength of Al-7Si-0.3Mg-0.6Fe alloy (T6 condition) [A= Al-7Si-0.3Mg-0.6Fe and B= A + 0.05% Ca]

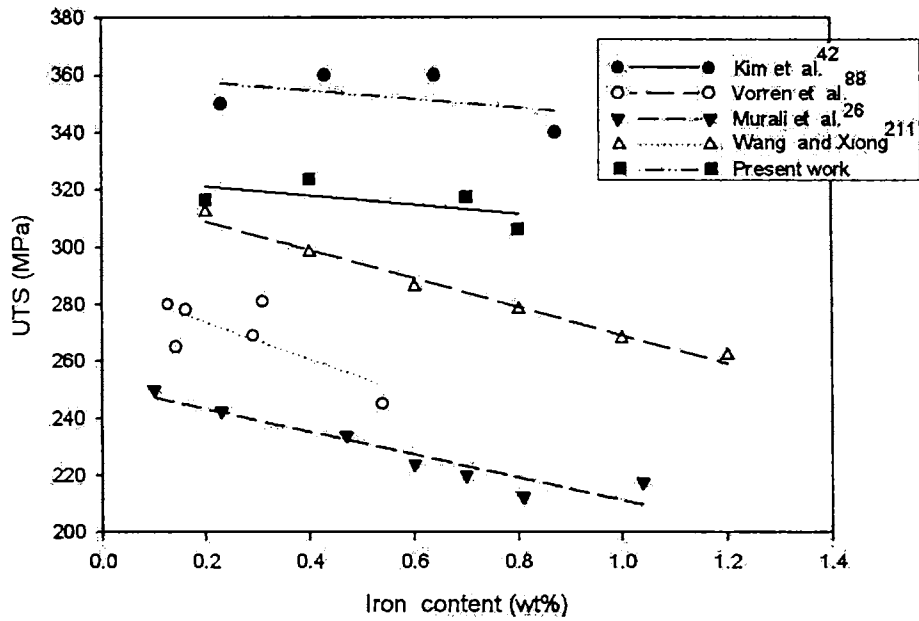


Figure 4.23: Empirical analysis of the variation of UTS with iron content in Al-Si-Mg and Al-Si-Cu alloys

Table 4.4: Empirical analysis of data for UTS versus Fe content

Investigator	Alloy	Casting	UTS Vs Fe (Linear fit)	
			Best fit equation	Correlation coefficient, $R^2$
Kim et al. <sup>42</sup>	Al-Si-Cu	PM	UTS= -15.8(%Fe)+324.2	0.9996
Vorren et al. <sup>88</sup>	Al-Si-Mg	PM	UTS= -49.7(%Fe)+318.8	0.9990
Murali et al. <sup>26</sup>	Al-Si-Mg	SM	UTS= -39.9(%Fe)+251.1	0.9996
Wang and Xiong <sup>211</sup>	Al-Si-Mg	SM	UTS= -65.2(%Fe)+286.8	0.9999
Present work	Al-Si-Mg	PM	UTS= -15.1(%Fe)+360.7	0.9997

[PM = Permanent Mould; SM = Sand Mould]

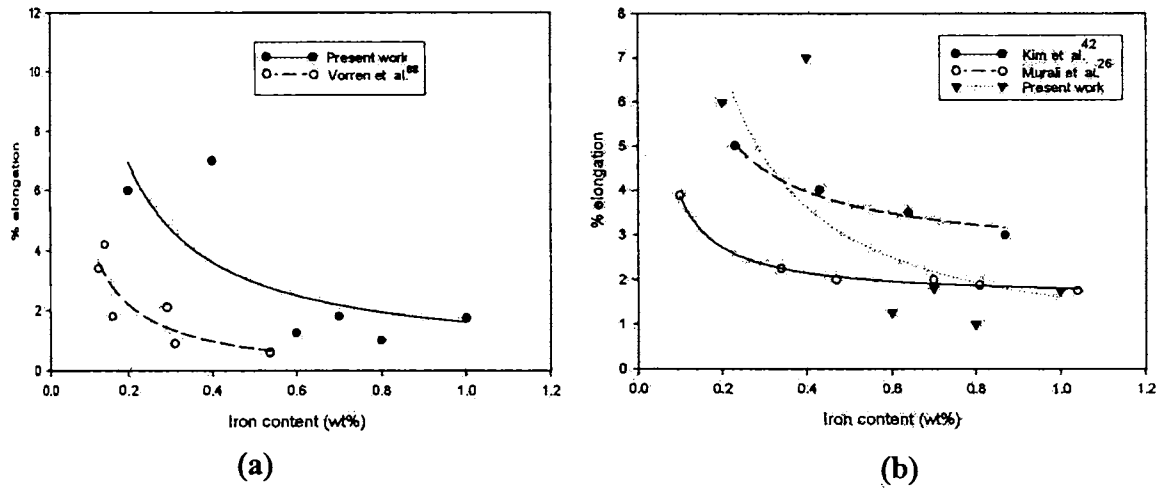


Figure 4.24: Empirical analysis of the variation of % elongation with iron content in Al-Si-Mg and Al-Si-Cu alloys

Table 4.5: Empirical analysis of data for % elongation versus Fe content

Investigator	Alloy	Casting	% Elongation Vs Fe (Polynomial fit)	
			Best fit equation	Correlation coefficient, $R^2$
Kim et al <sup>42</sup>	Al-Si-Cu	PM	$\%Elongation = 1.5766 + \frac{0.2295}{(\%Fe)}$	0.9995
Vorren et al <sup>88</sup>	Al-Si-Mg	PM	$\%Elongation = -0.2781 + \frac{0.4966}{(\%Fe)}$	0.9296
Murali et al <sup>26</sup>	Al-Si-Mg	SM	$\%Elongation = 2.4834 + \frac{0.5931}{(\%Fe)}$	0.9991
Present work	Al-Si-Mg	PM	$\%Elongation = 0.2663 + \frac{1.3392}{(\%Fe)}$	0.8402

[PM = Permanent Mould; SM = Sand Mould]

When comparing the present work with Vorren et al.<sup>88</sup> (both are Al-Si-Mg system and permanent mould casting), the values of UTS and % elongation reported in the latter are lower. This may be due to the varying mould wall thickness and mould preheating temperatures used in the two cases (20 and 32mm mould wall thickness and mould preheating temperatures of 573 and 693 K respectively). Similarly, the higher values of UTS achieved in the present work (permanent mould casting) than those of Murali et al.<sup>26</sup> and Wang and Xiong<sup>211</sup> (sand casting) is due to the difference in the solidification rate. Higher solidification rate results in reduction of the secondary dendrite arm spacing, less and better distributed porosity, reduction in the size of Fe-intermetallic phases and a finer eutectic Si structure. Further, it can be seen from Figure 4.23 that the trend in the variation of UTS with increasing iron in the present work is similar to the work of Kim et al.<sup>42</sup> on Al-Si-Cu alloy.

#### 4.2.4 Discussion

Increasing Fe content from (0.2 to 0.7 wt.%) in Al-7Si-0.3Mg alloy results in the precipitation of long needles/platelet  $\beta$ -phase, whose size and volume fraction increase with increasing iron content.

Calcium addition has refined the large platelet Fe intermetallics to very fine form and modified the eutectic Si to fine fibrous form. However, higher amount of Ca addition (0.05%) results in the precipitation of  $\text{Al}_2\text{CaSi}_2$  intermetallics. The refinement of  $\beta$ -platelets with Ca addition is due to the fragmentation of  $\beta$ -platelets by Ca. The reason for this fragmentation of the platelets could be attributed to the rejection of Si at the  $\beta$ -phase/Al matrix interface. The higher diffusion coefficient<sup>2</sup> of Si in Al ( $10^{-11}$  to  $10^{-8}$   $\text{cm}^2 \text{s}^{-1}$ ) compared to Fe ( $10^{-13}$  to  $10^{-12}$   $\text{cm}^2 \text{s}^{-1}$ ) in the temperature range 673 to 873 K would facilitate the destabilization of the  $\beta$ - $\text{Al}_5\text{FeSi}$  phase platelets in the presence of Ca. In the case of Sr, it has been reported<sup>273</sup> that the formation temperature of  $\beta$  phase is high enough to enhance the diffusion of Sr into the  $\beta$ -platelets (absorption), especially when the thickness of these platelets is of the order 1  $\mu\text{m}$ . Figure 4.25 schematically illustrates the decomposition of  $\beta$ - $\text{Al}_5\text{FeSi}$  platelets and the formation of Ca-containing intermetallics in Ca added alloys wherein (a), (b) and (c) indicate low, sufficient and excessive Ca contents respectively. A low

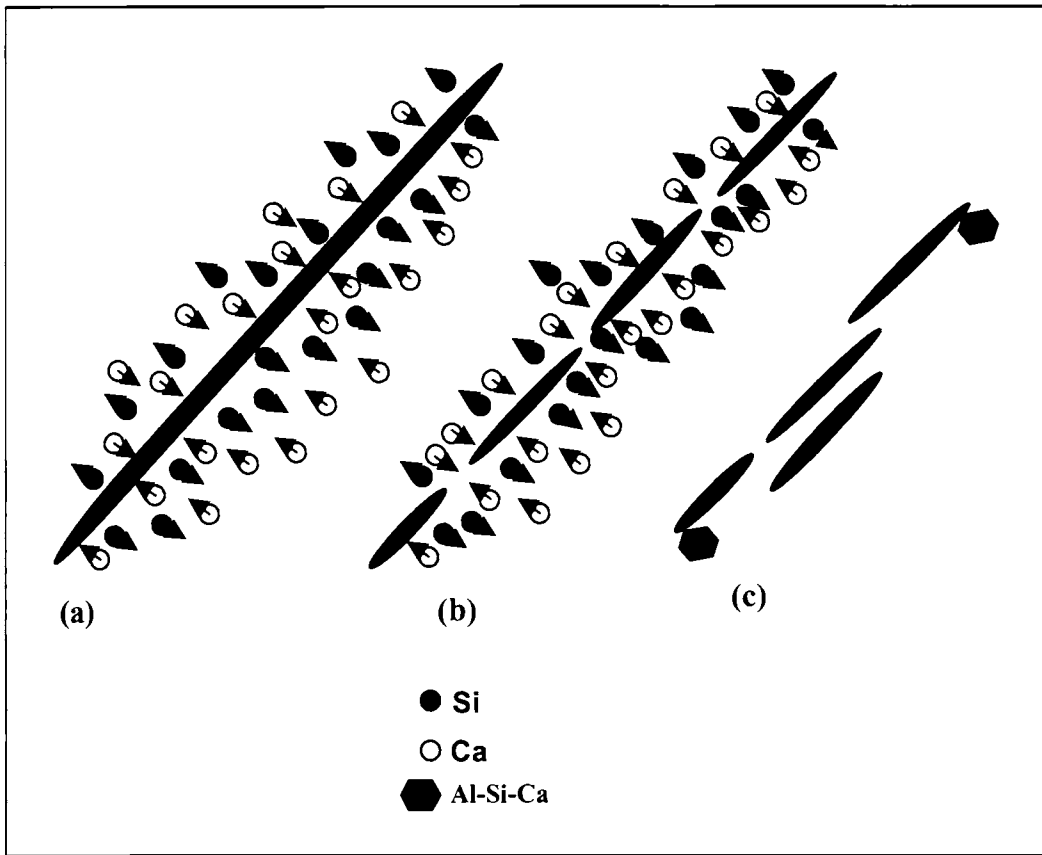


Figure 4.25: Schematic illustration of decomposition of  $\beta$  platelets with Ca addition

level of calcium induces no changes in the  $\beta$ -Al<sub>5</sub>FeSi platelets, whereas a sufficient amount of Ca content leads to fragmentation of the  $\beta$ -Al<sub>5</sub>FeSi platelets. On the other hand, an excessive amount of Ca will lead to fragmentation of the  $\beta$ -Al<sub>5</sub>FeSi platelets and precipitation of Al-Ca-Si intermetallic phase respectively. As this intermetallic phase is seen to be attached to the sides or the end of the  $\beta$ -phase platelets, it could be assumed that the Si rejected from the latter reacts with the Ca in the surrounding area, leading to the formation of the Al<sub>2</sub>CaSi<sub>2</sub> particles. This has been further confirmed by the SEM/EDS analysis (Figure 4.12) of the Al-7Si-0.3Mg-0.6Fe alloy where the Al-Ca-Si compound is seen to be attached to the side of the  $\beta$ -phase platelets. This is further supported by the work of Samuel et al<sup>195, 273</sup> on Sr addition to 6111 (Al-0.65Si-0.32Fe-0.86Cu-0.21Mn-0.89Mg-0.048Cr) and 319 (Al-6.2Si-3.7Cu) alloys.

It has been observed that the % porosity of the alloy increases as the iron content increases from 0.2 to 0.7wt.%. This may be due to the difficulty in the feeding of the liquid metal due to the presence of large intercepting  $\beta$ -platelets. This result is in accordance with the work of Samuel et al<sup>195</sup> on the effect of trace elements on  $\beta$ -Al<sub>5</sub>FeSi characteristics, porosity and tensile properties of 319 (Al-6.2Si-3.7Cu) alloy.  $\beta$ -Fe platelets are often found to be associated with shrinkage pores,<sup>273, 274</sup> and this observation is understood to be the direct result of their effect in increasing restrictions to feeding through the small interdendritic channels in the later stages of feeding. It has been reported<sup>274</sup> that the platelets are observed to form as an interlocking network and grow around pre-existing features in the microstructure. These relatively large and long  $\beta$ -platelets intersect and reduce the size of the interdendritic feeding paths, limiting feeding and thus increasing the driving force for pores to form.

It is interesting to note that the % porosity of 0.2, 0.4 and 0.7% Fe containing alloys is reduced with 0.005% Ca addition. This may be due to the degassing effect of calcium at low levels. This is supported by the work of Velasco et al.<sup>104</sup> There are several mechanisms that have been proposed to explain the changes in porosity that occurs as a result of adding eutectic modifiers to Al-Si alloys. First, the porosity formation at various Ca levels may be explained by the recent theory<sup>158</sup> that porosity

formation in hypoeutectic Al-Si alloys is strongly dependent on the eutectic solidification mode. EBSD analysis of the Ca-containing sample in the present work indicates that the eutectic nucleates in the interdendritic liquid away from the primary aluminium/liquid interface and the eutectic evolves with a front growing in a direction opposite to the thermal gradient, while in unmodified alloys the eutectic nucleates with a very high nucleation frequency adjacent to the dendrite tips throughout the sample. This is further supported by the results of Knuutinen et al.<sup>130</sup> showing a direct relationship between porosity and eutectic solidification mode in A356 alloy treated with different levels of Ba, Ca, Y and Yb. The principle implies the impact of the different modes of eutectic solidification and thus spatial distribution of evolving eutectic on the interdendritic permeability in the final stages of solidification. Such considerations therefore account for the overall solidification and feeding occurring in the sample, thus determining the overall feedability and feeding requirements of different regions of the casting. Therefore, at the intermediate Ca level (0.005%), the eutectic may display a mixed eutectic solidification mode, i.e. between that of the unmodified and Ca modified alloys, thus leading to a minimum of porosity for this particular casting with its solidification and feeding pattern. The role of feeding direction and influence of eutectic solidification mechanisms have been discussed in detail by Dinnis et al.<sup>275</sup> Secondly, In the case of Sr modified Al-Si melts, it has been reported that Sr does not alter the degassing rate of melts and it can react with hydrogen in the melt and precipitate as hydrides.<sup>268</sup> Since the values for free energy of formation of SrH<sub>2</sub> and CaH<sub>2</sub> are of the same order viz., -61.15 and -61.70 kJmol<sup>-1</sup>, respectively,<sup>276</sup> like Sr, Ca at very low levels may also react with the hydrogen present in the melt and form solid hydride particles, reducing the amounts of free hydrogen that can cause porosity. This could possibly explain the reduction of porosity for the 0.005% of Ca addition. However, further evidence is required to confirm such a hypothesis. Beyond this critical level of Ca, Ca containing oxide film might have caused ruptures in the usually protective Al<sub>2</sub>O<sub>3</sub> oxide film, leading to faster pickup of hydrogen. The increased porosity at 0.01% Ca may be due to the increased melt affinity for gas absorption.

The increase in electrical conductivity with calcium addition can be attributed to the modification of eutectic Si by Ca addition, which allows easier flow of electrons when compared to the untreated alloy, where the eutectic Si in platelet form acts as an impediment to the flow of electrons.

#### 4.2.5 Summary

1. Ca addition has dual role modifier of the eutectic Si and refiner of the long platelet  $\beta$ -Fe phases. The proposed mechanism of Fe-neutralization by Ca is the destabilization of the  $\beta$ -platelets and fragmentation of the long  $\beta$ -platelets into smaller sizes.
2. A low amount of Ca (0.005%) has reduced the porosity of the alloy probably due to the trapping of hydrogen as calcium hydride.
3. Higher Ca levels lead to faster pickup of hydrogen, probably due to the rupture of the protective  $\text{Al}_2\text{O}_3$  oxide film by the Ca containing oxide film.
4. Electrical conductivity is increased with Ca addition due to the modification of eutectic Si from acicular to fibrous form.
5. Ca addition has improved the % elongation of the alloy by 18, 14 and 44% and the impact strength by 44, 48 and 16% respectively at 0.2, 0.4 and 0.7% Fe contents.
6. Higher amount of Ca (0.05%) addition reduces the size of the platelet Fe-intermetallics to very fine form. A maximum improvement of 79.6% in impact strength has been achieved by 0.05% Ca addition to Al-7Si-0.3Mg-0.6Fe alloy. However, higher amount of Ca addition has led to the precipitation of  $\text{Al}_2\text{CaSi}_2$  intermetallics and higher porosity in the castings.
7. An empirical analysis carried out for comparing the results of the present work with those of the other researchers on the effect of increasing iron content on UTS and % elongation of Al-Si-Mg and Al-Si-Cu alloys has shown a linear and an inverse first order polynomial relationships respectively.

---

---

## CHAPTER 5

# EFFECT OF Mn, Be AND Sr AND THEIR INTERACTION WITH Ca IN Al-7Si-0.3Mg-xFe ALLOY

---

---

### 5.1 INTRODUCTION

Manganese is the most commonly used and the least expensive element for Fe neutralization in Al-Si alloys. Be has been found to be the most effective element in improving the mechanical properties of Al-Si-Mg alloys. However, Be is carcinogenic and the higher amounts of Mn required for iron neutralization lead to sludge formation affecting machinability.<sup>26,88,199,210,224</sup> Further, it has been reported that Mn does not significantly reduce the deleterious effect of Fe on fracture toughness.<sup>88</sup> It is evident from the previous chapter that Ca greatly increases the impact strength of Fe containing Al-7Si-0.3Mg alloy. Hence, a combination of Ca and Mn can improve both the tensile and impact properties of Fe containing Al-7Si-0.3Mg alloy. It has been observed that higher amount of Ca leads to porosity in the castings. A small amount of Be in Al-Si alloys is known to have several benefits. It preferentially oxidizes forming BeO on the surface of the casting, reducing Mg loss and making Mg available for forming the required volume of Mg<sub>2</sub>Si for strengthening.<sup>250</sup> Further, there are considerable evidences<sup>241,257,258</sup> for the Fe neutralizing effect of Sr in Al-Si-Cu alloys. In view of these beneficial effects of individual elements Mn, Be, Sr and Ca, the study mainly focuses on their combined effects.

### 5.2 METHODOLOGY

Al-7Si-0.3Mg-xFe alloys were prepared in 20 kg capacity crucible using ALTAB Fe compact (75% Fe and 25% Al). For each experiment, about 3 kg of the alloy was melted in a clay-graphite crucible of 5 kg capacity using an electric resistance furnace. The melt was subjected to fluxing and degassing using commercially available fluxes and degassing tablets respectively. Amount of Be to be

added was chosen as per the optimum level reported for the alloy in the literature.<sup>26</sup> The effect of Be, Mn Sr and Ca in Al-7Si-0.3Mg alloy both individually and in combination have been studied with an iron content of 0.8Fe. The main reason for the choice of a high Fe content alloy (about thrice the usual limit) was to promote the formation of large intermetallics in the microstructure. It has been found in the previous chapter that the optimum amount of Ca for Fe neutralization lies in the range of 0.03-0.04%. Since the modification effect of Ca and Sr is found to be nearly equal in the present work, the amount of Ca and Sr for the comparison and interaction study has been taken as 0.04%. The melting, casting, heat treatment and testing procedures are given in chapter 3.

## 5.3 RESULTS

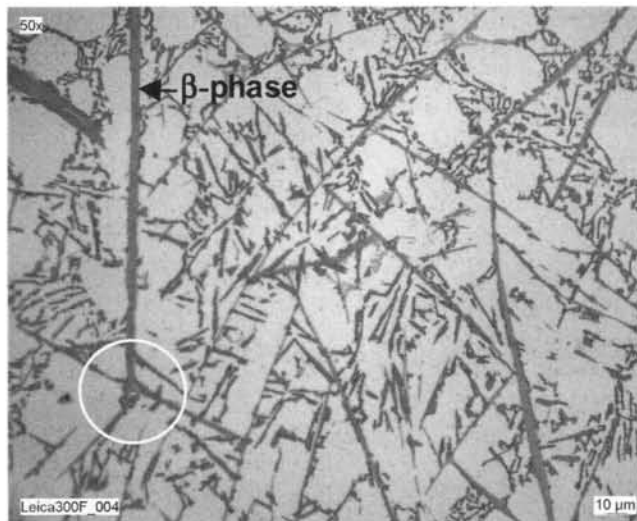
### 5.3.1 Microstructure

It is evident from chapter 4 that increasing Fe content in Al-7Si-0.3Mg alloy results in the precipitation of long platelet  $\beta$ -phase, whose amount and size increase with increasing Fe content. Figures 5.1 (a) and (b) show the typical as cast microstructures of permanent mould cast Al-7Si-0.3Mg-0.8Fe alloy. It has been seen that  $\beta$ -Fe platelets are present in the interdendritic regions as well as precipitated along with the eutectic Si. Smaller  $\beta$ -needles are branching out from the parent needle spanning across the matrix (Figure 5.1(a) circled area). This network of  $\beta$ -needles extending over large distances in the matrix may affect the feedability of the alloy during casting. Figure 5.1 (b) is a typical micrograph showing eutectic Si nucleating at several locations along the length of a large  $\beta$ -platelet.

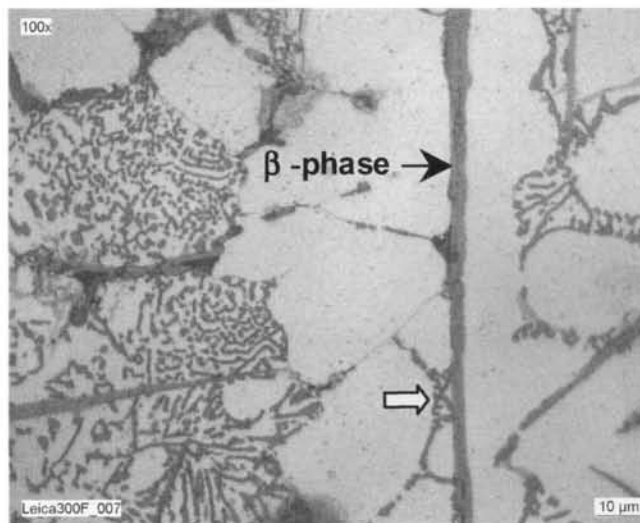
#### 5.3.1.1 Effect of Mn, Be and Sr

##### *Manganese*

Figure 5.2(a) shows the typical as cast microstructure of permanent mould cast Al-7Si-0.3Mg-0.6Fe alloy with 0.3% Mn addition. It is seen that platelet Fe-intermetallic phases have been replaced by Chinese script phases. At a higher amount of Mn (0.5%), Fe-rich intermetallics [Figure 5.2(b)] appear in Chinese script, star like and other compact shapes. On the other hand, 0.4% Mn addition to Al-7Si-0.3Mg-0.8Fe alloy results in both platelets and Chinese script Fe-intermetallics with the



(a)



(b)

**Figure 5.1: Typical microstructures of permanent mould cast Al-7Si-0.3Mg alloy with (a) 0.8% Fe, Circled area showing the branching of  $\beta$ -platelet and (b) Higher magnification of the branched platelet, arrow showing nucleation of eutectic Si by  $\beta$ -platelets**

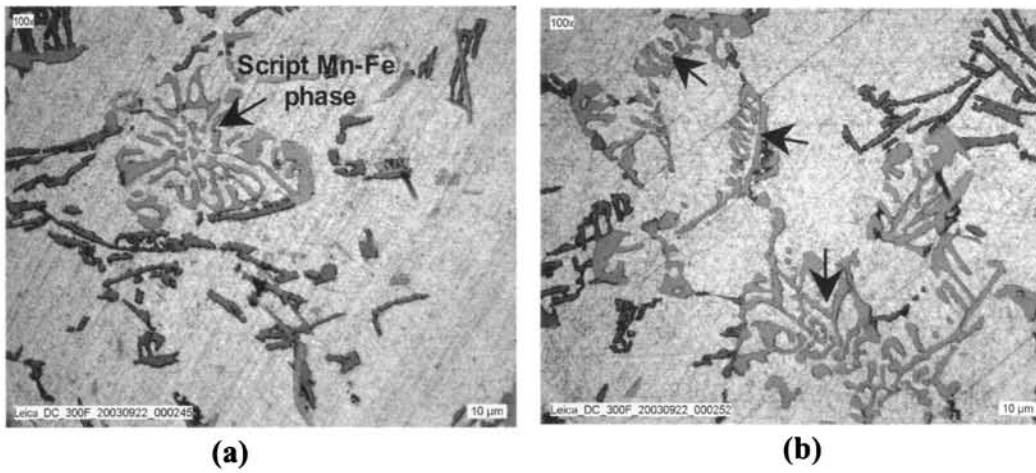


**Figure 5.2: Typical microstructures of permanent mould cast Al-7Si-0.3Mg-0.6Fe alloy treated with (a) 0.3% Mn and (b) 0.5% Mn [Arrows show the Mn-Fe phases]**

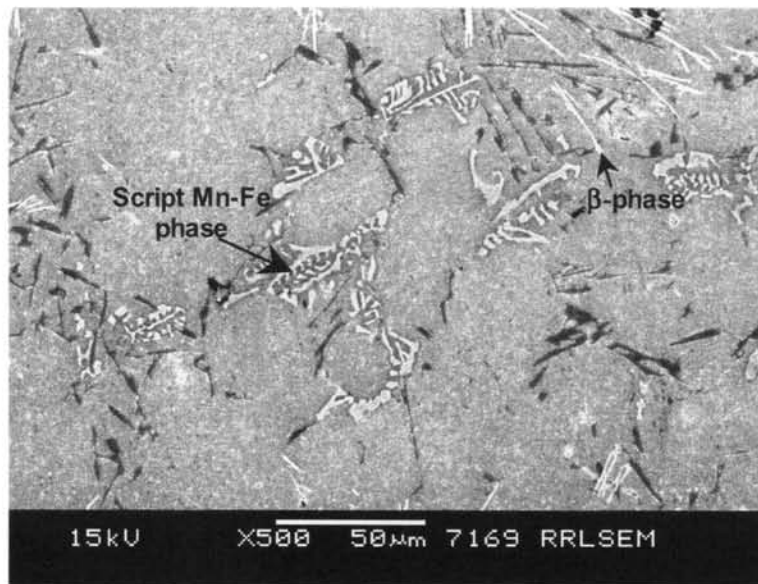


**Figure 5.3: SEM micrograph of Al-7Si-0.3Mg-0.8Fe alloy with 0.4% Mn addition**

dominance of the latter (Figure 5.3). The EDS analysis of the Mn-Fe compound in Al-7Si-0.3Mg-0.6Fe alloy treated with 0.3% Mn indicates the presence of Al, Si, Fe and Mn and their distributions are shown in Figure 5.4. The Mn-Fe phase has been identified as  $Al_{15}(Fe,Mn)_3Si_2$ . This is in agreement with that reported in literature.<sup>8</sup>

### *Beryllium*

Figures 5.5 (a) and (b) show the typical as cast microstructures of permanent mould cast Al-7Si-0.3Mg-0.8Fe alloy with Be (0.2%) addition. It is seen that Be addition replaces the platelet/needle like Fe-intermetallic phases by small spherical shape and Chinese script Fe-intermetallic phases. It is to be noted that Chinese script phases exist both inside the primary  $\alpha$ -Al dendrites as well as in the interdendritic regions. It is also observed that Be added sample cast in permanent mould shows refined Chinese script phases. On the other hand, in the case of sand cast Al-7Si-0.3Mg-1.0Fe alloy with Be (0.2%) addition, these Chinese script phases are found only inside the  $\alpha$ -Al dendrites (Figure 5.6). This observation is in line with that of Murali et al.<sup>26</sup> From the XRD pattern (Figure 5.7), the secondary phases identified in the Al-7Si-0.3Mg-0.8Fe and Al-7Si-0.3Mg-0.8Fe-0.2Be alloys are  $(Al_9FeSi_3$  and  $Al_5FeSi)$  and  $Al_2FeBe_3$  respectively.

### *Strontium*

Figures 5.8 (a) and (b) show the typical as cast microstructures of permanent mould cast Al-7Si-0.3Mg-0.8Fe alloy with strontium addition. It is seen that Sr modifies the eutectic Si to fine fibrous form and reduces the size of the platelet Fe intermetallics. It has also been observed that the platelet phases are precipitated along with the eutectic Si.

#### **5.3.1.2 Interaction of Mn, Be, Sr and Ca**

##### *Calcium and Manganese*

To study the combined effect of Ca and Mn, varying amounts of Ca (0.02, 0.05 and 0.08%) have been added to Al-7Si-0.3Mg-0.6Fe-0.3Mn alloy. It has been observed that addition of 0.02% Ca refines the eutectic Si to fibrous form. Some of the  $\beta$ -platelets have been fragmented as clearly seen in Figure 5.9 (a). However, 0.05% Ca addition has refined both eutectic Si and platelet Fe-intermetallics

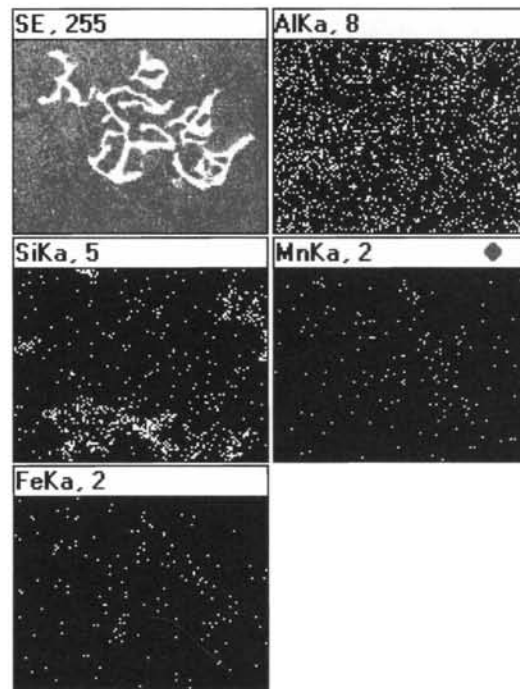


**Figure 5.4: EDS elemental X-ray mapping and elemental distribution of Chinese script Mn-Fe phase in Al-7Si-0.3Mg-0.6Fe alloy treated with 0.3% Mn**

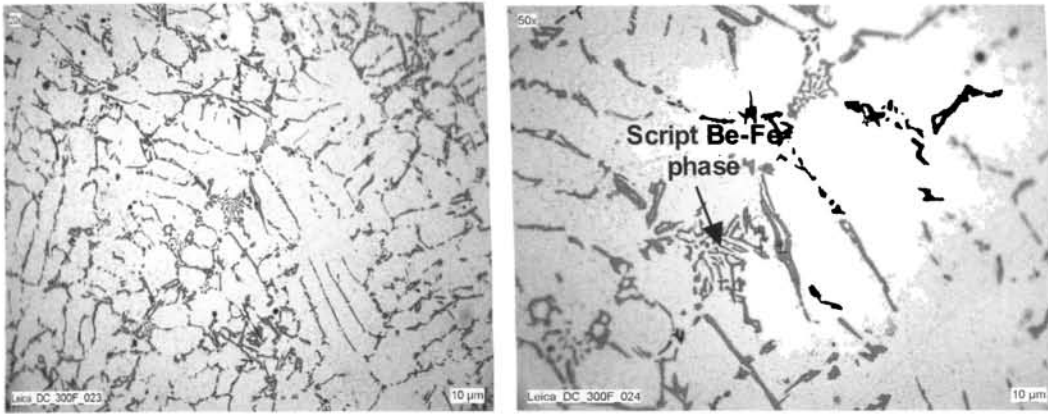


**Figure 5.5: Typical as cast microstructures of permanent mould cast Al-7Si-0.3Mg-0.8Fe-0.2Be alloy**

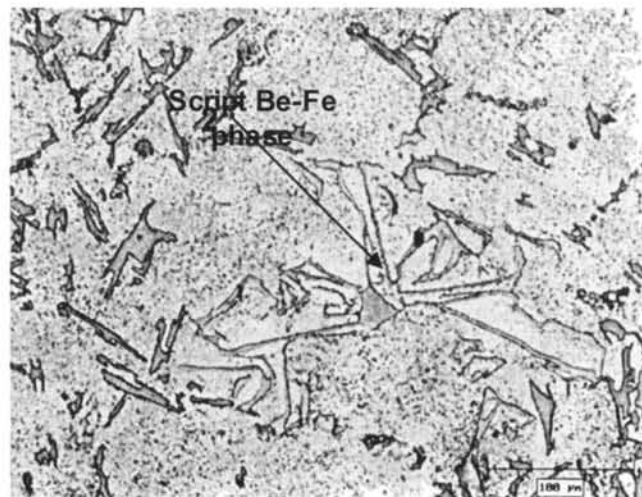


**Figure 5.6: Typical microstructure of sand cast Al-7Si-0.3Mg-1.0Fe-0.2Be alloy**

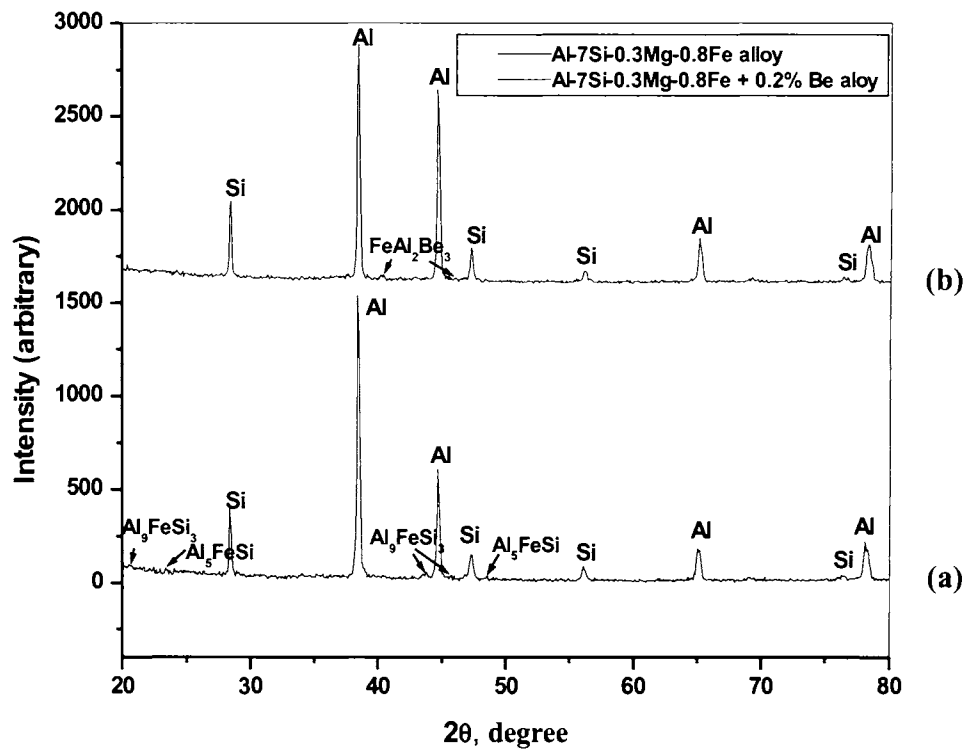
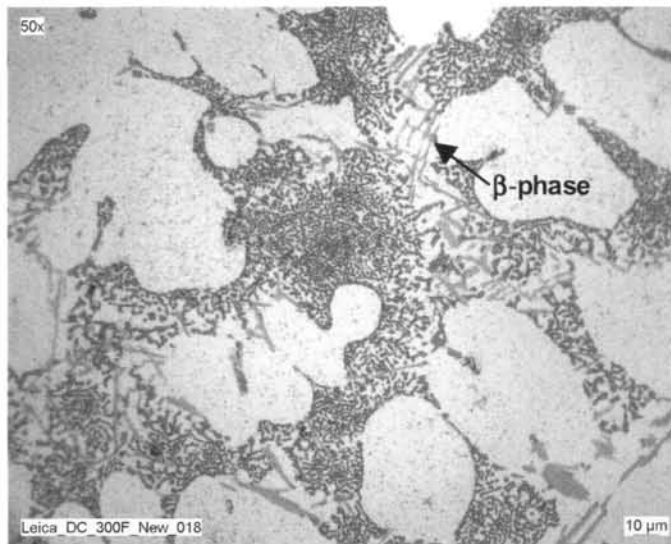
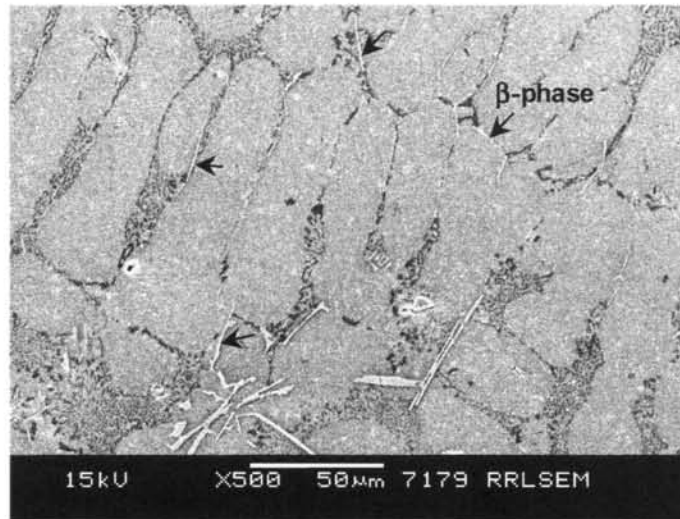


Figure 5.7: X-ray diffraction patterns of (a) Al-7Si-0.3Mg-0.8Fe and (b) Al-7Si-0.3Mg-0.8Fe-0.2Be alloys

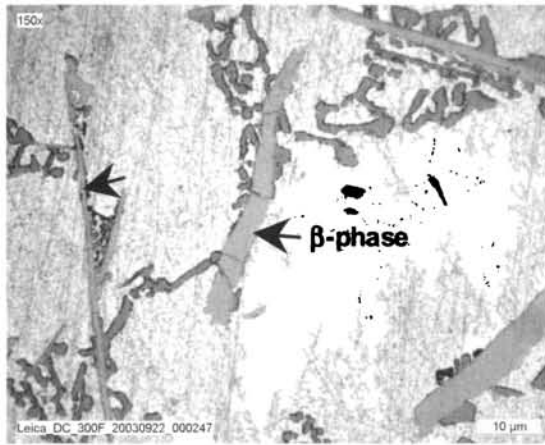


(a)

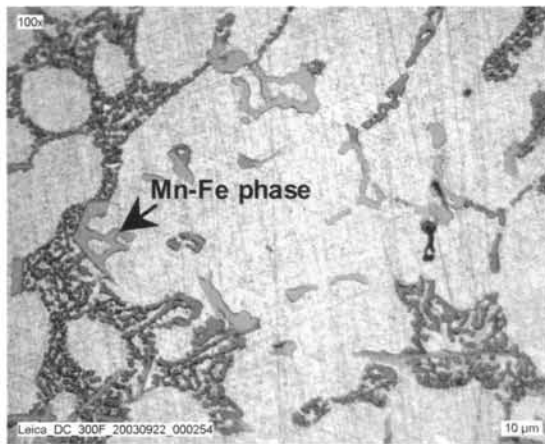


(b)

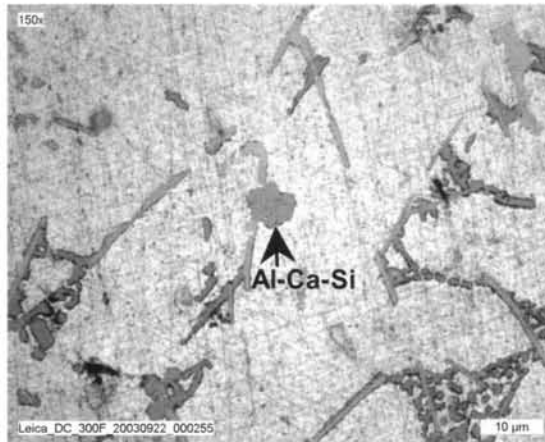
**Figure 5.8: Typical microstructures of permanent mould cast Al-7Si-0.3Mg-0.8Fe alloy treated with 0.04% Sr (a) Optical and (b) SEM micrographs**



(a)



(b)



(c)

**Figure 5.9: Typical microstructures of permanent mould cast Al-7Si-0.3Mg-0.6Fe-0.3Mn alloy with (a) 0.02 (b) 0.05 and (c) 0.08% Ca**

[Figure 5.9 (b)]. On the other hand, a higher amount of Ca addition (0.08%) to Al-7Si-0.3Mg-0.6Fe-0.3Mn alloy leads to coarsening of the  $\beta$ -platelets as shown in Figure 5.9 (c). Further, precipitation of Al-Ca-Si intermetallics has also been observed.

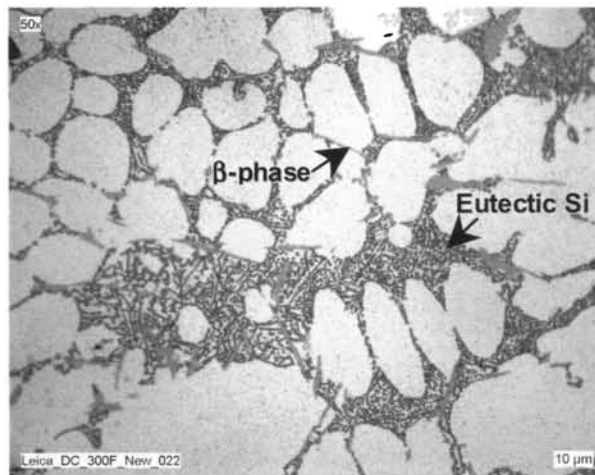
#### *Calcium and Beryllium*

Figure 5.10 shows the as cast microstructure of permanent mould cast Al-7Si-0.3Mg-0.8Fe alloy with Be and Ca additions and Figure 5.11 shows the as cast microstructures of sand mould cast Al-7Si-0.3Mg-1.0Fe alloy with Be and Ca additions. It is seen that addition of a trace amount of Be (0.005%) has no significant effect on the microstructure of the alloys. This observation has been confirmed by the average length of eutectic Si obtained by image analysis (Table 5.1). The variation in the average length of  $\beta$ -phase obtained by image analysis as a function of added elements is shown in Figure 5.12. It is clearly evident that the length of the  $\beta$ -phase is reduced by Ca and Be both individually and in combination.

#### *Manganese, Beryllium and Strontium*

As in the case of calcium, addition of a trace amount of Be (0.005%) in Sr (0.04%) added Al-7Si-0.3Mg-0.8Fe alloy has no significant effect on the microstructure. Both Mn-Fe and Be-Fe Chinese script intermetallic compounds have been observed (Figure 5.13) in the combined addition of Be (0.15%) and Mn (0.15%) in Al-7Si-0.3Mg-0.8Fe alloy. On the other hand, combined addition of Mn (0.3%) and Sr (0.04%) in Al-7Si-0.3Mg-0.8Fe alloy (Figure 5.14) leads to modification of the eutectic Si to fibrous form and precipitation of Mn-Fe Chinese script phases. Figure 5.15 shows the EDS elemental X-ray mapping and elemental distribution of Chinese script Mn-Fe phase in Al-7Si-0.3Mg-0.8Fe alloy with Be (0.15%)+Mn (0.15%) addition.

The microstructures of Al-7Si-0.3Mg-0.8Fe alloy treated without and with Mn, Be and Sr in T6 condition are shown in Figures 5.16 and 5.17 respectively and there is no significant change in the  $\beta$ -platelets by heat treatment. Similarly, the persistence of the Chinese script intermetallics even after heat treatment of the alloy with Mn and Be additions is also revealed [Figures 5.16 (b) and 5.17 (a)].



**Figure 5.10: Typical permanent mould cast microstructure of Al-7Si-0.3Mg-0.8Fe alloy with Be (0.005%)+Ca (0.04%) addition**

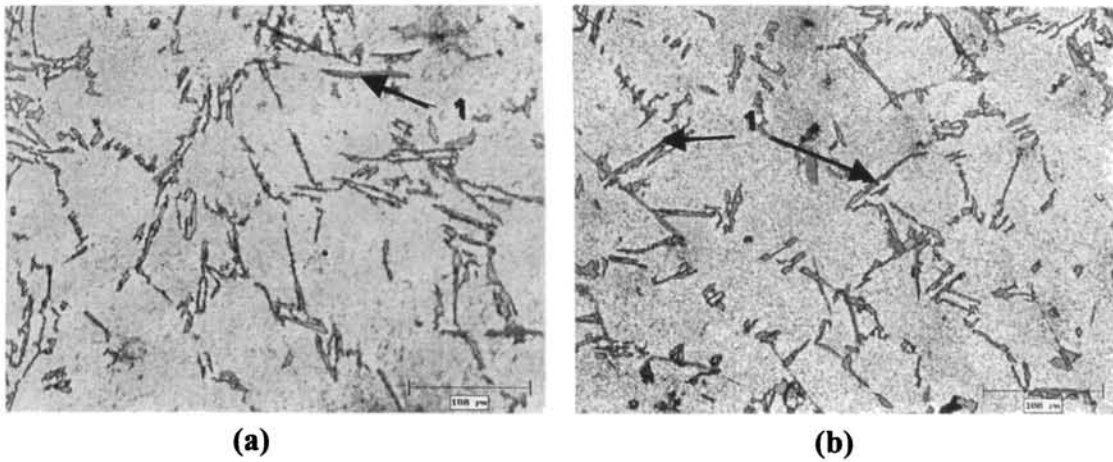


**Figure 5.11: Typical sand mould cast microstructures of Al-7Si-0.3Mg-1.0Fe alloy treated with (a) 0.015% Ca+0.005% Be and (b) 0.008% Ca + 0.007% Be [“1”- Platelet form of iron intermetallic compound]**

**Table 5.1: Average length of eutectic Si in Al-7Si-0.3Mg-1.0Fe alloy without and with Ca, Be and Ca+Be additions**

Alloy Code	Composition	Average length of eutectic Si ( $\mu\text{m}$ )
CF3	Al-7Si-0.3Mg-1.0Fe	32.6
CF3C	Al-7Si-0.3Mg-1.0Fe-0.015% Ca	16.8
CF3B	Al-7Si-0.3Mg-1.0Fe-0.2% Be	31.5
CF3CB1	Al-7Si-0.3Mg-1.0Fe-0.015% Ca-0.005% Be	18.6
CF3CB2	Al-7Si-0.3Mg-1.0Fe-0.008% Ca-0.007% Be	20.8

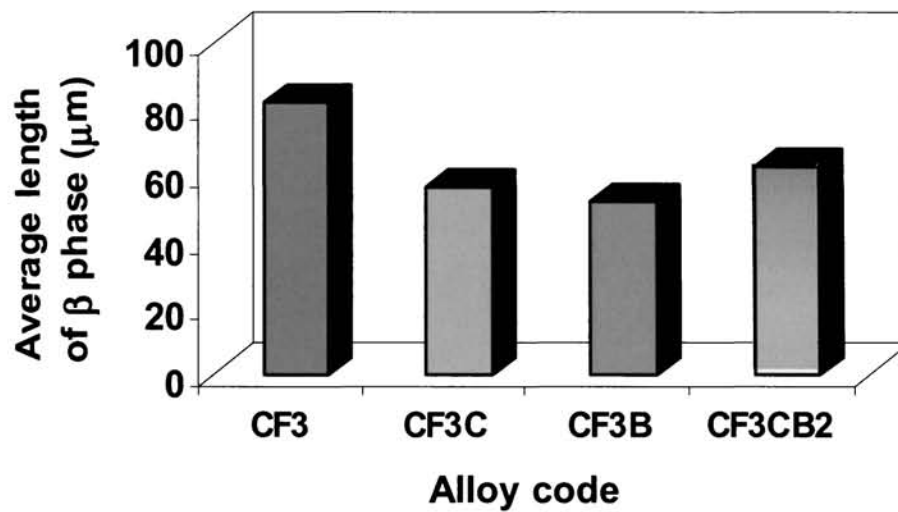


**Figure 5.12: Average length of  $\beta$  phase in Al-7Si-0.3Mg-1.0Fe alloy without and with Ca, Be and Ca+Be additions**

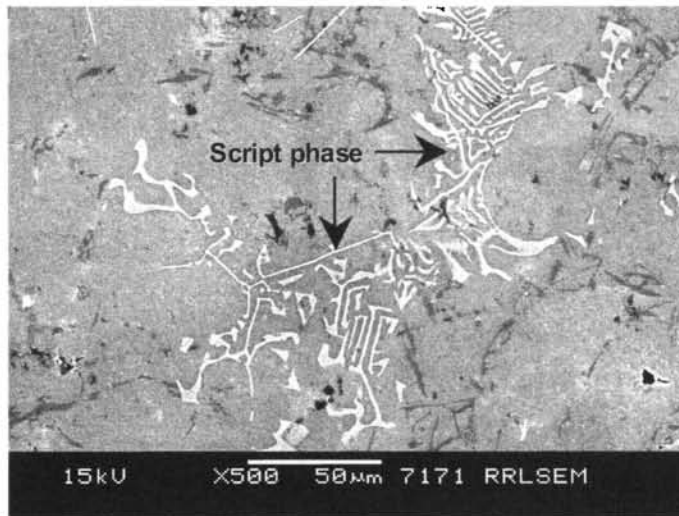


**Figure 5.13: SEM micrograph of Al-7Si-0.3Mg-0.8Fe alloy with Be (0.15%)+Mn (0.15%) addition**

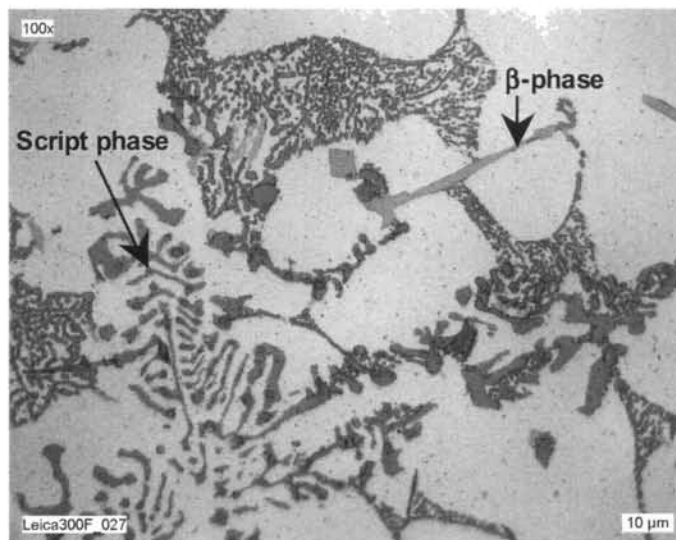


**Figure 5.14: Typical microstructure of permanent mould cast Al-7Si-0.3Mg-0.8Fe alloy with Mn (0.3%)+Sr (0.04%) addition**

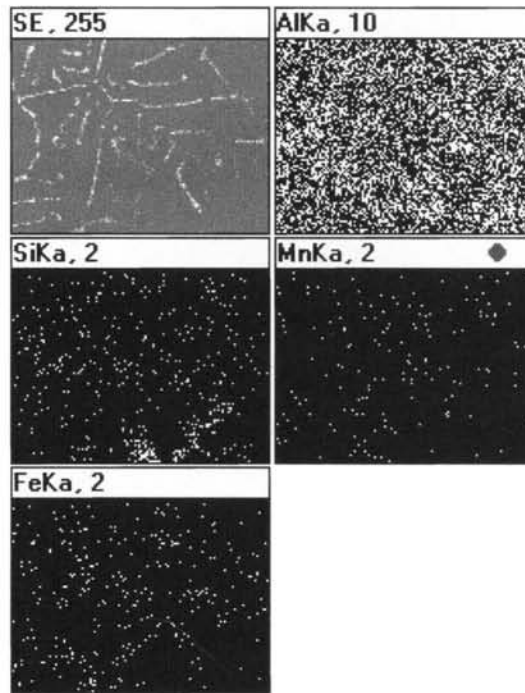
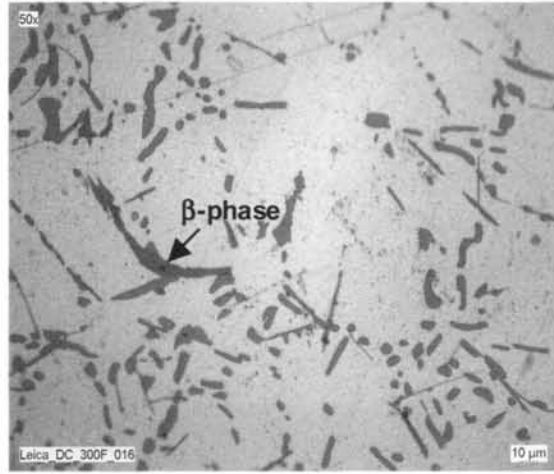
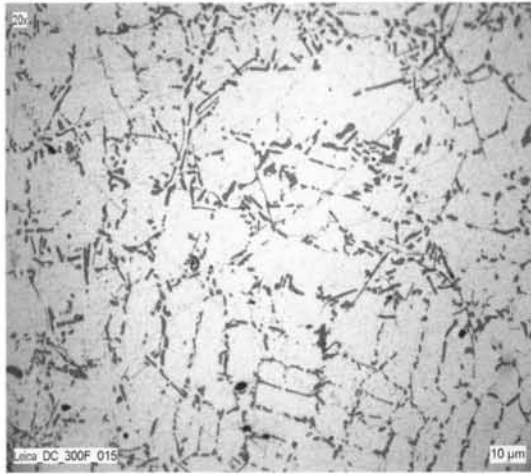
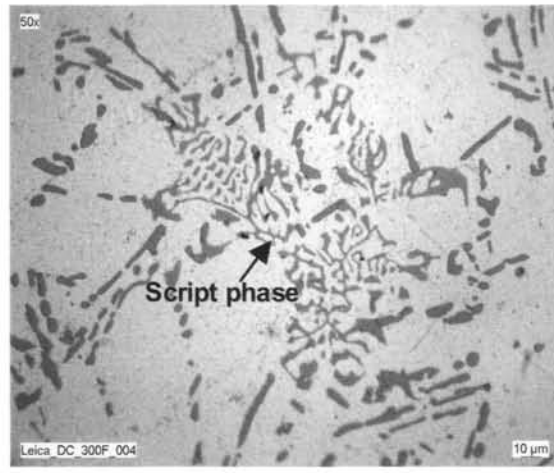
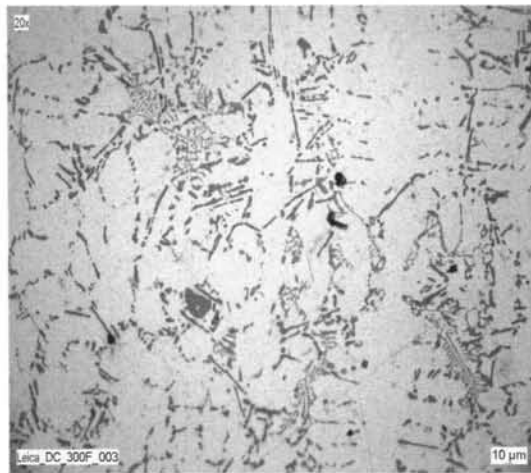


**Figure 5.15: EDS elemental X-ray mapping and elemental distribution of Chinese script Mn-Fe phase in Al-7Si-0.3Mg-0.8Fe alloy with Be (0.15%) + Mn (0.15%)**

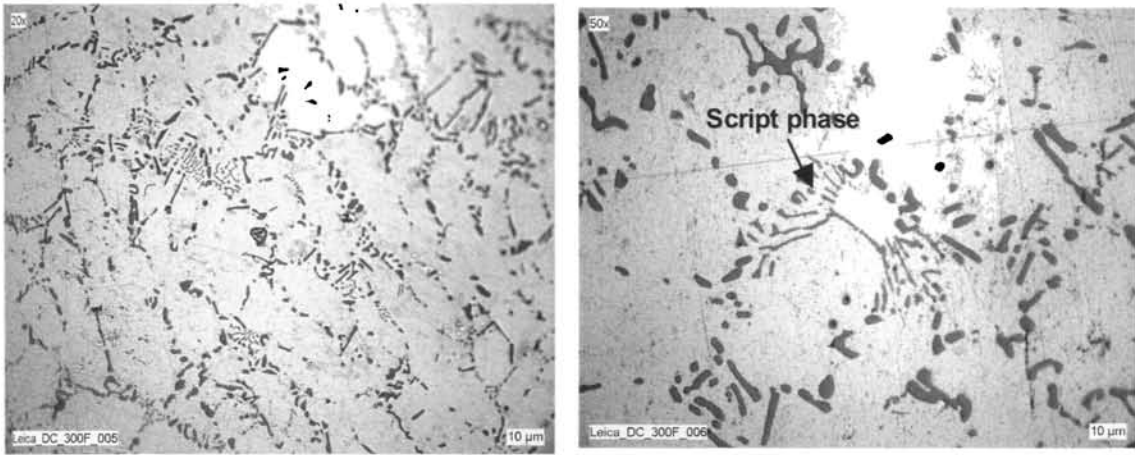


(a)

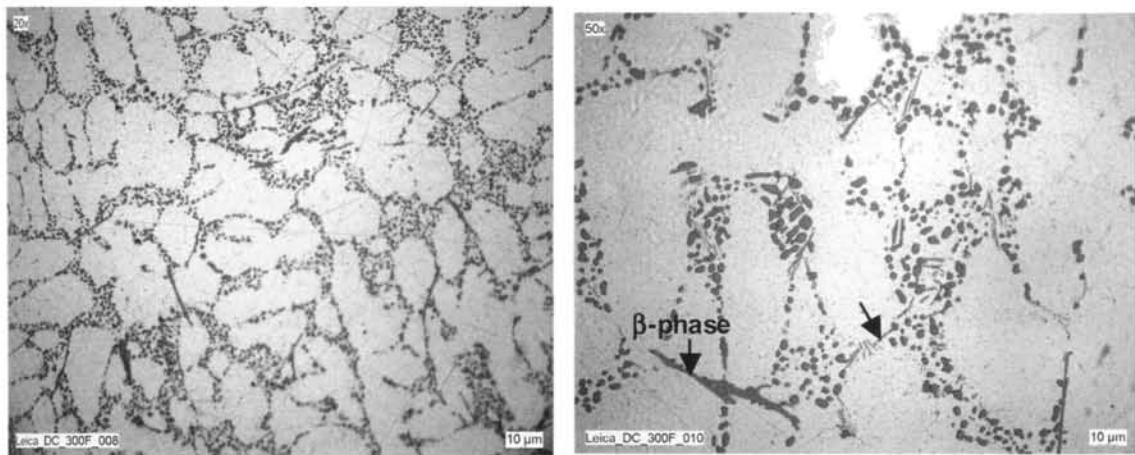


(b)

**Figure 5.16: Typical microstructures of Al-7Si-0.3Mg-0.8Fe alloy in T6 condition  
(a) without and (b) with 0.4% Mn**



(a)



(b)

**Figure 5.17: Typical microstructures of Al-7Si-0.3Mg-0.8Fe alloy in T6 condition with (a) 0.2% Be and (b) 0.04% Sr**

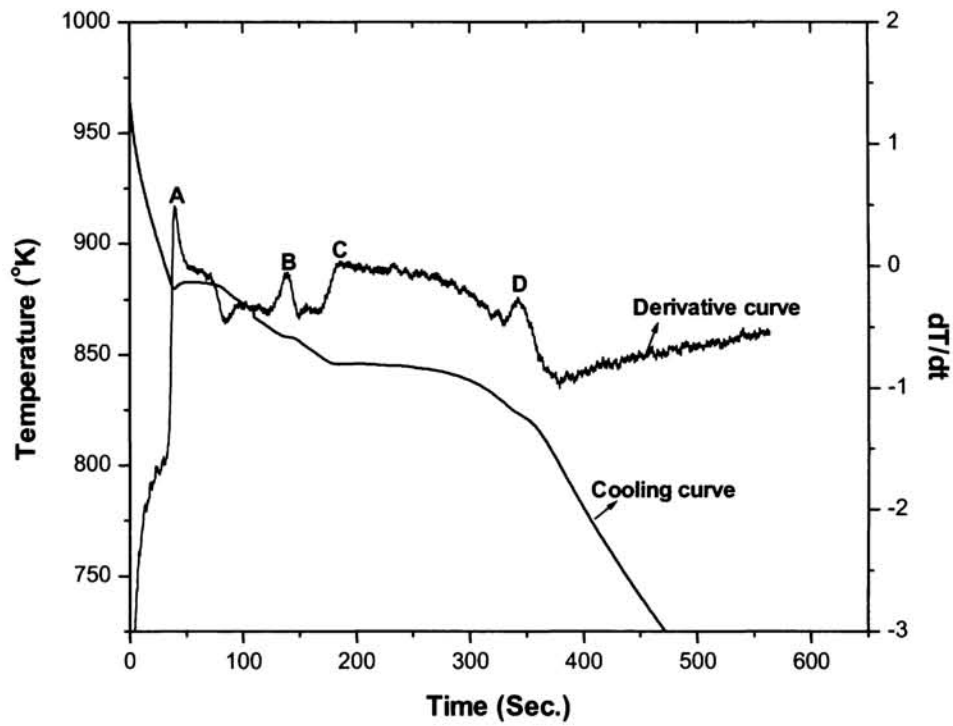
## 5.3.2 Solidification Behaviour

### 5.3.2.1 Thermal Analysis

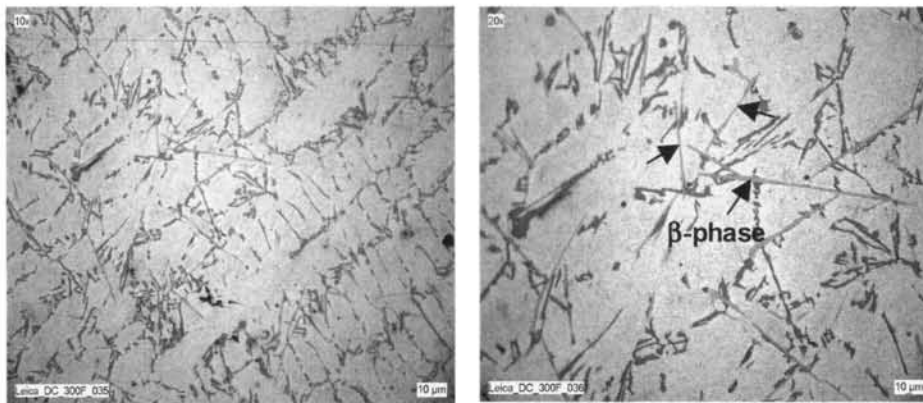
Figures 5.18-5.22 show the cooling curves and their first derivatives and the microstructures (at the centre of the thermal analysis sample, where the thermocouple tip was located) and Table 5.2 gives the alloys, thermal arrests and the phases formed in Al-7Si-0.3Mg-0.8Fe alloy without and with Be (0.2%), Mn (0.4%), Ca (0.04%) and Sr (0.04%) additions respectively. The first derivative is a measure of the instantaneous cooling rate along the cooling curve and is used here to signal the presence of minor slope changes on the curves. For each alloy sample, two cooling curves were taken to check repeatability. Figure 5.18 shows first thermal arrest point at 880.3 K, where the formation and growth of Al nuclei occur. After this arrest, the temperature of the solidifying alloy continues to decrease. Primary Al dendrites grow and the liquid is progressively enriched in Si and Fe. Second thermal arrest occurs at 858 K. This is caused by the latent heat fusion of the  $\beta$ -phase. Next arrest occurs at 845.9 K corresponding to the eutectic Si formation and growth. The final arrest point occurs at 823.8 K when the  $Mg_2Si$  phase is formed. On the other hand, the peak corresponding to  $\beta$  Fe-intermetallic is completely absent with Be (0.2%) addition. This shows that the  $\beta$  Fe phase has been changed to  $\alpha$ -(Be-Fe) phase as shown in the microstructure. However, the peak corresponding to  $\beta$  Fe-intermetallic phase formation is seen in the case of Mn, Ca and Sr additions. This is also evident from the microstructures (Figures 5.19-5.22) showing both platelet and Chinese script phases with Mn addition and refined platelet Fe intermetallics with Ca and Sr additions. Further, Ca and Sr additions decrease the eutectic temperature compared to the untreated alloy and the difference between the eutectic temperature of the untreated and Ca and Sr added sample is 6.6 and 8.7 K respectively. This is due the modification of eutectic Si by Ca and Sr additions to fine fibrous form as shown in the microstructures.

### 5.3.2.2 Differential Thermal Analysis

Differential Thermal Analysis (DTA) has been carried out in Al-7Si-0.3Mg-0.8Fe, Al-7Si-0.3Mg-0.8Fe-0.2Be and Al-7Si-0.3Mg-0.6Fe-0.5Mn alloys at a heating and cooling rate of 2° K/min and the corresponding DTA curves are given in Figures

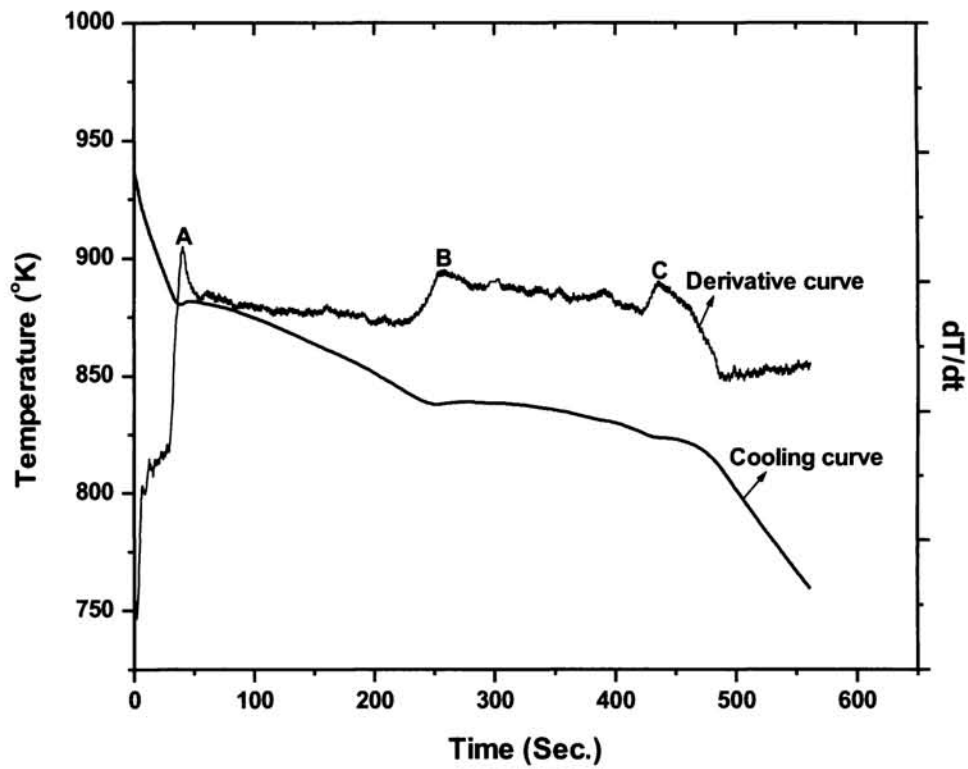


(a)

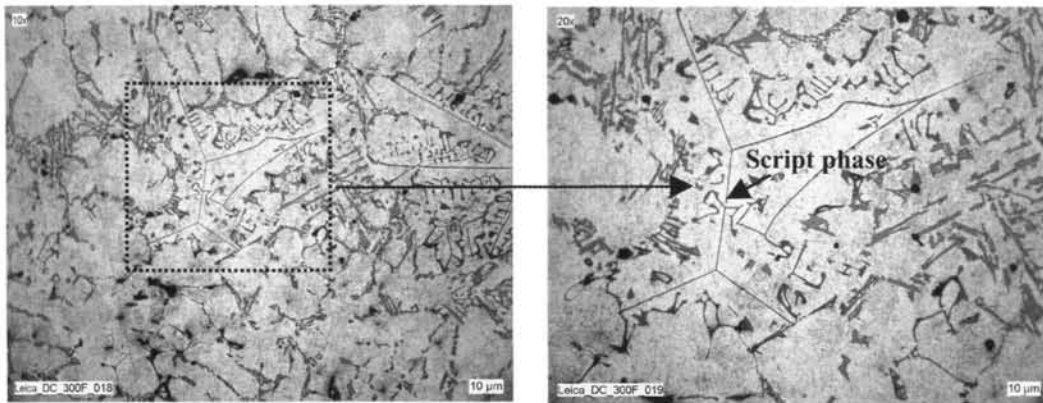


(b)

**Figure 5.18: (a) Cooling curve and its first derivative and (b) microstructures of Al-7Si-0.3Mg-0.8Fe alloy thermal analysis sample**

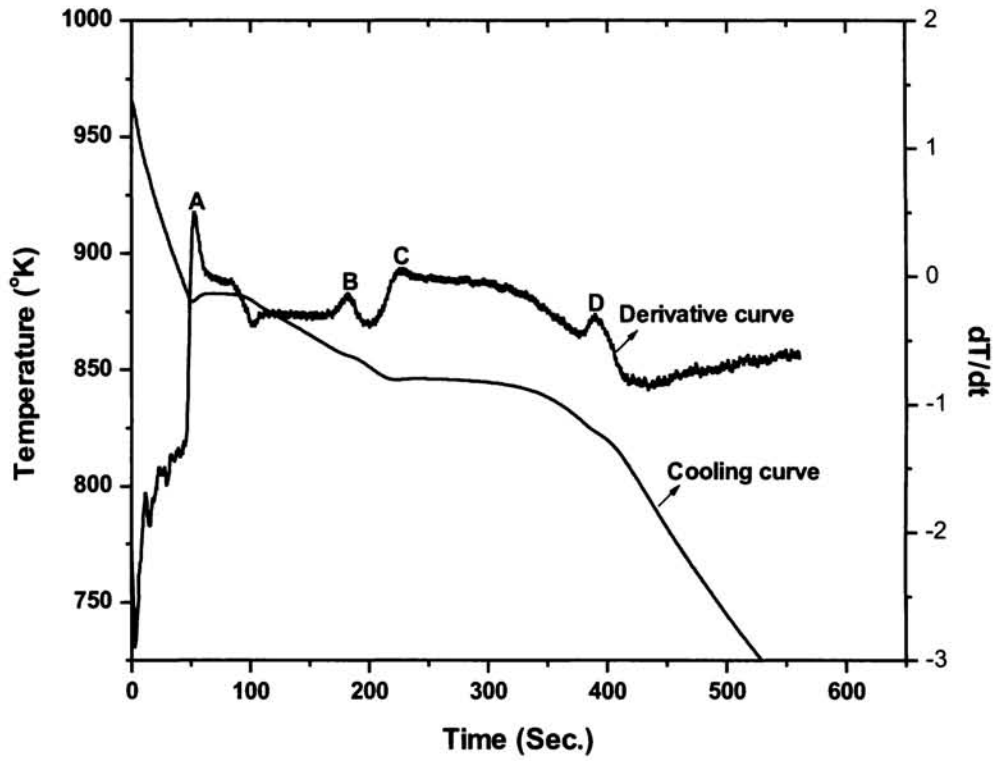


(a)

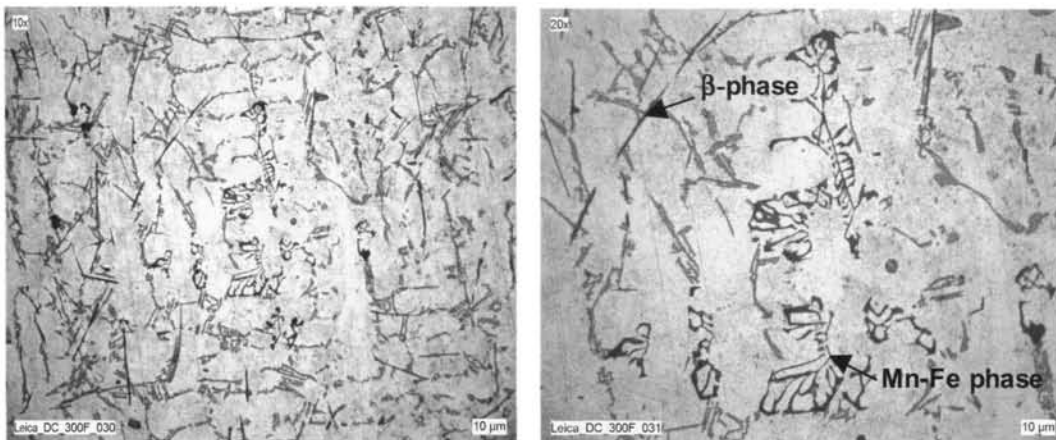


(b)

**Figure 5.19: (a) Cooling curve and its first derivative and (b) microstructures of Al-7Si- 0.3Mg-0.8Fe-0.2Be alloy thermal analysis sample**

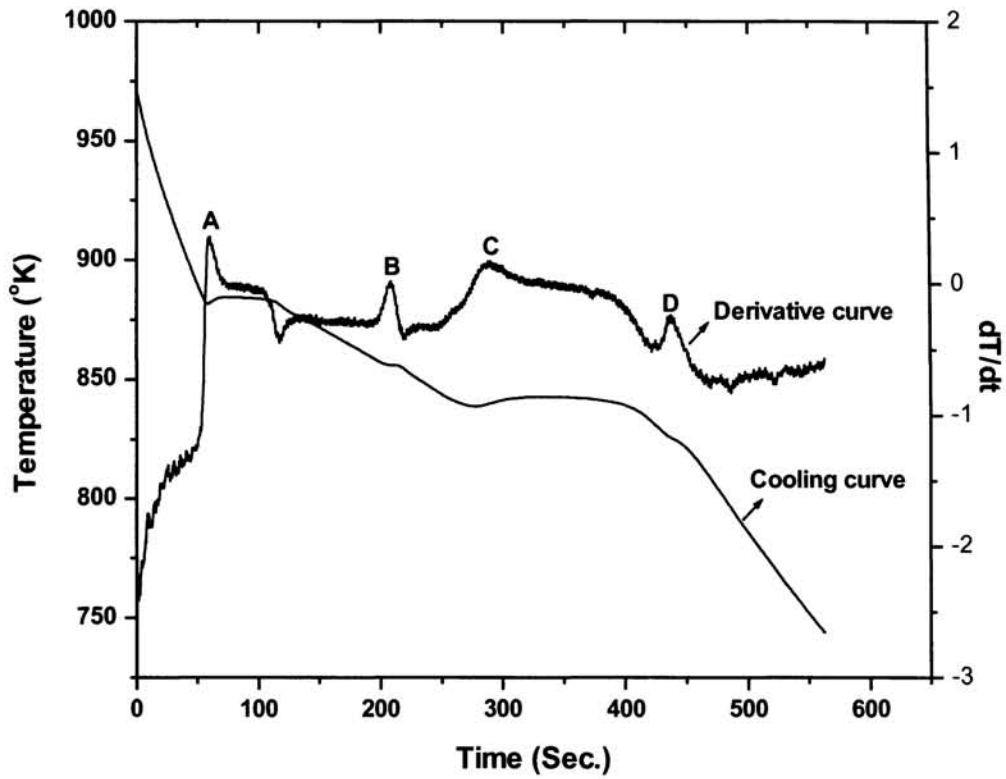


(a)

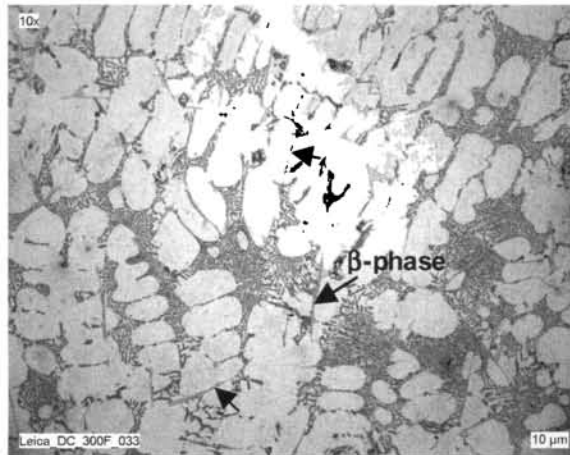


(b)

Figure 5.20: (a) Cooling curve and its first derivative and (b) microstructures of Al-7Si-0.3Mg-0.8Fe-0.4Mn alloy thermal analysis sample

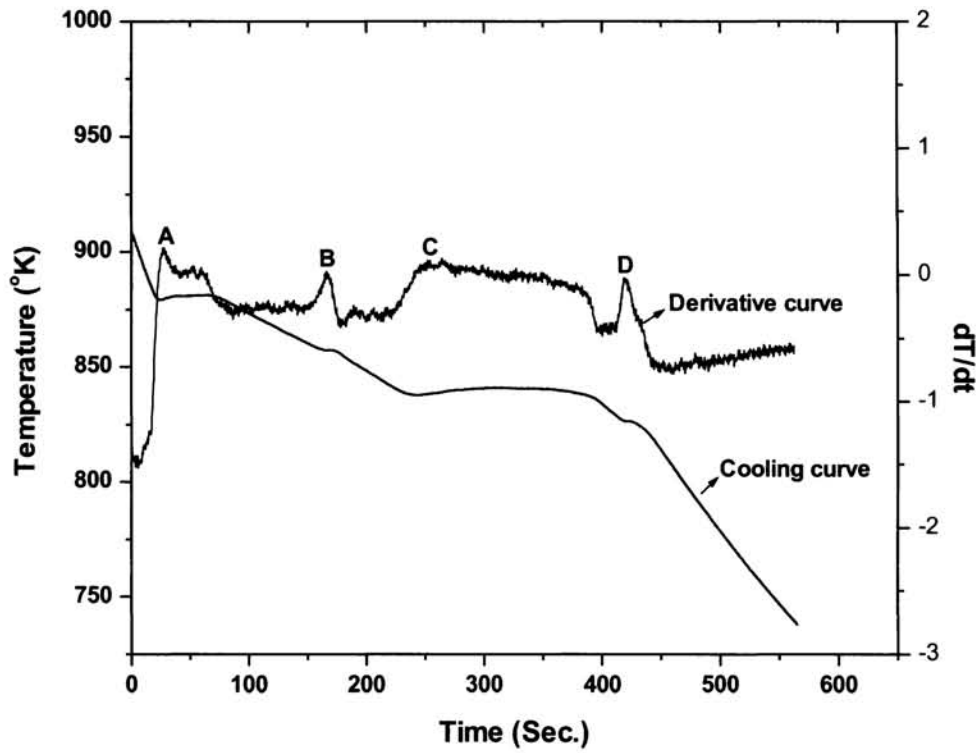


(a)

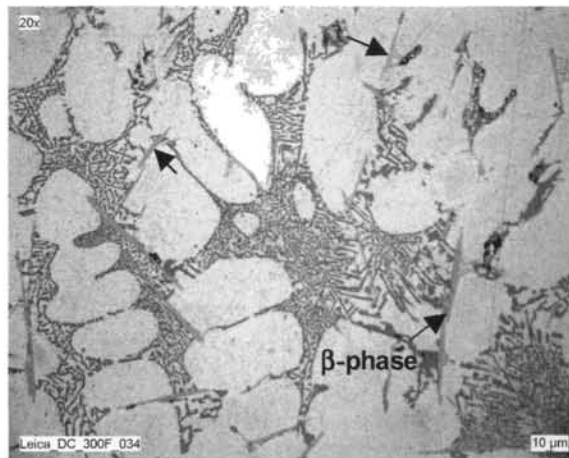


(b)

**Figure 5.21: (a) Cooling curve and its first derivative and (b) microstructure of Al-7Si-0.3Mg-0.8Fe-0.04Ca alloy thermal analysis sample (arrows show  $\beta$ -Fe intermetallic phase)**



(a)

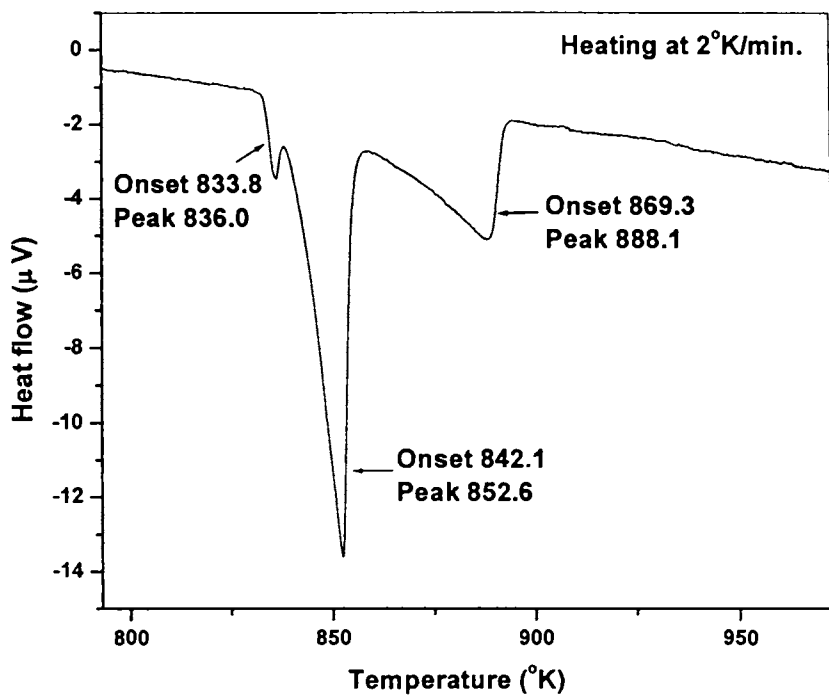


(b)

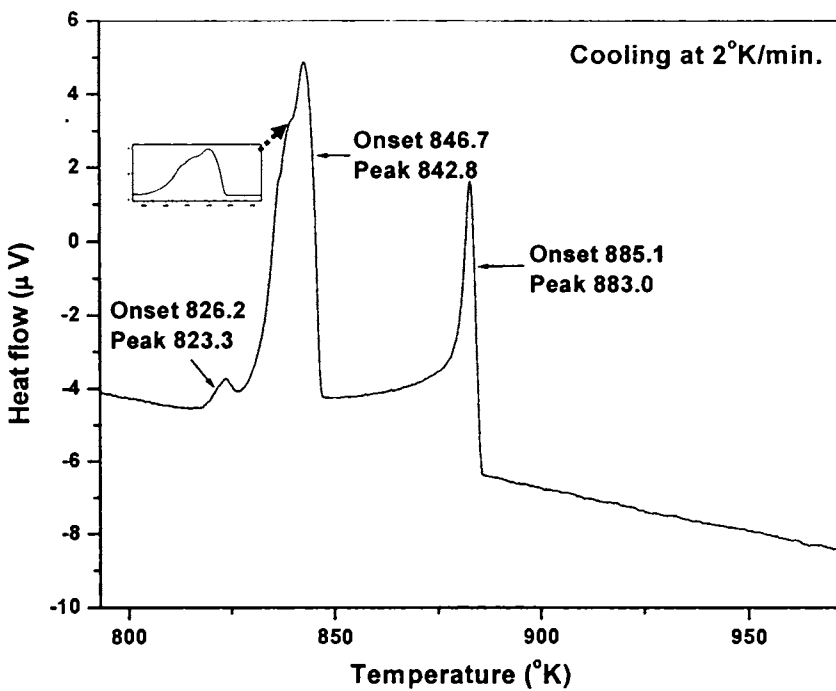
Figure 5.22: (a) Cooling curve and its first derivative and (b) microstructure of Al-7Si-0.3Mg-0.8Fe-0.04Sr alloy thermal analysis sample (arrows show  $\beta$ -Fe intermetallic phase)

**Table 5.2: Alloys, thermal arrests and the phases formed in Al-7Si-0.3Mg-0.8Fe alloy without and with Be, Mn, Ca and Sr additions**

Alloy	Thermal arrests		Phases formed
	Peak	Temperature (°K)	
Al-7Si-0.3Mg-0.8Fe	A	880.3	Primary $\alpha$ -Al Iron intermetallics Eutectic Si Mg <sub>2</sub> Si phase
	B	858.0	
	C	845.9	
	D	823.8	
Al-7Si- 0.3Mg-0.8Fe-0.2Be	A	880.7	Primary $\alpha$ -Al Eutectic Si Mg <sub>2</sub> Si phase
	B	838.1	
	C	823.7	
Al-7Si-0.3Mg-0.8Fe-0.4Mn	A	879.6	Primary $\alpha$ -Al Iron intermetallics Eutectic Si Mg <sub>2</sub> Si phase
	B	856.5	
	C	845.8	
	D	823.8	
Al-7Si-0.3Mg-0.8Fe-0.04Ca	A	882.1	Primary $\alpha$ -Al Iron intermetallics Eutectic Si Mg <sub>2</sub> Si phase
	B	855.9	
	C	839.3	
	D	826.4	
Al-7Si- 0.3Mg-0.8Fe-0.04Sr	A	879.3	Primary $\alpha$ -Al Iron intermetallics Eutectic Si Mg <sub>2</sub> Si phase
	B	857.2	
	C	837.2	
	D	826.7	

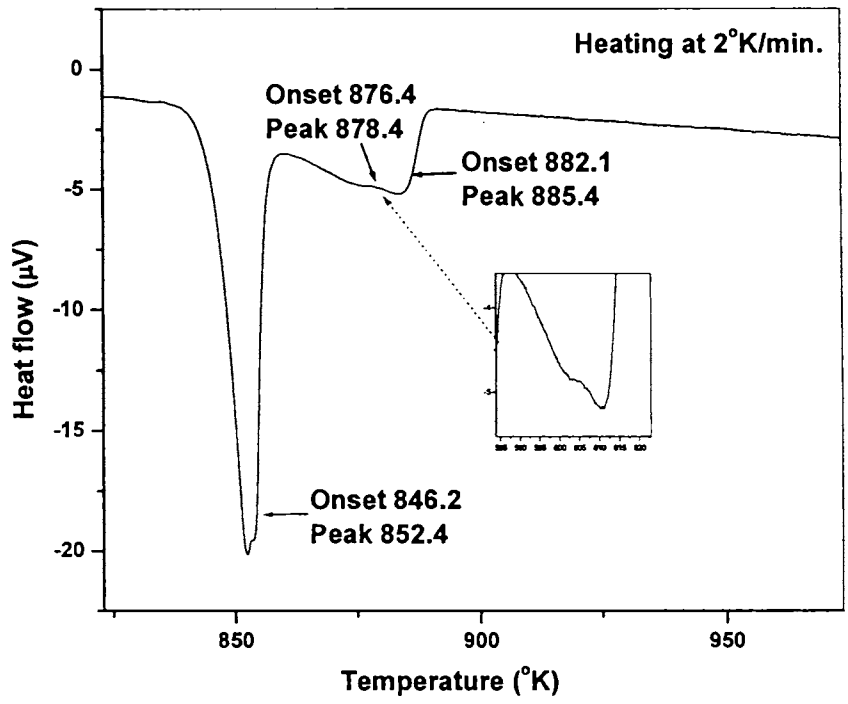


(a)

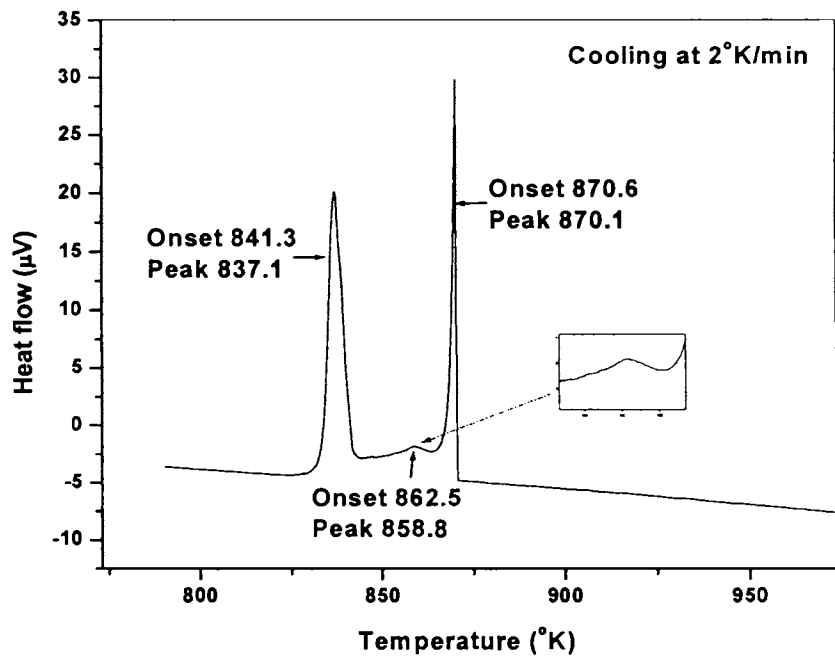


(b)

Figure 5.23: DTA curves of Al-7Si-0.3Mg-0.8Fe alloy (a) Heating and (b) Cooling at 2°K/min.

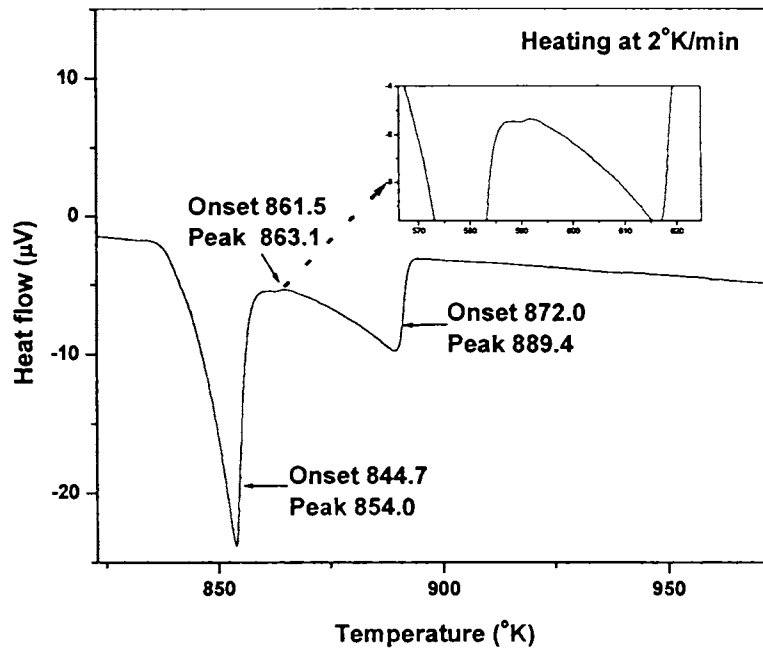


(a)

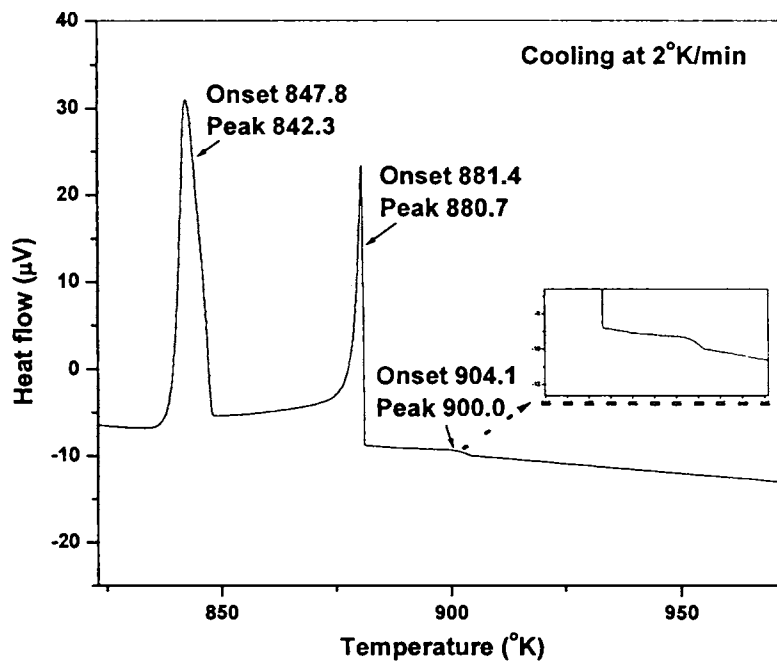


(b)

Figure 5.24: DTA curves of Al-7Si-0.3Mg-0.8Fe alloy with 0.2% Be addition  
(a) Heating and (b) Cooling at 2° K/min.



(a)



(b)

Figure 5.25: DTA curve of Al-7Si-0.3Mg-0.6Fe alloy with 0.5% Mn addition  
 (a) Heating and (b) Cooling at 2° K/min.

5.23-5.25. The peak corresponding to platelet Fe intermetallic could not be detected since it merges with the eutectic Si reaction as shown in the cooling curve (Figure 5.23). It is seen from the Figure 5.24 that the temperature of Be-Fe phase dissolution (heating curve) and the precipitation (cooling curve) are higher than the peak corresponding to  $\beta$ -Fe intermetallic phase formation (858 K from thermal analysis). As a result, the amount of free iron available to precipitate in the form of  $\beta$ -Al<sub>3</sub>FeSi is diminished. This is supported from the microstructural observation of the replacement of platelet Fe intermetallics by Chinese script phases. Similarly, the peak at 863 K (heating curve) in Figure 5.25 corresponds to Chinese script Mn-Fe-intermetallic phase reaction. The observation of sludge formation at higher Mn (0.5%) addition in the microstructure is supported from the appearance of a peak at 900 K (cooling curve).

### 5.3.3 Physical characteristics

#### 5.3.3.1 Porosity

Table 5.3 shows the effect of Ca, Mn and Ca + Mn on the porosity and electrical conductivity of Al-7Si-0.3Mg-0.6Fe alloy. It is seen that % porosity is increased with Ca (0.05%) addition compared to the untreated and other additions studied. The % porosity is lower with Mn followed by Ca + Mn additions. This may be due to the morphological change of large platelet Fe-intermetallic compounds to star like, Chinese script and other compact shapes. This result is in accordance with the work of Samuel et al<sup>195</sup> on the effect of Be, Mn, Cr and Sr on 319 (Al-6.2Si-3.7Cu) alloy, which has shown that the contours of the script phase facilitate the filling up of the liquid metal in between the dendrite arms of the phase (compared to the blocking action of the  $\beta$ -needles/platelets) and thereby reducing the amount of porosity.

#### 5.3.3.2 Electrical conductivity

The electrical conductivity of Ca added samples are higher than those of the untreated, Mn and Ca+Mn added samples (Table 5.3). This is due to the modification of eutectic Si by Ca addition to fibrous form, which allows easier flow of electrons compared to the platelet morphology.

**Table 5.3: % porosity and electrical conductivity of permanent mould cast Al-7Si-0.3Mg-0.6Fe alloy without and with Ca, Mn and Ca + Mn additions**

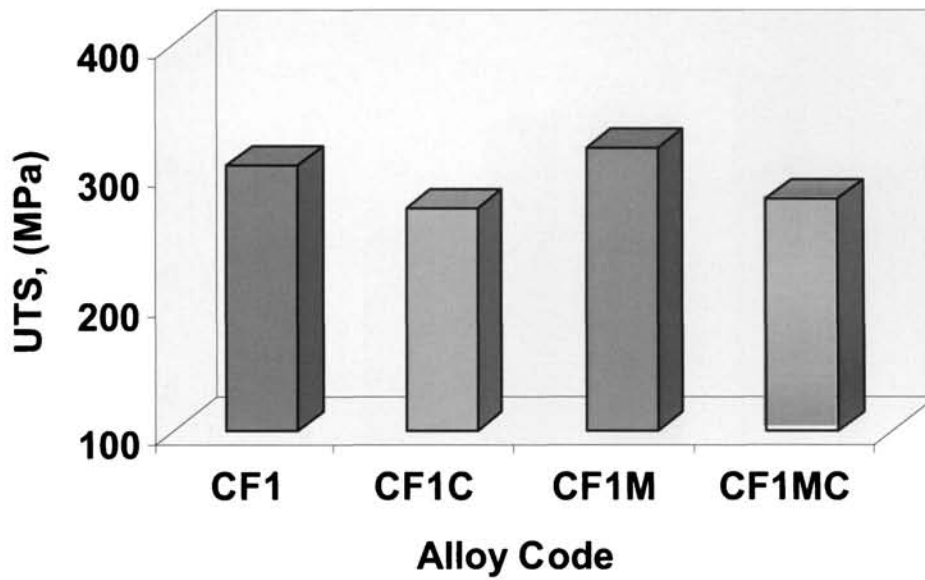
<b>Alloy Code</b>	<b>Addition</b>	<b>% Porosity</b>	<b>Electrical conductivity</b>
CF1	No addition	0.82	34
CF1C	0.005% Ca	1.27	36
CF1M	0.3% Mn	0.78	33
CF1MC	0.05% Ca +0.3% Mn	0.86	34

### 5.3.4 Mechanical Properties

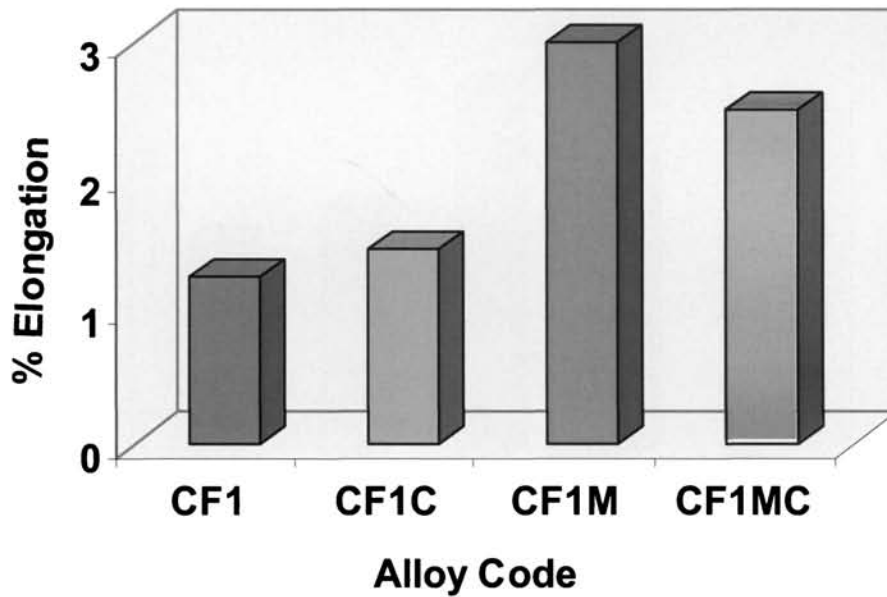
#### 5.3.4.1 Tensile properties

The ultimate tensile strength and % elongation of Ca, Mn and Ca+Mn added Al-7Si-0.3Mg-0.6Fe alloy cast in permanent mould are compared in Figures 5.26 (a) and (b) respectively. Mn (0.3%) addition has increased the ultimate tensile strength (UTS) nominally [4.2% improvement] compared to the untreated alloy. However, the addition of Ca and Ca+Mn has decreased the UTS by 11 and 8.8% respectively compared to untreated alloy. It has also been observed that the addition of Ca and Mn both individually and in combination increases the elongation of the alloy [Figures 5.26 (b)] compared to the untreated alloy. However, the maximum improvement in elongation (140%) is obtained with Mn (0.3%) followed by Ca+Mn and Ca addition, the latter showing only a nominal increase.

Figures 5.27 (a) and (b) show the variation of ultimate tensile strength and % elongation of Al-7Si-0.3Mg-1.0Fe alloy with Ca, Be and Ca + Be additions. Be (0.2%) addition has improved the UTS (26.3%) and elongation (71.4%) due to the morphological change of  $\beta$  needles to Chinese script form. The results obtained in the present study are in good agreement with the published data<sup>26</sup> concerning the effectiveness of Be as an iron neutralizer in Al-7Si-0.3Mg alloy. It has been observed



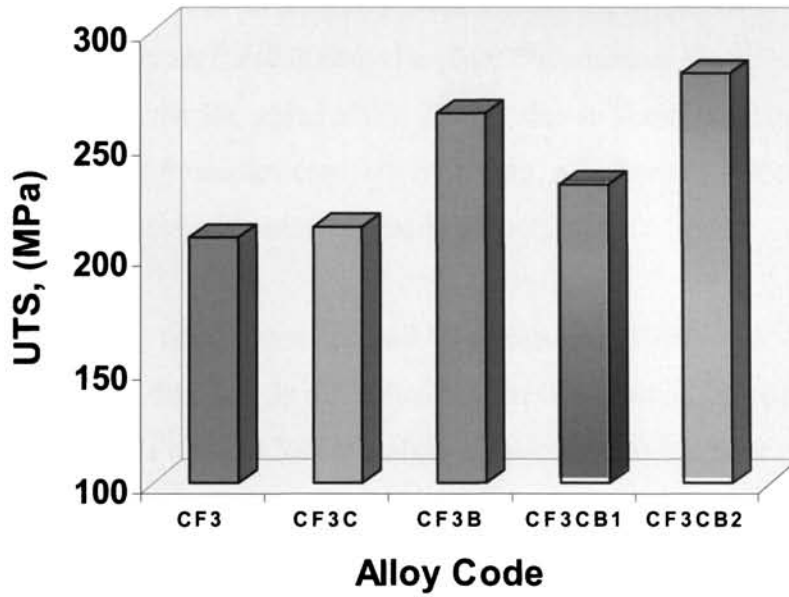
(a)



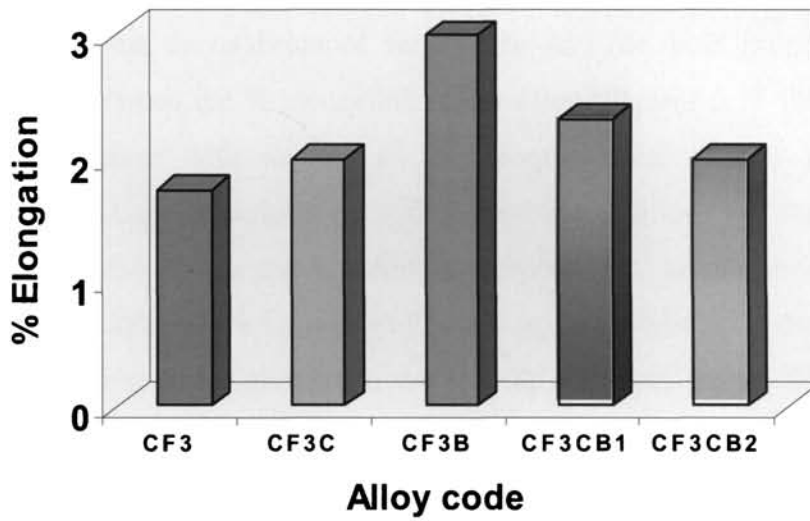
(b)

CF1: Al-7Si-0.3Mg-0.6Fe
CF1C: Al-7Si-0.3Mg- 0.6Fe +0.05% Ca
CF1M: Al-7Si-0.3Mg-0.6Fe +0.3%Mn
CF1MC: Al-7Si-0.3Mg- 0.6Fe +0.3%Mn+0.05% Ca

**Figure 5.26: Effect of Ca, Mn and Ca+Mn additions on the (a) UTS and (b)% elongation of Al-7Si-0.3Mg-0.6Fe alloy cast in permanent mould**



(a)



(b)

CF3: Al-7Si-0.3Mg-1.0Fe
CF3C: Al-7Si-0.3Mg-1.0Fe +0.015% Ca
CF3B: Al-7Si-0.3Mg-1.0Fe +0.2% Be
CF3CB1: Al-7Si-0.3Mg-1.0Fe +0.015% Ca+0.015% Be
CF3CB2: Al-7Si-0.3Mg-1.0Fe +0.008% Ca + 0.007% Be

Figure 5.27: Effect of Ca, Be and Ca+Be additions on the (a) UTS and (b) % elongation of Al-7Si-0.3Mg-1.0Fe alloy cast in permanent mould

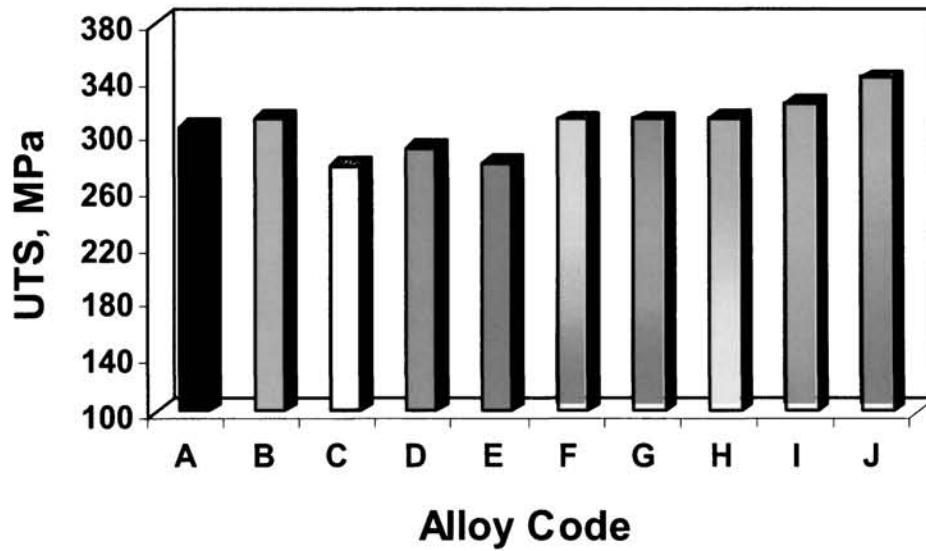
that a trace amount of Be addition to Al-7Si-0.3Mg-1.0Fe-0.015% Ca alloy improves both the UTS and elongation compared to Al-7Si-0.3Mg-1.0Fe and Al-7Si-0.3Mg-1.0Fe-0.015Ca alloys. The maximum improvement in tensile strength (34.5%) is obtained with Ca (0.008%)+Be (0.007%) addition. However, % elongation is low compared to the Be added alloy. This is due to insufficient amount of Ca to reduce the length of  $\beta$  needles completely. Hence, a higher amount of Ca with trace Be may give the best combination of tensile properties.

The ultimate tensile strength and % elongation of Al-7Si-0.3Mg-0.8Fe alloy treated with Be, Ca, Mn and Sr individually or in combination and cast in permanent mould are shown in Figures 5.28 (a) and (b) respectively. It has been observed that all additions except Ca, Sr and Mn increase the UTS compared to the untreated alloy. The highest improvement in UTS has been observed in the combined addition of Be (0.15%) and Mn (0.15%) to Al-7Si-0.3Mg-0.8Fe alloy. On the other hand, Ca (0.04%), Sr (0.04%) and Mn (0.4%) additions have reduced the UTS by 9.2, 5.3 and 8.6% respectively compared to that of untreated Al-7Si-0.3Mg-0.8Fe alloy. It has also been observed that the addition of Be, Ca, Sr and Mn both individually and in combination increases the % elongation of the alloy [Figures 5.28 (b)] compared to the untreated alloy. This is due to the morphological change of platelet Fe intermetallics to Chinese script form with Be and Mn additions and the refinement of platelet Fe phases with Ca and Sr additions respectively. Addition of Mn (0.3%) to Al-7Si-0.3Mg-0.8Fe-0.04% Ca and Al-7Si-0.3Mg-0.8Fe-0.04% Sr alloys leads to 75 and 167% improvement in elongation respectively compared to individual addition of Ca and Sr.

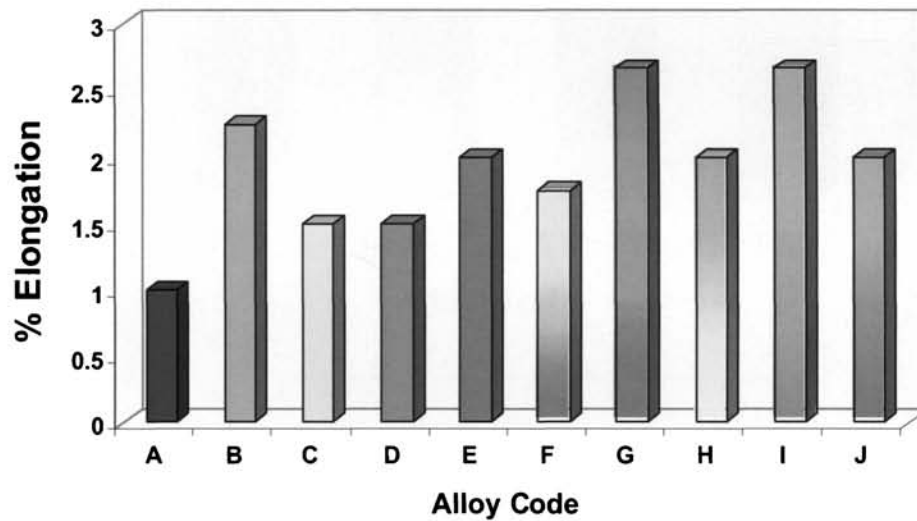
Be (0.2%) addition has shown significant improvement in elongation (125%). It is interesting to note that trace amount of Be (0.005%) with Ca and Sr (0.04%) has improved the UTS (2 and 5.5% respectively) and elongation (100 and 167% respectively) compared to the untreated and Ca and Sr alone added alloys.

#### **5.3.4.2 Impact Strength**

Figure 5.29 shows the impact strength of Al-7Si-0.3Mg-0.6Fe alloy with and without Ca, Mn and Ca+Mn additions. As reported in the previous chapter, impact



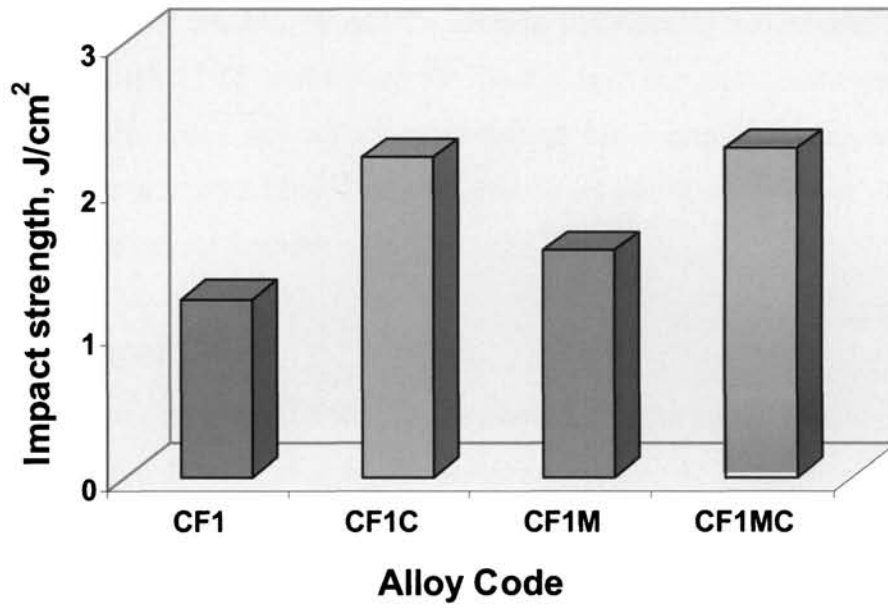
(a)



(b)

A: Al-7Si-0.3Mg-0.8Fe
B: Al-7Si-0.3Mg-0.8Fe +0.2% Be
C: Al-7Si-0.3Mg-0.8Fe +0.04% Ca
D: Al-7Si-0.3Mg-0.8Fe + 0.04% Sr
E: Al-7Si-0.3Mg-0.8Fe +0.4% Mn
F: Al-7Si-0.3Mg-0.8Fe +0.3% Mn+ 0.04% Ca
G: Al-7Si-0.3Mg-0.8Fe + 0.3% Mn+0.04% Sr
H: Al-7Si-0.3Mg-0.8Fe + 0.005% Be+0.04% Ca
I: Al-7Si-0.3Mg-0.8Fe + 0.005% Be+ 0.04% Sr
J: Al-7Si-0.3Mg-0.8Fe +0.15% Be+0.15% Mn

**Figure 5.28: Effect of Be, Mn, Sr and Ca individually and in combination on the (a) UTS and (b) % elongation of Al-7Si-0.3Mg-0.8Fe alloy**



CF1: Al-7Si-0.3Mg-0.6Fe
CF1C: Al-7Si-0.3Mg- 0.6Fe +0.05% Ca
CF1M: Al-7Si-0.3Mg-0.6Fe +0.3%Mn
CF1MC: Al-7Si-0.3Mg- 0.6Fe +0.3%Mn+0.05% Ca

**Figure 5.29: Effect of Ca, Mn and Ca+Mn additions on the impact strength of Al-7Si-0.3Mg-0.6Fe alloy**

strength has been greatly improved (80%) by Ca addition. However, only 27% improvement in impact strength has been observed in Mn added alloy. Ca+Mn addition shows 85% improvement. Further, the microstructural features observed in the fractographs of impact tested alloys [Figures 5.30 (a-d)] support these results. Ca added alloy shows more dimples, a characteristic of ductile fracture [Figure 5.31 (b)]. On the other hand, fractograph of Mn added alloy [Figure 5.31 (c)] shows the presence of a large number of cleavage fractured surface typical of a brittle failure.

The effect of Be, Mn, Sr and Ca addition individually and in combination on the impact strength of T6 heat-treated Al-7Si-0.3Mg-0.8Fe alloy is shown in Figure 5.31. It has been found that all additions except Mn improve the impact strength compared to the untreated alloy. However, combined addition of Mn with Ca, Sr and Be improves the impact strength.

#### 5.4 DISCUSSION

The large size of  $\beta$ -Al<sub>5</sub>FeSi platelet observed in the untreated alloys indicates that it must have formed at a higher temperature, i.e, as a pre-eutectic reaction (providing a longer time for its growth). On the other hand, the much smaller size of the  $\beta$ -platelets observed indicates that they are very likely the products of a co-eutectic reaction. It has been reported<sup>144, 200, 201</sup> that unlike the Si eutectic temperature, which is only marginally affected by variations in cooling rate, the  $\beta$ -phase start temperature decreases with decreasing iron content, increasing cooling rate and increasing melt superheat until it eventually merges with the Si eutectic temperature. Though the  $\beta$ -phase continues to crystallize until the end of the silicon eutectic reaction, the length of the primary  $\beta$ -phase needles greatly depends on the time interval between the  $\beta$ -phase start temperature and the silicon eutectic temperature. With decreasing  $\beta$ -phase start temperature, the  $\beta$ -phase growth time and therefore the length and volume fraction of this phase decrease until the  $\beta$ -phase start temperature merges with the silicon eutectic temperature.

It has been observed that the eutectic Si nucleates on the surface of the  $\beta$ -platelets [Figure 5.1 (b)]. This is supported from the work of Taylor et al.<sup>272</sup> It has

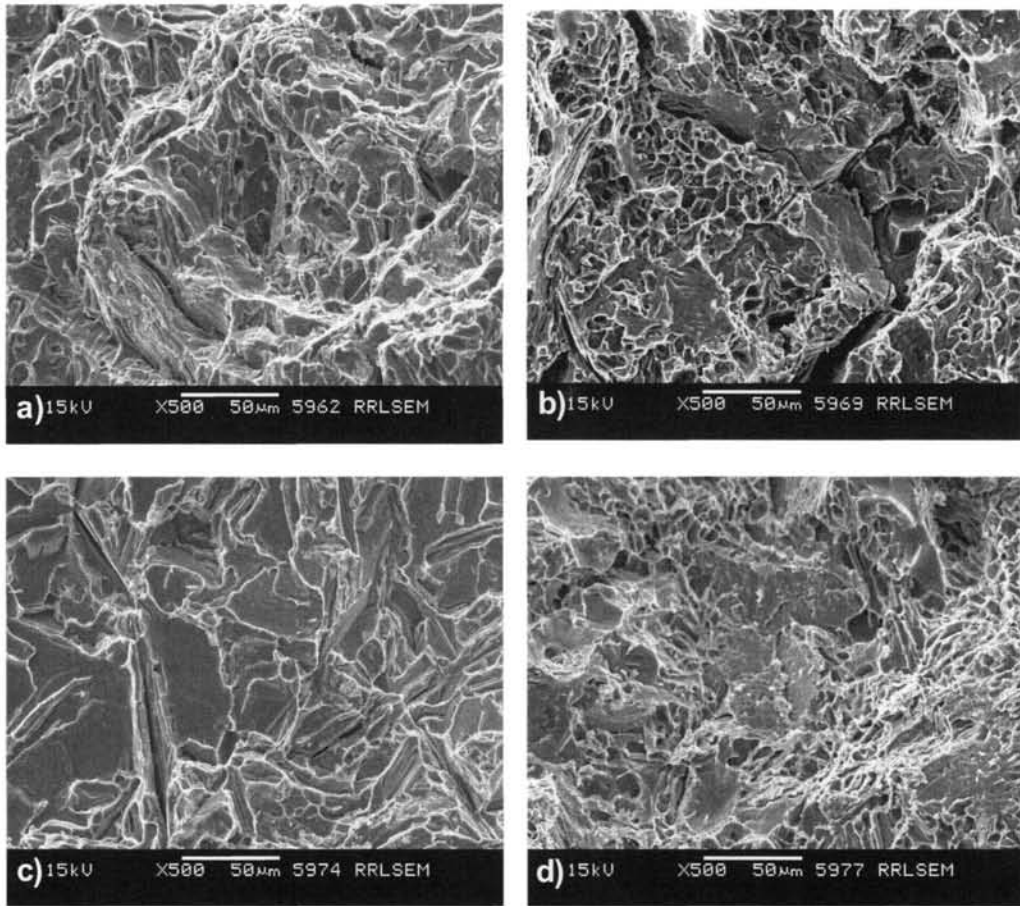
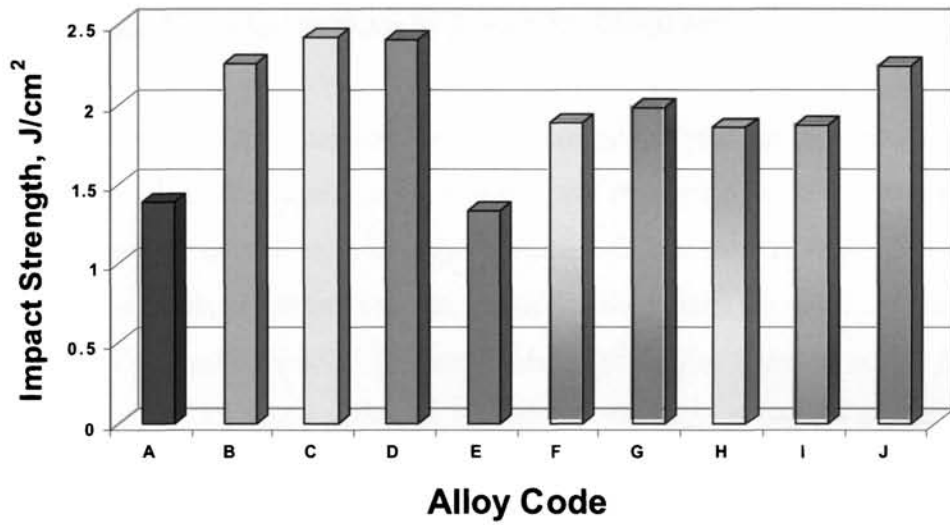


**Figure 5.30: Fractographs of impact tested Al-7Si- 0.3Mg- 0.6Fe alloy (a) without and with (b) 0.05% Ca (c) 0.3%Mn and (d) 0.3% Mn+0.05% Ca**



A: Al-7Si-0.3Mg-0.8Fe
B: Al-7Si-0.3Mg-0.8Fe +0.2% Be
C: Al-7Si-0.3Mg-0.8Fe +0.04% Ca
D: Al-7Si-0.3Mg-0.8Fe + 0.04% Sr
E: Al-7Si-0.3Mg-0.8Fe +0.4% Mn
F: Al-7Si-0.3Mg-0.8Fe +0.3% Mn+ 0.04% Ca
G: Al-7Si-0.3Mg-0.8Fe + 0.3% Mn+0.04% Sr
H: Al-7Si-0.3Mg-0.8Fe + 0.005% Be+0.04% Ca
I: Al-7Si-0.3Mg-0.8Fe + 0.005% Be+ 0.04% Sr
J: Al-7Si-0.3Mg-0.8Fe +0.15% Be+0.15% Mn

**Figure 5.31: Effect of Be, Mn, Sr and Ca individually and in combination on the impact strength of Al-7Si-0.3Mg-0.8Fe alloy**

been reported that the Si particles are often observed to grow from multiple locations along a single  $\beta$ -platelet. For eutectic Si to nucleate and grow on the  $\beta$ -platelets, the latter must form and present prior to the former. This is the case for the platelets that form as either a primary  $\beta$ -phase or as binary  $\beta$ -phase (a component of the Al- $\beta$ -Al<sub>5</sub>FeSi binary eutectic). Such platelets are well developed by the time the ternary eutectic Si begins to grow. This has been confirmed by the appearance of a peak at 858 K in Figure 5.18 corresponding to  $\beta$ -platelets formation.

Addition of Mn changes the morphology of platelet Fe intermetallic to Chinese script. This is because of the replacement of Mn by Fe, which can substitute each other, being transitional elements. However in the case of 0.5% Mn addition, agglomeration of the script and star like particles takes place [Figure 5.2 (b)]. In order to obtain the crystallization of the iron compound in the Chinese script form and avoid the needle like and polyhedral crystal morphology, a certain critical ratio of iron: manganese is required and this ratio depends on the cooling rate. Bakerud et al<sup>244</sup> have clearly explained the solidification sequence (Figure 2.13) with Mn addition in Al-7Si-0.3Mg alloy. According to Mondolfo,<sup>8</sup> (Fe,Mn)Al<sub>6</sub> is the first phase to form in the Al-Fe-Mn-Si system, which encompasses many commercial alloys. In many alloys, (Fe,Mn)Al<sub>6</sub> reacts peritectically with the liquid to form (FeMn)<sub>3</sub>Si<sub>2</sub>Al<sub>15</sub>. The rate of peritectic transformation depends on the equilibrium diagram and kinetic factors.<sup>280-283</sup>

Be (0.2%) has changed the morphology of platelet Fe compound to Chinese script and fine globules. Both Mn and Be additions lead to the precipitation of either coarse or fine Chinese script form of intermetallic phase with Fe at slow (thermal analysis sample, cooling rate 1.5° K/min) and fast cooling rates (permanent mould) respectively. It has also been observed in the present work that the Chinese script phases with Be addition forms only inside the  $\alpha$ -Al at slow cooling rate and both inside the  $\alpha$ -Al and in the interdendritic areas at high cooling rates. Murali et al<sup>210</sup> have reported that in the case Be (0.27%) added sand cast Al-7Si-0.3Mg alloy, the Be-Fe phase is formed inside the  $\alpha$ -Al, which is probably the result of a peritectic reaction. It has been observed from the DTA curves (Figures 5.24 and 5.25) that the Be-Fe and Mn-Fe phases precipitate at temperatures much higher than the formation

temperature of the  $\beta$ -phase. As a result, the amount of free iron available to precipitate in the form of  $\beta$ - $\text{Al}_5\text{FeSi}$  is diminished leading to the formation of Chinese script phase.

Be (0.2%) addition has significantly improved the tensile and impact properties. This is due to the morphological change of  $\beta$  needles to Chinese script form. This has been further confirmed from the cooling curve of Al-7Si-0.3Mg-0.8Fe-0.2Be alloy showing the absence of a peak corresponding to  $\beta$ -Fe intermetallic compared to the cooling curve without Be addition (Figures 5.18 and 5.19). The microstructures of Mn and Be added alloys in the T6 treated condition show the persistence of Chinese script phases. Further, it has been reported<sup>277</sup> that  $\alpha$ -AlFeMnSi particles have quite perfect crystals and hence the dissolution process is hindered by the lack of defects.

The improvement in elongation and impact strength with Sr addition is due to the fragmentation of the platelet Fe intermetallics and modification of the eutectic Si. This observation is in accordance with the work of Samuel et al<sup>195</sup> on Sr addition to Al-Si-Cu (319) alloy. The fragmentation of platelet Fe-intermetallic phase is clearly explained in the previous chapter.

It has been found that Mn addition improves the tensile properties. On the other hand, impact strength is not significantly improved. However, Mn in combination with Ca, Sr and Be improves the impact strength significantly. This is due to the modification of the eutectic Si from acicular to fibrous form. The most important observation in the present work is the attainment of the best combination of tensile and impact properties by Ca+Mn, Sr+Mn and Be+Mn additions to Al-7Si-0.3Mg-xFe alloys. Similarly, combined addition of a trace amount of Be (0.005%) to Ca and Sr improves the tensile properties significantly. This is due the fact that Be in trace amount in Al-Si alloys preferentially oxidizes forming BeO on the surface of the casting, cleans the melt surface and reduces gas pick up (and hence porosity) and Mg loss making Mg available for forming the required volume of  $\text{Mg}_2\text{Si}$  for strengthening.<sup>250</sup>

## 5.5 SUMMARY

1. Mn (0.3%) addition to Al-7Si-0.3Mg-xFe alloy changes the morphology of platelet iron phase to script form leading to significant improvement in tensile properties. However, there is no significant improvement in impact strength.
2. Be (0.2%) changes the platelet morphology of iron phase to Chinese script form, which are seen only inside the  $\alpha$ -Al in slow cooling (sand cast), both in the interdendritic as well as inside the  $\alpha$ -Al in fast cooling (permanent mould casting). This morphological change is responsible for the significant improvement in both the tensile and impact properties.
3. Combined additions of Ca + Mn, Be + Mn and Sr + Mn lead to improvement in both tensile and impact properties compared to individual additions and a synergistic effect of both the elements is achieved.
4. A trace amount of Be (0.005%) addition to Ca and Sr leads to superior tensile properties compared to Ca and Sr additions alone.

---

---

## CHAPTER 6

### CONCLUSIONS

---

---

In the present investigation, the dual beneficial effects of Ca viz., modification and Fe-neutralization, comparison of the effects of Ca and Sr with common Fe-neutralizers (Be and Mn) and the interaction of Be, Mn, Sr and Ca in a commercially important cast Al-7Si-0.3Mg alloy have been studied. The castings have been characterized with respect to their microstructure, % porosity and electrical conductivity, solidification behaviour and mechanical properties. The major observations and the conclusions drawn are given under each chapter. This chapter summarizes all of them together as well as highlights the significant contributions of this thesis to the knowledge and the avenues for future work.

1. Calcium modifies the platelet eutectic Si in Al-7Si-0.3Mg alloy to fibrous form. The optimum level of Ca required for modification so as to get the best mechanical properties lies in the range 0.01-0.02%.
2. Porosity of Ca (0.02%) added sample is lower than that treated with the well known modifier viz., Sr. The properties obtained with Ca (0.02%) addition are at par with those obtained with Sr (0.02%) addition.
3. Like Sr, higher amount of Ca also leads to the formation of higher porosity and Al-Ca-Si intermetallics.
4. Ca addition to Al-7Si-0.3Mg-xFe alloy modifies the eutectic Si and refines the long platelet  $\beta$ -Fe phases. The proposed mechanism of Fe-neutralization by Ca is the destabilization of the  $\beta$ -platelets and fragmentation of the long  $\beta$ -platelets into smaller ones.
5. A low amount of Ca (0.005%) has reduced the porosity of the alloy probably due to the trapping of hydrogen as calcium hydride.

6. Higher Ca levels lead to faster pickup of hydrogen probably due to the rupture of the protective  $\text{Al}_2\text{O}_3$  oxide film by the Ca containing oxide film.
7. Electrical conductivity is increased with Ca addition due to the change in eutectic Si morphology from acicular to fibrous form.
8. Ca addition has improved the % elongation and impact strength of Al-7Si-0.3Mg-xFe alloys significantly.
9. A high amount of Ca (0.05%) addition reduces the size of the platelet Fe-intermetallics to very fine form. A maximum improvement in impact strength has been achieved by 0.05% Ca addition to Al-7Si-0.3Mg-0.6Fe alloy. However, Ca at this level has led to the precipitation of  $\text{Al}_2\text{CaSi}_2$  intermetallics and higher porosity in the castings.
10. An empirical analysis carried out for comparing the results of the present work with those of the other researchers on the effect of increasing iron content on UTS and % elongation of Al-Si-Mg and Al-Si-Cu alloys has shown a linear and an inverse first order polynomial relationships respectively.
11. Mn (0.3-0.5%) addition to Al-7Si-0.3Mg-xFe alloy changes the morphology of platelet iron phase to script form. This has led to a significant improvement in tensile properties. However, there is no significant improvement in impact strength.
12. Be (0.2%) addition to Al-7Si-0.3Mg-xFe alloy changes the platelet morphology of iron phase to Chinese script form. This morphological change has resulted in significant improvement in both the tensile and impact properties.
13. Combined additions of Ca + Mn, Sr + Mn and Be + Mn have yielded improvement in both tensile and impact properties compared to individual additions.
14. A trace amount of Be (0.005%) addition to Ca and Sr leads to superior tensile properties compared to Ca and Sr additions alone.

## **6.1 SIGNIFICANT CONTRIBUTIONS OF THE PRESENT INVESTIGATION TO THE KNOWLEDGE**

1. Dual role of calcium viz., Modification and Fe-neutralization leading to improved elongation and impact properties in Al-7Si-0.3Mg-xFe alloys.
2. The properties obtained with Ca (0.02%) modification are at par with those obtained with the well known modifier viz., Sr (0.02%).
3. The optimum level of Ca in high Fe containing Al-7Si-0.3Mg alloy with respect to its fragmentation effect on the  $\beta$ -Fe intermetallic phase lies in the range 0.03-0.04%.
4. A trace amount of Be (0.005%) addition to Ca and Sr in Al-7Si-0.3Mg-xFe alloy leads to superior tensile properties compared to Ca and Sr additions alone.
5. The limitation on the impact properties of Al-7Si-0.3Mg-xFe alloy by Mn addition has been overcome by the combined addition of Mn with Ca and/or Sr and a synergistic effect of both the elements is achieved.
6. Judicious combinations of the iron neutralizers studied can pave the way for increased utilization of secondary or recycled aluminium alloys, requiring minimum energy.

## **6.2 AVENUES FOR FUTURE WORK**

1. Low amount of Ca (0.005%) reduced the porosity of the alloy probably due to the trapping of hydrogen as calcium hydride. However, further work is required to confirm such a hypothesis.
2. Understanding of the three-dimensional morphology of iron-containing intermetallics using modelling techniques.
3. Processing of Aluminium Matrix Composites using Ca as wetting promoter and Fe-neutralizer by liquid stir casting technique where lot of Fe will be introduced through the steel rod used for stirring.

## REFERENCES

1. Alan B. Deross: "Aluminum Casting Technology", p.31, American Foundrymen's Society, Inc., Des Plaines, Illinois.
2. John. E. Hatch: 'Aluminum: Properties and Physical Metallurgy', 200-211; 140: 1984, American Society for Metals, Metals Park, Ohio.
3. [www.mineralresourcesforum.org](http://www.mineralresourcesforum.org)
4. J.A. Taylor: Int. J. Cast Metals, 1995, 8(4), 225-252.
5. B. Closset and J.E. Gruzleski: AFS Trans. 1982, 90, 453-464.
6. A.M. Samuel, A. Pennors, C. Villeneuve and F.H. Samuel: Int. J. Cast Metal Res., 2000, 13, 231-253.
7. V.P. Itkin, C.B. Alcock, P.J. Van Ekeren and H.A.J. Oonk: 'Binary Alloy phase Diagrams', 2<sup>nd</sup> edn, 2.42; 1992, Ohio, ASM Materials Park.
8. L.F. Mondolfo: 'Aluminum Alloys: Structure and Properties', 1976, London, Butterworths.
9. Teng-Shih and Fang-Shea Shih: Int. J. Cast Met. Res., 1998, 10, 273-
10. A.M. Samuel, P. Quellet, F.H. Samuel and H.W. Doty: AFS Trans., 1997, 105, 951-962.
11. H. De La Sablonniere and F.H. Samuel: Int. J. Cast Met. Res., 1996, 9, 195
12. P. Quellet, F.H. Samuel, D. Gloria and S. Valtierra: Int. J. Cast Met. Res., 1997, 10, 67.
13. <http://www.world-aluminium.org>
14. [www.uneptie.org/outreach/wssd/contributions/sector\\_reports](http://www.uneptie.org/outreach/wssd/contributions/sector_reports)
15. F. Paray, B. Kulunk and J.E. Gruzleski: Int.J.Cast Metals Res., 2000, 13, 17-37.
16. G.K. Sigworth, S. Shivkumar and D. Apelian: AFS Trans. 1989, 97,811-824.

17. M. Tsukuda, M. Harada, T. Suzuki and S. Kokie: J. Jpn. Inst. Light Metals 1978, **28**(3), 109.
18. R.C. Harris, S. Lipson and H. Rosenthal: AFS Trans. 1956, **64**, 470.
19. W.A. Bailey: Foundry, May 1964, 54.
20. J. Sulinski: AFS Trans., 1967, **75**, 548-566.
21. T. Gaspar, "Effect of trace elements in superalloys", Metals and Ceramics Information Center, No.145, Mar.(1985).
22. G.J. Simensen,"Quality Assurance of DC-Casting of Aluminium", Continuous Casting: Melting -Casting-Control, DGM Informations Gessellschaft, pp.305-318 (1986).
23. B.L. Tuttle, A. Keslinke, D. Twarog and E. Daniels: AFS Trans., 1989, **97**, 889-902.
24. Shu-Zu Lu and A. Hellawell: Metall. Trans., 1987, **18A**(10), 1721-1733.
25. B.S. Murthy, S.A. Kori and M. Chakraborty: Int. Mater. Rev., 2002, **47**(1), 3-29.
26. S. Murali, K.S. Raman and K.S.S. Murthy: Int. J. Cast Metals, 1994, **6**, 189-198.
27. Y. Kobayashi, M. Niinomi, M. Yamoka and Y. Shimomara, J. Jpn. Inst. Light Met. 1993, **43**, 472.
28. C.J. Machovec, G.E. Byczynski, J.W. Zindel and I.A. Godlewski: AFS Trans., 2000, **108**, 439-444.
29. C.R. Loper, Jr and J.-I. Cho: AFS Trans., 2000, **108**, 667-672.
30. W. Martin: US Pat. No.3, 128, 176, Apr.7, 1964.
31. J. Glowonia, P. Bolechata, and Z. Kutig: Krzepiece Met. Stapon 1979, **1**, 70-8.
32. G. Bernd and J. Helmut: Stoeperitidende 1980, **46**(6), 168-9,171-3.
33. G. Bernd and J. Helmut: Giesserei 1980, **67**(1), 8-13 (Ger)
34. Y. Tsumura, A. Sakukibaru, K. Toyada and M. Ishikawa: J. Japan, Inst. Light Metals, 1980, **30**, 239-245.

35. R. Cook: Scandinavian Metallurgical Co.: 19; 1998, Wimbledon Hill Road, London, SW19 7LZ, UK.
36. B.P. Christian, E.-J. Friedrich and K. Thomas: *Giessereiforschung* 1982, **34** (3), 111-117 (Ger.)
37. A.G. Cooper Gwyer and H.W. Lewis Phillips: US Pat. No.1, 657, 389, Jan.24, 1928.
38. S. Baliktay and S. Honer: *Giesserei*, 1982, **69**, 397-402 (in German)
39. T. Kobayashi, H.J. Kim, and M. Niinomi: *Materials Science and Technology*, 1997, **13** (6), 497-502.
40. T. Kobayashi: in Proc. Conf. '6th International Conference on Aluminum Alloys', Toyohashi, Japan, 5-10; 1998.
41. T. Kobayashi, T. Ito, Q. Yao and N. Fatahalla: *Materials Science and Technology*, 1999, **15** (6), 1037-1043.
42. H.J. Kim, T. Kobayashi and T. Ito: *Materials Science Forum*, 1996, **217-222**, 1395-1400.
43. P.V. Bonsignore and E.J. Daniels: *Modern casting*, 1991, **81**(5), 28-29.
44. P.V. Bonsignore and E.J. Daniels: in Proc. Conf. 'Light Metals 1995', 12-16; 1995, Warrendale, PA, Minerals, Metals and Materials Society/AIME.
45. G. Piatti: *J. Mater. Sci.* 1983, **18**(8), 2471-83 (Eng).
46. D. Moore and L.R. Morris: Alcan Research and Development Ltd., Can.CA 1, 113, 282.
47. D. Moore and L.R. Morris: *Jpn. Kokai Tokyo Koho* 78, 125, 918.
48. Wu Qingling, Ma Higsheng and Ma Longxiang: *Dongbei Gongxueyuan Xuebao* 1984, **38**, 37-42 (ch).
49. V.K. Portnoi and V.M. Henko: *Izv. Vyssh. Uchebn. Zaved, Tsevetn. Metall.* 1984, (3), 70-4 (Russ).
50. Liquan Ma and Zhen-Lun Song: *Scripta Mater.* 1998, **39**(11), 1523- 1528.
51. S. Akiyama, H. Ueno, K. Koji, A. Imagawa, S. Nagata, K. Morimoto, T. Nishikawa and M. Itoh: US Pat. No. 4, 713, 277, Dec 1987.

52. Y. Sugimura, J. Meyer, M.Y. He, H. Bart-Smith, J. Grenstedt and A.G. Evans: *Acta Mater.*, 1997, **45**(12), 5245-5259.
53. Zhen-Lun Song, Liquan Ma, Zhao-Jin Wu and De-Ping He: *J. Mater. Sci.* 2000, **35**, 15-20.
54. W. Keng, Q. Wei, C. Shaojun and L. Yixian: *Zhongguo Youse Jinshu Xuebao* 1998, 8 (Suppl.1), 80-85 (Ch).
55. Sh. Chu and Q. Niu, K. Wu: *Huagong Yejin (Eng.Chem.Metall.)*, 1998, **19**(3), 260-265 (in Chinese).
56. A. Kawabe, A. Oshida, T. Kobayashi and H. Toda: *Keikinzoku* 1999, **49**(4), 149-154 (Japan).
57. T. Hikosaka, K.M. Ki and N.I. Kawamoto: *Alutopica (Jpn.)* Feb. 1988, **18**(2), 56-65.
58. C.H. Chiu and C.F. Yang: *Chukung (J. Chin. Foundrymen's Assoc.)*, Dec. 1999, **25**(4), 22-35 (in Chinese).
59. J. Choh, Z. Ebihara and T. Oki: *J. Jpn. Inst. Light Met.*, Oct. 1988, **38**(10), 600-607.
60. T. Namai, Y. Osava and M. Kikuchi: *Trans. Jpn. Foundrymen's Soc.* Apr. 1986, **5**, 29-32.
61. Hitachi Chemical Co.: *CA*, **98** (10): 165566a
62. Agency Of Industrial Sciences and Technology: *Jpn. Kokai Tokyo Koho JP* 81, 141, 960.
63. K. Hirohiko, K. Toshitake and N. Hideo: *Jpn. Kokai Tokyo Koho JP* 10 121, 167(Japan).
64. S. Towato, S. Yamada and T. Ohwaki: *Trans. Jpn. Inst. Met.*, 1985, **26**(8), 565-570.
65. S. Sugiyama, F. Toshiyasu, I. Horoshi and S. Yoshiya: (Sumitomo Light Metals Industries Ltd.), *Jpn. Kokai Tokyo Koho JP* 56. 011.
66. I. Yamamoto, T. Umino, Y. Shinoda and H. Yoshino, Nadagawa corrosion protecting Co., Ltd. (Tokyo, JP); Mitsui mining & smelting Co. (Tokyo, JP): *US Pat. No. 4,631,172*, Dec. 23, 1986.

67. S. Yoshifusa and H. Yuji: (Sumintomo Light Metal Industries, Ltd., Japan), Jpn. Kokai Tokyo Koho JP 2000 167, 689.
68. S. Yoshifusa and H. Yuji: (Sumintomo Light Metal Industries, Ltd., Japan), Jpn. Kokai Tokyo Koho JP 2000 153, 387.
69. Furukawa Aluminum Co. Ltd.: Jpn. Kokai Tokyo Koho JP 58 32, 222.
70. W. Kunio and M. Shiro: (Sumiko Boshoku K.K.; Sumitomo Metal Mining Co., Ltd., Japan), Jpn. Kokai Tokyo Koho JP 11 61, 307.
71. Furukawa Aluminum Co. Ltd., Nippondenso Co. Ltd.: Jpn. Kokai Tokyo Koho JP 60 89, 540.
72. D.L. Chidree: Kaisen Aluminum & Chemical Corporation, USA, PCT Int. Appl. WO 98 45, 082.
73. Furukawa Aluminum Co. Ltd.: Jpn. Kokai Tokyo Koho JP 80 100, 950.
74. H. Kawase and M. Yamaguchi: Furukawa aluminum Co., Ltd. (Tokyo, JP): US Pat. No. 4, 172, 923.
75. D. Amitava, A. Colin Mc Lean, Jr. B. Richard Liser, B. Debasis and D. Santosh Kumar (Allied Corp.): CA, 103(6): 75022n
76. Furukawa Aluminum Co. Ltd., Nippondenso Co. Ltd.: Jpn. Kokai Tokyo Koho JP 60 89, 542.
77. G.B. Parker, Reynolds Metals Company (Richmond, VA): US Pat. No. 5,469,911, Nov. 28, 1995.
78. O. Tokinori: (Furukawa Electric Co., Ltd., Japan), Jpn. Kokai Tokyo Koho JP 11 246, 926.
79. O. Tokinori and S. Takahiro: (Furukawa Electric Co., Ltd., Japan), Jpn. Kokai Tokyo Koho JP 11 246, 927.
80. Kobe Steel Ltd.: Jpn. Kokai Tokyo Koho JP 59 56, 565.
81. Nippon Light Metal Co. Ltd.: CA, 100 (2): 25183h.
82. K. Toshihiko, T. Yoshinobu, S. Yoshiyuki, T. Yoshishige and A. Kiyooki (Sumitomo Electric Industries, Ltd., Japan): Jpn. Kokai Tokyo Koho JP 11 158, 572.

83. Sumitomo Electric Industries Ltd.: Jpn. Kokai Tokyo Koho JP 59 190, 336.
84. Kobe Steel Ltd: Jpn. Kokai Tokyo koho JP 81, 133, 444.
85. S. Nishi and M. Morishita (Kobe Steel Ltd., Japan), Jpn. Kokai Tokyo Koho JP 11 350, 053.
86. S.J. Cytron (United States Dept. of the Army): US Pat. Appl. US 367, 693.
87. S.S. Sreeja Kumari, R.M. Pillai and B.C. Pai: Int. Mater.Rev., 2005, **50**(4), 216-238.
88. D. Vorren, J.E. Evesen and T.B. Pederson: AFS Trans., 1984, **92**, 459-466.
89. K. Radhakrishna and S. Seshan: Int. J. Cast Met. Res., 1989, **2**, 34-38.
90. M.C. Flemings, T.Z. Kattamis and B.P. Bardes: AFS Trans., 1991, **99**, 501-506.
91. L.A. Narayanan, F.H. Samuel and J.E. Gruzleski: AFS Trans., 1992, **100**, 383
92. D.R. Irani and V. Kondic: AFS Trans., 1969, **77**, 208-211.
93. H. Iwahori, K. Yonekura, Y. Yamamoto and M. Nakamura: AFS Trans.,1990, **98**,167-173.
94. J. Campbell: Castings, 1<sup>st</sup> edn., 1991, Butterworth Heinemann, Oxford, United Kingdom
95. H. Shahin: Scand. J. Metallurgy, 1985, **14**, 306-312.
96. G. Laslaz and P. Laty: AFS Trans., 1991, **99**, 83-90.
97. P.S. Mohanty, F.H. Samuel and J.E. Gruzleski: Proc.Int.Symp.on Light Metals Processing and Applications, Canadian Institute of Mining, Metallurgy and Petroleum, Montreal, 1994, pp.273-282.
98. D. Argo and J.E. Gruzleski: AFS Trans., 1988, **96**, 65-74.
99. G.K. Sigworth, C. Wang, H. Huang and J.T. Berry: AFS Trans., 1994, **102**, 245-260.
100. N. Roy, P.R. Louchez and F.H. Samuel: J. Mater. Sci., 1996, **31**, 4725-4740.
101. X. Cao and J.Campell: AFS Trans., 2000, **108**, 391-400.

102. Q.S. Hamed, R. Elliott and P.S. Cooper: in Proc. Conf. 'Light Metals 1992', 1391; 1991, Warrendale PA, USA, The Minerals, Metals & Materials Society.
103. K.R. Van Horn: 'Aluminum-Vol. I. Properties, Physical metallurgy and Phase Diagrams', 179; 1967, Ohio, Metals Park, American Society for Metals.
104. E. Velasco, J.E. De La Rosa, F. Hernandez, J.F. Mojica, S. Valtierra and R. Colas: in Proc. Conf. 'Light Metals 1998', 993-1001; 1998, Warrendale, PA, Minerals, Metals and Materials Society/AIME.
105. A.K. Dahle, J. Hjelen and L. Arnberg: in Proc. 4th Decennial Int. Conf. 'Solidification Processing', 527; 1997, Eds. J. Beech and H. Jones, Sheffield, UK.
106. A.K. Dahle, J. Hjelen and L. Arnberg: in Proc. 14th International Congress on Electron Microscopy (ICEM-14), Symposium U, Vol. II, 135; 1998, Cancun, Mexico.
107. D. Emadi and J.E. Gruzleski: AFS Trans., 1994, **102**, 307-312.
108. Q.T. Fang and D.A. Granger: AFS Trans., 1989, **97**, 989-1000.
109. J.E. Gruzleski, Hadiak, H. Campbell and B. Closset: AFS Trans., 1986, **94**, 147-154.
110. P.N. Crepeau: Modern Casting, 1997, **87(7)**, 39-41.
111. C.E. Ransley and H. Neufeld: J.Inst.Metals, 1947-48, **74**, 599-620.
112. C.E. Ransley and D.E.J. Talbot: Z.Metallkunde, 1955, **46**, 328.
113. M.F. Jordan: J.Inst.Metals, 1962-1963, **91**, 48-53.
114. P.M. Thomas and J.E. Gruzleski: Metall.Trans.B, 1978, **9B**, 139-141.
115. J.E. Gruzleski and B. Closset: "The treatment of Liquid Aluminum-Silicon Alloys", 1990, American Foundrymen's Society, Illinois.
116. D.P. Kanicki and W.M. Rasmussen: Modern Casting 1990, **80(2)**, 55-58.
117. P.S. Mohanty, F.H. Samuel and J.E. Gruzleski: Metall.Trans.A, 1993, **24A**, 1845-1856.

118. X.G. Chen and S. Engler: AFS Trans., 1994, **102**, 673-682.
119. W.L. Orchan, M.H. Mulazimoglu and J.E. Gruzleski: AFS Trans., 1991, **99**, 653-659.
120. E. Di Russo: *Aluminio*, 1960, **29**(3), 121-127.
121. J.R. Denton and J.A. Spittle: *Mater. Sci. Tech.*, 1985, **1**, 305-311.
122. K. Hiroshi and A. Yoji: *Journal of Japan Foundry Engineering Society*, 1997, **67**(7), 556-561.
123. A.F. Fakhman, A.M. Mikhailov, A.V. Kurdyumov and S.V. Inkin: *Tsvetnye Metally*, 1983, **24**, 84-85.
124. A.S. Fedosov and A.V. Kurdyumov: *Tsvetnye Metally*, 1985, **26**, 60-61.
125. E.N. Pan, H.S. Chiou and G.J. Liao: *Trans. Am. Foundrymen's Soc.*, 1991, **99**, 605-621.
126. N.L. Kutsenok, I.N. Ganiev and V.N. Yanchuk: *Metal Science and Heat Treatment (USSR)*, 1987, **29**, 146-149.
127. S. Holecek: *Aluminum*, 1973, **49**, 811-812.
128. K.E. Honer and Y. Zhang: *Giesserei Forschung*, 1987, **39**, 34-38.
129. M. Shigeo and M. Tomoya: *Light Met.* 1960, **10**(45), 394-396.
130. A. Knuutinen, K. Nogita, S.D. McDonald and A.K. Dahle: *J. Light Metals*, 2001, **1**(4), 241-249.
131. M. Montani, O. Yamashita, T. Suzuki and K. Sakaki: *Foundry Engineering*, 1996, **68**(8), 691-696.
132. A.V. Kurdyumov, A.S. Fedosov and S.V. Inkin: *Liteinoe Proizvodstvo*, 1990, **11**, 12-13.
133. S. Holecek: *Slevarenstvi*, 1976, **24**(1), 9-10.
134. S. Holecek: *Sb.Vys. Sk. Chem.-Technol. Praze, Anorg. Chem. Technol.*, 1977, 12.
135. A. Abdollahi and J.E. Gruzleski: *Int. J. Cast Metals Res.*, 1998, **11**, 145-155.
136. J.A. Taylor, G. Schaffer and D.H. St John: *Metall. TransA.*, 1999, **30A**, 1651-1655.

137. M. Claude Mascre: *Fonderie*, 1955, **108**, 4330-4336.
138. H. Iwahori, H. Takamiya, K. Yonekura, Y. Yamamoto and M. Nakamura: *Casting* 1988, **60**(9), 590-595.
139. J.E. Eklund, On the Effects of Impurities on the solidification and mechanical behaviour of primary and secondary commercial purity aluminium and aluminium alloys, Ph.D Thesis, Helsinki University of Technology, Helsinki, Finland, June 1993.
140. N. Roy, A.M. Samuel and F.H. Samuel: *Metall. Mater. Trans.*, 1996, **27A**, 415-429.
141. E.L. Rooy: *AFS Trans.*, 1985, **93**, 935-938.
142. E.L. Rooy, "Aluminium and Aluminium Alloys", *Metals Handbook: Vol.15-Casting* (ASM, Metals Park, Ohio, 9<sup>th</sup> edn., 1988), pp.745-770.
143. L. Anantha Narayanan, F.H. Samuel and J.E. Gruzleski: *Metall.Trans.* 1994, **25A**, 1761-1773.
144. B. Chamberlin and V.J. Zabek: *AFS Trans.*, 1973, **81**, 322-327.
145. M.M. Makhoulf and H.V. Guthy: *J. Light Met.*, 2001, **1**, 199-218.
146. B.M. Closset and S. Khan: in Proc. Conf. 'Light Metals 1990', 869; 1990, Warrendale, PA, TMS.
147. W. Wang and J. E. Gruzleski: *Mater. Sci. Technol.*, 1989, **15**, 471.
148. M. Garat, G. Laslaz, S. Jacob, P. Meyer, P.H. Guerin and R. Adam: *AFS Trans.*, 1992, **100**, 821-832.
149. G.K. Sigworth: *AFS Trans.*, 1983, **91**, 7-16.
150. V.P. Efimenko, A.A. Baranov, V.Z. Kisun'ko, Y.B. Bychkov and A.G. Progunova: *Soviet J. Non-Ferrous Met. Res.*, 1982, **10**, 461-465.
151. D. Li: *Foundry (China)*, January 1985, 27-32.
152. Jian Zengyun, Shang Baolu and Lu Deyang: *J.Chinese Rare Earth Soc.*, 1990, **8**, 206-211.

153. B.J. Ye, C.R. Loper Jr, D.Y. Lu and C.S. Kang: AFS Trans., 1985, **93**, 533-544.
154. A.I. Gavrilov, A.A. Anikin, K.I. Vlaskina, E.I. Gurevich and M.A. Ismailov: Soviet Castings Technology, February 1987, 77-79.
155. M. Ravi, U.T.S. Pillai, B.C. Pai, A.D. Damodaran and E.S. Dwarakadasa: Metall. Trans., 1996, **27A** (5), 1283-1292.
156. L.M. Hogan and M. Shamsuzzoha: Materials Forum, 1987, **10**, 270.
157. M. Shamsuzzoha and L.M. Hogan: J. Cryst. Growth, 1986, **76**, 429.
158. A.K. Dahle, J. Taylor and D.A. Graham: Aluminum Trans., 2000, **3**, 17-30.
159. A.K. Dahle, K. Nogita, J.W. Zindel, S.D. Mc Donald and L.M. Hogan: Metall. Trans., 2001, **32A**, 949-960.
160. K. Nogita and A.K. Dahle: Mater. Trans., 2001, **42**(3), 393-396.
161. J.R. Davis: "ASM Handbook-Casting, Vol.15", 9<sup>th</sup> edn., ASM International, Materials Information Society, Ohio.
162. P.K. Kissling and J.F. Wallace: Foundry, April 1963, p.74.
163. A. March: Molten Aluminum Processing, Feb.1986, 245-267.
164. M.B. Gokhshtein and L.S. Vasil'eva: Metallov, 1970, (7), 42-44.
165. V.D. Belov, A.V. Kurdyumov and S.V. Inkin: Soviet Non-Ferrous Metals Research, 1981, **9**(6), 497-500.
166. K. Nogita, A. Knuutinen, S.D. Mcdonald and A.K. Dahle: J. Light Metals, 2001, **1**(4), 219-228.
167. Y. Tsumura: J. Jpn. Inst. Light Met., 1955, **5**, 135-143.
168. M. Sasaki and Y. Yamada: US Pat. No. 5, 303, 764, Apr.19, 1994.
169. A. Knuutinen, K. Nogita, S.D. Mcdonald and A.K. Dahle: J. Light Metals, 2001, **1**(4), 229-240.

170. A.L. Greer, P.S. Cooper, M.W. Meredith, W. Schneider, P. Schumacher, J.A. Spittle and A. Tronche: *Advanced Engineering Materials*, 2003, **5**, 81–91.
171. D.G. McCartney: *Int. Mater. Rev.*, 1989, **34**, 247-260.
172. G.P. Jones and J. Pearson: *Metall. TransB.*, 1976, **7B**, 223-234.
173. K.P. Kashyap and T. Chandrashekar: *Bull. Mater. Sci.*, 2001, **24**, 345-353.
174. A.A. Abdel-Hamid: *Z. Metallkde*, 1989, **80**, 566-569.
175. M. Abdel-Reihim, N. Hess and W. Reif: *Metall. (Berlin)*, 1983, **37(6)**, 571-573.
176. C.R. Loper and J.-I. Cho: *Trans. Am. Foundrymen's Soc.* 2000, **108**, 585-592.
177. M.H. Fox and M. Nilmani: in *Proc. Conf. Third Australasian Asian Pacific Conference on 'Dross Minimization - Its Relationship to Melting and Melt Handling Practice'*, 239 - 254: 1993, Melbourne, Aluminum Cast House Technology; Theory and Practice.
178. Rob Brooks: Materials Center, NPL (Private Communication)
179. S. Venkatewaran, R.M. Mallya and M.R. Seshadri: *AFS Trans.*, 1986, **94**, 701-708.
180. D. Argo and J.E. Gruzleski: *Int. J. Cast Met. Res.*, 1989, **2**, 109-112.
181. W.H.M. Alsem, P.C. Van Wigggen and M. Vader, in *Proc. Conf. TMS, Light Metals 1992*, San Diego, 1992, pp.821-829.
182. John Campbell: Department of Metallurgy and Materials, The University of Birmingham (Private Communication).
183. Y. Tsumura, A. Sakakibara, K. Toyoda and S. Hara: *J. Japan Inst. Light Metals*, 1972, **22**, 369-376 (in Japanese)
184. G. Chai, *Dendrite Coherency During Equiaxed Solidification in Aluminium Alloys*, Ph.D Dissertation, Stockholm University, 1994.
185. S. Morimoto, N. Ohishi and S. Okada: *AFS Trans.*, 1987, **95**, 39-46.

186. D. Apelian, S. Shivkumar and G. Sigworth: AFS Trans., 1989, **97**, 727-742.
187. B. Closset, R.A.L. Drew and J.E. Gruzleski: AFS Trans. 1986, **94**, 9-16.
188. B.A. Parker, D.S. Saunders and J.R. Griffiths: Metals Forum, 1982, **5**(1).
189. F.N. Rhines and M. Aballe: Met.TransA, 1986, **17A**, 2139-2152.
190. T.J. Shin, D.N. Lee, and J. Korean Inst.Met., **23**(10), pp.1116-1122 (1985).
191. M. Tsukuda, T. Suzuki, M. Harada and S. Koike: Report from Kobe Steel (R&D), 1978, **28**(2), pp.60-64.
192. P.Y. Zhu, Q.Y. Liu and T.X. Hou: AFS Trans. 1985, **93**, 609-614.
193. J.W. Martin and R.D. Doherty: "Stability of Microstructures in Metallic Systems", Cambridge University Press, Cambridge, UK (1980).
194. S.S. Sreeja Kumari, R.M. Pillai and B.C. Pai: in the Proc. Conf. on Light Metals and Composites for Strategic and Societal Needs, RRL-Trivandrum, October 23–24<sup>th</sup>, 2002.
195. A.M. Samuel, F.H. Samuel, C. Villeneuve, H.W. Doty and S. Valtierra: Int. J. Cast Metals Res. **14** (2001) 97-120.
196. R. Ahmad and R. Marshall, Effect of Superheating on Iron-rich Plate type Compounds in Al-Si Alloy, Int. J. Cast Metal Res., **15** (2003) 497-504.
197. S.S. Sreeja Kumari, R.M. Pillai, and B.C. Pai: Indian Foundry Journal 2002, **48** 27-31.
198. W. Khalifa, F.H. Samuel and J.E. Gruzleski: Metall.Trans. 2003, **34A**, 807-825.
199. G. Gustafsson, J. Thorvaldsson and G.L. Dunlop: Metall. Trans. 1986, **17A**, 45-52.
200. R. Mackay and J.E. Gruzleski: Int.J.Cast Met.Res., 1997, **10**, 131-145.
201. S. Tang and T. Sritharan: Mater. Sci. Technol., 1998, **14**, 738-742.
202. A. Couture: AFS. Int. J. Cast Met.Res.,1981, **6**, 9-17
203. T.O. Mbuya, B.O. Odera and S.P. Ng'ang'a: Int.J.Cast Met.Res., 2003, **16**(5), 451-465.

204. M. Makhlouf, L. Wang, D. Apelian and L. Yang: AFS Trans., 1999, **107**, 501-505.
205. J.E. Hatch: 'Aluminum: Properties and Physical Metallurgy', ASM INTERNATIONAL, Metals Park, OH, 1984.
206. L. Wang, M. Makhlouf and D. Apelian: Int. Mater. Rev., 1995, **40** (6), 225-252.
207. L. Wang, D. Apelian and M. Makhlouf: AFS Trans., 1999, **107**, 231-238.
208. D.A. Granger, R.R. Sawtell and M.M. Kersker: AFS Trans., 1984, **92**, 579-586.
209. C.H. Caceres, C.J. Davidson, J.R. Griffiths and Q.G. Wang: Metall. Trans.A, 1999, 30A, 2611-2618.
210. S. Murali, K.S. Raman and K.S.S. Murthy: Mater. Sci. Engg., 1995, **A190**, 165-172.
211. Y. Wang and Y. Xiong: Mater. Sci. Eng., 2000, **A280**, 124-127.
212. Y.-H. Tan, S.-L. Lee and Y.-L. Lin: Metall.Trans.A, 1995, **26A**(5), 1195-1205.
213. Y.-H. Tan, S.-L. Lee and H.-Y. Wu: Int.J.Fatigue, 1996, **18**(2), 137-147.
214. Y.-H. Tan, S.-L. Lee and Y.-L. Lin: Metall.Trans.A, 1995, **26A**(11), 2937-2945.
215. F.H. Samuel, P.Quellet, A.M. Samuel and H.W. Doty: Metall.Trans.A, 2001, **29A**(12), 2871-2884.
216. G.E. Nagel Jr, J.P. Mouret and J. Dubruelh: AFS Trans., 1983, **91**, 157-160.
217. G. Atxaga, A. Pelayo and A.M. Irisarri: Mater. Sci. Technol., 2001, **17**(4), 445-450.
218. L. Wang, D. Apelian and M. Makhlouf: AFS Trans., 1998, **106**, 155-162.
219. P. Jonason: AFS Trans., 1992, **100**, 601-607.
220. C. Mascre: Fonderie, 1955, **108**, 4330.
221. L. Grand: Fonderie, 1964, **217**, 95-100
222. R.C. Lemon and H.Y. Hunsicker: AFS Trans. 1956, **64**, 255-260.

223. S. Murali, K.S. Raman and K.S.S. Murthy: *Int. J. Cast Met. Res.* 1991, **4**(1), 31-35.
224. S. Murali, K.S. Raman and K.S.S. Murthy: *Met.Sci. Engg.* 1992, **A151**, 1-10.
225. B. Closset and J.E. Gruzleski: *Metall.TransA*, 1982, **13A**, 945-951.
226. J.L. Estrada and J. Duszczyk: *J. Mater. Sci.*, 1990, **25**, 886.
227. J. Iglessis, C. Frantz and M. Gantois: *Mem. Sci. Rev. Metall.*, 1977, p.237.
228. A.M. Samuel, F.H. Samuel. H.W. Doty and S. Valtierra: *AFS Trans.* 2001, **116**, 679-696.
229. G. L. Armstrong: SAE, Article no. 780249, 1978.
230. L.F. Mondolfo and J.G. Barlock: *Metall. Trans.*, 1975, **6B**, 565-572.
231. Y. Awano and Y. Shimizu: *AFS Trans.* 1990, **98**, 889-895.
232. Wanqi Jie, Zhongwei Chen, W. Reif and K. Muller: *Metall. Trans.*, 2003, **34A**, 799-806.
233. X. Bian, G. Zhang, S. Zhao and J. Ma: *Int. J. Cast Metals Res.* 1992, **5**, 39-41.
234. X. Liu, X. Bian, Y. Liu, G. Zhang and J. Ma: *Acta Metallurgica Sinica*, 1997, **33**, 1062-1068.
235. C.Y. Kim, O. Umezawa and K. Nagai: *Metals and Materials*, 1998, **4**, 1027-1031.
236. C.Y. Kim, O. Umezawa and K. Nagai, *The Third International Conference on Ecomaterials*, p.99, Ecomaterials Forum, The Society of Non-Traditional Technology, Tsukuba, Japan (1997)
237. O. Umezawa and K. Nagai: *Trans. Mater. Res. Soc. Jap.* 1996, **20**, 190.
238. O. Umezawa and K. Nagai, *The Third International Conference on Ecomaterials*, p.59, Ecomaterials Forum, The Society of Non-Traditional Technology, Tsukuba, Japan (1997)
239. W.A. Bailey: *Mod. Cast* 1964, Aug. 443-454.

240. S.G. Shabestari, M. Mahmudi, M. Emamy and J. Campbell: *Int. J. Cast Metals Res.*, 2002, **15**, 17-24.
241. A.M. Samuel, F.H. Samuel and H.W. Doty: *J. Mater. Sci.*, 1996, **31**, 5529-5539.
242. V.A. Kozhanov, I.S. Alekseichuk and Yu. B. Bychkov: *Tsvetnye Metally*, 1985, **26**, 91-92.
243. D.L. Colwell and R.J. Kissling: *AFS Transactions*, 1961, **69**, 610-616.
244. L. Bakerud, G. Chai and J. Tamminen, *Solidification Characteristics of Aluminum Alloys*, AFS/Skanaluminum (1990)
245. D.A. Granger: *AFS Trans.*, 1991, **99**, 379-383.
246. K.T. Kashyap, S. Murali, K.S. Raman and K.S.S. Murthy: *Mater. Sci. Technol.*, 1993, **9**, 189-203.
247. N.A. Belov and T.A. Kurdyumova: *Russ. Metall.*, 1989, **2**, 207-212.
248. V.S. Zolotarevsky, A.A. Axenov and N.A. Belov: *Key Engineering Materials*, 1990, **44-45**, 347-364.
249. P.S. Wang, Y.J. Liauh, S.L. Lee and J.C. Lin: *Materials Chemistry and Physics*, 1998, **53**, 195-202.
250. K.G. Wikle: *AFS Trans.*, 1978, **86**, 513-518.
251. T. Otani, T. Kato, K. Arai and R. Otsuka: *Light Met. (N.Y)* 1981, 855-870.
252. T. Otani, O. Watanabe and M. Sakaguchi: *US Pat. No. 4*, 377, 425, Mar.22, 1983.
253. L.R. Morris and F.B. Miners: *US Pat. No. 3*, 926, 690, Dec.16, 1975.
254. F.H. Samuel, A.M. Samuel, H.W. Doty and S. Valtierra: *Metall. Trans.*, 2001, **32A**, 2061-2075.
255. G.K. Sigworth: *Modern casting*, July 1987, pp.23-25.
256. M.M. Haque and V. Kondic: in *Proceedings of a International Symposium, Light Metals; Science and Technology*, Trans. Tech Publications, Switzerland, 1985, pp.159-170 (1985).

257. A. Pennors, A.M. Samuel, F.H. Samuel and H.W. Doty: AFS Trans., 1998, **106**, 251-264.
258. T. Sato, H. Tezuka and P. Ashtari: Mater. Trans., Dec.2003, **44**(12), 2611-2616.
259. T. Suzuki and N. Oshiro: US Pat. No. 6, 336, 955, Jan.8, 2002.
260. K. Akihiko, T. Hiroyasu and T. Koichi: Nippon Imono Kyokai Zenkoku Koen Taikai Koen Gaiyaoshu, 1994, **125**, 9.
261. H. Nakae, H. Kanamoro and K.-K. Song: in Proc. 3rd Asian Foundry Congress, 8-10; 1995 Kyongju, South Korea.
262. S. El-Hadad, A.M. Samuel, F.H. Samuel, H.W. Doty and S. Valtierra: Int. J. Cast Met. Res., 2003, **15**(5), 551-564.
263. A.V. Vakhovbov, F.N. Alidzhanov, T.D. Dzhuraev and I.N. Ganiev: Dokl. Akad. Nauk. Tadzh. SSR 1978, **21**(11), 35-8 (Russ).
264. K. Kobayashi, S. Tsukahara and S. Yamada: Kenkyu Hokoku-Kanto Gakuin Daigaku Kogakubu 1999, **43**(1), 1-7 (Japanese).
265. V.K. Afanas'ev and A.N. Prudnikov: Izv. Vyssh. Uchebn. Zaved., Chern. Metall. 2000, (12), 27-28 (Russ).
266. I.-S. Kwon, J.-H. Kim, K.-M. Kim and E.-P. Yoon: J. Korean Inst. Met. Mater., 1998, **36**(9), 1444-1450 (in Korean).
267. A.K. Dahle, S.D. Mc Donald and K. Nogita: in 'Advances in Aluminum Casting Technology II', 1-10; 2 002, M. Tiryakioglu and J. Campbell (eds), ASM International, USA.
268. S. Jacob, M. Garat, G. Laslaz, P. Meyer, P. Guerin and R. Adam: Hommes et Fonderie, 1995, **258**, 45-54.
269. 'The Properties and Characteristics of Aluminium Casting Alloys', published by The Association of Light Alloy Refiners and Smelters, 3 Albermarle Street, London, W1x3HF, June 1973.
270. T. Ware, A.K. Dahle, S. Charles, M.J. Couper: Advances in Aluminum Casting Technology II, ASM International (USA), 2002, pp. 159-168.

271. C.H. Caceres: *Int. J. Cast Metals Res.*, 1998, 10, 293-299.
272. J.A. Taylor, G.B. Schaffer and D.H. StJohn, *Metall.Trans.A*, 1999, 30A, (Part III), 1657-1662.
273. F.H. Samuel, A.M. Samuel, H.W. Doty and S. Valtierra, *Metall.Trans.A*, 2001, 32A, 2061-2075.
274. L. Lu and A.K. Dahle: *Metall.Trans.A*, 2005, 36A, 819-835.
275. C. Dinnis, J.A. Taylor and A.K. Dahle: *Scripta Materialia*, 2005, 53(8), 955-958.
276. W.M. Mueller, J.P. Blackledge and G.G. Libowitz: 'Metal Hydrides', Academic Press Inc., New York. 1968, p. 202.
277. L. Anantha Narayanan, F.H. Samuel and J.E. Gruzleski: *Metall.Trans.* 1995, 26A, 2161-2174.
278. C.M. Dinnis, A.K. Dahle and J.A. Taylor, *AFS Trans.*, 2005.
279. D.H. St John, L.M. Hogan, *Acta Metal. Mat.* 1987, 35, 171-174.
280. H.P. Ha, J.D. Hunt, *Met. Mater. Trans. A* 2000, 31A, 29-34.
281. H. Fredriksson, T. Nyle, *Met. Sci.* 1982, 16, 283-294.
282. H.W. Kerr, J. Cisse, G.F. Bolling, *Acta Met.* 1974, 22, 676-677.
283. D.H. St John, *Acta Metall. Mater.* 1990, 38, 631-636.

## AWARDS AND PUBLICATIONS BASED ON THE THESIS WORK

### AWARDS

1. **“Best Paper Presentation award”** for the technical paper entitled “Investigation on the Structure and Properties of Be and Ca Added Al-7Si-0.3Mg-1.0Fe Alloy” presented at “National Symposium of Research Scholars-4”, held at IIT-Madras, Sept. 27–28, 2002.
2. **“Best Paper Presentation award”** for the technical paper entitled “Microstructural characterization of calcium added Al-7Si-0.3Mg-xFe alloy”, presented at “NMD-ATM-2004”, Indian Institute of Metals, Trivandrum, Nov. 17–19, 2004.

### PAPERS IN JOURNALS

#### Scientific Citation Index (SCI) Journal

1. “The Role of Calcium in Aluminum Based Alloys and Composites”  
**S.S. Sreeja Kumari**, R.M. Pillai and B.C. Pai,  
International Materials Review, 2005, **50(4)**, 216-238.  
*[Fourth Highest Impact Factor (3.68) Journal in Materials Science]*
2. “Influence of Ca on the structure and properties of Al-7Si-0.3Mg alloy”,  
**S.S. Sreeja Kumari**, R.M. Pillai, K. Nogita, A.K. Dahle and B.C. Pai,  
Metallurgical and Materials Transactions A, 2006 (in press).
3. “Effect of Be, Mn and Ca on the structure and properties of Al-7Si-0.3Mg-0.8Fe alloy”, **S.S. Sreeja Kumari**, R.M. Pillai, T.P.D. Rajan and B.C. Pai, International Journal of Cast Metals Research (communicated)
4. “Investigation on the Structure and Properties of Be and Ca Added Al-7Si-0.3Mg-1.0Fe Alloy” **S.S. Sreeja kumari**, R.M. Pillai and B.C. Pai  
Trans. Indian Inst. Met., August 2003, **56(4)**, 357-361.

#### Non Scientific Citation Index (SCI) Journal

1. “Effect of Iron in Al-7Si-0.3Mg Alloy”  
**S.S. Sreeja Kumari**, R.M. Pillai and B.C. Pai,  
Indian Foundry Journal, Jan 2002, **48 (1)**, 27-31.

## PAPERS IN CONFERENCE PROCEEDINGS

### International Conference

1. "Evaluation of Calcium as an Iron Neutralizer in Al-7Si-0.3Mg Alloy"  
S.S. Sreeja Kumari, R.M. Pillai and B.C. Pai, in the Proceedings of International Conference on Non-Ferrous Metals-2002 organized by NFTDC, Hyderabad, pp. 102-107, June 28-29, 2002.
2. "Beneficial Effects of Calcium in Aluminium Alloys"  
S.S. Sreeja Kumari, R.M. Pillai and B.C. Pai, in the Proceedings of International Conference on Aluminium (INCAL-03) organized by Aluminium Association of India, New Delhi, April 23-25<sup>th</sup>, 2003.
3. "Mitigating the Ill Effects of Iron in Primary and Secondary Al-Si Alloys",  
S.S. Sreeja Kumari, R. M. Pillai and B. C. Pai, in the Proceedings of 3<sup>rd</sup> International Conference on Advanced Manufacturing Technology (ICAMT 2004), pp.977-982, May 11-13, 2004, Malaysia.
4. "Influence of Ca, Be and Mn on the Structure and Properties of 356 Alloy",  
S.S. Sreeja Kumari, R.M. Pillai and B.C. Pai, in the John Campbell Honorary Symposium, TMS (The Minerals, Metals & Materials Society), pp.273-282, Feb. 13-17, 2005, San Francisco, California.

### National Conference

1. "Effects of Ca on density, electrical conductivity, mechanical properties and microstructure of Al-7Si-0.3Mg alloy" S.S. Sreeja kumari, R.M. Pillai and B.C. Pai in the Proceedings of Third National Symposium of Research Scholars on Metals and Materials, IIT Madras, pp.104-118, Sept 8-9, 2000.
2. "Investigation on the Structure and Properties of Be and Ca Added Al-7Si-0.3Mg-1.0Fe Alloy", S.S. Sreeja kumari, R.M. Pillai and B.C. Pai presented in the Third National Symposium of Research Scholars on Metals and Materials, IIT Madras, Sept 27-28, 2002.
3. "Effect of Trace Elements on Cast Al-Si Alloys"  
S.S. Sreeja kumari, R.M. Pillai and B.C. Pai in the Proceedings of Light Metals and Composites for Strategic and Societal Needs, RRL-Trivandrum, October 23-24<sup>th</sup>, 2002.
4. "Effect of Mn and Ca on the structure and properties of Al-7Si-0.3Mg-0.4Fe alloy", S.S. Sreeja Kumari, R.M. Pillai and B.C. Pai, in the Proceedings of 52<sup>nd</sup> Indian Foundry Congress, pp.91-96, Feb. 6-8<sup>th</sup>, 2004.

G8940

**Other Conference Presentations:**

1. "Mechanism of iron neutralization by Be, Mn and Ca in Al-7Si-0.3Mg-0.8Fe alloy", **S.S. Sreeja Kumari**, R.M. Pillai and B.C. Pai presented in "FDM-NMD-ATM-2005", Indian Institute of Metals, at IIT-Chennai, during Nov.12–16<sup>th</sup>, 2005.
2. "Microstructural characterization of calcium added Al-7Si-0.3Mg-xFe alloy", **S.S. Sreeja Kumari**, R.M. Pillai, B.C. Pai, S.G.K. Pillai and P. Prabhakar Rao presented in "NMD-ATM-2004", Indian Institute of Metals, at Trivandrum, during Nov.17–19<sup>th</sup>, 2004.
3. "Role of calcium in Aluminium-Silicon alloys" **S.S. Sreeja Kumari**, R.M. Pillai and B.C. Pai presented in "NMD-ATM-2000", Indian Institute of Metals, at Bhilai, during Nov. 14–17<sup>th</sup>, 2000.

